ECMWF COPERNICUS REPORT

Copernicus Atmosphere Monitoring Service

# Validation report of the CAMS near-real time global atmospheric composition service

## December 2017 - February 2018

Issued by: KNMI

Date: 4 June 2018

Ref: CAMS84_2015SC3_D84.1.1.11_2018DJF_v1

IMPLEMENTED BY ECMWF

# Validation report of the CAMS near-real-time global atmospheric composition service. Period December 2017 - February 2018

***EDITORS:***
H.J. ESKES (KNMI), A. WAGNER (MPG), M. SCHULZ (METNO),
Y. CHRISTOPHE (BIRA-IASB), M. RAMONET (LSCE)

***AUTHORS:***
S. BASART (BSC), A. BENEDICTOW (METNO), Y. BENNOUNA (CNRS-LA),
A.-M. BLECHSCHMIDT (IUP-UB), S. CHABRILLAT (BIRA-IASB), H. CLARK (CNRS-LA),
E. CUEVAS (AEMET), H. FLENTJE (DWD), K. M. HANSEN (AU), U. IM (AU),
J. KAPSOMENAKIS (AA), B. LANGEROCK (BIRA-IASB), K. PETERSEN (MPG),
A. RICHTER (IUP-UB), N. SUDARCHIKOVA (MPG), V. THOURET (CNRS-LA),
T. WARNEKE (UBC), C. ZEREFOS (AA)

**REPORT OF THE COPERNICUS ATMOSPHERE MONITORING SERVICE, VALIDATION SUBPROJECT.**

AVAILABLE AT:
HTTP://ATMOSPHERE.COPERNICUS.EU/QUARTERLY_VALIDATION_REPORTS

***CITATION:***
VALIDATION REPORT OF THE CAMS NEAR-REAL-TIME GLOBAL ATMOSPHERIC COMPOSITION SERVICE: PERIOD DECEMBER 2017 - FEBRUARY 2018.
H.J. ESKES, A. WAGNER, M. SCHULZ, Y. CHRISTOPHE, M. RAMONET, S. BASART, A. BENEDICTOW, Y. BENNOUNA, A.-M. BLECHSCHMIDT, S. CHABRILLAT, H. CLARK, E. CUEVAS, H. FLENTJE, K.M. HANSEN, U. IM, J. KAPSOMENAKIS, B. LANGEROCK, K. PETERSEN, A. RICHTER, N. SUDARCHIKOVA, V. THOURET, T. WARNEKE, C. ZEREFOS, COPERNICUS ATMOSPHERE MONITORING SERVICE (CAMS) REPORT, CAMS84_2015SC3_D84.1.1.11_2018DJF_v1.pdf, MAY 2018.

***STATUS:***
VERSION 1, FINAL

***DATE:***
4/6/2018

# Executive Summary

The Copernicus Atmosphere Monitoring Service (http://atmosphere.copernicus.eu, CAMS) is a component of the European Earth Observation programme Copernicus. The CAMS global near-real time (NRT) service provides daily analyses and forecasts of reactive trace gases, greenhouse gases and aerosol concentrations. This document presents the validation statistics and system evolution of the CAMS NRT service for the period up to 1 March 2018. Updates of this document appear every 3 months.

This summary is split according to service themes as introduced on the CAMS website: air quality & atmospheric composition, climate forcing, ozone layer and UV. Specific attention is given to the ability of the CAMS system to capture recent events. We focus on the 'o-suite' composition fields, which are the daily analyses and forecasts produced by the IFS (Integrated Forecast System) modelling system at ECMWF, using the available meteorological and atmospheric composition observations which are ingested in the ECMWF 4D-Var assimilation system. The model and assimilation configuration is summarised in section 2. We furthermore assess the impact of the composition observations by comparing the validation results from the 'o-suite' to a 'control' configuration without assimilation. Also, the pre-operational high-resolution forecasts of $CO_2$ and $CH_4$ are assessed in this report.

The o-suite data delivery for the period December 2017 - February 2018 was good, with an availability of 98.33% at 10 and 22 utc (two forecasts per day).

## Air quality and atmospheric composition

### *Tropospheric ozone ($O_3$)*

Model ozone is validated with respect to surface and free tropospheric ozone observations from the GAW and ESRL networks, IAGOS airborne data and ozone sondes. For free tropospheric ozone against sondes the o-suite modified normalized mean biases (MNMBs) are on average smaller ±10% over the Northern Hemisphere (NH), and between ± 20% for stations in the Tropics (Fig. S1). For December 2017 to February 2018 good agreement is found over the NH mid latitudes in the free troposphere, which is confirmed with IAGOS evaluations over Paris, Amsterdam and Frankfurt. In the UTLS region, the control runs shows a better correspondence with the observations. By the end of September 2017 the o-suite and control run switched to a new version, which shows in larger ozone mixing ratios in the control run. The o-suite slightly underestimates surface ozone over Europe, North America and West Africa during December 2017 to February 2018 with MNMBs of around -10%. For Antarctica the o-suite partly overestimates ozone, whereas the control run has a large negative bias.

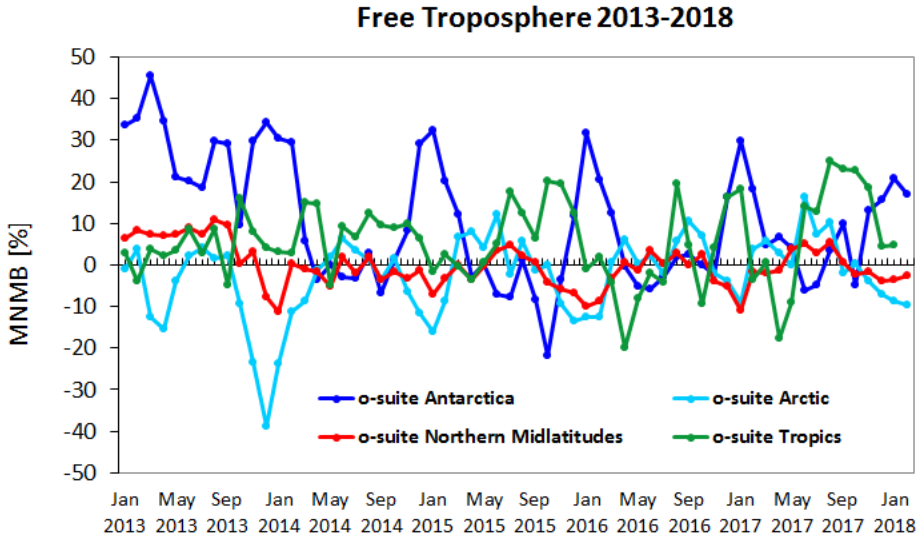


Figure S1: Time series of MNMB of ozone in the o-suite, compared against ozone sondes, averaged over different latitude bands. The free troposphere is defined here as the layer between 750 and 300 hPa.

### *Tropospheric Nitrogen dioxide ($NO_2$)*

Model validation, with respect to SCIAMACHY/Envisat $NO_2$ data before April 2012 and GOME-2/MetOp-A $NO_2$ data afterwards, shows that tropospheric $NO_2$ columns are well reproduced by the NRT model runs, indicating that emission patterns and $NO_x$ photochemistry are generally well represented, although modelled shipping signals are more pronounced than in the satellite retrievals. Tropospheric $NO_2$ columns over some local emission hotspots (e.g. Moscow, and Persian Gulf) are overestimated, while wintertime emissions over Europe are underestimated. Since December 2014, the agreement between satellite retrievals and model results for time series over East-Asia and Europe is better than for previous years (Fig. S.2), as observed columns of $NO_2$ decreased recently, likely associated with reduced emissions, and (in contrast to the observations) simulated values show an increase over the whole timeseries available. Spring and summertime values over East-Asia are overestimated by the o-suite since 2015, a feature which did not occur for previous years. Mainly in summer and autumn the models regularly show an overestimation over several regions with fire activity (Canada, Siberia, and Nepal). Evaluation against MAX-DOAS observations shows an overestimation over Xianghe with MBs of around 75%.

### *Tropospheric Carbon Monoxide (CO)*

Model validation with respect to GAW network surface observations, IAGOS airborne data, FTIR observations (NDACC and TCCON) and MOPITT and IASI satellite retrievals reveals that the seasonality of CO can be reproduced well by both model versions. A small, consistent negative bias of -5% against MOPITT appears in the o-suite throughout the year over Europe and the US, but for the last year it is further reduced. Also compared to IAGOS aircraft observations over Europe and Asia, modelled free tropospheric CO mixing ratios show an underestimation compared to the measurements. This is consistent with the results of modelled CO mixing ratios against GAW surface stations in Europe and Asia, where the o-suite slightly underestimates the observations with MNMBs around 5%.

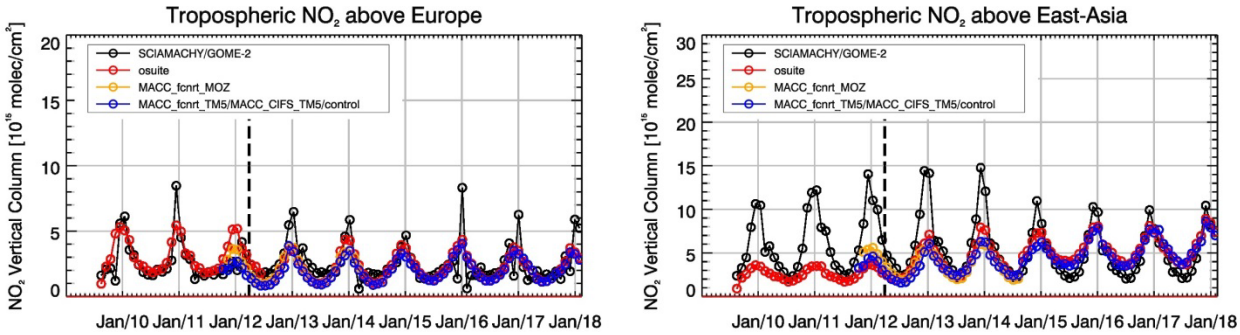


Figure S.2: Time series of tropospheric $NO_2$ columns from SCIAMACHY (up to March 2012), GOME-2 (from April 2012 onwards) compared to model results for Europe and East-Asia. The o-suite is in red, control is in blue (the model run without data assimilation is termed control since Sep 2014).

***Formaldehyde***

Model validation, with respect to SCIAMACHY/Envisat HCHO data before April 2012 and GOME-2/MetOp-A HCHO data afterwards, shows that modelled monthly HCHO columns represent well the magnitude of oceanic and continental background values and the overall spatial distribution in comparison with mean satellite HCHO columns. Compared to GOME-2 satellite retrievals, an overestimation of values regularly occurs over Australia and Central Africa, which could be both related to biogenic emissions or fire emissions. For time series over East-Asia and the Eastern US, both regions where HCHO columns are probably dominated by biogenic emissions, models and retrievals agree rather well. However, the yearly cycle over East-Asia is underestimated by the models.

The validation of model profiles with ground-based UV-VIS DOAS measurements over Xianghe, near Beijing, and over La Reunion shows that background column values are underestimated by around 15-40%, in agreement with satellite observations for this region. Also local pollution events are not captured correctly, in part due to the relatively coarse horizontal resolution of the global models, and in part associated with uncertainties in HCHO and precursor emissions. Note that no formaldehyde observations are assimilated in the system.

***Aerosol***

We estimate that the o-suite aerosol optical depth showed an average positive bias in the latest three months of +20%, measured as modified normalized mean bias against daily Aeronet (V3 level 1.5) sun photometer data. The +3 day forecasted aerosol distribution shows 17% less aerosol optical depth (AOD) than that from the initial forecast day, as shown in Figure S.3-a. The spatio-temporal correlation, shown in figure S.3-b, shows small month-to-month variation in DJF 2017-2018 about 0.78, indicating the simulation reproduces approximately 50% of the day to day AOD variability across all Aeronet stations. After better performance of the o-suite in spring 2017 there still seems to be a small decay in January and February 2018, which is partly associated with a high AOD bias in Southern Latitudes and more sea salt. The o-suite forecast at +3 days shows slightly lower correlation, as a consequence of imperfect forecasted meteorology and fading impact of the initial assimilation of MODIS AOD and MODIS fire info on model performance. However, the forecast and also control experiment have improved clearly since February 2017. The second o-suite running each day at 12UTC shows almost identical performance as the o-suite starting at 00UTC.

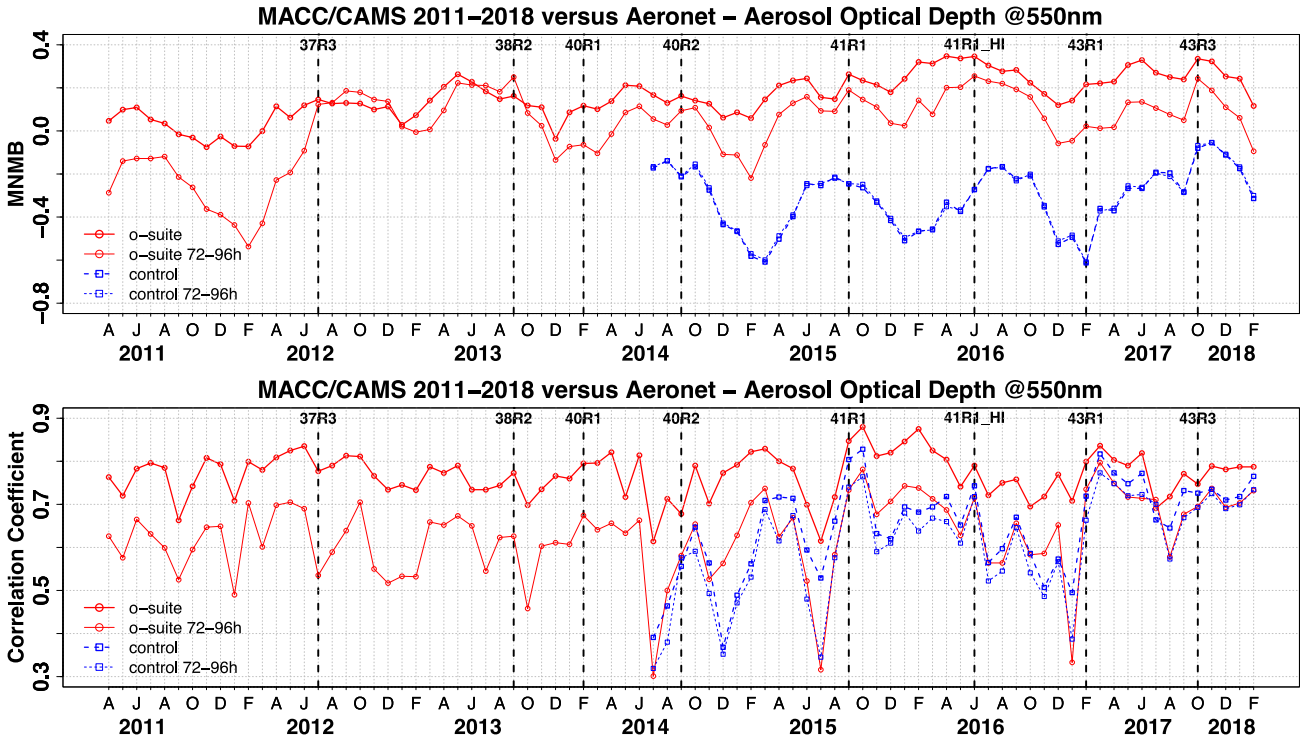


Figure S.3. Aerosol optical depth at 550nm in IFS 00Z model simulations for April 2011 – February 2018 against daily matching Aeronet Version3 level 1.5 data. a) Modified normalized mean bias (MNMB); o-suite (thick red curve); o-suite at last forecast day (light red curve); Control (blue dashed); Control at last forecast day (light blue dashed); b) Corresponding correlation coefficient. Model version changes are marked as vertical bars.

The AOD performance of the o-suite with respect to the AERONET data exhibits no pronounced seasonal cycle since 2014. Since October 2017, there is 45% more sea salt and 25% less sulphate .

The aerosol Ångström exponent contains information about the size distribution of the aerosol, and implicitly composition. The o-suite continues to show a positive global bias against Aeronet (V3 Level 1.5) data of +11%, indicating too fine particles in the model. The composition has changed considerably since February 2017, with now as much organic aerosol AOD as sulfate AOD.

PM10 data are used directly as defined by the IFS system. An evaluation of these PM10 surface concentrations against an average from data in the period 2000-2009 at 160 background sites in North America and Europe indicate that PM10 concentrations exhibit in the latest period an underestimation with MNMB bias of -30% in Europe and a slight overestimation in North America. The fraction of data within factor 2 of observed values has increased compared to earlier years.

From December to February, CAMS model can simulate the main areas of dust activity in North Africa and the Middle East although it underestimates the AOD observations particularly over the Bodélé (in Mali). During winter, the o-suite model can reproduce the daily variability of AERONET observations with a correlation coefficient of 0.79 in average for all the AERONET sites in comparison with control with a correlation coefficient of 0.74. These results are close to those obtained by the SDS-WAS Multi-model ensemble of 0.81. In terms of MB, both CAMS experiments (o-suite and control) as well as the SDS-WAS Multi-model underestimate the AERONET observations

resulting in an MB of -0.08 for all these experiments. Tropical North Atlantic region presents the best results of the AERONET comparison with correlation coefficients of 0.92. In the Sahel, o-suite presents strong underestimations (MB of -0.30) despite that the model can reproduce the observed daily variability (with a correlation value of 0.58 for o-suite). Over long-range transport regions, the performance of o-suite is particularly limited over sub-Tropical North Atlantic region, Western Iberian Peninsula and Western Mediterranean (with correlation coefficients between 0.30 and 0.55). This is a consequence of the low AOD concentration observed during this period in these AERONET sites. Otherwise, the comparison of 48h and 72h forecasts for both CAMS experiments shows that the prediction is stable during the 3-days forecasts with correlation coefficients of 0.79 (0.72), 0.75 (0.73) and 0.73 (0.72) respectively to 24, 48 and 72h forecasts for all the sites for o-suite (control). In the Sahara region, the correlation coefficient is better at 48h and 72h than forecast.

Aerosol backscatter coefficients in Germany are low-biased in the planetary boundary layer (PBL). Possible reasons are missing of ammonia and nitrate in the model (foreseen to be activated soon), assumption of too high particle densities (for pure compact materials) in the mass to backscatter conversion, and the lack of vertical transport barrier at the top of the PBL, causing dilution with free troposphere air. Free troposphere (FT) background backscatter coefficients are biased high, probably due to wrong re-distribution between PBL and FT. This is not fixed by the assimilation, which instead adds aerosol to the whole profile. The bias on a specific level thus depends on its relative position w.r.t. to the BLH.

The model BLH agrees reasonably (within few 100 m) with observations under favourable measurement conditions. Very often, however, meteorological conditions prevent formation, unambiguousness or detectability of the BLH or make the latter a challenge.

***System performance in the Arctic***

The CAMS model runs are validated using surface ozone measurements from the ESRL-GMD and the IASOA networks (6 sites) and ozone concentrations in the free troposphere are evaluated using balloon sonde measurement data.

For the period from December 2014 to January 2018 the simulations of the surface ozone concentrations are on average in good agreement with the observations apart from ozone depletion events in spring (March to June).

During December 2017 – January 2018 there is generally an underestimation of the ozone concentrations in the Arctic troposphere, both for the surface measurements (MNMB up to -20%) and for the free troposphere (MNMB up to -9%). The underestimation of tropospheric ozone concentrations in winter by IFS appear to be recurring over the past years.

***System performance in the Mediterranean***

The model is compared to surface $O_3$ observations from the AirBase network. Our analysis shows that model MNMBs vary between -35% and 10% over the Mediterranean shore of Spain. Over France, Gharb and Malta both runs underestimates surface ozone concentrations by -5% and -15% respectively while over Cyprus both models reproduce well surface ozone mean concentrations (MNMBs≈0). Temporal correlation coefficients between simulated and observed surface ozone for both the o-suite and control runs are highly significant over the entire Mediterranean from Gibraltar to Cyprus.

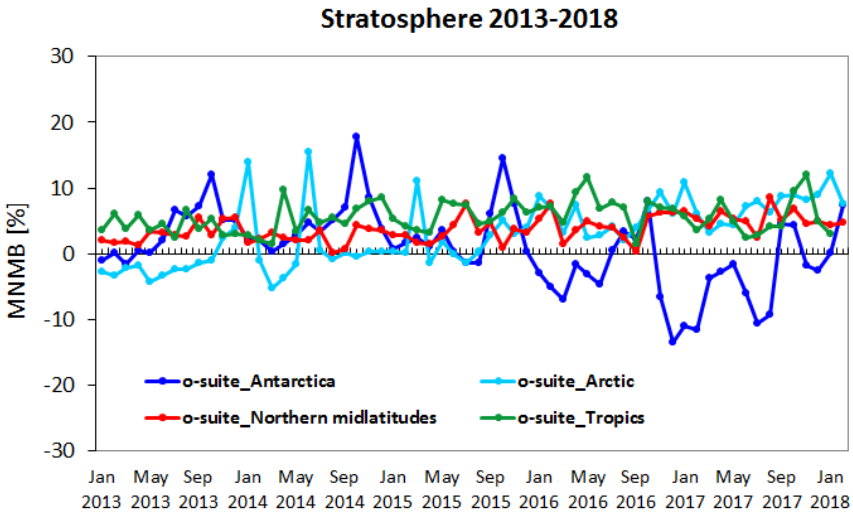


Figure S.4: MNMBs (%) of ozone in the stratosphere from the o-suite against aggregated sonde data in the Arctic (light blue), Antarctic (dark blue) northern midlatitudes (red) and tropics (green) ) from 2013 to February 2018.

CAMS o-suite can reproduce the daily variability of AERONET observations. In Western, Central and Eastern Mediterranean, the correlation coefficient increases from 0.50, 0.66 and 0.63 to 0.59, 0.67 and 0.65, respectively for control and o-suite during winter. Underestimations observed in the Mediterranean Basin in control are corrected in o-suite introducing overestimations in the whole Mediterranean Basin except in Italian sites. This results in an increase of MB from -0.02, -0.03 and 0 for control to 0.01, 0.01 and 0.01 for o-suite. The highest peaks on CAMS AOD simulations are linked to desert dust sources. Dust activity was exceptional high over the Mediterranean during this winter. At surface levels, both CAMS experiments show similar skill scores in comparison with EIONET observations indicating the limited impact of the data assimilation at surface levels. Otherwise, CAMS model can reproduce the daily variability of the most intense dust events observed by PM sites but highly overestimates some aerosol events associated to maritime aerosols.

## Climate forcing

### *Greenhouse gases*

Pre-operational high-resolution forecasts of $CO_2$ and $CH_4$ have been compared to ICOS surface (15 sites) and TCCON total column (3 sites) measurements, for a one year period from December 2016 to March 2018. Most of the stations are located in Europe (9 ICOS and 2 TCCON sites) providing a better representativeness over this continent. The third TCCON station is located in the tropical Indian ocean, at La Réunion Island, where two surface stations are also monitoring $CO_2$ and $CH_4$ at the surface, one being installed at sea level, the other on a mountain site 2195 m asl.

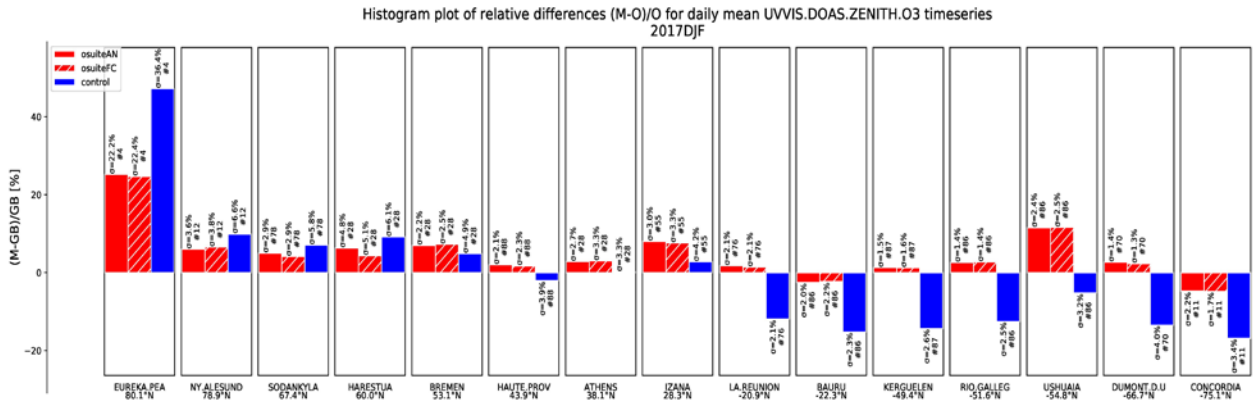


Figure S.5: Relative biases during quarter DJF 2017 - 2018 for 15 UVVIS stations measuring stratospheric ozone columns with ZENITH measurement geometry (stations sorted with decreasing latitude).

Both surface and total column observations show two main issues:

- an overestimation of the $CO_2$ seasonal cycle in North Hemisphere by about ±1%. Longer term comparison (2 years) at La Reunion indicates an overestimation of the simulated trend compared to TCCON time series.
- an increasing $CH_4$ bias up to 2% in early 2018 observed at all sites

## Ozone layer and UV

### *Ozone partial columns and vertical profiles*

Ozone columns and profiles have been compared with the following observations: vertical profiles from balloon-borne ozonesondes; ground-based remote-sensing observations from the NDACC (Network for the Detection of Atmospheric Composition Change, http://www.ndacc.org); and satellite observations by two instrument (OMPS-LP, ACE-FTS). Furthermore, the o-suite analyses are compared with those delivered by the independent assimilation system BASCOE.

Compared to ozone sondes (Fig. S.4) the model $O_3$ partial pressures are slightly overestimated in all latitude bands (MNMB between 4 and +12%) except above Antarctica.

Comparisons with the NDACC network include 15 stations for UVVIS stratospheric columns, microwave profiles for Ny Alesund (78.9°N) and Bern (47°N) and LIDAR profiles at Hohenpeissenberg (47.8°N) and Observatoire Haute Provence (OHP), France (43°N). The comparison with the UVVIS stations (Fig. S.5) are generally in agreement with the o-suite, while it indicates a latitudinal dependence of the biases for the control run. The result from MWR and LIDAR comparisons for the current period are in line with those of previous reports.

The comparison with independent satellite observations is generally in good agreement for the considered period: for ACE-FTS, the NMB is mainly within 10% between 5km and 40km, and mostly within 5% between 15km and 35km except in the tropics. OMPS-LP has updated the version for its level-2 product (to version 2.5, on altitude grid only). This results in different bias patterns compared to previous versions.

***Other stratospheric trace gases***

Due to the lack of stratospheric chemistry in the C-IFS-CB05 scheme, the only useful product in the stratosphere is ozone. Other species, like $NO_2$, have also been evaluated but the results are only indicative.

## Events

During end-January and early-February, there was an exceptional and *intense dust activity over the Mediterranean*. On 30th January a dust outbreak with origin in Algeria affected Southern Iberian Peninsula and Western Mediterranean. On 2nd February, a new dust event with origin in Algeria-Tunisia border was affecting Central-Eastern Mediterranean achieving high aerosol concentrations (up to 1.3 in Greece). After this later event, the Eastern Mediterranean again affected by two more consecutive dust event with origin in Libya. CAMS o-suite can timely reproduce the spatial distribution of the different dust plumes over the Mediterranean in comparison with the available observations. However, a high AOD/DOD ratio is observed over the dust affected areas inducing DOD underestimations.

During the *mid-October European dust event*, the Storm Ophelia pushed warm and dusty air from Africa northwards. CAMS o-suite timely reproduced the spatial distribution of the different dust plumes over the North Atlantic on 12-16 October and affected Northwestern Spain on 15 October and United Kingdom on 16 October as observed by MODIS. The whole episode is well simulated by CAMS o-suite in the North Atlantic and Europe. We can see how CAMS o-suite tracks fairly well the changes in both shape and size of the dust layer throughout the dusty period and how the AOD levels are enhanced on 15 October in Northwestern Spain coinciding with the location of the fires.

A prominent *fire event* was studied, namely the Portugal fires in mid-October 2017 and the plume transport over Europe. We found that for CO the fire plume location and transport was well predicted, but with differences in intensity compared to satellite observations.

# Table of Contents

# 1. Introduction

The Copernicus Atmosphere Monitoring Service (CAMS, http://atmosphere.copernicus.eu/) is a component of the European Earth Observation programme Copernicus. The CAMS global near-real time (NRT) service provides daily analyses and forecasts of trace gas and aerosol concentrations. The CAMS near-real time services consist of daily analysis and forecasts with the ECMWF IFS system with data assimilation of trace gas concentrations and aerosol properties. This document presents the system evolution and the validation statistics of the CAMS NRT global atmospheric composition analyses and forecasts. The validation methodology and measurement datasets are discussed in Eskes et al. (2015).

In this report the performance of the system is assessed in two ways: both the longer-term mean performance (seasonality) as well as its ability to capture recent events are documented. Table 1.1 provides an overview of the trace gas species and aerosol aspects discussed in this CAMS near-real time validation report. This document is updated every 3 months to report the recent status of the near-real time service. The report covers results for a period of at least one year to document the seasonality of the biases. Sometimes reference is made to other model versions or the reanalysis to highlight aspects of the near-real time products.

This validation report is accompanied by the "Observations characterization and validation methods" report, Douros et al. (2017), which describes the observations used in the comparisons, and the validation methodology. This report can also be found on the global validation page, http://atmosphere.copernicus.eu/user-support/validation/verification-global-services.

Key CAMS NRT products and their users are: Boundary conditions for regional air quality models (e.g. AQMEII, air quality models not participating in CAMS); Long range transport of air pollution (e.g. LRTAP); Stratospheric ozone column and UV (e.g. WMO, DWD); 3D ozone fields (e.g. SPARC). As outlined in the MACC-II Atmospheric Service Validation Protocol (2013) and MACC O-INT document (2011), relevant user requirements are quick looks of validation scores, and quality flags and uncertainty information along with the actual data. This is further stimulated by QA4EO (Quality Assurance Framework for Earth Observation, http://www.qa4eo.org) who write that “all earth observation data and derived products is associated with it a documented and fully traceable quality indicator (QI)”. It is our long-term aim to provide such background information. The user is seen as the driver for any specific quality requirements and should assess if any supplied information, as characterised by its associated QI, are "fit for purpose" (QA4EO task team, 2010).

CAMS data are made available to users as data products (grib or netcdf files) and graphical products from ECMWF, accessible through the catalogue on http://atmosphere.copernicus.eu/.

A summary of the system and its recent changes is given in section 2. Section 3 gives an overview of the performance of the system from a seasonal (climatological) perspective, for various species. Section 4 describes the performance of the system during recent events. Extended validation can be found online via regularly updated verification pages, http://atmosphere.copernicus.eu/user-support/validation/verification-global-services. Table 1.2 lists all specific validation websites that can also be found through this link.

Table 1.1: Overview of the trace gas species and aerosol aspects discussed in this CAMS near-real time validation report. Shown are the datasets assimilated in the CAMS analysis (second column) and the datasets used for validation, as shown in this report (third column). Green colors indicate that substantial data is available to either constrain the species in the analysis, or substantial data is available to assess the quality of the analysis. Yellow boxes indicate that measurements are available, but that the impact on the analysis is not very strong or indirect (second column), or that only certain aspects are validated (third column).

| Species, vertical range | Assimilation | Validation |
|---|---|---|
| Aerosol, optical properties | MODIS Aqua/Terra AOD<br>PMAp AOD | AOD, Ångström: AERONET, GAW, Skynet, MISR, OMI, lidar, ceilometer |
| Aerosol mass (PM10, PM2.5) | MODIS Aqua/Terra | European AirBase stations |
| $O_3$, stratosphere | MLS, GOME-2A, GOME-2B, OMI, SBUV-2, OMPS | Sonde, lidar, MWR, FTIR, OMPS, ACE-FTS, OSIRIS, BASCOE and MSR analyses |
| $O_3$, UT/LS | MLS | IAGOS, ozone sonde |
| $O_3$, free troposphere | Indirectly constrained by limb and nadir sounders | IAGOS, ozone sonde |
| $O_3$, PBL / surface | - | Surface ozone: WMO/GAW, NOAA/ESRL-GMD, AIRBASE |
| CO, UT/LS | IASI, MOPITT | IAGOS |
| CO, free troposphere | IASI, MOPITT | IAGOS, MOPITT, IASI, TCCON |
| CO, PBL / surface | IASI, MOPITT | Surface CO: WMO/GAW, NOAA/ESRL |
| $NO_2$, troposphere | OMI, partially constrained due to short lifetime | SCIAMACHY, GOME-2, MAX-DOAS |
| HCHO | - | GOME-2, MAX-DOAS |
| $SO_2$ | GOME-2A, GOME-2B (Volcanic eruptions) | - |
| Stratosphere, other than $O_3$ | - | $NO_2$ column only: SCIAMACHY, GOME-2 |
| $CO_2$, surface, PBL | | ICOS |
| $CO_2$, column | | TCCON |
| $CH_4$, surface, PBL | | ICOS |
| $CH_4$, column | | TCCON |

Table 1.2: Overview of quick-look validation websites of the CAMS system.

| |
|---|
| Reactive gases – Troposphere |
| GAW surface ozone and carbon monoxide:<br>http://macc.copernicus-atmosphere.eu/d/services/gac/verif/grg/gaw/gaw_station_ts!CIFS/TM5 AN<br>IAGOS tropospheric ozone and carbon monoxide:<br>http://www.iagos.fr/cams/<br>Surface ozone from EMEP (Europe) and NOAA-ESRL (USA):<br>http://www.academyofathens.gr/cams<br>Tropospheric nitrogen dioxide and formaldehyde columns against satellite retrievals:<br>http://www.doas-bremen.de/macc/macc_veri_iup_home.html<br>Tropospheric CO columns against satellite retrievals:<br>http://cams.mpimet.mpg.de |
| Reactive gases - Stratosphere |
| Stratospheric composition:<br>http://www.copernicus-stratosphere.eu<br>NDACC evaluation in stratosphere and troposphere (the NORS server)<br>http://nors-server.aeronomie.be |
| Aerosol |
| Evaluation against Aeronet stations:<br>http://aerocom.met.no/cams-aerocom-evaluation/<br>More in-depth evaluations from the Aerocom website:<br>http://aerocom.met.no/cgi-bin/aerocom/surfobs_annualrs.pl?PROJECT=CAMS&MODELLIST=CAMS-VALreports&FULL=explicit&INFO=nohover&PERFORMANCE=ind&YEARFILTER=ALLYEARS&PSFILTER=ALLVARS&Type0=SCATTERLOG&Ref0=AERONETSunNRT&Run0=ECMWF_OSUITE&Parameter0=OD550_AER&St<br>WMO Sand and Dust Storm Warning Advisory and Assessment System (SDS-WAS) model intercomparison and evaluation:<br>http://sds-was.aemet.es/forecast-products/models |
| Satellite data monitoring |
| Monitoring of satellite data usage in the Reanalysis and Near-Real-Time production:<br>http://copernicus-atmosphere.eu/d/services/gac/monitor/ |

Naming and color-coding conventions in this report follow the scheme as given in Table 1.3.

Table 1.3. Naming and color conventions as adopted in this report.

| **Name in figs** | **experiment** | **Color** |
|---|---|---|
| {obs name} | {obs} | black |
| o-suite D+0 FC | 0001 | red |
| Control | gsyg | blue |
| High-resolution greenhouse gas | ghqy | orange |

# 2. System summary and model background information

The specifics of the different CAMS model versions are given below (section 2.1) including an overview of model changes. Other systems used in CAMS are listed in section 2.2. An overview of products derived from this system is given in section 2.3. Timeliness and availability of the CAMS products is given in section 2.4.

## 2.1 System based on the ECMWF IFS model

Key model information is given on the CAMS data-assimilation and forecast run o-suite and its control experiment, used to assess the performance of the assimilation. The forecast products are listed in Table 2.1. Table 2.2 provides information on the satellite data used in the o-suite. Further details on the different model runs and their data usage can be found at http://atmosphere.copernicus.eu/documentation-global-systems.
Information on older MACC experiment types, including MACC_fcnrt_MOZ and MACC_CIFS_TM5 can be found in older Validation reports available from http://www.gmes-atmosphere.eu/services/aqac/global_verification/validation_reports/.

### 2.1.1 o-suite

The o-suite consists of the IFS-CB05 chemistry combined with the CAMS bulk aerosol model. The chemistry is described in Flemming et al. (2015) and Flemming et al. (2017), aerosol is described in Morcrette et al. (2009). The forecast length is 120 h. The o-suite data is stored under **expver '0001'** of **class 'MC'**. On 21 June 2016 the model resolution has seen an upgrade from T255 to T511, and forecasts are produced twice per day. The latest upgrade of the system took place on 26 September 2017. Here a summary of the main specifications of this version of the o-suite is given.

- The meteorological model is based on IFS version cy43r3_CAMS. The model resolution is T511L60. See also http://atmosphere.copernicus.eu/implementation-ifs-cycle-43r3cams.
- The modified CB05 tropospheric chemistry is used (Williams et al., 2013), originally taken from the TM5 chemistry transport model (Huijnen et al., 2010)
- Stratospheric ozone during the forecast is computed from the Cariolle scheme (Cariolle and Teyssèdre, 2007) as already available in IFS, while stratospheric NOx is constrained through a climatological ratio of $HNO_3/O_3$ at 10 hPa.
- Monthly mean dry deposition velocities are based on the SUMO model provided by the MOCAGE team.
- Data assimilation is described in Inness et al. (2015) and Benedetti et al. (2009) for chemical trace gases and aerosol, respectively. Satellite data assimilated is listed in Table 2.2 and Fig. 2.1.
- Anthropogenic and biogenic emissions are based on MACCity (Granier et al., 2011) and a climatology of the MEGAN-MACC emission inventories (Sindelarova et al., 2014)
- NRT fire emissions are taken from GFASv1.2 (Kaiser et al. 2012).

Table 2.1: Overview of model runs assessed in this validation report.

| Forecast system | Exp. ID | Brief description | Upgrades (e-suite ID) |
|---|---|---|---|
| o-suite | 0001 | Operational CAMS DA/FC run | 20170926-present<br>20170124-20170926<br>20160621-20170124<br>20150903-20160620<br>20140918-20150902 |
| Control | gsyg<br>gnhb<br>gjjh<br>geuh<br>g4o2 | control FC run without DA | 20170926-present (gsyg)<br>20170124-20170926 (gnhb)<br>20160621-20170124 (gjjh)<br>20150901-20160620 (geuh)<br>20140701-20150902 (g4o2) |
| GHG run | ghqy<br>gf39 | High resolution T1279,<br>NRT $CO_2$ and $CH_4$ without DA | 20160301-present (ghqy)<br>20150101-20160229 (gf39) |

Table 2.2: Satellite retrievals of reactive gases and aerosol optical depth that are actively assimilated in the o-suite.

| Instrument | Satellite | Provider | Version | Type | Status |
|---|---|---|---|---|---|
| MLS | AURA | NASA | V3.4 | O3 Profiles | 20130107 - |
| OMI | AURA | NASA | V883 | O3 Total column | 20090901 - |
| GOME-2A | Metop-A | Eumetsat | GDP 4.7 | O3 Total column | 20131007 - |
| GOME-2B | Metop-B | Eumetsat | GDP 4.7 | O3 Total column | 20140512 - |
| SBUV-2 | NOAA-19 | NOAA | V8 | O3 21 layer profiles | 20121007 - |
| OMPS | Suomi-NPP | NOAA / EUMETSAT | | O3 Profiles | 20170124 - |
| IASI | MetOp-A | LATMOS/ULB | - | CO Total column | 20090901 - |
| IASI | MetOp-B | LATMOS/ULB | - | CO Total column | 20140918 - |
| MOPITT | TERRA | NCAR | V5-TIR<br>V7-TIR | CO Total column | 20130129 -<br>20160124 - |
| OMI | AURA | KNMI | DOMINO V2.0 | NO2 Tropospheric column | 20120705 - |
| OMI | AURA | NASA | v003 | SO2 Tropospheric column | 20120705-20150901 |
| GOME-2A/2B | METOP A/B | Eumetsat | GDP 4.7 | SO2 Tropospheric column | 20150902 - |
| MODIS | AQUA / TERRA | NASA | Col. 5 Deep Blue<br>Col. 6, 6.1 | Aerosol total optical depth, fire radiative power | 20090901 -<br>20150902 -<br>20170124 - |
| PMAp | METOP-A<br>METOP-B | EUMETSAT | | AOD | 20170124 -<br>20170926 - |

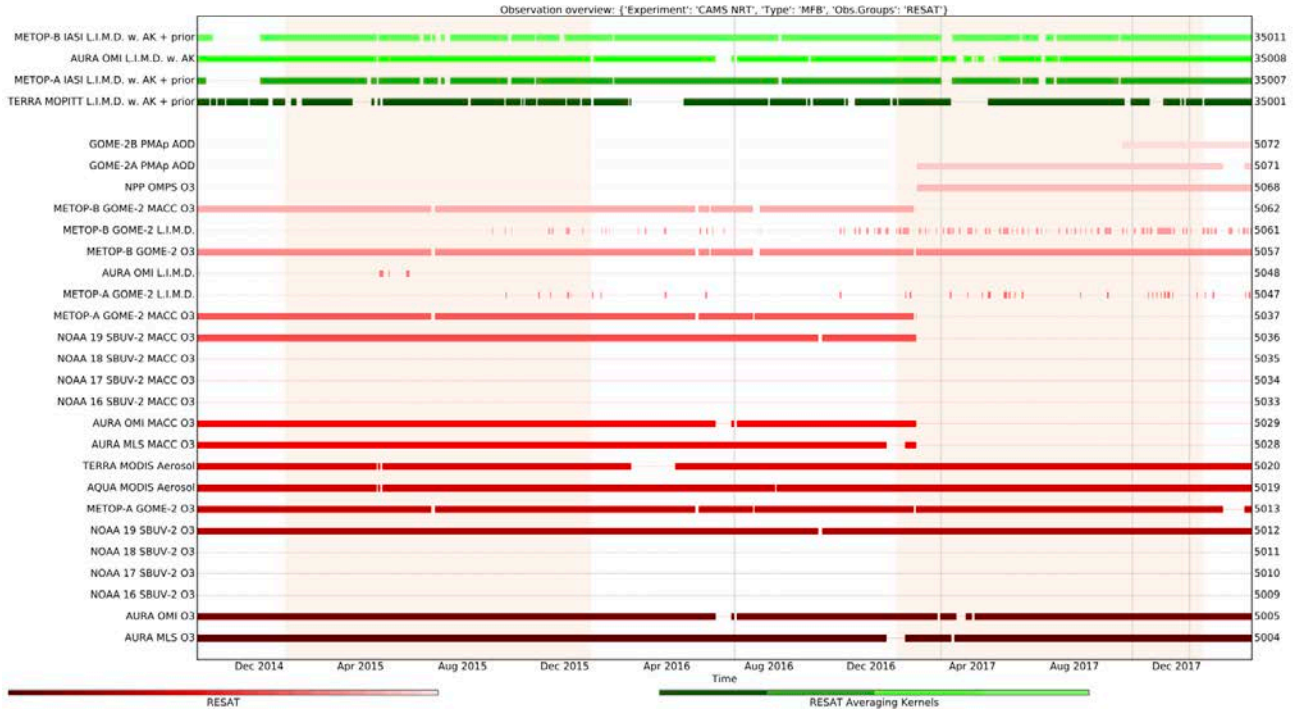


Figure 2.1: Satellite observation usage in the real-time analysis, for ozone, CO, aerosol AOD, from Oct. 2014 onwards. Top four rows: products assimilated with averaging kernels. New assimilated products since the 24 January 2017 upgrade are the PMaP AOD including GOME-2B and OMPS ozone profile observations. Note that the lines mentioning "MACC O3" should be discarded.

The aerosol model includes 12 prognostic variables, which are 3 bins for sea salt and desert dust, hydrophobic and hydrophilic organic matter and black carbon, sulphate aerosols and its precursor trace gas $SO_2$ (Morcrette et al., 2009). Aerosol total mass is constrained by the assimilation of MODIS AOD (Benedetti et al. 2009). A variational bias correction for the MODIS AOD is in place based on the approach used also elsewhere in the IFS (Dee and Uppala, 2009).

New source scheme for Secondary Organic Aerosols (part of the Organic Matter), based on scaled CO emissions. This is a change form the current AEROCOM-based emissions. The impact is an increase of organic matter aerosol concentrations. The upgrade of 24 January 2017 introduced the following adjustments: 1. Reduced dust emissions over Taklamakan desert and India. 2. Dust emissions adjusted towards more larger particles. 3. Reduction in sulphate aerosol. 4. Mass fixer for aerosols.

A brief history of updates of the o-suite is given in Table 2.4, and is documented in earlier MACC-VAL reports:
http://www.gmes-atmosphere.eu/services/aqac/global_verification/validation_reports/.

A list with changes concerning the assimilation system can be found at
http://atmosphere.copernicus.eu/user-support/operational-info/global-system-changes.
The CAMS o-suite system is upgraded regularly, following updates to the ECMWF meteorological model as well as CAMS-specific updates such as changes in chemical data assimilation. These changes are documented in e-suite validation reports, as can be found from the link above. Essential model upgrades are also documented in Table 2.4.

On 26 September 2017 the system has been upgraded to cy43r3. A validation report for this upgrade is available here:
https://atmosphere.copernicus.eu/sites/default/files/repository/CAMS84_2015SC2_D84.3.1.3_201706_esuite_v1_0.pdf

### 2.1.2 Control

The control run (current expver = **gsyg** since 26/11/2017; older versions are gnhb / gjjh / geuh / g4o2) applies the same settings as the respective o-suites, based on the coupled IFS-CB05 system with CAMS aerosol for cy41r1/cy40r2, except that data assimilation is not switched on. The only two exceptions with regard to this setup are:

- at the start of every forecast the ECMWF operational system is used to initialise *stratospheric* ozone, considering that stratospheric ozone, as well as other stratospheric species are not considered to be a useful product of this run. The reason for doing so is that this ensures reasonable stratospheric ozone as boundary conditions necessary for the tropospheric chemistry.
- The full meteorology in the control run is also initialized from the ECMWF operational NWP analyses. Note that this is different from the o-suite, which uses its own data assimilation setup for meteorology. This can cause slight differences in meteorological fields between o-suite and control, e.g. as seen in evaluations of upper stratospheric temperatures.

### 2.1.3 High-resolution $CO_2$ and $CH_4$ forecasts

The pre-operational forecasts of $CO_2$ and $CH_4$ use an independent setup of the IFS as the osuite, at a resolution of TL1279, i.e. ~16 km horizontal, and with 137 levels. This system runs in NRT, and does not apply data assimilation for the greenhouse gases.

The land vegetation fluxes for $CO_2$ are modelled on-line by the CTESSEL carbon module (Boussetta et al., 2013). A biogenic flux adjustment scheme is used in order to reduce large-scale biases in the net ecosystem fluxes (Agusti-Panareda, 2015). The anthropogenic fluxes are based on the annual mean EDGARv4.2 inventory using the most recent year available (i.e. 2008) with estimated and climatological trends to extrapolate to the current year. The fire fluxes are from GFAS (Kaiser et al., 2012).

Methane fluxes are prescribed in the IFS using inventory and climatological data sets, consistent with those used as prior information in the $CH_4$ flux inversions from Bergamaschi et al. (2009). The anthropogenic fluxes are from the EDGAR 4.2 database (Janssens-Maenhout et al, 2012) valid for the year 2008. The biomass burning emissions are from GFAS v1.2 (Kaiser et al., 2012).

The high resolution forecast experiments analyzed in this report correspond to two experiments:

- "gf39" from Jan 2015 to Feb 2016. This run was set up to replace run gcbt, which had a bug in the code resulting in spikes in concentration fields.
- "**ghqy**" from March 2016 to present. The initial conditions used in ghqy on 1st of March 2016 are from the GHG analysis (experiment gg5m). Furthermore, the meteorological analysis used to initialize the ghqy forecast changed resolution and model grid in March 2016.

The high-resolution model run also include a linear CO scheme (Massart et al., 2015).

Table 2.4: Long-term o-suite system updates.

| Date | o-suite update |
|---|---|
| 2009.08.01 | Start of first NRT experiment f7kn with coupled MOZART chemistry, without aerosol. Also without data assimilation. |
| 2009.09.01 | Start of first MACC NRT experiment f93i, based on meteo cy36r1, MOZART v3.0 chemistry, MACC aerosol model, RETRO/REAS and GFEDv2 climatological emissions, T159L60 (IFS) and 1.875°×1.875° (MOZART) resolution. |
| 2012.07.05 | Update to experiment fnyp: based on meteo cy37r3, MOZART v3.5 chemistry, where changes mostly affect the stratosphere, MACCity (gas-phase), GFASv1 emissions (gas phase and aerosol), T255L60 (IFS) and 1.125°×1.125° (MOZART) resolution. Rebalancing aerosol model, affecting dust. |
| 2013.10.07 | Update of experiment fnyp from e-suite experiment fwu0: based on meteo cy38r2, no changes to chemistry, but significant rebalancing aerosol model. Assimilation of 21 layer SBUV/2 ozone product |
| 2014.02.24 | Update of experiment fnyp from e-suite experiment fzpr: based on meteo cy40r1. No significant changes to chemistry and aerosol models. |
| 2014.09.18 | Update to experiment g4e2: based on meteo cy40r2. In this model version IFS-CB05 is introduced to model atmospheric chemistry. |
| 2015.09.03 | Update to experiment g9rr: based on meteo cy41r1. |
| 2016.06.21 | Update to experiment 0067: based on meteo cy41r1, but a resolution increase from T255 to T511, and two production runs per day |
| 2017.01.24 | Update to cycle 43R1_CAMS, T511L60 |
| 2017.09.26 | Update to cycle 43R3_CAMS, T511L60 |

## 2.2 Other systems

### 2.2.1 BASCOE

The NRT analyses and forecasts of ozone and related species for the stratosphere, as delivered by the Belgian Assimilation System for Chemical ObsErvations (BASCOE) of BIRA-IASB (Lefever et al., 2014; Errera et al., 2008), are used as an independent model evaluation of the CAMS products. The NRT BASCOE product is the ozone analysis of Aura/MLS-SCI level 2 standard products, run in the following configuration (version 05.07):

- The following species are assimilated: $O_3$, $H_2O$, $HNO_3$, HCl, HOCl, $N_2O$ and ClO.
- It lags by typically 4 days, due to latency time of 4 days for arrival of non-ozone data from Aura/MLS-SCI (i.e. the scientific offline Aura/MLS dataset).
- Global horizontal grid with a 3.75° longitude by 2.5° latitude resolution.
- Vertical grid is hybrid-pressure and consists in 86 levels extending from 0.01 hPa to the surface.

- Winds, temperature and surface pressure are interpolated in the ECMWF operational 6-hourly analyses.
- Time steps of 20 minutes, output every 3 hours

See the stratospheric ozone service at http://www.copernicus-stratosphere.eu/. It delivers graphical products dedicated to stratospheric composition and allows easy comparison between the results of o-suite, BASCOE and TM3DAM. The BASCOE data products (HDF4 files) are also distributed from this webpage. Other details and bibliographic references on BASCOE can be found at http://bascoe.oma.be/. A detailed change log for BASCOE can be found at http://www.copernicus-stratosphere.eu/4_NRT_products/3_Models_changelogs/BASCOE.php.

### 2.2.2 TM3DAM and the multi-sensor reanalysis

One of the MACC products was a 30-year reanalysis, near-real time analysis and 10-day forecast of ozone column amounts performed with the KNMI TM3DAM data assimilation system, the Multi-Sensor Reanalysis (MSR) system (van der A et al., 2010, 2013),
http://www.temis.nl/macc/index.php?link=o3_msr_intro.html.
The corresponding validation report can be found at
http://www.copernicus-atmosphere.eu/services/gac/global_verification/validation_reports/.

The NRT TM3DAM product used for the validation of the CAMS NRT streams is the ozone analysis of Envisat/SCIAMACHY (until April 2012), AURA/OMI, and MetOp-A/GOME-2, run in the following configuration:

- total $O_3$ columns are assimilated
- Global horizontal grid with a 3° longitude by 2° latitude resolution.
- Vertical grid is hybrid-pressure and consists in 44 levels extending from 0.1 hPa to 100 hPa.
- Dynamical fields from ECMWF operational 6-hourly analysis.

An update of the MSR (MSR-2) was presented in van der A et al. (2015), which extended the record to 43 years based on ERA-interim reanalysis meteo and with an improved resolution of 1x1 degree.

### 2.2.3 SDS-WAS multimodel ensemble

The World Meteorological Organization's Sand and Dust Storm Warning Advisory and Assessment System (WMO SDS-WAS) for Northern Africa, Middle East and Europe (NAMEE) Regional Center (http://sds-was.aemet.es/) has established a protocol to routinely exchange products from dust forecast models as the basis for both near-real-time and delayed common model evaluation. Currently, twelve regional and global models (see the complete list in the following link https://sds-was.aemet.es/forecast-products/forecast-evaluation/model-inter-comparison-and-forecast-evaluation/at_download/file) provides daily operational dust forecasts (i.e. dust optical depth, DOD, and dust surface concentration).

Different multi-model products are generated from the different prediction models. Two products describing centrality (multi-model median and mean) and two products describing spread (standard deviation and range of variation) are daily computed. In order to generate them, the model outputs are bi-linearly interpolated to a common grid mesh of 0.5º x 0.5º. The multimodel DOD (at 550 nm) Median from nine dust prediction models participating in the SDS-WAS Regional Center is used for the validation of the CAMS NRT streams.

## 2.3 CAMS products

An extended list of output products from the NRT stream o-suite are available as 3-hourly instantaneous values up to five forecast days. These are available from ECMWF (through ftp in grib2 and netcdf format, http://atmosphere.copernicus.eu/global-near-real-time-data-access ).

## 2.4 Availability and timing of CAMS products

The availability statistics provided in Table 2.6 are computed for the end of the 5-day forecast run, and are obtained from July 2012 onwards. The CAMS production KPI is defined as the percentage of cycles in which all the general data dissemination tasks are completed before the deadlines: 10 UTC for the 00 and 22 UTC for the 12 run. This was in part based on requirements from the regional models. We note that at present most regional models can still provide their forecasts even if the global forecast is available a bit later. Note that since 21 June 2016 two CAMS forecasts are produced each day.

For the period December 2017 - February 2018, 98.33% of the forecasts were delivered on time. There were three significant delays: two caused by corrupted input data (each causing ~2 hours delay) and one by HPC power failure (6 hours delay).

Table 2.6: Timeliness of the o-suite from Dec 2014 to the end of February 2018. From June 2016 onwards CAMS has produced two forecasts per day.

| **Months** | **On time, 22 utc** | **80th perc** | **90th perc** | **95th perc** |
|---|---|---|---|---|
| Dec-Feb '14-'15 | 97% | D+0, 19:43 | D+0, 20:28 | D+0, 21:13 |
| Mar-May 2015 | 96% | D+0, 19:38 | D+0, 21:03 | D+0, 21:40 |
| Jun-Aug 2015 | 95% | D+0, 20:24 | D+0, 20:53 | D+0, 21:54 |
| Sept-Nov 2015 | 95% | D+0, 19:44 | D+0, 20:55 | D+0, 21:51 |
| Dec-Feb '15-'16 | 100% | D+0, 18:39 | D+0, 18:57 | D+0, 19:43 |
| Mar-May 2016 | 98% | D+0, 19:32 | D+0, 19:47 | D+0, 20:00 |
| Jun-Aug 2016<br>(00 and 12 cycle) | 100% | D+0, 08:53<br>D+0, 20:55 | D+0, 09:04<br>D+0, 21:01 | D+0, 09:18<br>D+0, 21:18 |
| Sep-Nov 2016 | 98.9% | D+0, 08:44<br>D+0, 20:44 | D+0, 08:51<br>D+0, 20:48 | D+0, 08:52<br>D+0, 20:51 |
| Dec 2016 -<br>Feb 2017 | 99.4% | D+0, 09:02<br>D+0, 21:01 | D+0, 09:11<br>D+0, 21:02 | D+0, 09:18<br>D+0, 21:04 |
| Mar-May 2017 | 100% | D+0, 09:08<br>D+0, 21:07 | D+0, 09:14<br>D+0, 21:09 | D+0, 09:19<br>D+0, 21:11 |
| Jun-Aug 2017 | 100% | D+0, 09:05<br>D+0, 21:05 | D+0, 09:07<br>D+0, 21:08 | D+0, 9:09<br>D+0, 21:10 |
| Sep-Nov 2017 | 100% | D+0, 09:02<br>D+0, 21:00 | D+0, 09:05<br>D+0, 21:04 | D+0, 9:09<br>D+0, 21:07 |
| Dec 2017 -<br>Feb 2018 | 98.33% | D+0, 08:55<br>D+0, 20:54 | D+0, 08:59<br>D+0, 20:59 | D+0, 09:01<br>D+0, 21:02 |

# 3. Tropospheric Ozone

## 3.1 Validation with sonde data in the free troposphere

Model profiles of the CAMS runs were compared to free tropospheric balloon sonde measurement data of 38 stations taken from the NDACC, WOUDC, NILU and SHADOZ databases for February 2017 to February 2018 (see Fig. 3.1.1 - 3.1.2). Towards the end of the period, the number of available soundings decreases, which implies that the evaluation results may become less representative. The figures contain the number of profiles in each month that are available for the evaluation. The methodology for model comparison against the observations is described in Douros et al., 2017. The free troposphere is defined as the altitude range between 750 and 200hPa in the tropics and between 750 and 300hPa elsewhere.

In all zonal bands MNMBs for the o-suite are mostly within the range ±25%, for all months, see Fig. 3.1.1.-3.1.2. The control run generally shows larger negative MNMBs, (up to -40%).

Over the Arctic, the o-suite mostly shows slightly positive MNMBs during summer and spring (MNMBs up to 16%), while during the winter season the MNMBs get negative (within -9%) see, Fig. 3.1.1.

Over the NH mid-latitudes MNMBs for the o-suite are on average close to zero all year round (maxima are -4% to +6%), which is generally a clear improvement compared to the control run, which shows larger negative MNMBs during the respective period.

Over the Tropics, ozone mixing ratios are overestimated by the o-suite (up to 25%) by the o-suite, see Fig. 3.1.2.

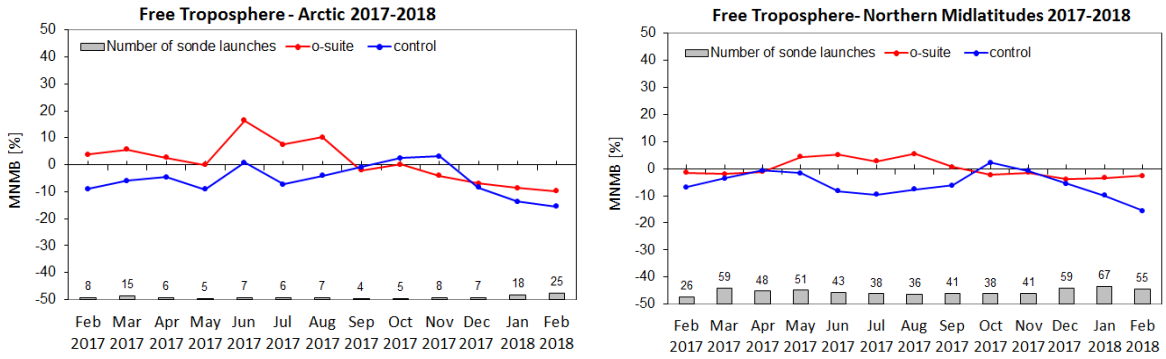


Figure 3.1.1: MNMBs (%) of ozone in the free troposphere (between 750 and 300 hPa) from the IFS model runs against aggregated sonde data over the Arctic (left) and the Northern mid latitudes (right). The numbers indicate the amount of individual number of sondes.

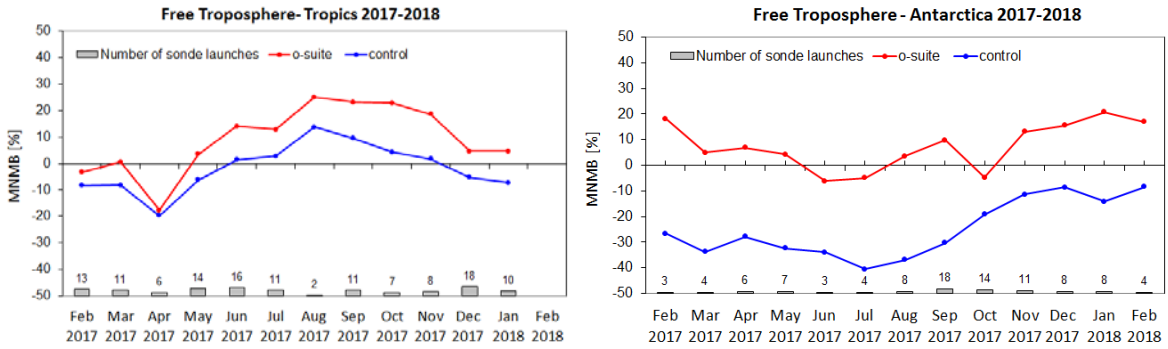


Figure 3.1.2: MNMBs (%) of ozone in the free troposphere (between 750 and 200hPa (Tropics) / 300hPa) from the IFS model runs against aggregated sonde data over the Tropics (left) and Antarctica (right). The numbers indicate the amount of individual number of sondes.

## 3.2 Ozone validation with IAGOS data

The daily profiles of ozone measured at airports around the world, are shown on the website at http://www.iagos.fr/macc/nrt_day_profiles.php. For the period from December 2017 - February 2018, the data displayed on the web pages and in this report include only the data as validated by the instrument PI. The available flights and available airports are shown in Fig. 3.2.1 top and bottom respectively. Performance indicators have been calculated for different parts of the IAGOS operations.

Eight aircrafts were operating during this period. With these seven aircrafts, operating fully over the three month period, we can expect a total of about 1680 flights. The actual number of flights within the period was 510 (1020 profiles) giving a performance of 30 %. These flights are shown in Fig. 3.2.1 (top). Sixty one percent (61%) of the operational flights had usable measurements of ozone and 38% of flights had usable CO. Delivering these $O_3$ and CO data were two aircraft from Lufthansa operating from Frankfurt, two aircraft operated by Air France based in Paris, one from Cathay Pacific, one from China Airlines based in Taipei and one from Hawaiian Airlines since mid-October 2017, with flight operations from Honolulu. Fig. 3.2.1 (bottom) shows the available airports, with a plotting circle scaled to the highest number of flights at an airport.

*Europe*

Fig. 3.2.2 presents ozone timeseries at Paris during December 2017 - February 2018. Ozone is well represented throughout the profiles until the UTLS region when ozone is generally overestimated, with the control run performing consistently better than the o-suite. Some examples of individual profiles are presented in Fig. 3.2.3.

At Paris (Fig. 3.2.3) the profiles on 10 December 2017 and 22 February 2018 show an increase in ozone values in the free troposphere between 5000 m and 6000 m reaching about 80 ppbv and 100 ppbv respectively. This peak is well detected by CAMS-global whereas control run is providing a nearly constant profile. On 2 and 29 December the profiles at Paris show low tropopause which is well reproduced by CAMS global, but not by control run.

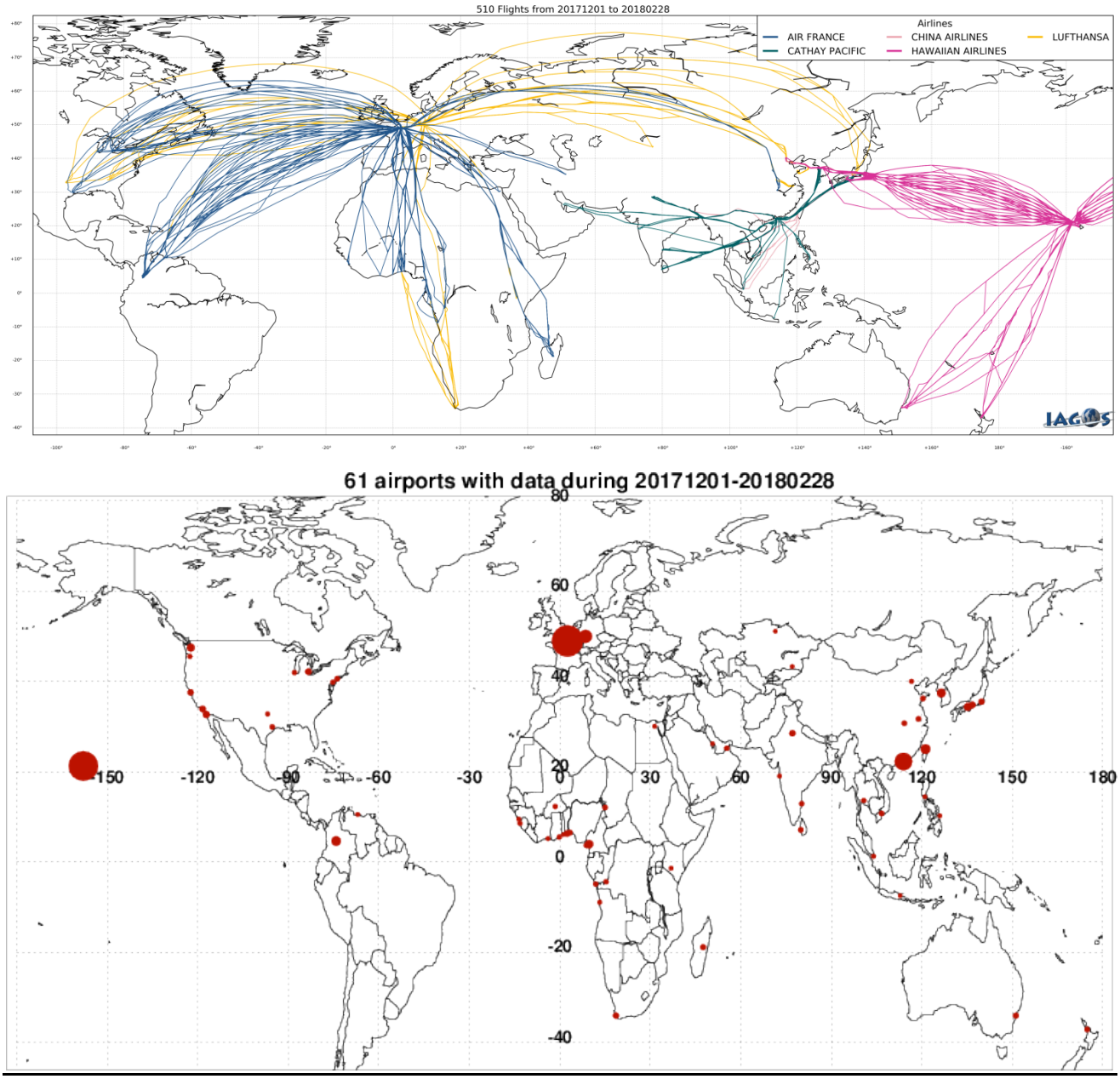


Figure 3.2.1. Map of the flights (top) and the visited airports (bottom) during the period December 2017 - February 2018, by the IAGOS-equipped aircraft. The size of the plotting circle represents the number of profiles available.

Fig. 3.2.3 also shows ozone profiles at Frankfurt on 29 December 2017 and 20 January 2018 with a peak of about 120 ppbv in the UTLS around the altitude of 7000 m likely due to stratospheric intrusions. This peak is not reproduced by the models, and CAMS-global fails to determine the altitude of tropopause which is found at an altitude close to the observed peak

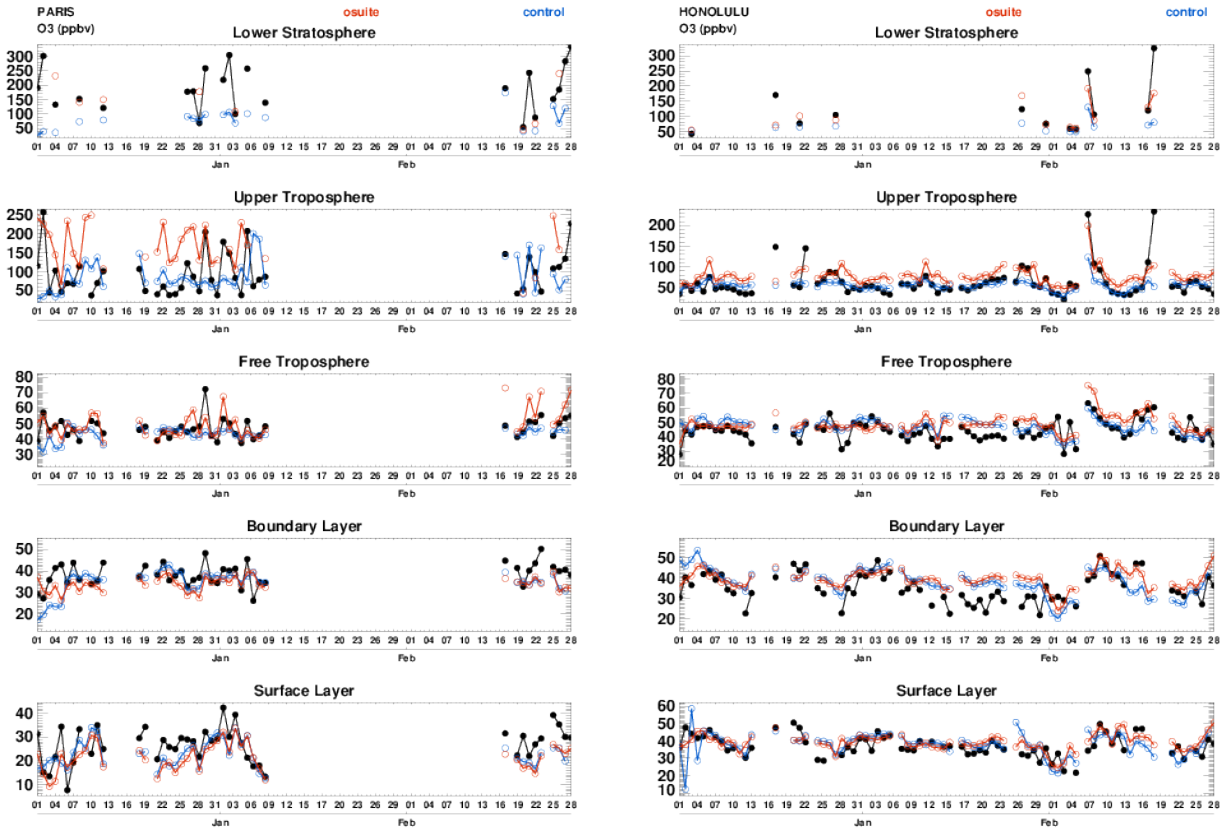


Figure 3.2.2. Time series of daily mean ozone over Paris and Honolulu during December 2017 – February 2018 for 5 layers, Surface, Boundary layer, Free Troposphere, Upper Troposphere and Lower Stratosphere.

*West Africa*

Several destinations across West Africa have been visited during the period December 2017 – February 2018. These include some situated on the Gulf of Guinea (Accra, Cotonou, Conakry) where pollution from oil industries has effects on the profiles all year round, some situated inland (N'Djamena), and some in the southern hemisphere (Kinshasa). All these cities are subject to anthropogenic emissions from vehicles and to biomass burning during the dry season, from December to March and from June to October in the northern and southern hemisphere respectively. In Fig. 3.2.4 examples of ozone profiles sampled in this region are shown. These ozone profiles present anomalies in the boundary layer and/ or in the free troposphere likely related to forest fires as they are often correlated with peaks in CO (see section 4.2). The profiles with complex shapes (i.e. with several maxima) such as in Accra, Conakry, N'djamena and Cotonou are reproduced by the models, with better performance of the o-suite as compared to the control run. In the case of Kinshasa on 7$^{th}$ and 8$^{th}$ December, the strong increase in ozone values between 2000 m and 4000 m reaching about 110 ppbv is not detected by the models. For these dates the plume observed for CO is also missed by the models (see CO section).

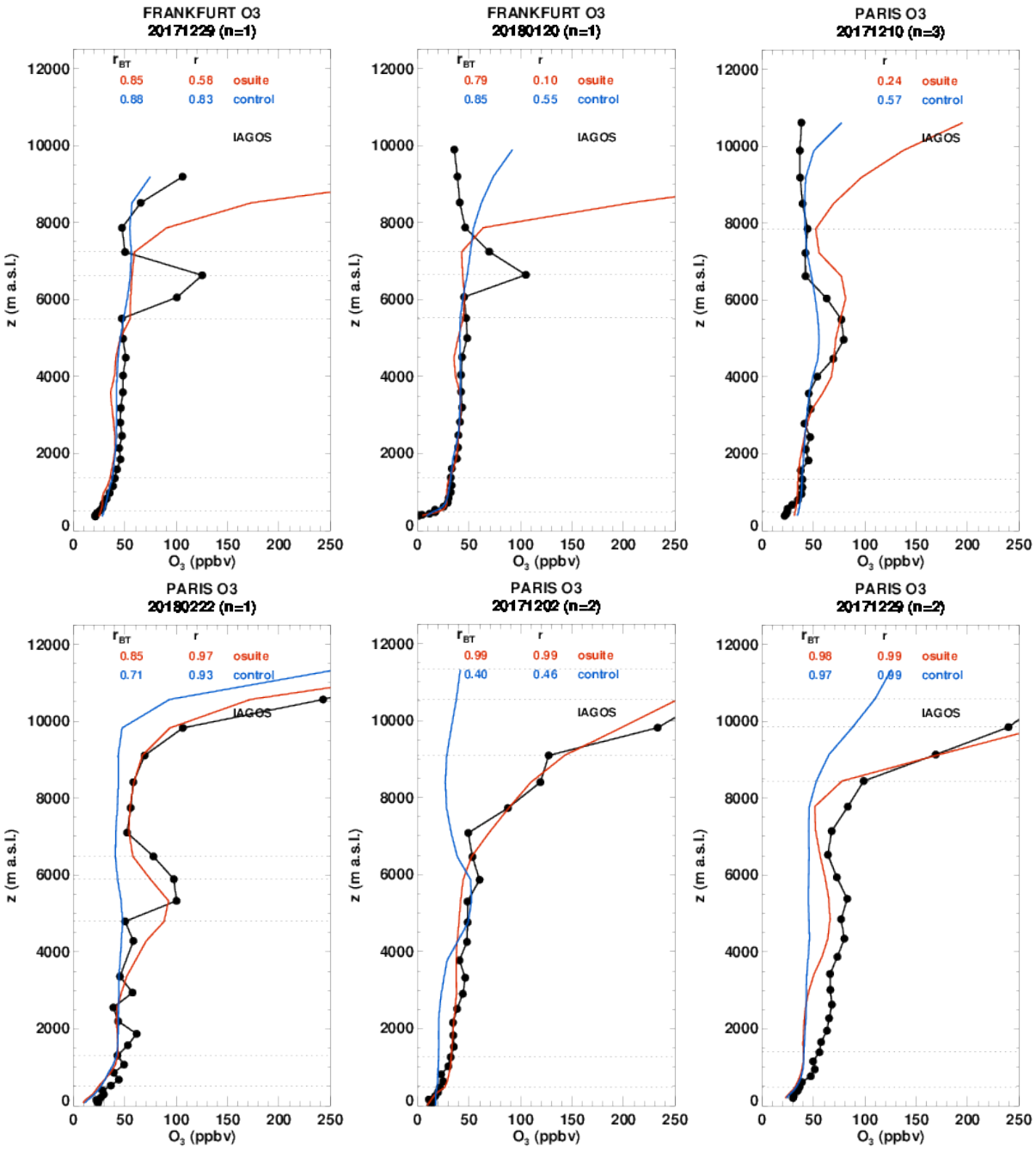


Figure 3.2.3. Selection of daily profiles for ozone from IAGOS (black) and the two NRT runs (o-suite:red, control: blue) over Europe during December 2017 – February 2018.

*North America*

At North American airports ozone is slightly underestimated at the surface, and the largest discrepancies between models and observations are found in the UTLS where the results can be very different. In the profiles shown in Fig. 3.1.2.5, CAMS global performs better than control run in Chicago (4th January 2018) and Detroit (28th December2017) where the model detects an increase in

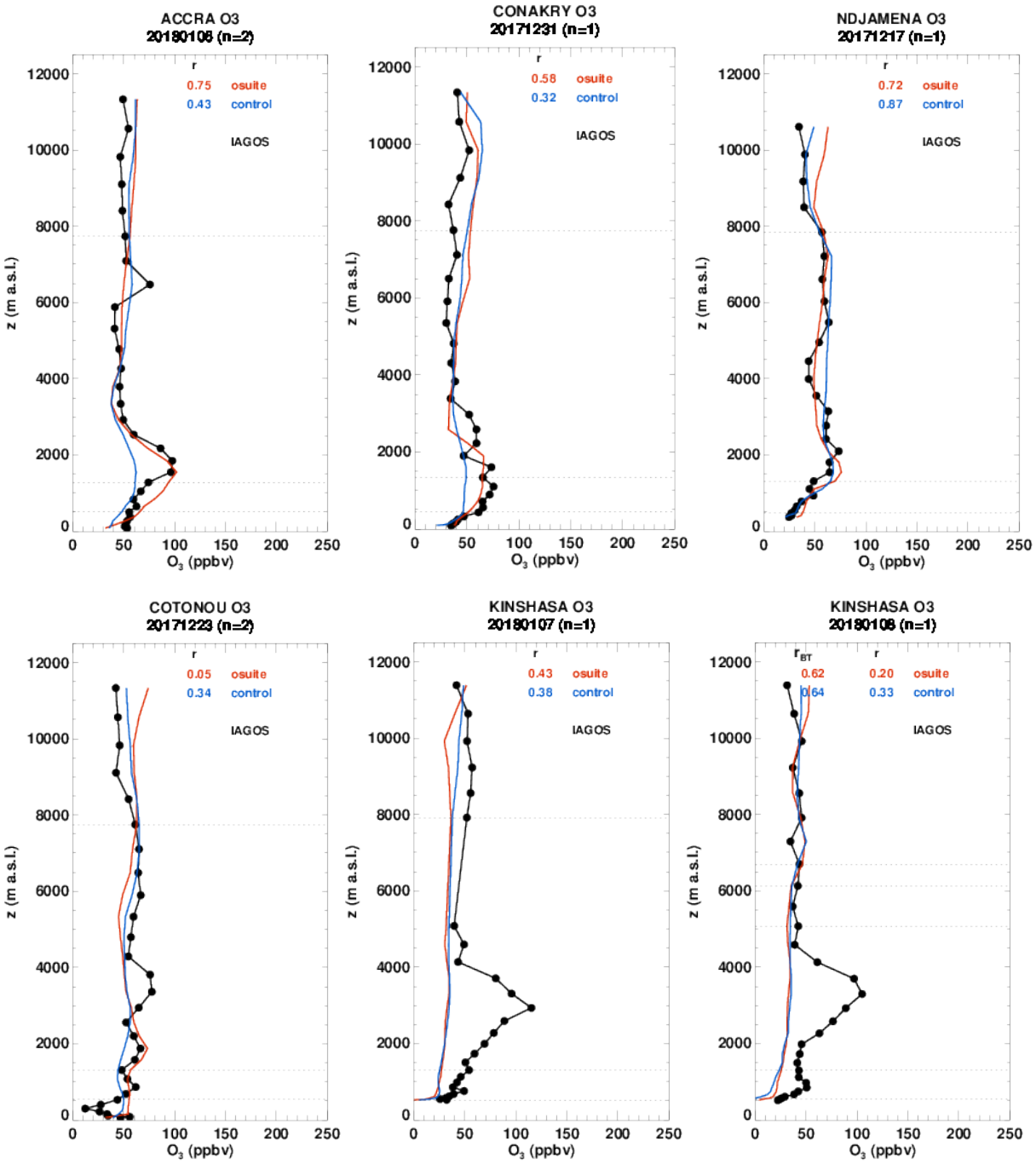


Figure 3.2.4. Selection of daily profiles for ozone from IAGOS (black) and the two NRT runs (o-suite:red, control: blue) over West Africa during December 2017 – February 2018.

ozone in the upper troposphere likely due to the intrusion of stratospheric air. At Seattle (26th January 2018), the control run underestimates ozone in the UTLS, whereas the o-suite overestimates $O_3$ with slightly better results in bias. At New York on 8th January 2018 the observed tropopause is very low, this not detected by any of the models. At San Diego on 5th December 2017, the peak observed near 5000 m of about 100 ppbv is related to the transport of smoke from bush fires in Mexico.

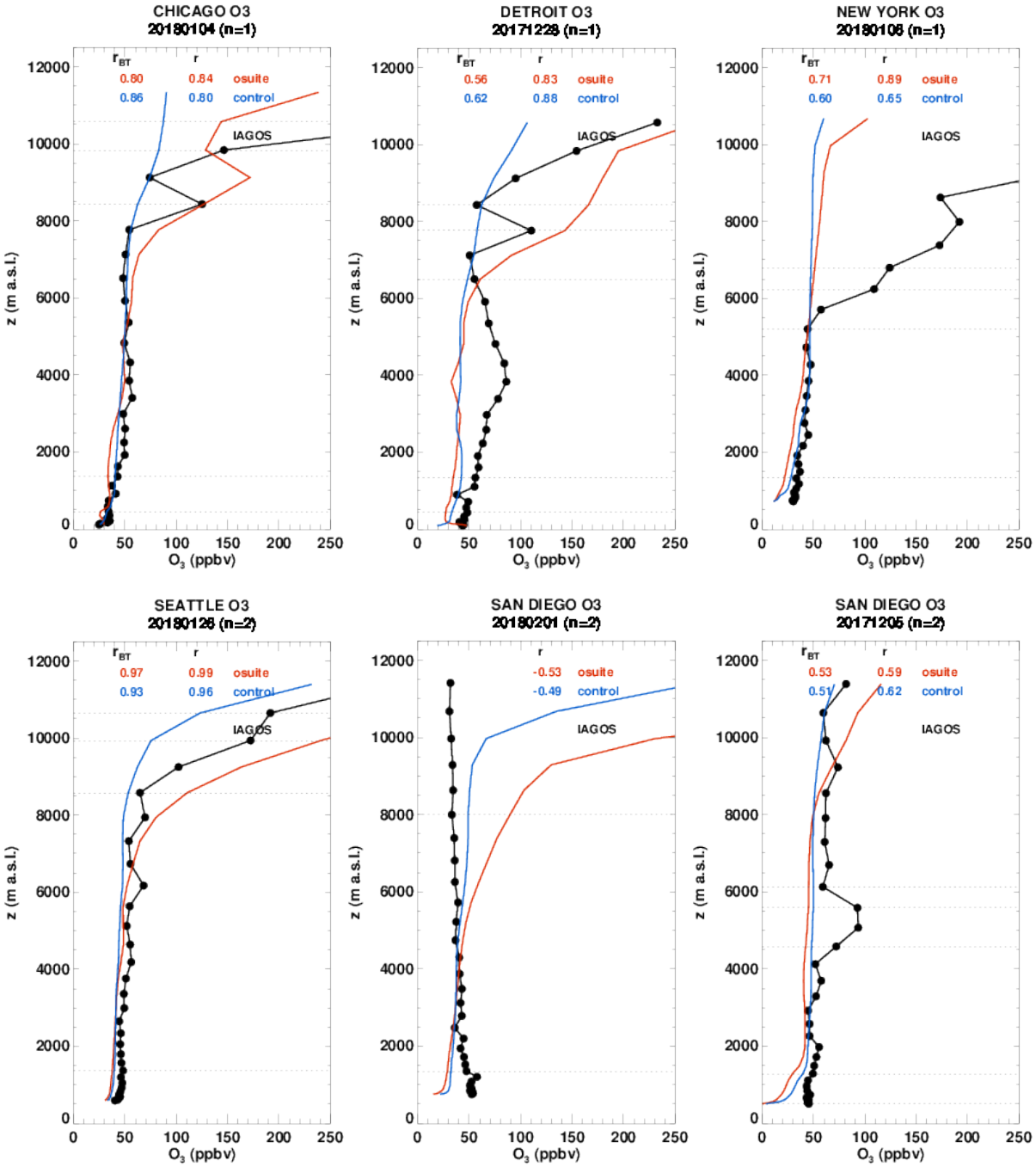


Figure 3.2.5. Selection of daily profiles for ozone from IAGOS (black) and the two NRT runs (o-suite: red, control: blue) over North America during December 2017 – February 2018.

*Asia*

Taipei, which is the capital and largest city of Taiwan, is a highly urbanized area ranked among the largest cities in the world according to population density. Air pollution in Taipei is mostly attributed to domestic (vehicle exhaust in particular) and transboundary pollution blowing from China. Smog episodes are frequent and can last several days as the city is surrounded by small mountains which prevent the dispersion of pollutants. Taipei is often visited during December 2017 – February 2018

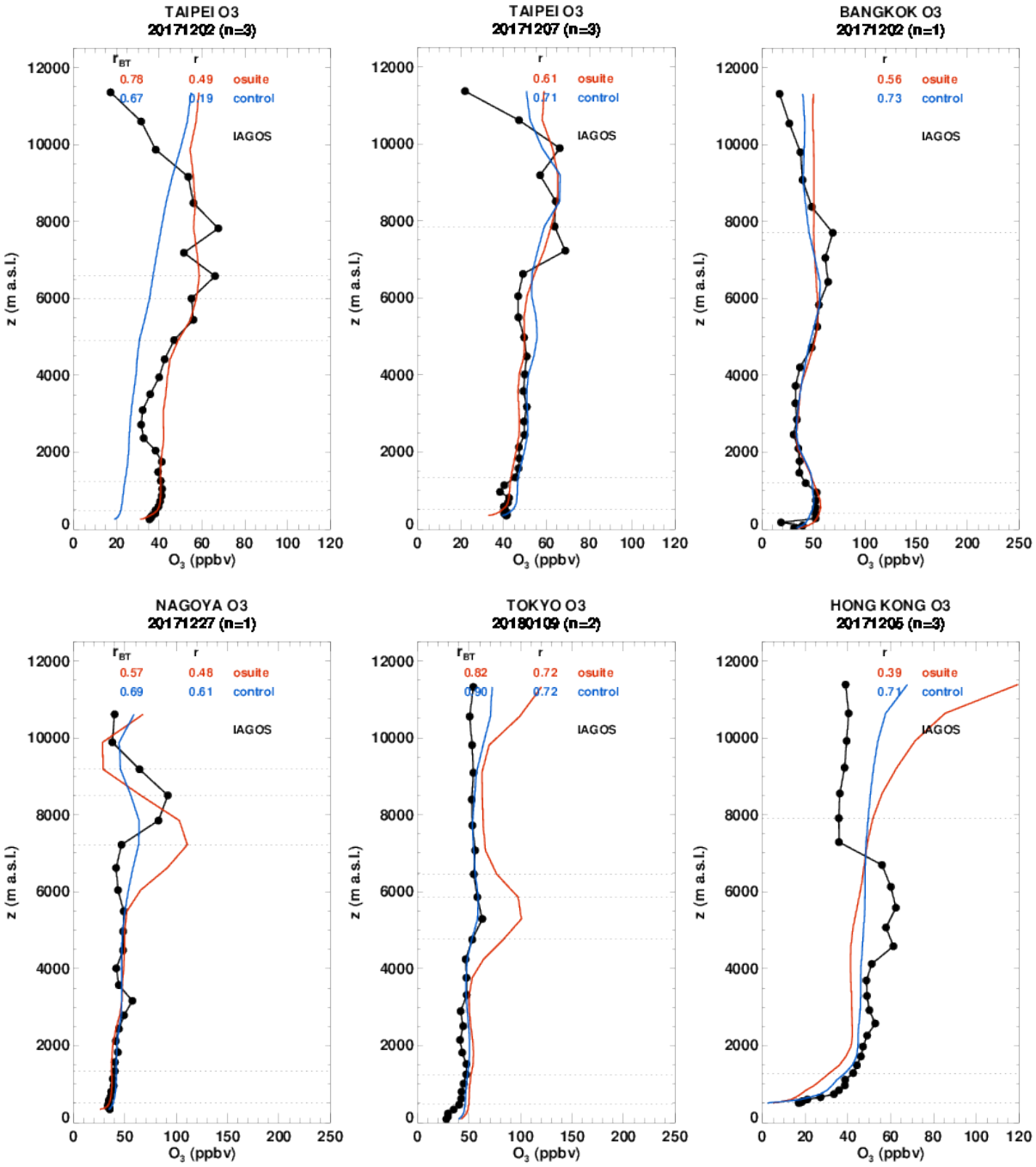


Figure 3.2.6 Selection of daily profiles for ozone from IAGOS (black) and the two NRT runs (o-suite:red, control: blue) over Northeastern Asia during December 2017 – February 2018.

(Fig. 3.2.1). The profiles at Taipei (Fig. 3.2.6) presents a wide ozone anomaly between 4000 m and 10 000 m on 2nd December, and between 7000 m and 10500 m on 7th December, with values reaching about 70 ppbv. These feature likely results from the transport of polluted air from China exported from the continent to Taipei. In the first case, the o-suite performs much better than the control run, whereas in the second case both models behave similarly showing good results. There are also a few profiles at other locations in Asia, Hong Kong, Tailandia (Bangkok) and in Japan (Nagoya, Tokyo). The profiles in Fig. 3.2.6 at these airports exhibit increases and also sometimes

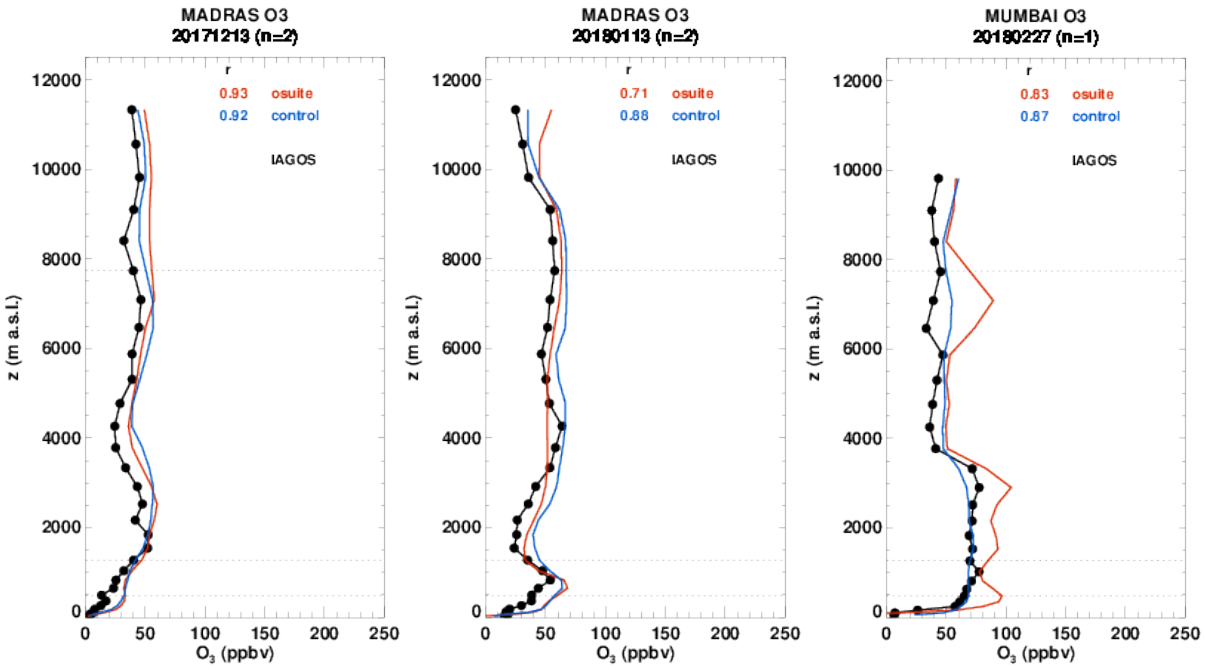


Figure 3.2.7. Selection of daily profiles for ozone from IAGOS (black) and the two NRT runs (o-suite: red, control: blue) over India during December 2017 – February 2018.

strong peaks in the upper troposphere (see at Nagoya) corresponding to the transport of air pollutants generated on the Chinese continent. The pollution plumes are well detected by the os-uite in Nagoya and Tokyo at an altitude close to that of the observations, but the o-suite overestimates the magnitude of these plumes. These events of pollution transport are also detected by the control run, but the strongest events are underestimated. In the profile at Hong Kong on 5th December 2017, between 4000 m and 6000 m ozone values are of about 60 ppbv. In this example, both the o-suite and the control do not reproduce this feature.

*India*

A few profiles are available at Indian airports. In Fig. 3.2.7 three profiles are presented: at Madras on 13th December 2017 and 13th January 2018, and at Mumbai on 27th February 2018. At Madras, the shape of these profiles present two maxima of ozone, one in the boundary layer and another in the free troposphere. The shape and magnitude of these profiles are well reproduced by both models. At Mumbai on 27th February 2018, ozone values reach about 80 ppbv in the boundary layer and are nearly constant up to 4000 m altitude. Both the o-suite and the control run show a good correspondence with the observations, however, with better performance of the control run while the o-suite shows an overestimation of around 25%.

*Pacific*

As mentioned in SON 2017 report, the Hawaiian aircraft started monitoring operations in October 2017. The pristine environment of the Island makes Hawaii a key location for addressing air quality and climate change issues, and for the validation of models. During the period December 2017 – February 2018, the airport of Honolulu has been sampled continuously (Fig. 3.2.2). On the 2nd December (Fig. 3.2.8), the profile at Honolulu shows a slight anomaly with values reaching about 60

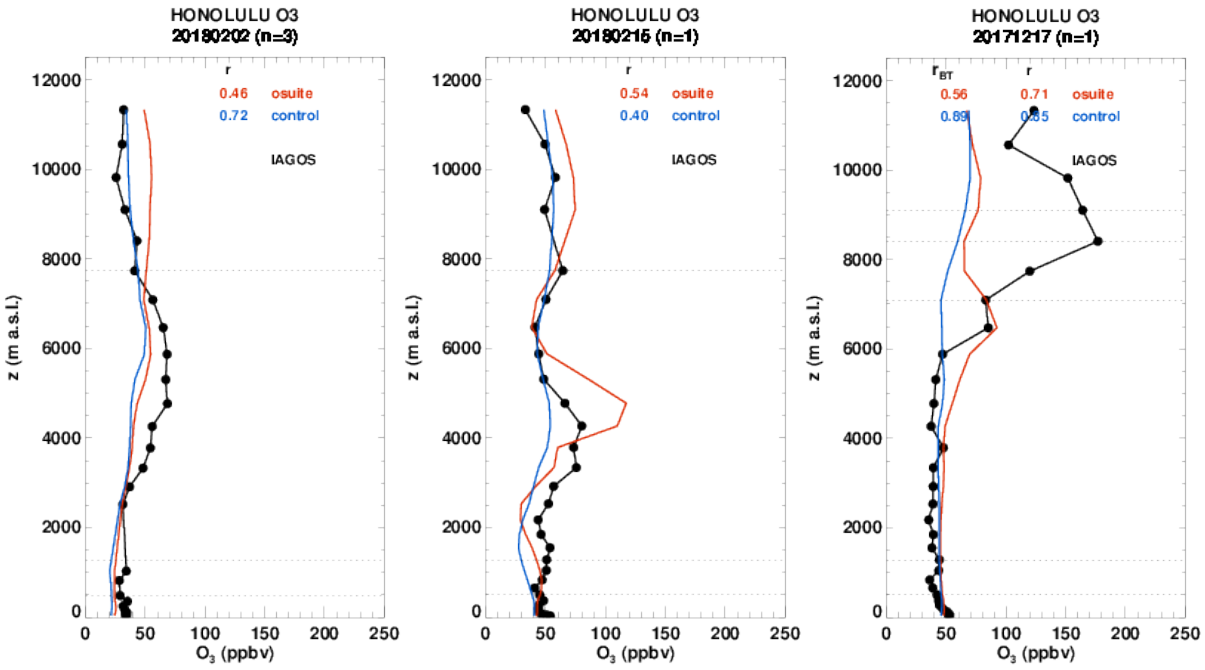


Figure 3.2.8. Selection of daily profiles for ozone from IAGOS (black) and the two NRT runs (o-suite: red, control: blue) over the Pacific during December 2017 – February 2018.

ppbv in the free troposphere between 2000 m and 8000 m. The models behave similarly and detect a very slight increase in ozone values which are underestimated as compared to observations. On 15th February a small peak of ozone is observed between 4000 m and 5000 m with 80 ppvb. This anomaly is well detected by the o-suite around the same altitude with a slightly sharper shape peaking at 120 ppbv (overestimation of 50%). The shape of the profile is well reproduced by the control run but the values are underestimated by nearly 40%. On 17th December, there is a high increase of ozone values between 6000 m and 10 000 m, with a maximum of 180 ppbv in the UTLS near 8000 m. The o-suite exhibits an increase of ozone values at a lower altitude around 6000 m but with a largely underestimated magnitude.

## 3.3 Validation with GAW and ESRL-GMD surface observations

For the Near Real Time (NRT) validation, 14 GAW stations and 8 ESRL stations are currently delivering $O_3$ surface concentrations in NRT, and the data are compared to model results. In the following, a seasonal evaluation of model performance for the 2 NRT runs (o-suite and control) has been carried out for the period from June to August 2017. The latest validation results based on GAW stations can be found on the CAMS website, http://www.copernicus-atmosphere.eu/d/services/gac/verif/grg/gaw/, and based on ESRL on http://www.academyofathens.gr/kefak/cams/index.html.

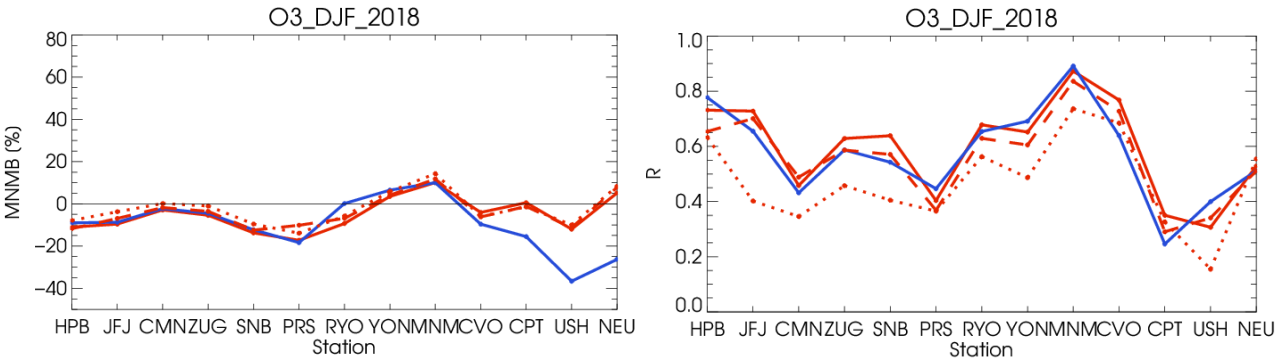


Figure 3.3.1: Modified normalized mean bias in % (left) and correlation coefficient (bottom right) of the NRT model runs compared to observational GAW data in the period December 2017 to February 2018 (o-suite: solid red, D+0: red-dashed, D+4: red-points, and control: blue).

Modified normalized mean biases in % (left, panel) and correlation coefficients (right, panel) for different forecasts days (D+2, red-dashed and D+4, red- pointed) with respect to GAW observations are shown in Figs. 3.3.1 and 3.3.2. It indicates that MNMBs for both o-suite and control run mostly remain stable till the D+4 (forecast run from 96h to 120h). Correlations between simulated and observed surface ozone values remain almost stable till D+2 (forecast run from 48h to 72h), but then drop (correlations for D+4 are lower than correlations for D+2 and D+0), see Fig. 3.3.1 and 3.3.2, right graph).

A comparison of the seasonal-mean MNMB over Europe (Fig. 3.3.3) from December 2012 to present shows that the MNMB over European GAW stations is minimal during the winter season, and tends to increase in other months. Also on average the MNMB for the o-suite shows a slight improvement over the years, while it remains higher, and more variable for the consecutive control runs. Temporal correlation is consistently better for control than for the o-suite.

Results are summarized in Figs 3.3.1 and 3.3.3.

Looking at different regions, for European stations (HPB, JFJ, ZUG, SNB, CMN, PRS), observed $O_3$ surface mixing ratios are slightly underestimated by both model runs. MNMBs are between -2 and -18%, see Fig. 3.3.1. Correlations for the European stations are between 0.40 and 0.73 for the o-suite and between 0.43 and 0.77 for the control run, see Fig. 3.3.1.

Over Arctic stations (EUK, BRW), both runs overestimate surface ozone values at Point Barrow station ($MNMB_{control}$≈25%, $MNMB_{o\text{-}suite}$≈15%) while at Eureka (EUK) both runs underestimate it ($MNMB_{control}$≈-5%, $MNMB_{o\text{-}suite}$≈-20%). Correlations between simulated and observed surface ozone are fair for the o-suite (r≈0.20 at EUK and r≈0.25 at BRW) and higher for the control run (r≈0.3 at EUK and r≈0.50 at BRW)

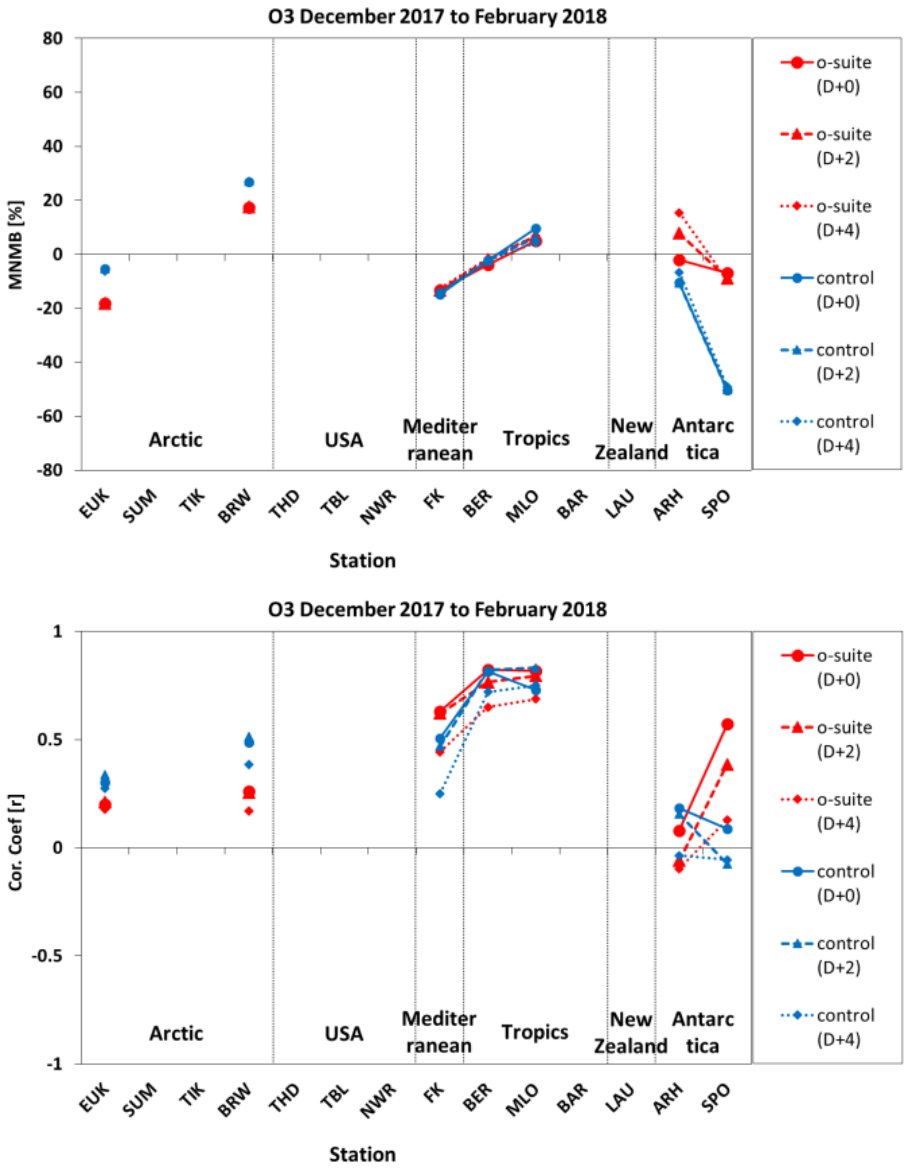


Figure 3.3.2: Modified normalized mean bias in % (left) and correlation coefficient (right) of the NRT forecast runs compared to observational ESRL data in the period December 2017 to February 2018. Circles correspond to D+0, triangles to D+2 and rhombs to D+4 metrics respectively. We note that data were not available yet for the US and New Zealand for this semester.

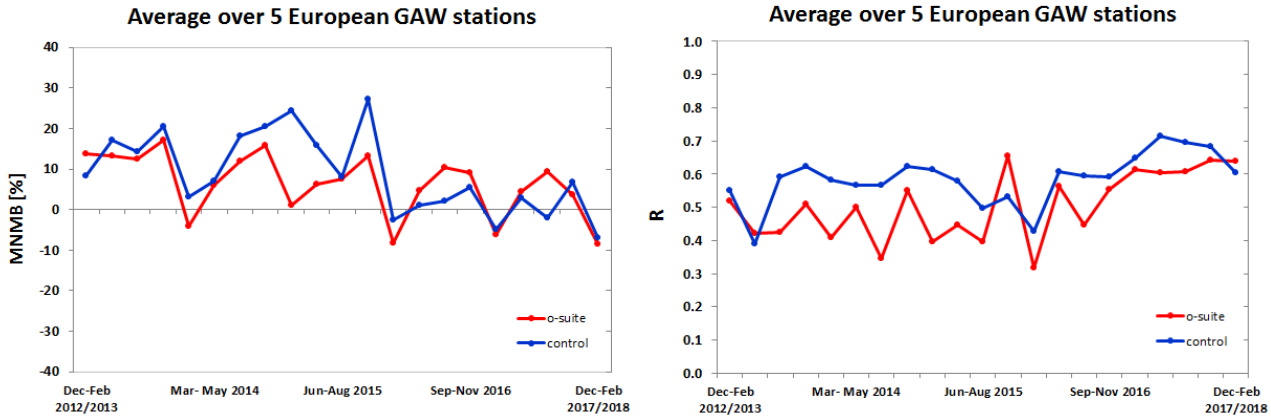


Figure 3.3.3: Long term (Dec. 2012 – February 2018) evolution of seasonal mean MNMB (left) and correlation (right), as averaged over 5 GAW stations in Europe, for o-suite (red) and control (blue).

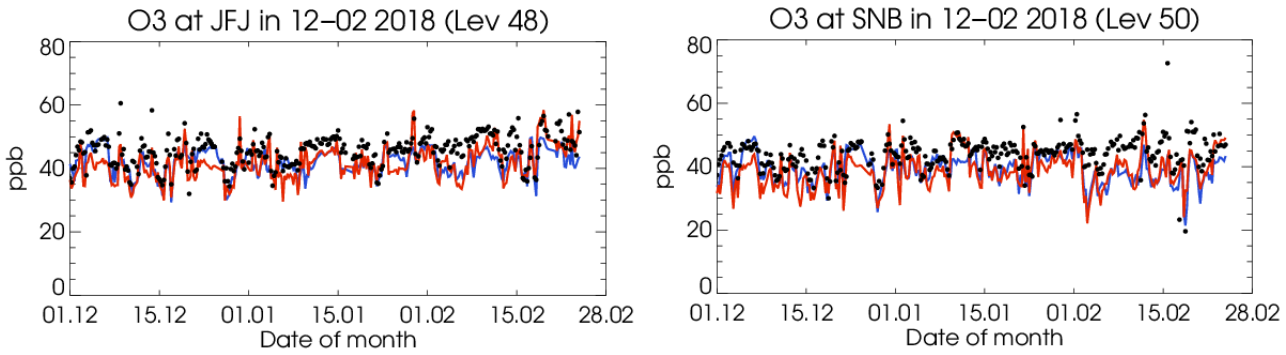


Figure 3.3.4: Time series for the o-suite (red) and control (blue) compared to GAW observations at Jungfraujoch (39.03°N, 141.8°E) and Sonnblick (47.05°N, 12.96°E)

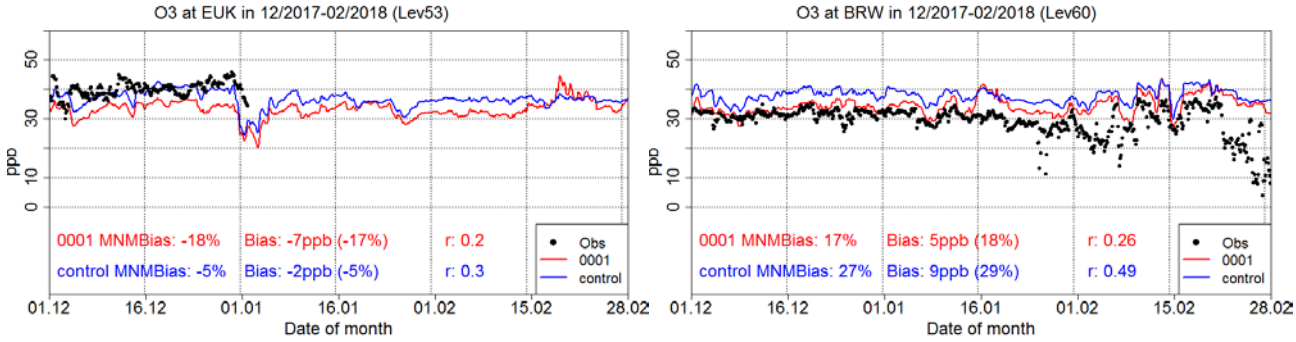


Figure 3.3.5: Time series for the o-suite (red) and control (blue) compared to ESRL observations at Eureka, Canda station (80.05°N, 86.42°W, left) and Point Barrow, Alaska station (40.12°N, 105.24°W, right).

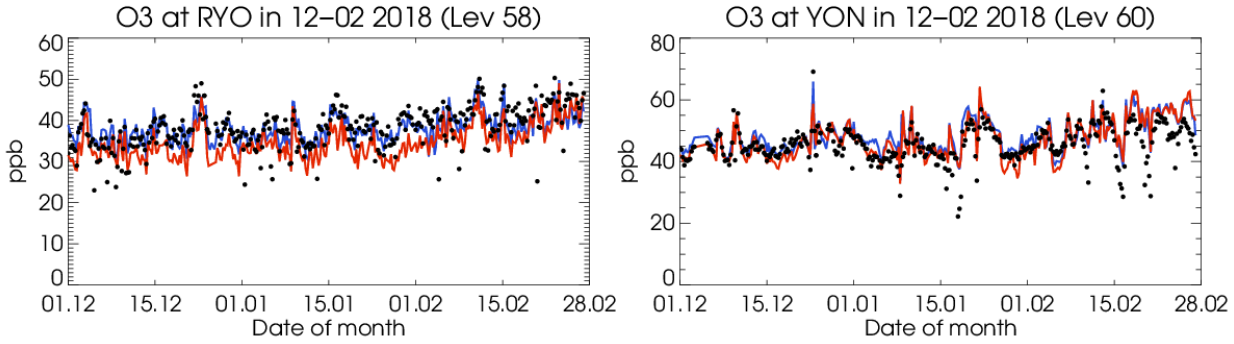


Figure 3.3.6: Time series for the o-suite (red) and control (blue) compared to GAW observations at Ryori (39.03°N, 141.82°E) and Yonagunijima (24.47°N, 123.02°E).

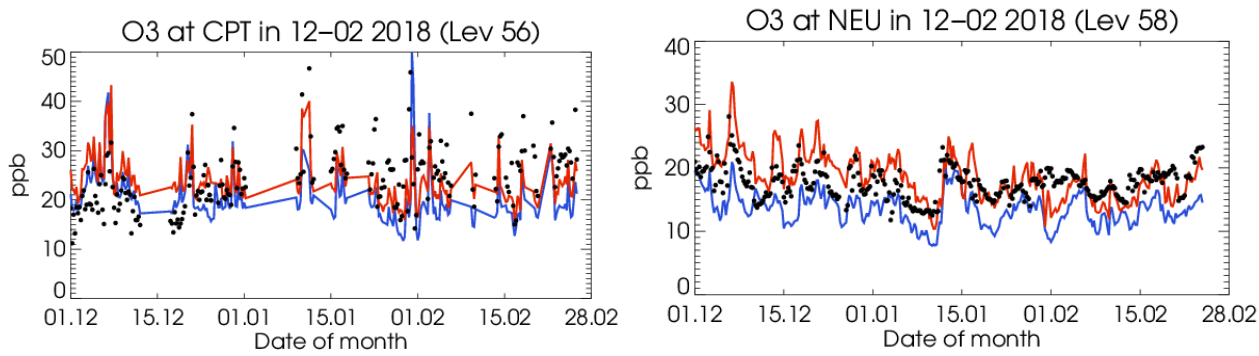


Figure 3.3.7: Time series for the o-suite (red) and control (blue) compared to GAW observations (black dots) at Cape Point (34.55°S, 18.48°W) and GAW observations at Neumayer (70.65°S, 8.25°W).

For stations located in Asia (RYO, YON, MNM) both runs show very accurate results with MNMBs within ± 10%, see Fig 3.3.6. Correlation coefficients range between 0.65 and 0.89.

Both runs reproduce well surface ozone mean values at Bermuda (BER) and overestimate observed ozone slightly by 5% at Mauna Loa (MLO) station in the Tropics. Correlations between simulated and observed surface ozone are high for both the o-suite and the control run over Bermuda and Mauna Loa stations (r>0.7)

Thanks to the data assimilation, $O_3$ mixing ratios of the southern hemispheric stations (CPT, USH) are accurately reproduced with MNMBs between 5 and -12%. Correlation coefficients range around 0.30 and 0.52. The control run shows a strong negative offset between -15% and -36%, see Fig 3.3.7.

Finally for South Pole station in Antarctica (SPO) and Neumayer station (NEU), the data assimilation corrects the negative offset in the control run: MNMBS o-suite = -5% (SPO), 5% (NEU), MNMBs control: -50% (SPO), -26% (NEU), see Fig 3.3.7 (right panel). At Arrival Heights station (ARH) the o-suite overestimates surface ozone values by 10% while the control run underestimates it by -3%. Correlations between simulated and observed surface ozone are weak for both runs at ARH station (r≈0.0), see Fig. 3.3.8. Over SPO the o-suite reproduces better than the control run the surface ozone variability ($r_{o\text{-}suite}$≈0.6, $r_{control}$≈0.1).

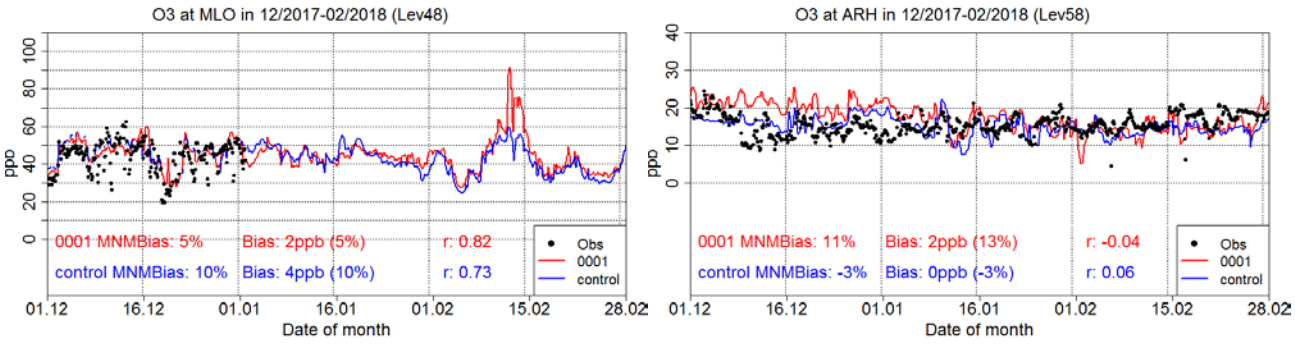


Figure 3.3.8: Time series for the o-suite (red) and control (blue) compared to ESRL observations (black dots) at Mauna Loa, Hawaii USA station (19.54°N, 24.42°W) and at Arrival Heights, Antarctica station (77.80°S, 13.22°W).

## 3.4 Validation with AirBase observations in Mediterranean

The surface ozone validation analysis over the Mediterranean is based on an evaluation against station observations from the Airbase Network (http://acm.eionet.europa.eu/databases/airbase/). In addition, 2 stations from the Department of Labour Inspection - Ministry of Labour and Social Insurance, of Cyprus (http://www.airquality.dli.mlsi.gov.cy/) are used in the validation analysis. For the validation analysis, stations in the Mediterranean located within about 100 km from the shoreline of the Mediterranean shore are used. Table 3.4.1 shows the names, coordinates, elevation and the MNMBs and correlations obtained with the 2 forecast runs (o-suite and control). It indicates that the variance explained by each station of both the o-suite and control is high and correlations are highly significant over Western, Central and Eastern Mediterranean, with the exception of Ak-Pardines station in Spain. It should be noted that the control run mostly reproduces the mean concentrations of surface ozone slightly better while the o-suite slightly better reproduces the surface ozone day to day variability (see Table 3.4.1).

In terms of biases, both runs mostly underestimate surface ozone values over the Mediterranean shore of Spain (MNMBs between -35% and 10% depending on the stations). Over the stations Plan Aups/Ste Baume in France and Gharb in Malta both the o-suite and the control run underestimate surface ozone concentrations by -5% and -15% respectively. Finally over Oros Troodos and Agia Marina stations in Cyprus both models accurately reproduce surface ozone mean concentrations (MNMBs≈0%; see also 3.4.1, lower graphs).

The spatial distribution of MNMBs and the correlation coefficients of the o-suite over the Mediterranean are shown in 3.1.4.2, where correlations over the entire Mediterranean from Gibraltar to Cyprus are highly significant. On the other hand it clearly shows the better o-suite performance over the Eastern Mediterranean compared to the Mediterranean shore of Spain and Central Mediterranean in terms of biases.

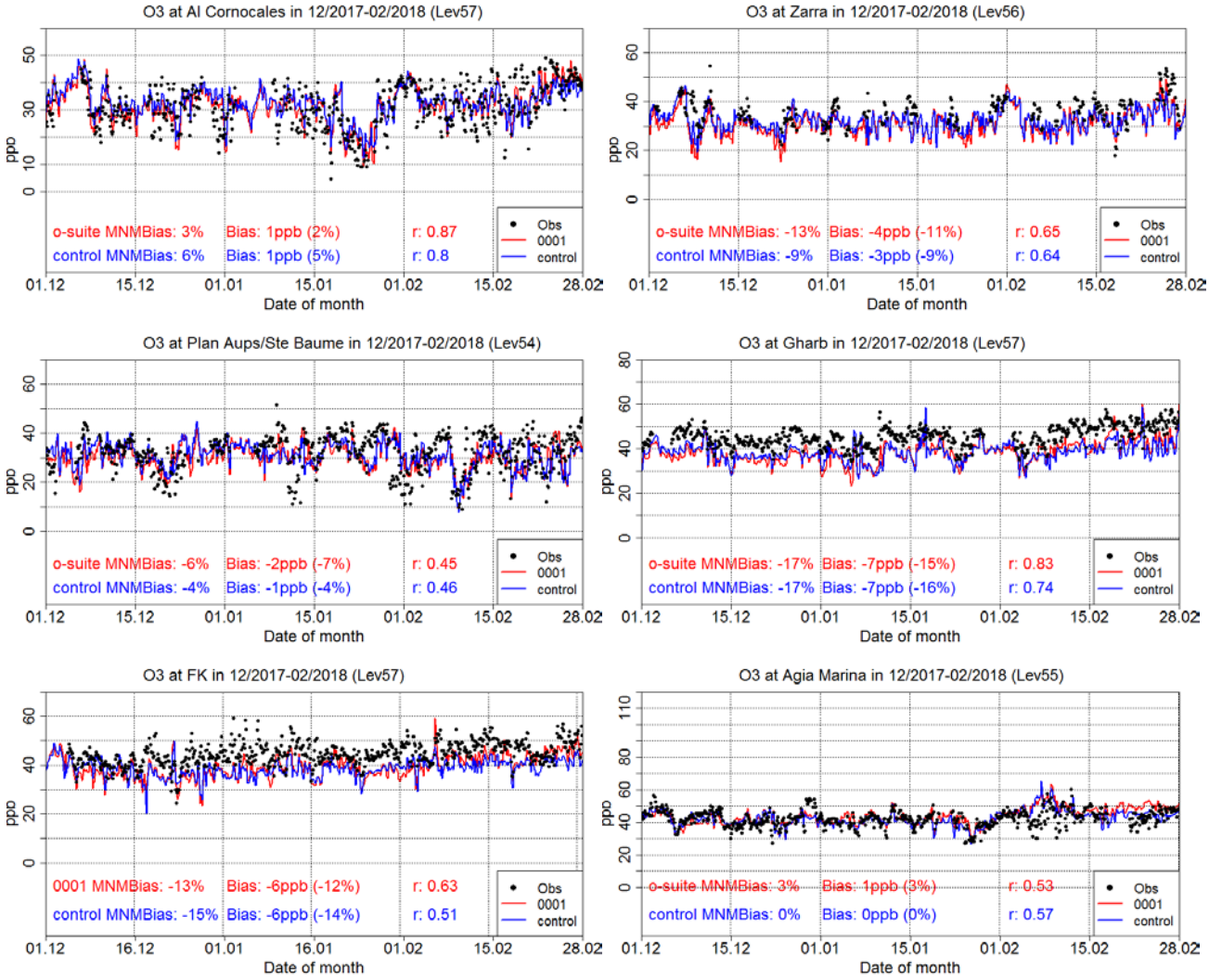


Figure 3.4.1: Time series for the o-suite (red) and Control (blue) compared to Airbase observations at Al Cornocales, Spain station (36.23°N, 5.66 °W, top left), at Zarra, Spain station (39.08°N, 1.10°W, top right), at Plan Aups/Ste Baume, France station (43.34°N, 5.73°E, center left), at Gharb, Malta station (36.07°N, 14.20°E, center right), at Finokalia, Crete/Greece station (35.32°N, 35.67°E, low right) and compared to observations provided by the Department of Labour Inspection - Ministry of Labour and Social Insurance of Cyprus, at Agia Marina, Cyprus station (35.04°N, 33.06 °E, low right).

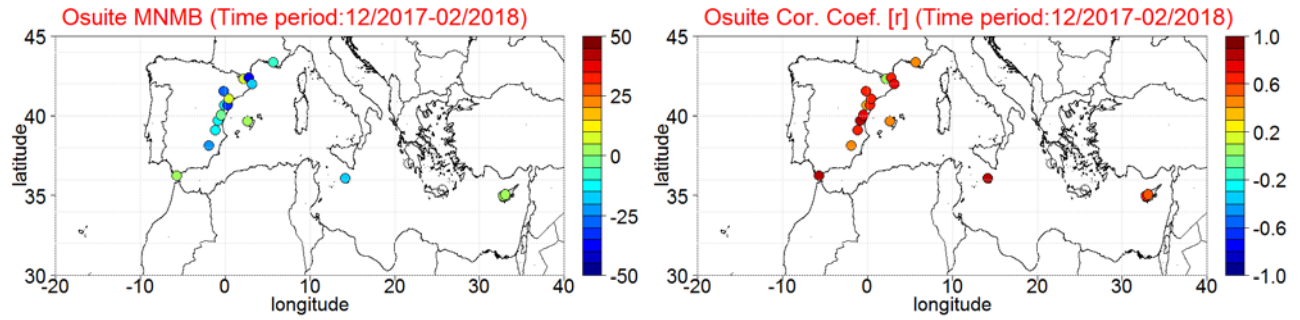


Figure 3.4.2 Spatial distribution of MNMB in % (left) and correlation coefficient (right) of the o-suite run compared to observational data during the period from 1 December 2017 to 28 February 2018.

Table 3.4.1: Coordinates, elevation, corresponding model level (level 60 is the surface level), as well as validation scores (MNMBs and correlations for the period DJF 2017-2018) obtained with the 2 forecast runs (o-suite and control), for each one of the selected Mediterranean stations. MNMBs and correlations with blue denote stations where control run performs better while with red are denoted stations where o-suite performs better.

| | | | | | | Distance from the | MNMB | | Cor. Coef | |
|---|---|---|---|---|---|---|---|---|---|---|
| Station Name | Stat_ID | Lon | Lat | Alt (m) | Level | shore (km) | o-suite | control | o-suite | control |
| Al Cornocales | ES1648A | -5.66 | 36.23 | 189 | 57 | 16 | 2.7 | 5.8 | 0.87 | 0.80 |
| Caravaka | ES1882A | -1.87 | 38.12 | 1 | 60 | 73 | -22.7 | -19.9 | 0.50 | 0.43 |
| Zarra | ES0012R | -1.10 | 39.08 | 885 | 56 | 70 | -12.6 | -9.4 | 0.65 | 0.64 |
| VIillar Del Arzobispo | ES1671A | -0.83 | 39.71 | 430 | 60 | 48 | -11.3 | -6.8 | 0.83 | 0.79 |
| Cirat | ES1689A | -0.47 | 40.05 | 466 | 60 | 37 | -3.4 | 1.2 | 0.80 | 0.79 |
| Bujaraloz | ES1400A | -0.15 | 41.51 | 327 | 60 | 60 | -27.1 | -21.3 | 0.70 | 0.69 |
| Morella | ES1441A | -0.09 | 40.64 | 1150 | 53 | 51 | -10.8 | -7.5 | 0.40 | 0.22 |
| Bc-La Senia | ES1754A | 0.29 | 40.64 | 428 | 59 | 21 | -31.0 | -26.3 | 0.67 | 0.65 |
| Ay-Gandesa | ES1379A | 0.44 | 41.06 | 368 | 58 | 15 | 7.3 | 12.0 | 0.68 | 0.58 |
| Ak-Pardines | ES1310A | 2.21 | 42.31 | 1226 | 57 | 81 | 6.8 | 8.7 | 0.10 | 0.05 |
| Hospital Joan March | ES1827A | 2.69 | 39.68 | 172 | 57 | 3 | 0.2 | 3.2 | 0.45 | 0.44 |
| Al-Agullana | ES1201A | 2.84 | 42.39 | 214 | 60 | 25 | -38.2 | -33.0 | 0.66 | 0.64 |
| Av-Begur | ES1311A | 3.21 | 41.96 | 200 | 56 | 9 | -15.6 | -10.6 | 0.75 | 0.70 |
| Plan Aups/Ste Baume | FR03027 | 5.73 | 43.34 | 675 | 54 | 21 | -6.1 | -3.5 | 0.45 | 0.46 |
| Gharb | MT00007 | 14.20 | 36.07 | 114 | 57 | 31 | -16.8 | -17.2 | 0.83 | 0.74 |
| Aliartos | GR0001R | 23.11 | 38.37 | 110 | 59 | 18 | NA | NA | NA | NA |
| NEO | - | 21.67 | 37.00 | 50 | 60 | 2 | NA | NA | NA | NA |
| Finokalia | GR0002R | 25.67 | 35.32 | 250 | 57 | 4 | NA | NA | NA | NA |
| Oros Troodos | - | 32.86 | 34.95 | 1819 | 49 | 11 | 1.8 | 1.2 | 0.68 | 0.53 |
| Agia Marina | CY0002R | 33.06 | 35.04 | 532 | 55 | 14 | 2.9 | 0.4 | 0.53 | 0.57 |

## 3.5 Validation with IASOA surface observations

Model results were compared to $O_3$ observations from the Villum Research Station, Station Nord in north Greenland (81.6°N 16.7°W), Alert Nunavut, Canada (82.5°N 62.5°W), Eureka, Nunavut, Canada (80.1°N 86.4°W), Zeppelin Mountain, Svalbard (78.9°N 11.9°E), and Tiksi, Russia (71.6°N 128.9°E) from the IASOA network, Fig. 3.5.1.

The data from Svalbard and VRS are covering the period from December 2014 to February 2018. Data from Eureka covers the period August 2016 – December 2017, data from Alert covers the period January 2016 – December 2017 and data from Tiksi covers the period September 2016 – February 2018. Ozone depletion events in March – June in 2015, 2016 and 2017 are not captured by the model simulations during spring at any of the sites. These events are related to halogen chemistry reactions that are not represented in the model simulations. The simulations are on average in good agreement with the observations apart from the spring depletion events.

For the period December 2017 – February 2018 the measurements are not quality controlled. The model simulations underestimate the measured $O_3$ concentrations at all sites but one, resulting in a negative bias of -15% to -20% for the o-suite and -4% to -11% for the control run (Table 3.5.1). The measurements at Tiksi are overestimated (2% and 13%). The negative bias in the winter period is seen to be a recurring event (Fig. 3.5.1). Note that the measurements from Svalbard for June-November 2017 have been invalidated. The control run performs better than the o-suite in terms of the bias, which is lower for all sites, while the correlation is better for the o-suite for the two sites with full data coverage; r = 0.47 – 0.74 for the o-suite compared to r = 0.15 – 0.68 for the control run.

Table 3.5.1. Normalised Mean Bias (NMB) and correlation coefficient (r) of the Control and the O-suite simulations for the sites Alert, Eureka, Svalbard, Tiksi and Villum Research Station (VRS) for the period December 2017 – February 2018.

| | | NMB | R |
|---|---|---|---|
| **Alert** | o-suite | -0.15* | 0.31* |
| | control | -0.04* | 0.48* |
| **Eureka** | o-suite | -0.15* | 0.04* |
| | control | -0.04* | 0.17* |
| **Svalbard** | o-suite | -0.18 | 0.74 |
| | control | -0.10 | 0.68 |
| **Tiksi** | o-suite | 0.02** | 0.10** |
| | control | 0.13** | 0.26** |
| **VRS** | o-suite | -0.20 | 0.47 |
| | control | -0.11 | 0.15 |

*Only data for 1 month.

**Only data for ~2 months

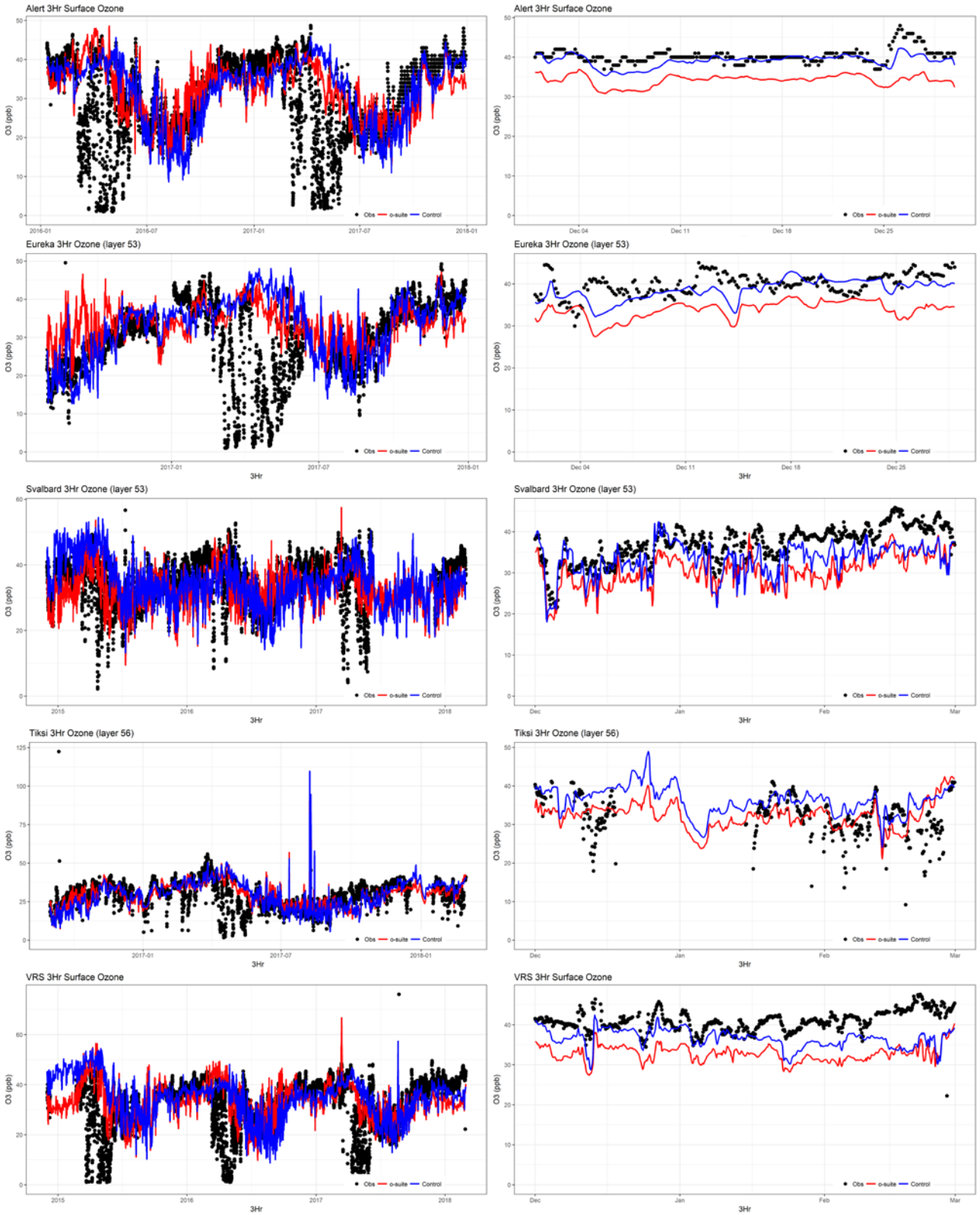


Figure 3.5.1: Time series for o-suite (red) and Control (blue) compared to observations (black dots) at Alert, Nunavut, Canada (Top row) Eureka, Nunavut, Canada (second row), Svalbard (third row), Tiksi, Russia (fourth row) and the Villum Research Station, Station Nord, Greenland (bottom row) for the full period (left) and for December-February (right).

# 4. Carbon monoxide

## 4.1 Validation with Global Atmosphere Watch (GAW) Surface Observations

For the Near-Real-Time (NRT) validation, 11 GAW stations have delivered CO surface mixing ratios in NRT and data is compared to model results as described in Douros et al (2017) and is used for CAMS model evaluation for December – February 2018. The latest validation results can be found on the CAMS website: http://www.copernicus-atmosphere.eu/d/services/gac/verif/grg/gaw/

For stations in the Northern Hemisphere, both runs mostly show slightly negative MNMBs. For the stations located in the Southern Hemisphere, the control shows a strong positive offset, which is corrected by the data assimilation for the o-suite.

For stations in Europe, and the Southern hemisphere, the MNMBs and correlation coefficients indicate that the forecast remains stable till the D+4 (forecast run from 96h to 120h).

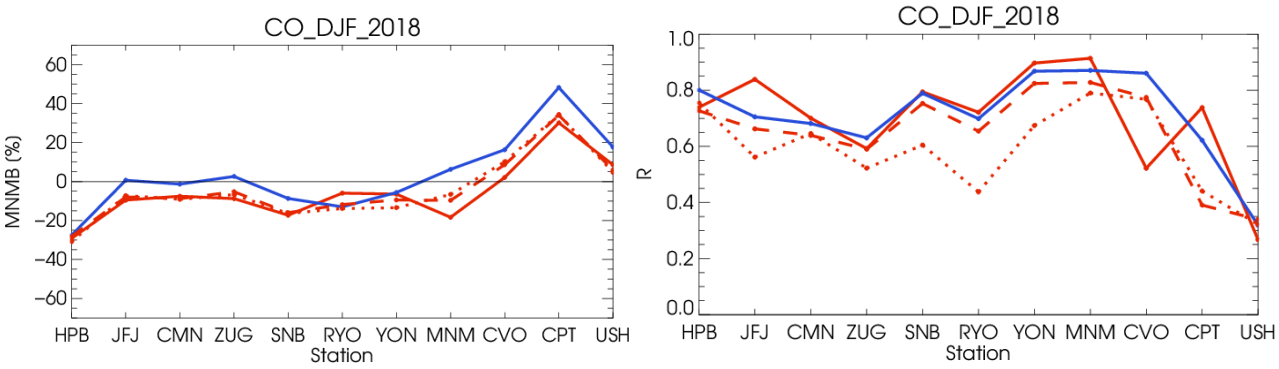


Figure 4.1.1: Modified normalized mean bias in % (left) and correlation coefficient (bottom right) of the NRT model runs compared to observational GAW data in the period December 2017 to February 2018 (o-suite: solid red, D+0: red-dashed, D+4: red-points, and control: blue).

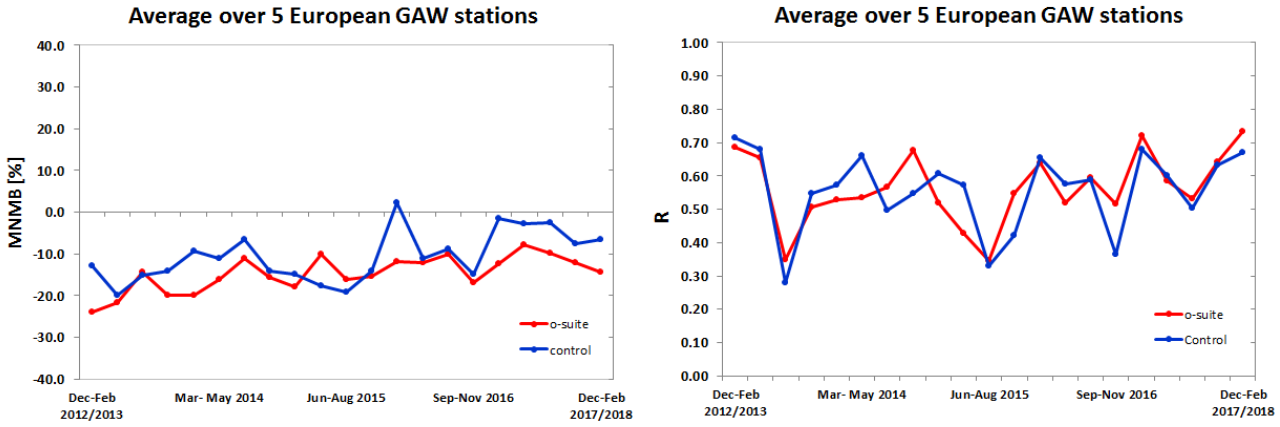


Figure 4.1.2: Long term (Dec. 2012 – February 2018) evolution of seasonal mean MNMB (left) and correlation (right), as averaged over 5 GAW stations in Europe, for o-suite (red) and control (blue).

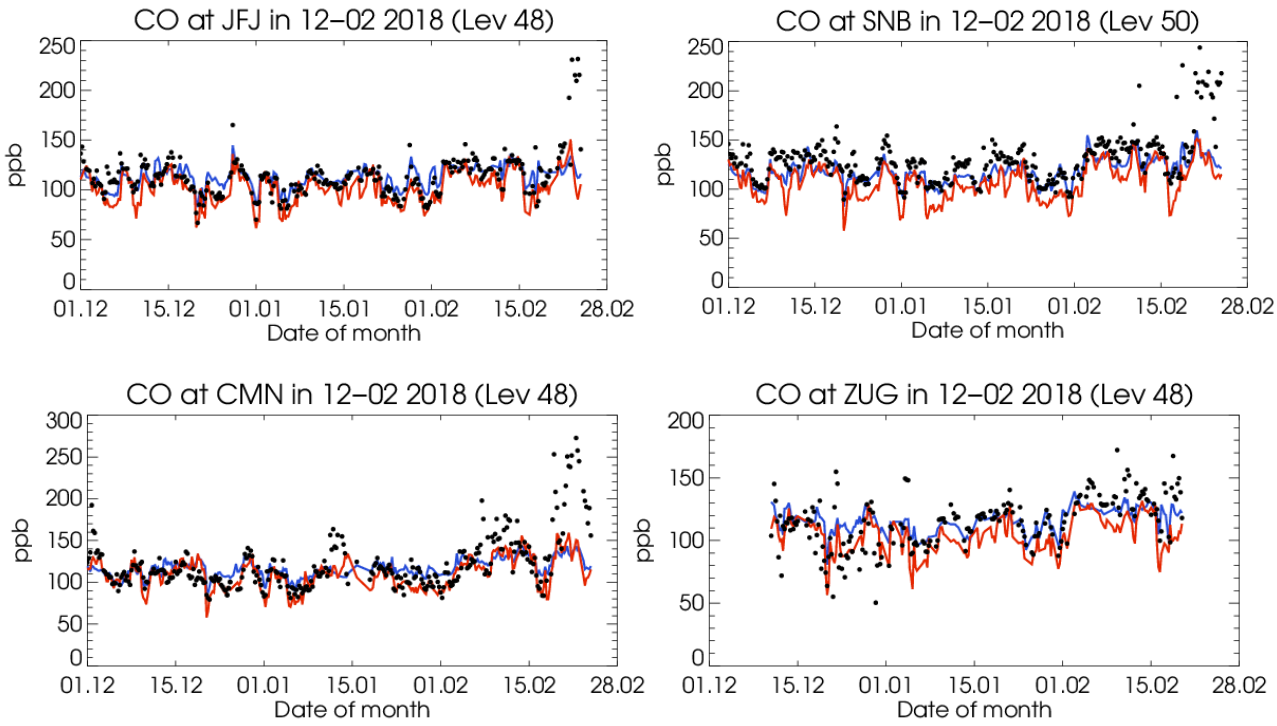


Figure 4.1.3: Time series for the o-suite (red) and control (blue) compared to GAW observations at, Jungfraujoch (46.5°N, 7.9°E), Sonnblick (47.05°N, 12.96°E), Monte Cimone (44.18°N, 10.70°E) and Zugspitze (47. 4°N, 10.9°E).

A comparison of the seasonal-mean MNMB over Europe (Fig. 4.1.2) from December 2012 to present shows a slowly improving MNMB from about -20% in 2013 to -10% for more recent periods. Temporal correlation remains relatively constant at r=0.6 on average.

For European stations, the o-suite shows an underestimation of observed CO mixing ratios, with MNMBs between -7% and -29%. The control shows higher CO mixing ratios for European stations with MNMBs between 0% and -27%. Both models did not capture an increase of CO mixing ratios caused by cold- weather induced temperature inversion by the end of February. Correlation coefficients are between 0.59 and 0.73 for the o-suite and between 0.63 and 0.80 for the control run.

For stations in Asia (RYO, YON, MNM) the o-suite and control mostly show a good correspondence with the observations with MNMBs between -6 and -18% for the o-suite and between 6% and -12% for the control run, see Fig. 4.1.5. Correlation coefficients range between 0.69 and 0.91.

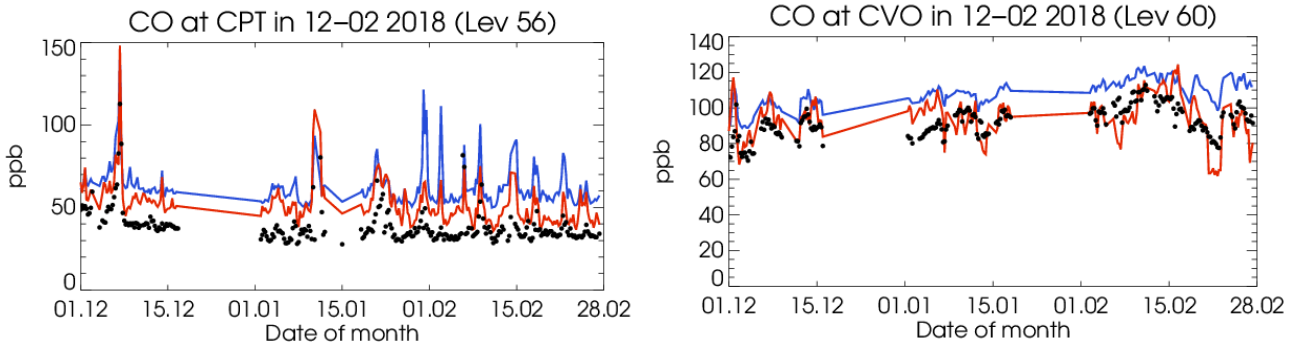


Figure 4.1.4: Time series for the o-suite (red) and control (blue) compared to GAW observations at Cape Point (34.35°S, 18.5°E) and Cape Verde (16.9°N, 24.9°W).

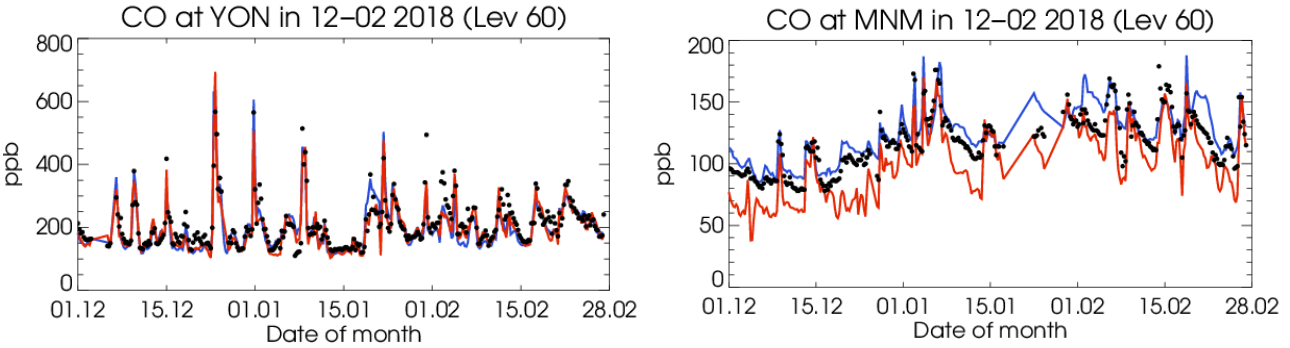


Figure 4.1.5: Time series for the o-suite (red) and control (blue) compared to GAW observations at Yonagunijima (24.47°N, 123.02°E) and Minamitorishima (24.29°N, 153.98°E).

## 4.2 Validation with IAGOS Data

The daily profiles of ozone and CO measured at airports around the world are shown on the website at http://www.iagos.fr/macc/nrt_day_profiles.php. For the period December 2017 to February 2018, data from several aircraft have been validated, as discussed in Sec. 3.2.

Figure 4.2.1 shows the time series of daily mean values in different atmospheric layers over Paris. At Paris, the models underestimate CO in both the boundary and surface layer. This behavior is more obvious in the individual profiles over Europe (Fig. 4.2.2). In the low stratosphere, the models overestimate the amount of CO, while there is good agreement between models and observations in the free and upper troposphere.

As mentioned in regional report, episodes of high CO in the surface layer are observed at the beginning of December and at the end of February (Fig. 4.2.2). On 3rd December surface mixing ratios reach more than 350 ppbv. The beginning of December has been characterized by particularly cold temperatures below seasonal which might explain the increase in local emissions. This episode is detected by the o-suite although largely underestimated with a mixing ratio at the surface being 40% lower. Regarding the control run, the episode is not detected at all and the profile is almost constant with an ozone mixing ratio of 50 ppbv.

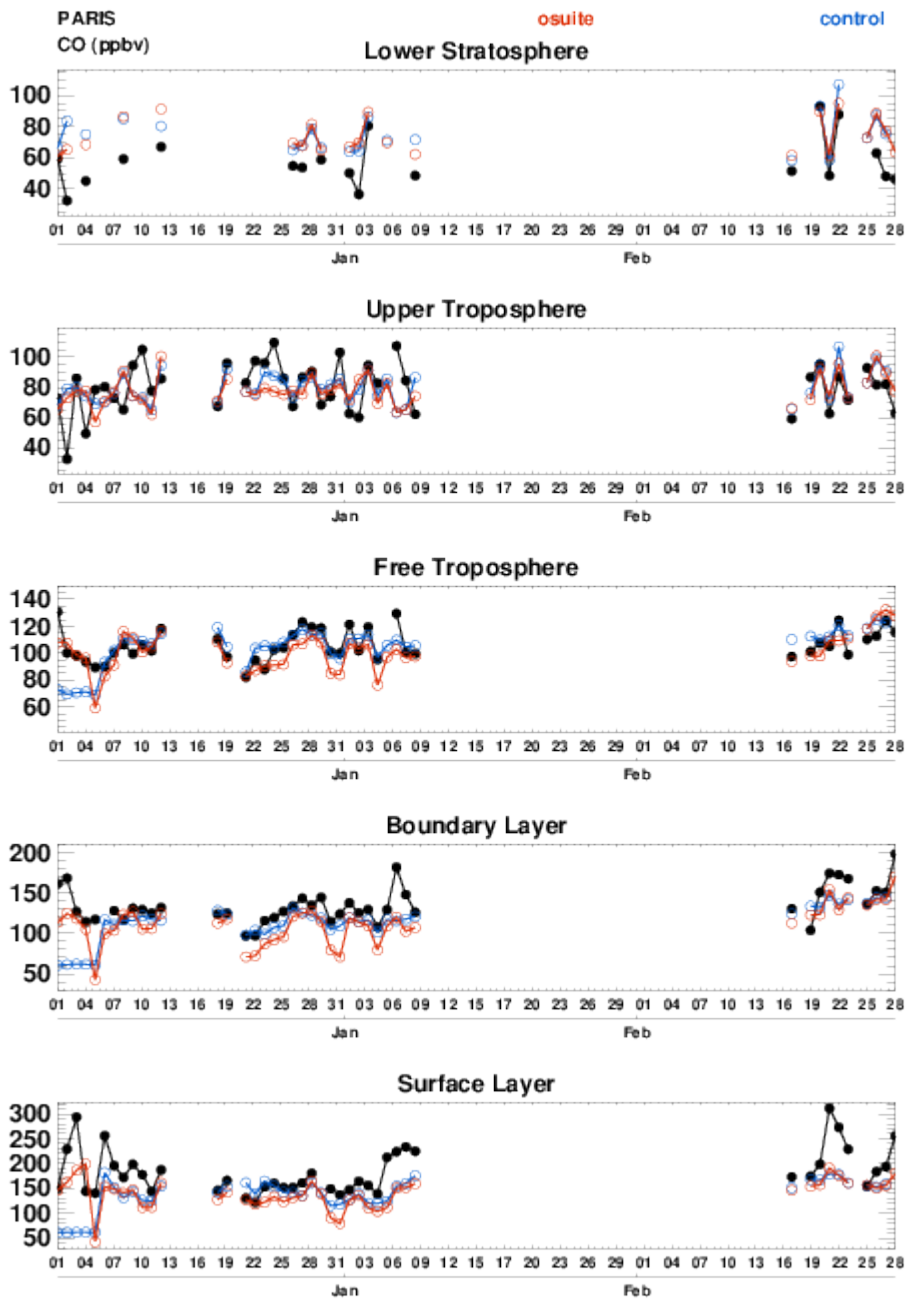


Figure 4.2.1. Time series of daily mean CO over Paris during December 2017 – February 2018 for 5 layers, Surface, Boundary layer, Free Troposphere, Upper Troposphere and Lower Stratosphere.

At the end of February cold air from Siberia has spread across Europe. On 21nd February, CO mixing ratio in the surface also reaches values of 350 ppbv. The o-suite and control run give similar results largely underestimating surface mixing ratios with a value of 200 ppbv at the surface. During the last week of February, several other profiles for CO are available at Paris, and most of them show mixing ratios beyond 200 ppbv in the surface. For these profiles, the results of the models are to those obtained for the 21th February.

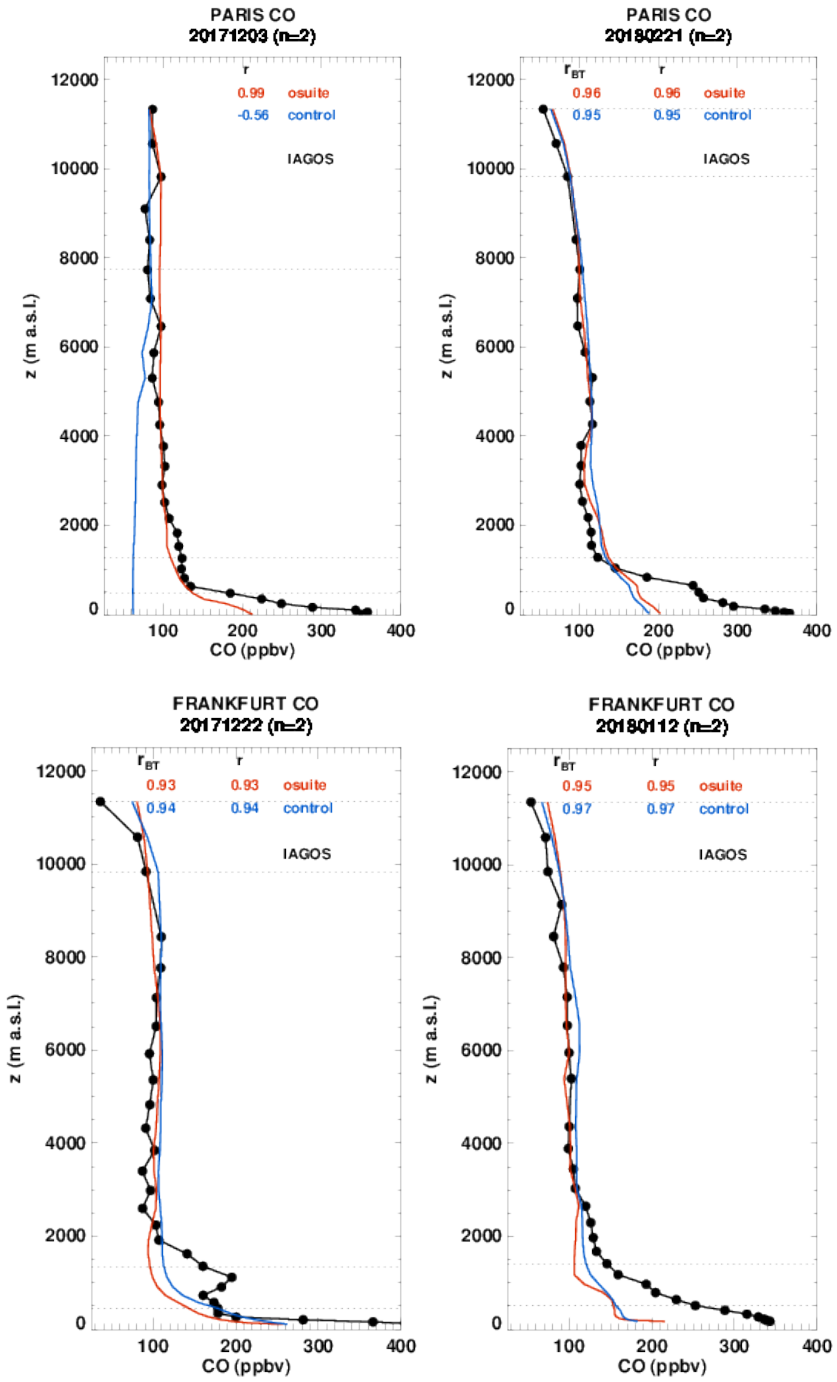


Figure 4.2.2 Selection of daily profiles for ozone from IAGOS (black) and the two NRT runs (o-suite: red, control: blue) over Europe during December 2017 – February 2018.

Figure 4.2.2 also shows a profile at Frankfurt on 22$^{th}$ December and 12$^{th}$ January where mixing ratio at the surface is 450 ppbv in the first case and 350 ppbv in the second case. The results of both models are similar with underestimation of about 40% and 50% in the surface and boundary layer respectively.

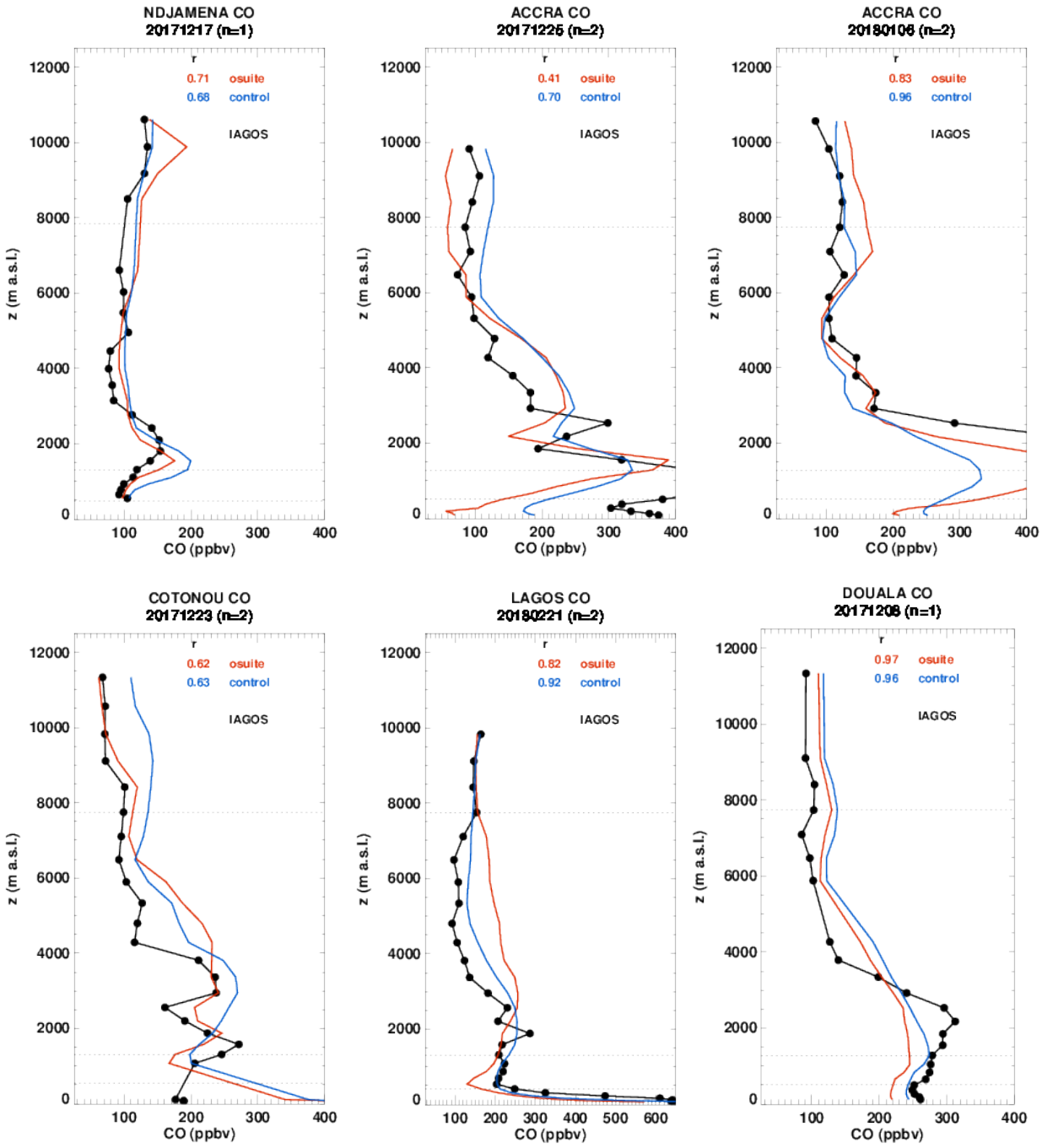


Figure 4.2.3-a Profiles of CO from IAGOS (black) and the two NRT runs over West Africa during December 2017 – February 2018.

*West Africa*

Fig. 4.2.3-a-b highlights some examples of profiles for CO over West Africa sampled by Air France aircraft during December 2017 – February 2018. The profiles presented here are for airports of N'djamena, Accra, Cotonou, Lagos, Douala and Kinshasa. These cities are affected by anthropogenic emissions from vehicles, oil industries, and from biomass burning which stretches across Africa just north of the equator from December to March and south of the equator from June to October. The

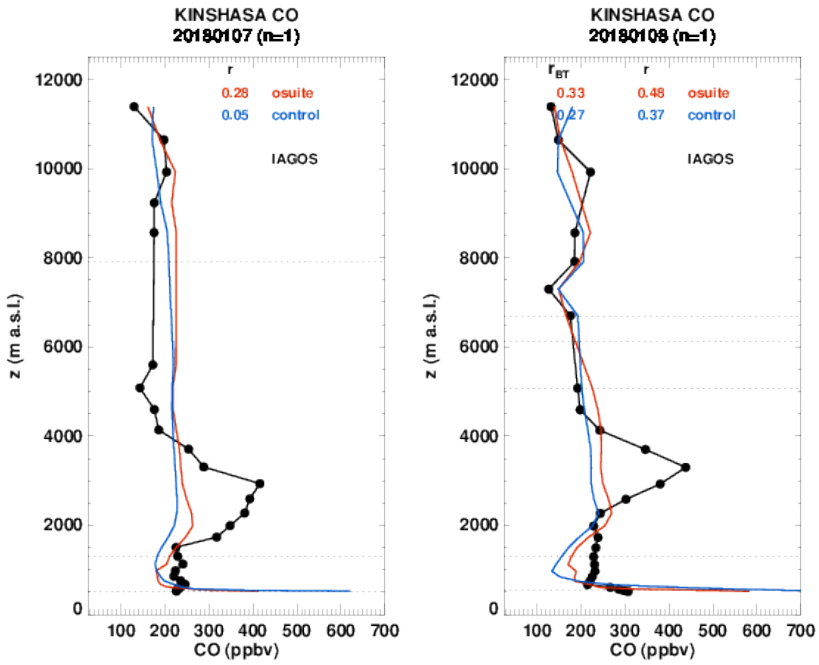


Figure 4.2.3-b Profiles of CO from IAGOS (black) and the two NRT runs over West Africa during December 2017 – February 2018.

high mixing ratios of CO in the surface and boundary layer at Accra on 25th December 2017 and 6th January 2018 might be explained by the occurrence of local fires but also by the transport of smoke from Central African Republic and South Sudan. Both models reproduce well the complex shape of the profile, but the values are underestimated in both surface and boundary layer with slightly better performance of the o-suite. Similar results are found in Cotonou on 23th December 2017 with a slightly better performance of the o-suite which detects the double peak shape of the profile as compared to the profile obtained by the control run which shows only a maximum. The profile at Douala on the 6th December can also be explained by the presence of fires on the coast nearby, as well as by the transport of smoke from the Central African Republic and South Sudan. The results of the two models are very close and the shape of the profile is similar to the observation with smaller gradients in the free troposphere. The plumes observed at Kinshasa on the 7th and 8th December 2017 peak at 400 ppbv near 3000 m altitude. These two plumes are not detected by the models, whereas the surface concentrations are largely overestimated. On 17th December 2017 a profile is available at N'djamena, showing a small peak of CO in the lower part of the free troposphere near 2000 m. For this case the models show a good performance. The peak is located at a slightly lower altitude by both models, and the results of the o-suite provide a magnitude slightly closer to the observations as the control run. The profile at Lagos on 21th February 2018 exhibits high mixing ratios at the surface attributed to local pollution and also in the lower part of the free troposphere associated with the transport of pollution from fires in the surrounding area. The plumes that are described here are correlated to high ozone values (see ozone section) when available. This is the case for the examples of N'djamena, Accra, Cotonou and Kinshasa. Regarding the results in the UTLS at all airports, they differ from profile to profile (underestimation/overestimation) and it is not always the same model which shows the best performance.

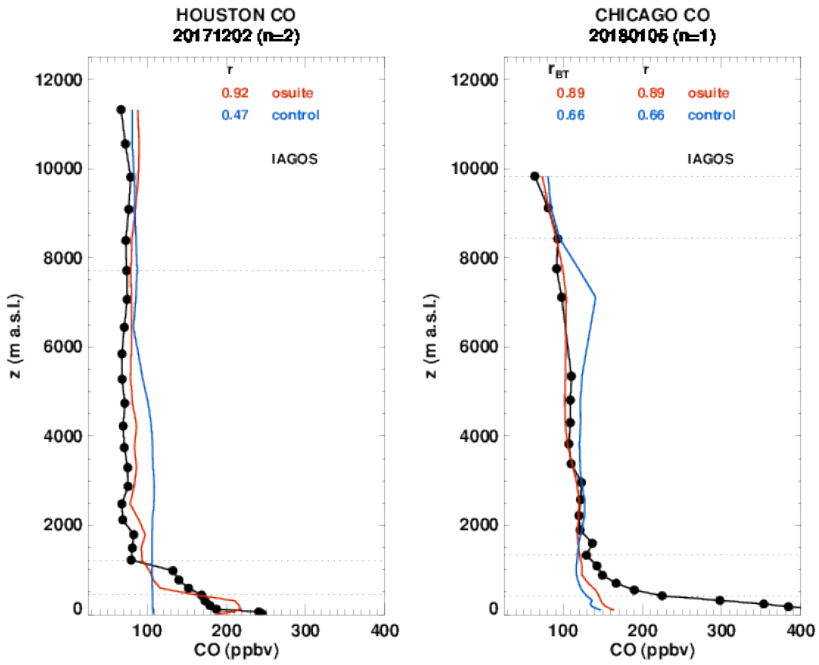


Figure 4.2.4. Profiles of CO from IAGOS (black) and the two NRT runs over North America during December 2017 – February 2018.

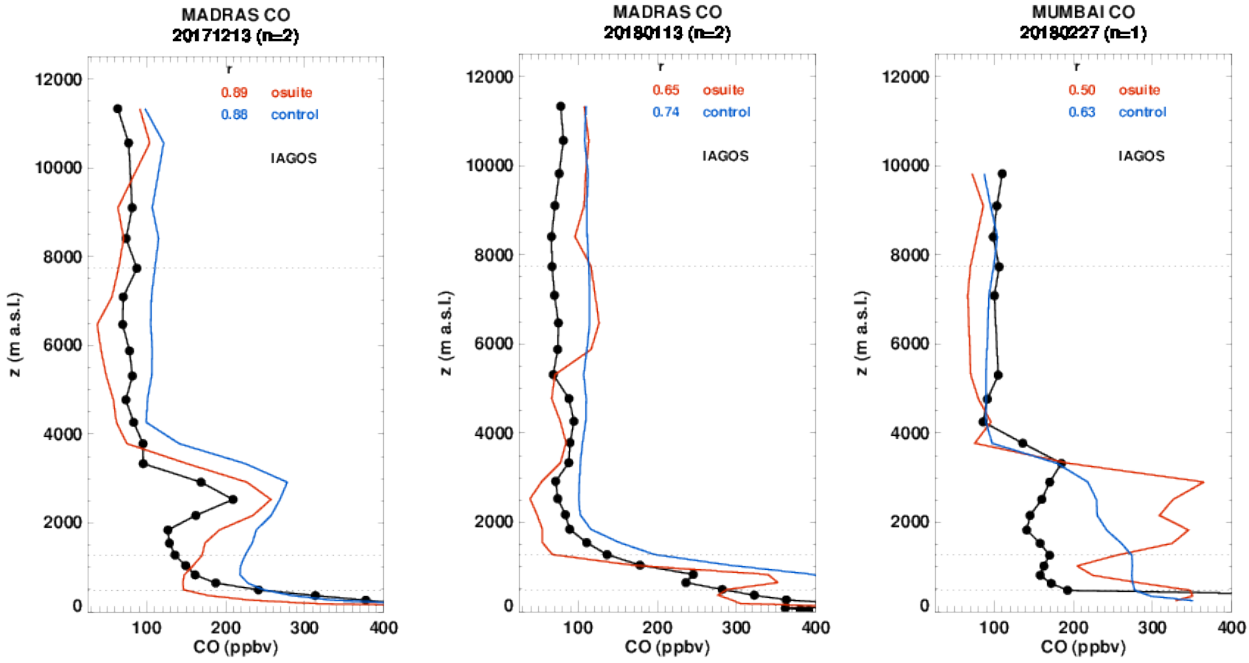


Figure 4.2.5: Profiles of CO from IAGOS (black) and the two NRT over India during December 2017 – February 2018.

*North America*

In North American airports similarly to Europe, it has been shown in previous reports that CO is usually underestimated in the surface and boundary layer by the two runs, while there is a good agreement in the free troposphere. In the profiles at Houston on the 2nd December (see Fig. 4.2.4), surface mixing ratios reached 250 ppbv and in this case the o-suite performs much better than the control run, which largely underestimates CO values in the surface and boundary layer with a nearly constant CO profile. At Chicago on the 5th January 2018, both models fail to detect the extremely high CO at the surface which overpasses 400 ppbv. The results in the UTLS are similar for both models and there is good agreement with the observations.

*India*

In addition to urban emissions, air quality is also affected by agricultural fires, in particular in northern India particular during the period April to May (pre-monsoon period) and October to November (post-monsoon). Two profiles at Madras and one at Mumbai are presented in Fig. 4.2.5. The two profiles at Madras (13th December 2017 and 13th January 2018) present high mixing ratios of CO in the surface layer reaching about 400 ppbv. On the 13th of December the profile also exhibits a peak of 200 ppbv near 2500 m. Both models show good performances in the surface layer. In the boundary layer and the free troposphere both models overestimate CO with a better performance shown by the o-suite. At Mumbai on the 27th February 2018, CO mixing ratios are nearly constant from the boundary layer up to 4000 m with a value of 150 ppbv. This feature is detected by both models, but the shape of the profile obtained by the o-suite is more similar to the observations whereas smoother gradients are obtained by the control run. However the o-suite overestimates largely the mixing ratio values in the lower part of the free troposphere, and the magnitude given by the control run agrees better with the observations. For all profiles, in the UTLS the behavior of the models can be very different (i.e. underestimation/overestimation), and the model showing better performance is not always the same one.

*Asia*

Fig. 4.2.6 highlights profiles at several locations in China, Japan and Korea. In all profiles CO underestimations are largest in the boundary layer and in the lower part of the free troposphere for both runs, which show very similar results. Sometimes the mixing ratio in the surface layer can also be largely underestimated. The best agreement is found in the upper troposphere for both models which behave similarly. It should be noted that most profiles sampled at Hong Kong airport during the reported period show the largest underestimations in the surface and boundary layer reaching 75% in the worst case. In the example of Fig.4.2.6 for Hong Kong the underestimation is of about 50%. The profile at Seoul exhibit extreme values of CO mixing ratios up to an altitude of 4000 m. Although surface values are well reproduced by the models, there is an underestimation of CO in the boundary layer and lower part of the free troposphere of around 50%.

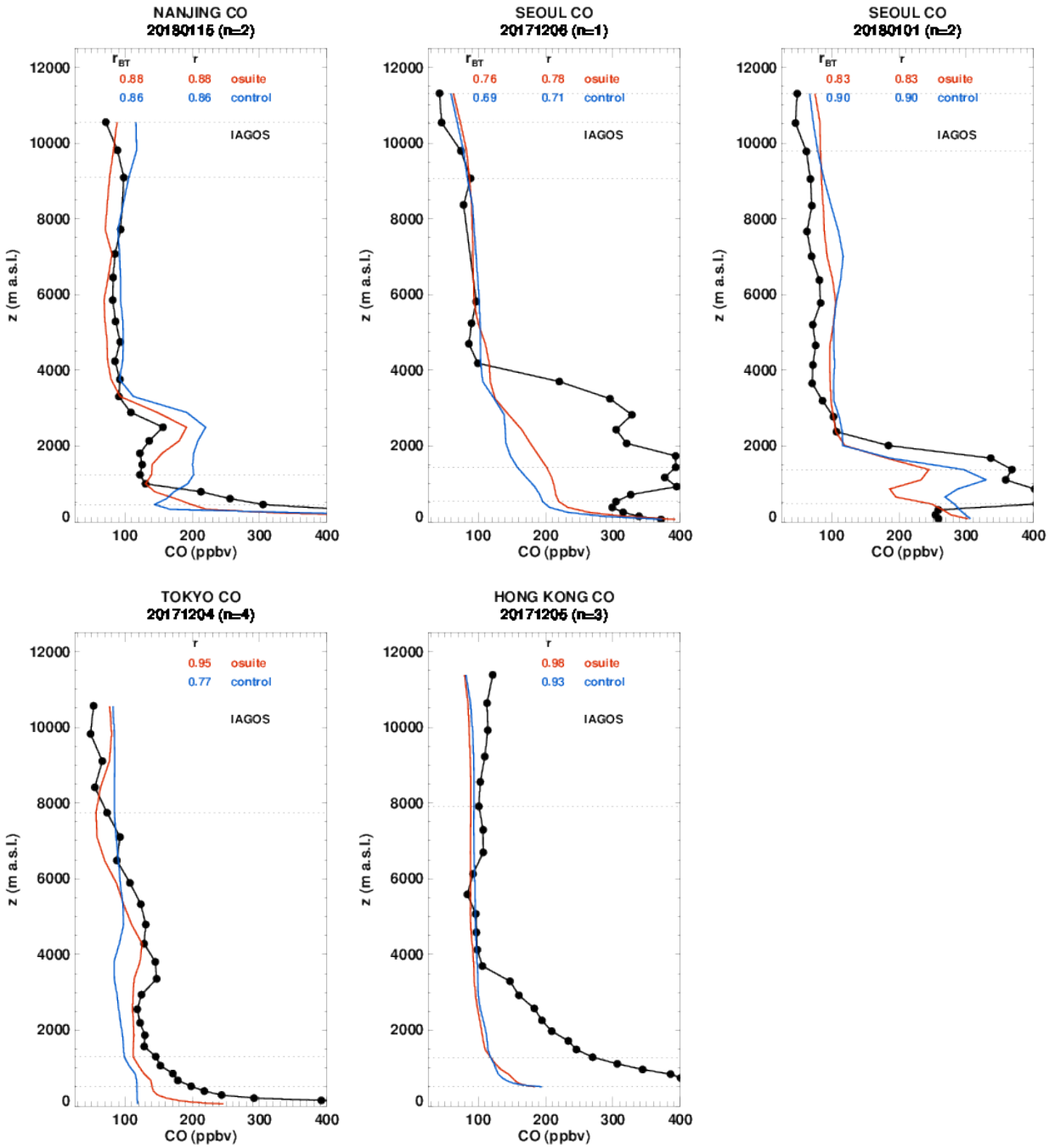


Figure 4.2.6 Profiles of CO from IAGOS (black) and the two NRT over North Eastern Asia during December 2017 – February 2018.

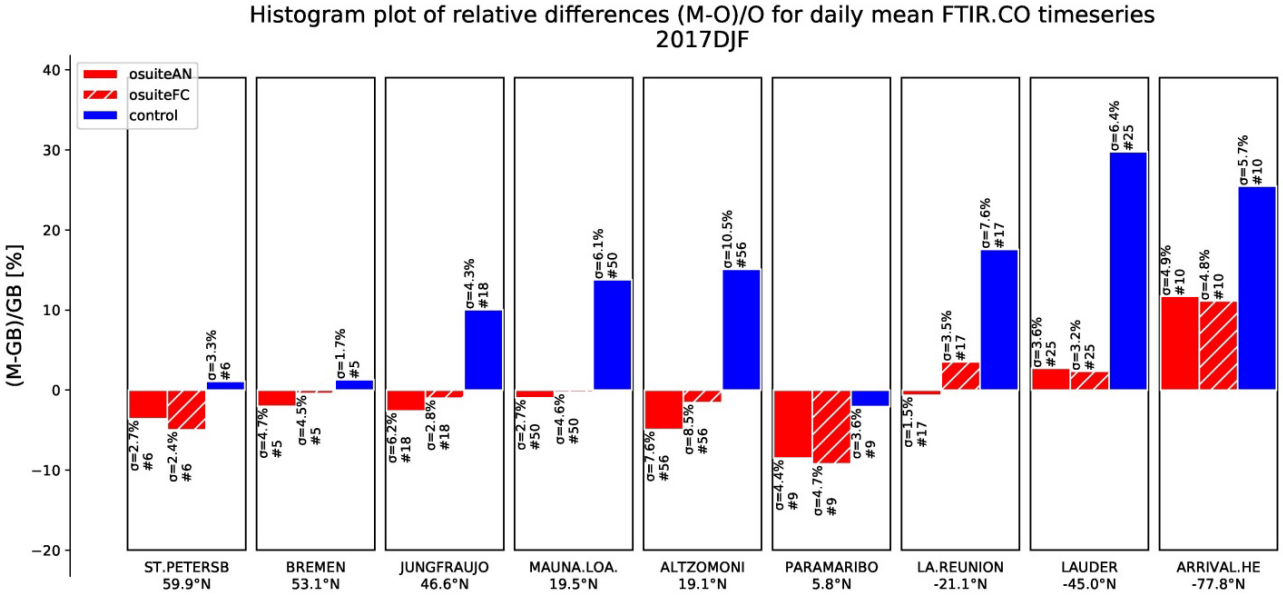


Figure 4.3.1: Seasonal relative mean bias (MB, %), standard deviation (STD, %) and number of observations used for the considered period DJF 2017 - 2018, compared to NDACC FTIR observations. The overall uncertainty for the CO measurements is approximately 5%. Stations are sorted with decreasing latitude (northern to southern hemisphere).

## 4.3 Validation against FTIR observations from the NDACC network

In this section, we compare the CO profiles of the CAMS models with FTIR measurements at different FTIR stations within the NDACC network. These ground-based, remote-sensing instruments are sensitive to the CO abundance in the troposphere and lower stratosphere, i.e. between the surface and up to 20 km altitude. Tropospheric CO profiles and columns are validated (up to 10km). A description of the instruments and applied methodologies can be found at http://nors.aeronomie.be.

Figure 4.3.2 show that the tropospheric columns of CO agree well. All biases for the o-suite AN and 1d FC are within the measurements uncertainty.

For all stations except Paramaribo, the control run overestimates the background CO with MBs up to 20%-30% in the southern hemisphere. The bias seems to increase with decreasing latitude.

The Taylor diagrams in Figure 4.3.3 provide information on the correlation of all three models under consideration with the FTIR time series. Leaving out the sites with few measurements, the assimilation has a positive effect on the correlation coefficient except at Jungfraujoch (site (4)). Looking at the correlation values, the o-suite 1d FC seems to perform better than the o-suite AN, in particular at Jungfraujoch, where the correlation decreases from 0.85 to a value below 0.4. This is not observed in other seasons

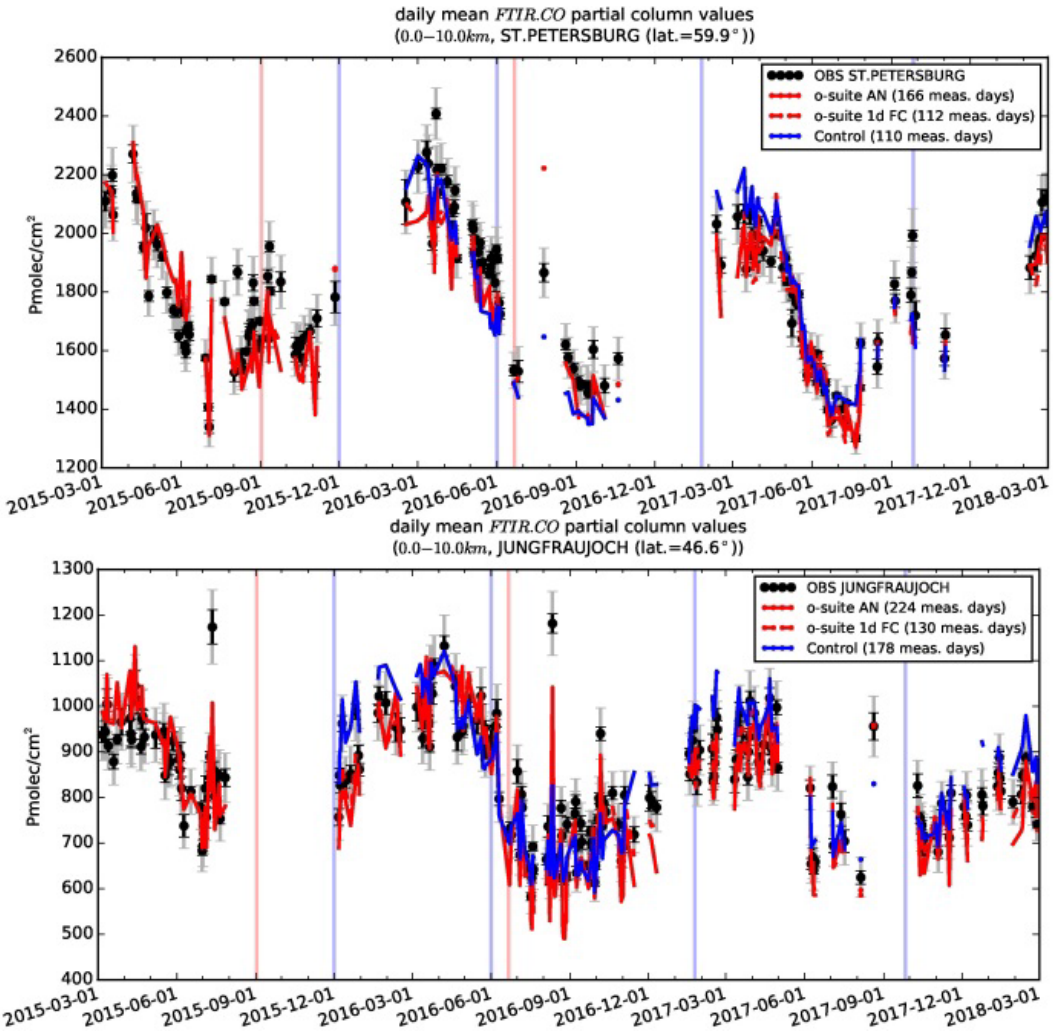


Figure 4.3.2: Daily mean values of tropospheric CO columns (till 10km) by the o-suite (AN and 1d FC, red) and the Control run (blue) compared to NDACC FTIR data at St Petersburg and Jungfraujoch for the period March 2015-March 2018. Vertical lines show the corresponding model upgrades.

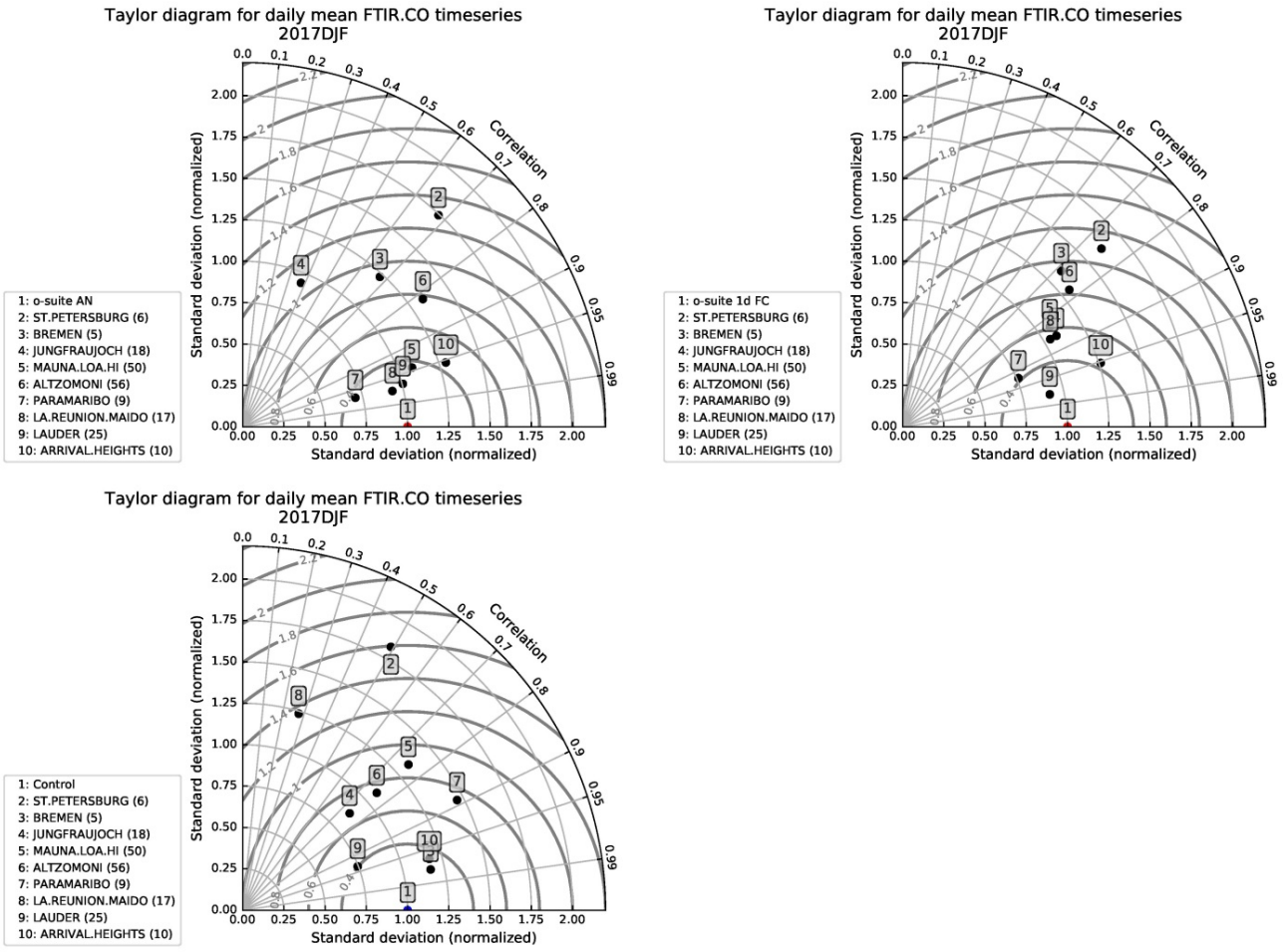


Figure 4.3.3: Taylor diagrams relating the standard deviations for the model and GB time series and their correlation. All time series are normalized such that the std of the model is 1. Some sites have only few measurements (St-Petersburg (2)). At Jungfraujoch (4) and St-Petersburg (2) the correlation of the o-suite 1d FC is higher than the correlation of the o-suite AN with the GB time series.

## 4.4 Evaluation with MOPITT and IASI data

In this section, modeled CO total columns are compared to MOPITT versions 6 and 7 (thermal infrared radiances) (Emmons et. al., 2009, Deeter et al., 2010) and IASI satellite retrievals (Clerbaux et al., 2009). Figure 4.4.1 shows the global distribution of CO total columns retrieved from MOPITT V7 (top left) and IASI (top right) and the relative biases of the model runs with respect to MOPITT V7, averaged for January 2018. Both, MOPITT and IASI show high values over the biomass burning area in central Africa and slightly enhanced values over East Asia. IASI values are higher in the above mentioned regions and depict a very distinct high concentration spot in Asia, which is not the case in MOPITT observations. The modeled CO geographical distribution and magnitude of values show that the model performs reasonably. The relative difference between the model runs and MOPITT shows that both model runs overestimate CO total column over East China of up to 40 % and over biomass burning areas in central Africa and the central part of South America of up to 30% (in the control run it is up to 40%). In general, the o-suite performs better than the run without data assimilation, with some overestimation in the tropics and the high southern latitudes and

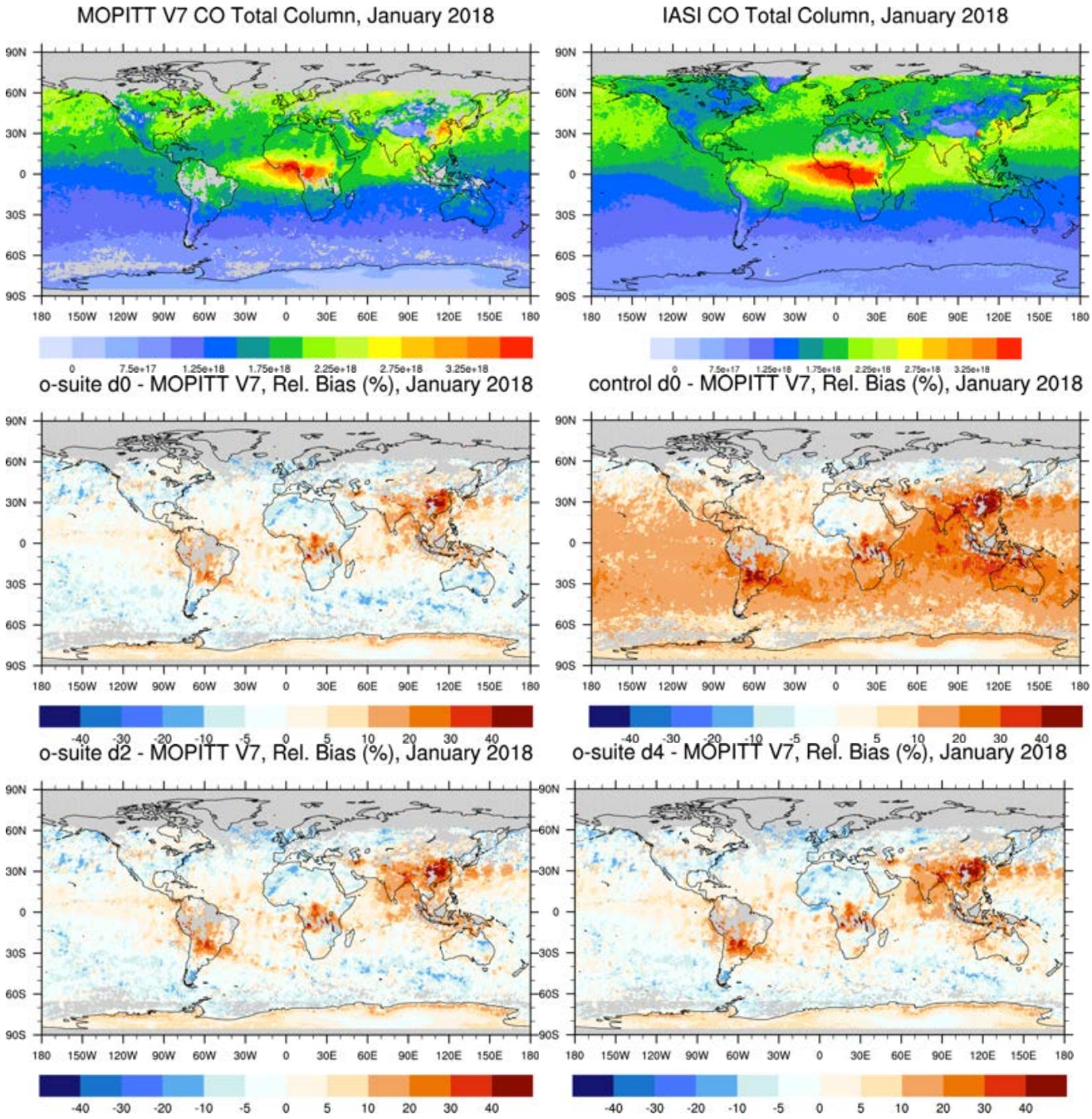


Fig. 4.4.1: CO total column for MOPITT V7 (top left) and IASI (top right) satellite retrievals and relative difference between the model runs and MOPITT for January 2018: o-suite (middle left), control run (middle right), o-suite 2nd forecast day (bottom left), o-suite 4th forecast day (bottom right). Grey color indicates missing values.

underestimations in the mid-latitudes of up to 20%. The control run shows overestimations for the whole Southern Hemisphere by about 20-30% with regional exceptions over the northern mid-latitudes and western Africa. Figure 4.4.1 shows no significant difference between the o-suite analysis and 2nd and 4th forecast days. Figure 4.4.2 shows time series of CO total column for MOPITT V6 and V7, IASI and the model runs over the eight selected regions. For the comparison with MOPITT, the modelled CO concentrations were transformed using MOPITT V7 averaging kernels

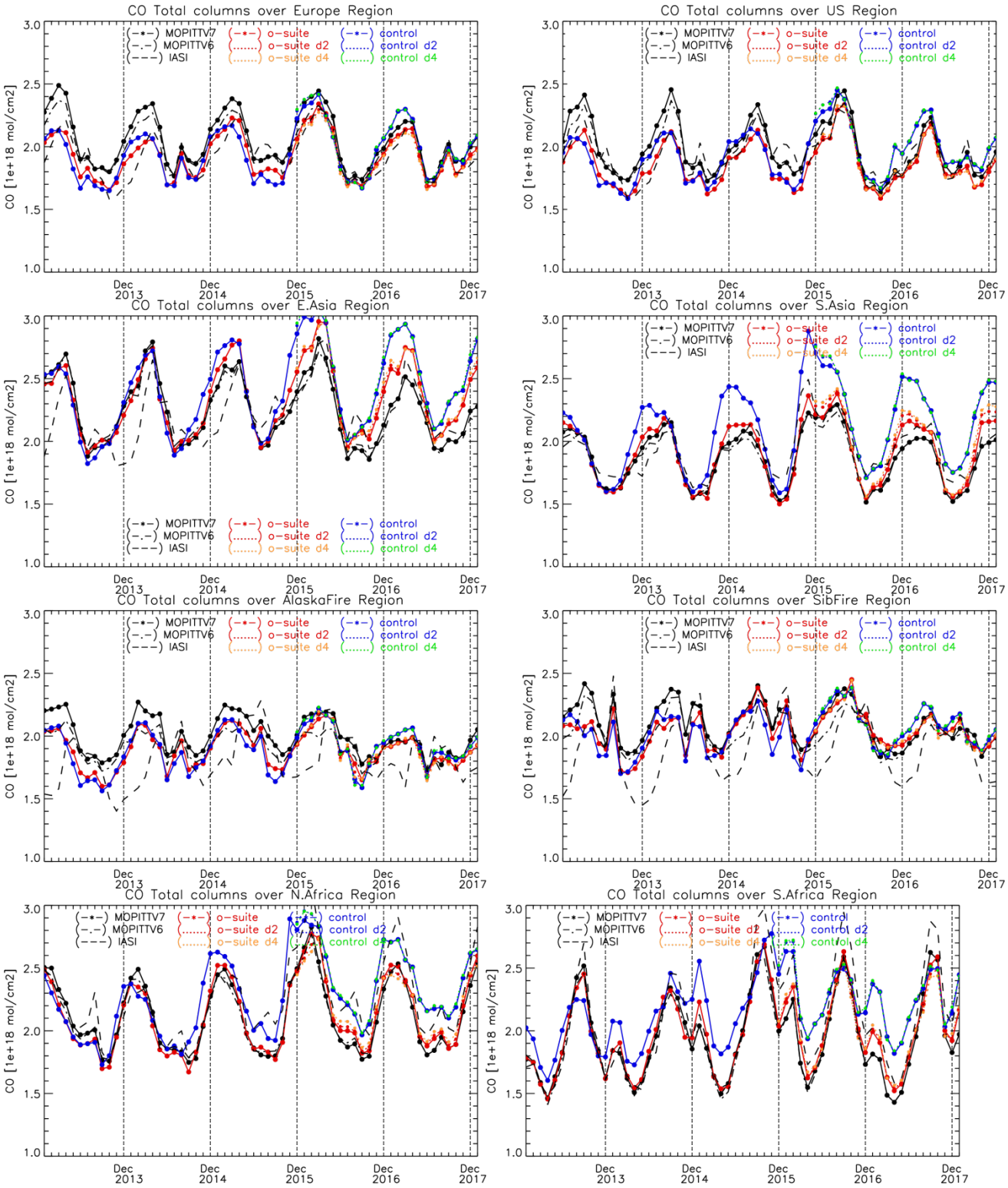


Fig. 4.4.2: Time series of CO total column for satellite retrievals MOPIT V6 and V7, IASI (black) and the model runs over the selected regions: o-suite (red, solid), control (blue, solid), o-suite 2nd forecast day (red, dotted), o-suite 4th forecast day (orange, dotted), control 2nd forecast day (blue, dotted), control 4th forecast day (green, dotted).

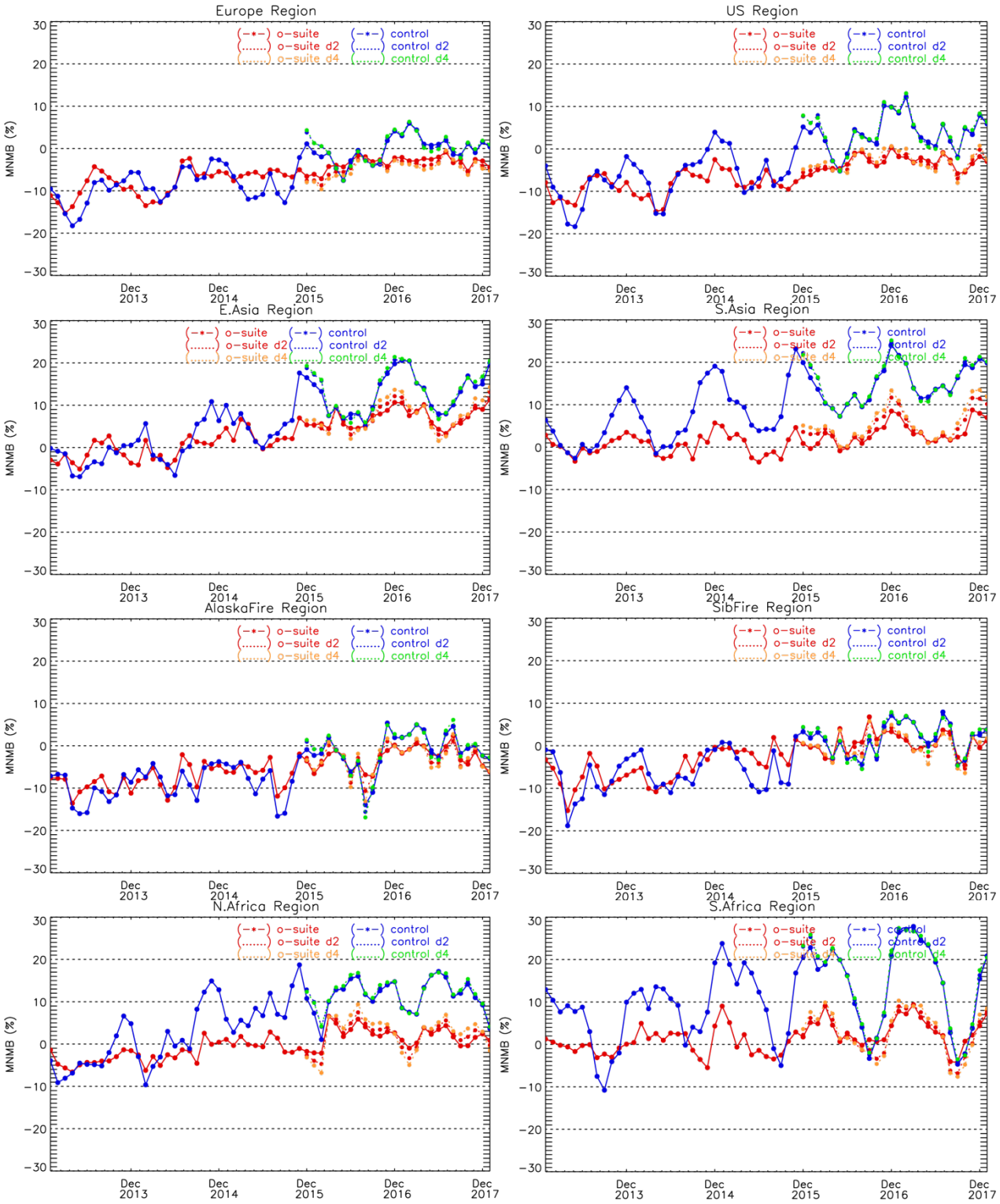


Fig. 4.4.3: Modified normalized mean bias (%) for CO total column from the model simulations vs MOPITT V7 retrievals over selected regions. O-suite (red, solid), control run (blue, solid), o-suite 2nd forecast day (red, dotted), o-suite 4th forecast day (orange, dotted), control 2nd forecast day (blue, dotted), control 4th forecast day (green, dotted).

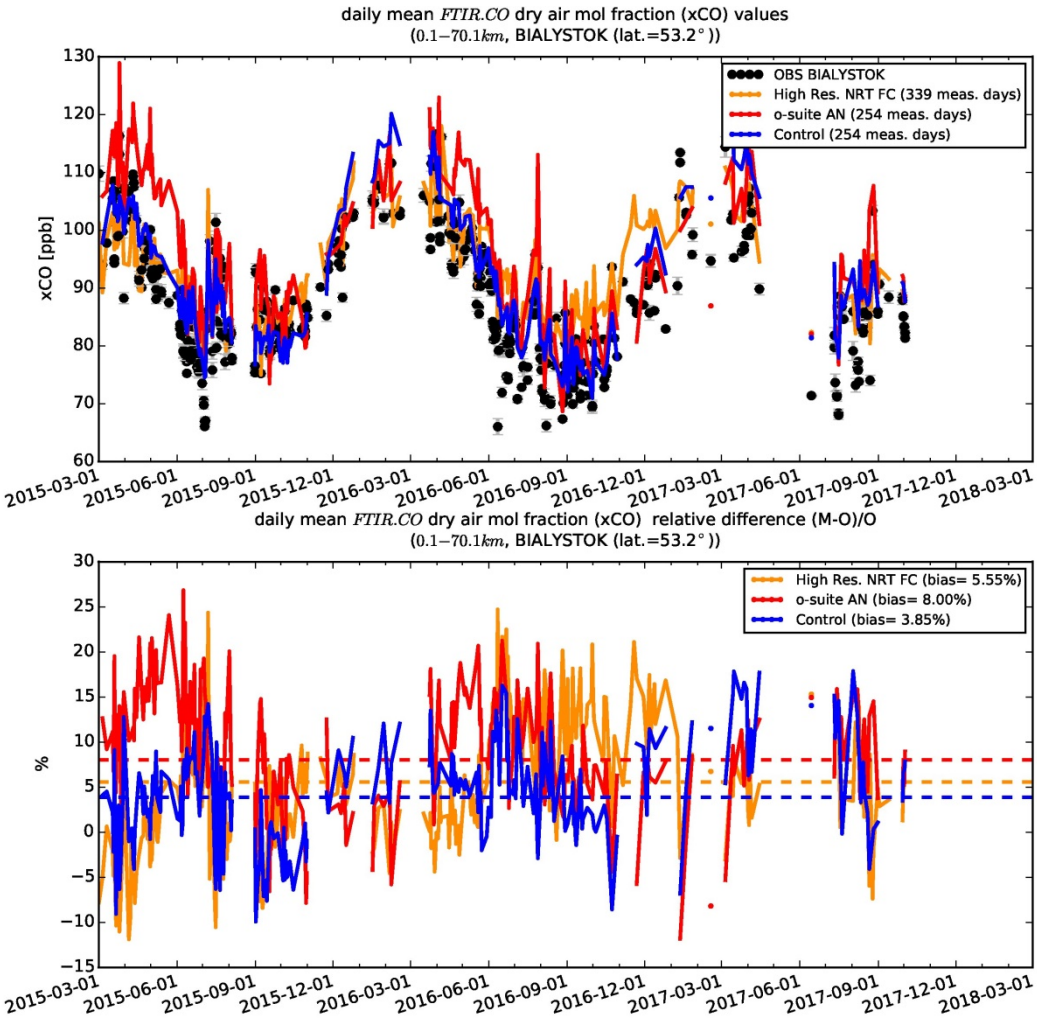


Figure 4.5.1: Time series and relative difference of column averaged mole fractions of carbon monoxide (CO) at the TCCON site Bialystok compared to the o-suite (red), control (blue) and the high resolution NRT FC model (yellow).

The modified normalized mean bias (MNMB) of the model runs compared to MOPITT V7 (Fig. 4.4.3) allow quantifying the impact of the assimilation on the model performance. The o-suite model runs show negative biases over Europe, the US and Alaskan fire regions with some seasonal exceptions. The control run shows a systematic positive bias of up to 20% over South Asia in November-December 2014, 2015, 2016, and 2017. Over southern Africa the control run overestimates satellite retrieved values up to 25% in the seasonal maximum in winter and spring 2015, 2016, and 2017. In general, the o-suite is within +/- 10% in all regions, while the control run shows larger biases in East and South Asia and North and South Africa, as well as stronger seasonal cycle. For the control run, d0, d2 and d4 forecast days are almost similar. For the o-suite run, d2 and d4 forecast days show growing positive/negative biases of up to 5 % compared to the analysis d0 in East and South Asia and North and South Africa. In winter 2017/2018 the o-suite shows better agreement with the satellite observations than the control run over the US, Asian and African regions and the Siberian fire region with biases within 10 %. The o-suite shows a systematic growing positive bias within 5% for d2 and d4 in autumn-winter in East and South Asia and in summer-autumn in North Africa and a negative growing bias within 5% in winter in North Africa and autumn in South Africa.

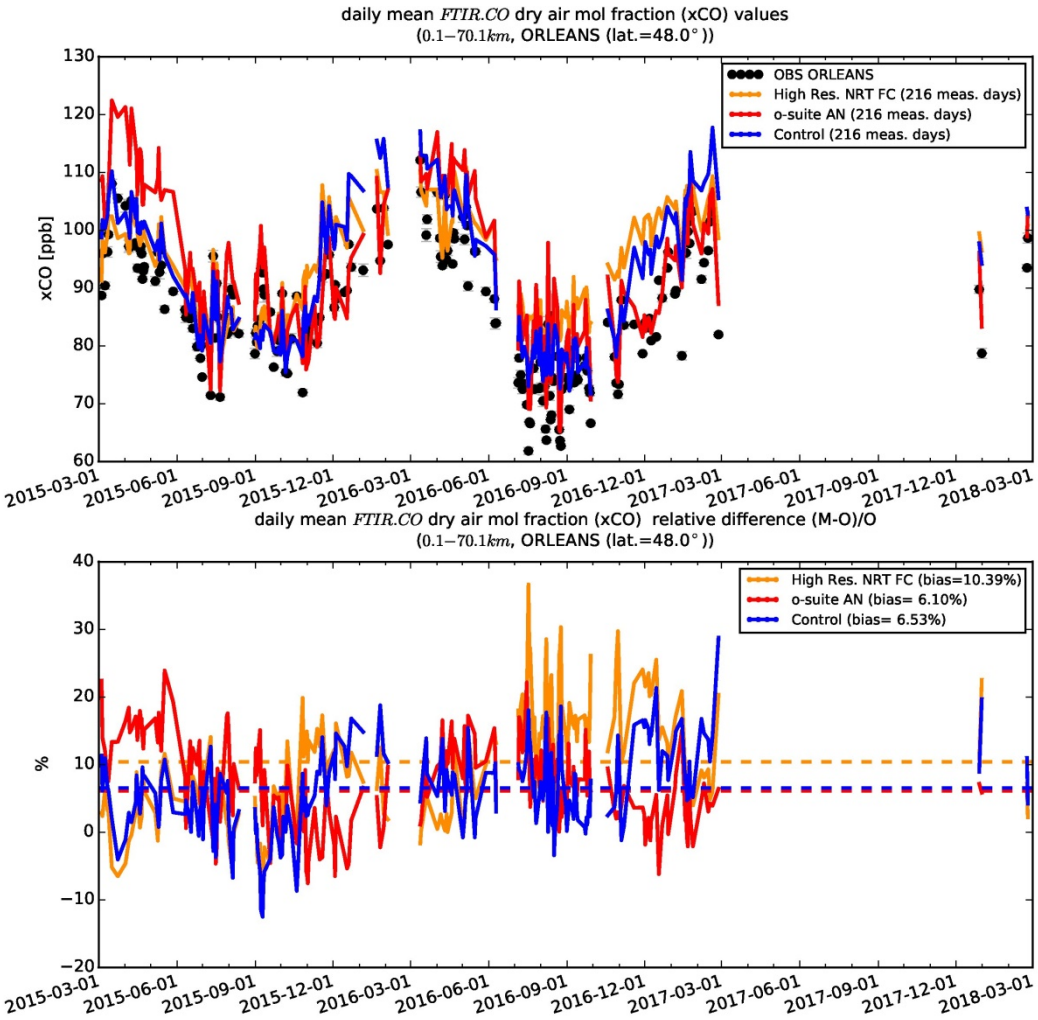


Figure 4.5.2: Time series and relative difference of column averaged mole fractions of carbon monoxide (CO) at the TCCON site Orleans compared to the o-suite (red), control (blue) and the high resolution NRT FC model (yellow).

## 4.5 Evaluation against TCCON CO

For the validation column averaged mole fractions of CO (denoted as XCO) from the Total Carbon Column Observing Network (TCCON) are used. Column averaged mole fractions provide different information content than the in situ measurements and are therefore complementary to the in situ data. The observations are compared with the high-resolution CO simulations, the o-suite, as well as the control run. Only measurements within 2.5h around local noon have been used for the comparison. The reason is that at high solar zenith angles the comparisons worsen due to the averaging kernels. This issue is being investigated.

In the reporting period problems occurred at the TCCON sites Bialystok and Orleans resulting in gaps in the time series. These problems include a broken computer, problems with the spectrometer as well as the solar tracker. For some periods of the reporting period data might become available at a later stage.

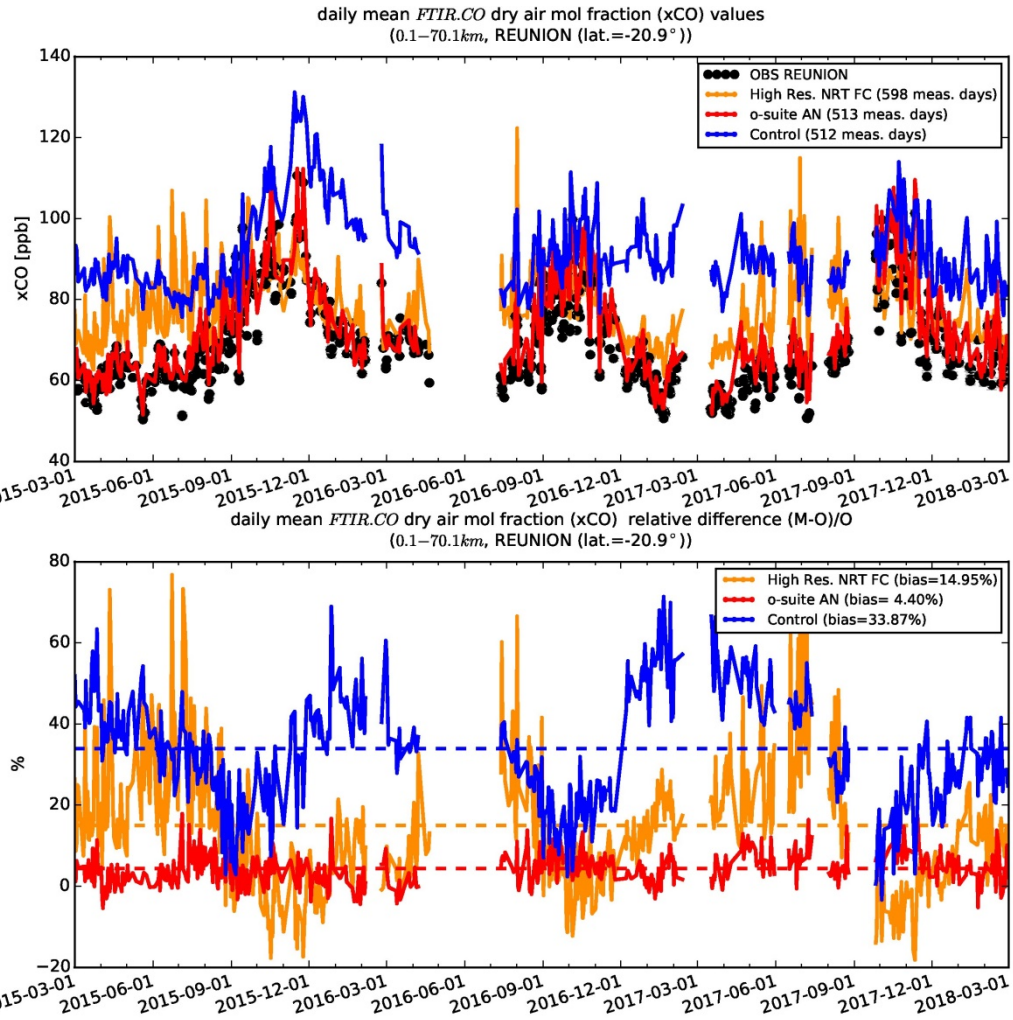


Figure 4.5.3: Time series and relative difference of column averaged mole fractions of carbon monoxide (CO) at the TCCON site Reunion compared to the o-suite (red), control (blue) and the high resolution NRT FC model (yellow).

At Bialystok on average all model simulations overestimate the XCO (Fig. 4.5.1), which is in agreement with the CO at Orleans (Fig. 4.5.2). However, the seasonality is well represented.

At Reunion (4.5.3) the o-suite captures the seasonality and agrees with the measurements quite well. The control run as well as the high resolution FC CO model simulations show strong deviations from the measurements.

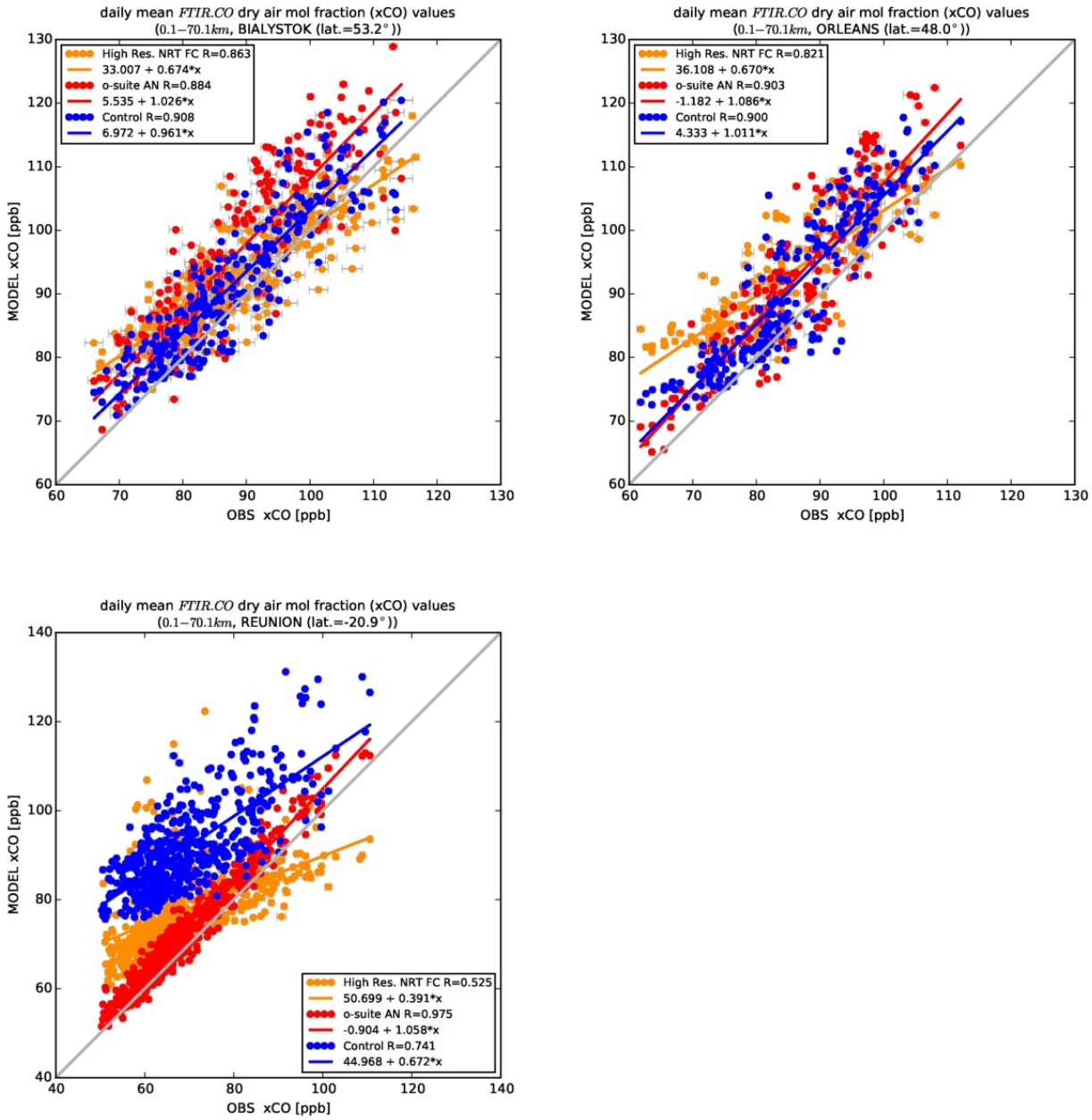


Figure 4.5.4: Scatter plots for the measured CO column averaged mole fractions and the high resolution NRT FC data for the TCCON sites Bialystok (top left), Orleans (top right) and Reunion (bottom left).

# 5. Tropospheric nitrogen dioxide

## 5.1 Evaluation against GOME-2 retrievals

In this section, model columns of tropospheric $NO_2$ are compared to SCIAMACHY/Envisat $NO_2$ satellite retrievals (IUP-UB v0.7) [Richter et al., 2005] for model data before April 2012, and to GOME-2/MetOp-A NO2 satellite retrievals (IUP-UB v1.0) [Richter et al., 2011] for more recent simulations. This satellite data provides excellent coverage in space and time and very good statistics. However, only integrated tropospheric columns are available and the satellite data is always taken at the same local time, roughly 10:00 LT for SCIAMACHY and 09:30 LT for GOME-2, and at clear sky only. Therefore, model data are vertically integrated, interpolated in time and then sampled to match the satellite data. GOME-2 data were gridded to model resolution (i.e. 0.4° deg x 0.4° deg). Model data were treated with the same reference sector subtraction approach as the satellite data. Uncertainties in $NO_2$ satellite retrievals are large and depend on the region and season. Winter values in mid and high latitudes are usually associated with larger error margins. As a rough estimate, systematic uncertainties in regions with significant pollution are on the order of 20% – 30%.

Figure 5.1.1 shows global maps of GOME-2 and model monthly mean tropospheric $NO_2$ columns as well as differences between retrievals and simulations for January 2018 as an example of the maps for winter 2017/2018. The overall spatial distribution and magnitude of tropospheric $NO_2$ is well reproduced by both model runs, indicating that emission patterns and $NO_x$ photochemistry are reasonably represented. Some differences are apparent between observations and simulations, with generally larger shipping signals simulated by the models. For example, shipping signals are much more pronounced in model simulations to the south of India. Wintertime emissions over central European pollution hotspots are largely underestimated (a feature known from previous NRT reports). However, other local maxima of values observed over anthropogenic emission hotspots in East Asia (e.g. over the heavily populated Sichuan Basin; 30°N, 105°E), India and others such as Teheran, Mecca and Moscow are overestimated. There also is an overestimation over large parts of the US.

Closer inspection of the seasonal variation of tropospheric $NO_2$ in some selected regions (Fig. 5.1.2) reveals significant differences between the models and points to some simulation problems. Over regions where anthropogenic emissions are major contributors to $NO_x$ emissions, models catch the shape of the satellite time series rather well. However, over East-Asia absolute values and seasonality were in previous years strongly underestimated by all model runs (most likely due to an underestimation of anthropogenic emissions), with the o-suite showing the best results since an upgrade in July 2012. As $NO_2$ column retrievals decreased since 2014, model simulated values are in better agreement with the satellite retrieved ones for recent years. However, this decrease in values is not reproduced by the simulations which in contrast to satellite observations show an increase over the complete timeseries of simulations available and as such, the better agreement for more recent years cannot be attributed to an improvement of the simulations. Springtime and summertime model values increased in 2015 compared to previous years, which is in contrast to the satellite retrievals, so that the simulated values for the summers since 2015 are about 50% larger than satellite retrieved ones. As for East-Asia, a decrease in satellite retrieved values also occurs for

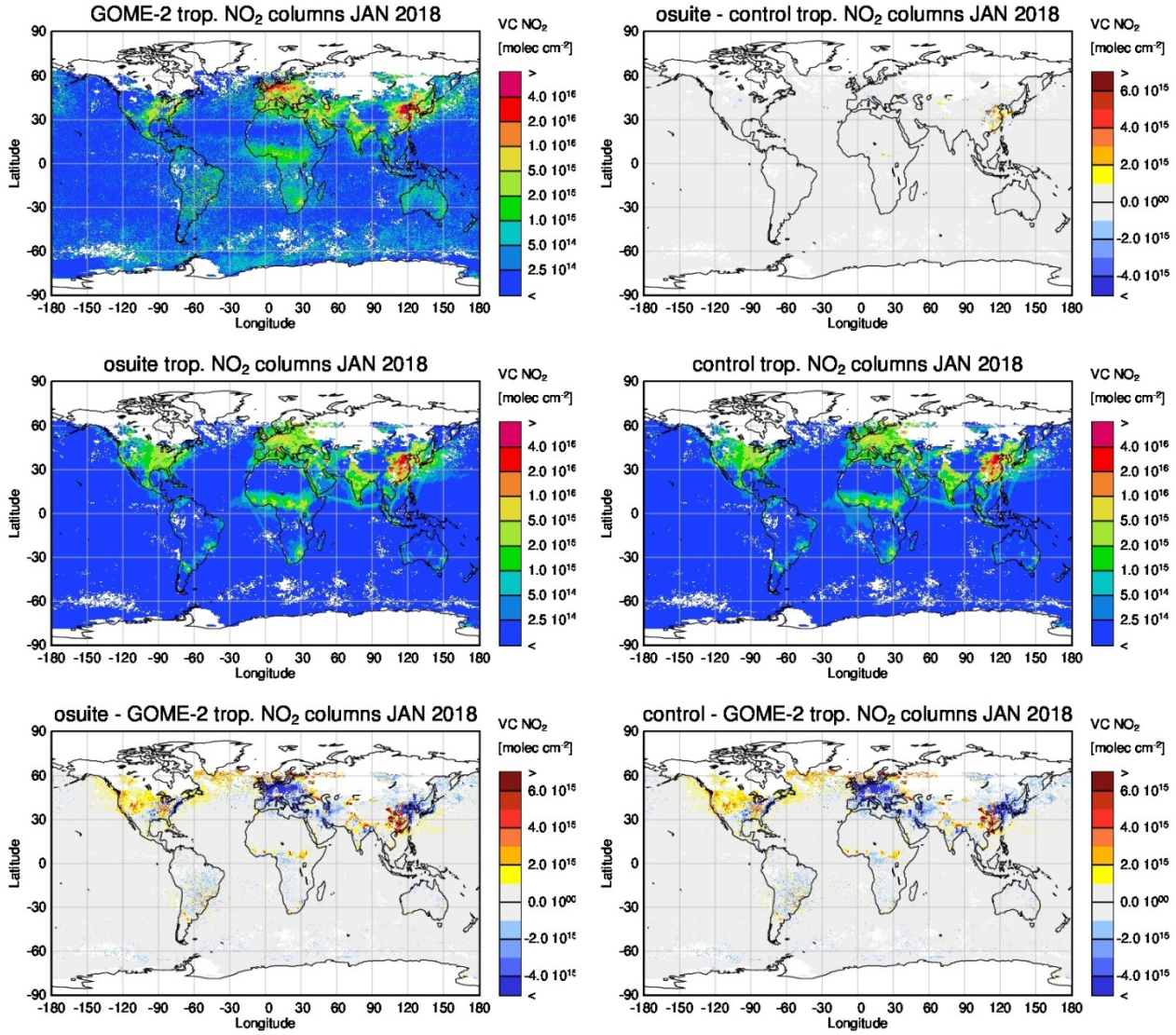


Figure 5.1.1: Global map comparisons of satellite retrieved and model simulated tropospheric $NO_2$ columns [molec $cm^{-2}$] for January 2018. The top row shows monthly mean tropospheric $NO_2$ columns retrieved by GOME-2 as well as the difference between o-suite and control, the second row shows the corresponding tropospheric $NO_2$ columns for model simulated averages. The third row shows differences of monthly means between models and GOME-2. GOME-2 data were gridded to model resolution (i.e. 0.4° deg x 0.4° deg). Model data were treated with the same reference sector subtraction approach as the satellite data.

Europe where a peak is usually found around January, which is, as a result, only slightly underestimated by the models for January 2015. The underestimation of tropospheric $NO_2$ columns over Europe may be caused to some extent by a change of emission inventories in 2012. However, the situation changed over the last three winter periods, for which GOME-2 shows (compared to previous years) a strong increase in January peak values, combined with a decrease in values for December and February, which is not reproduced by the models. It is not clear if the GOME-2 observations are realistic here, although a first inspection of daily GOME-2 satellite images did not point to problems regarding the retrieval.

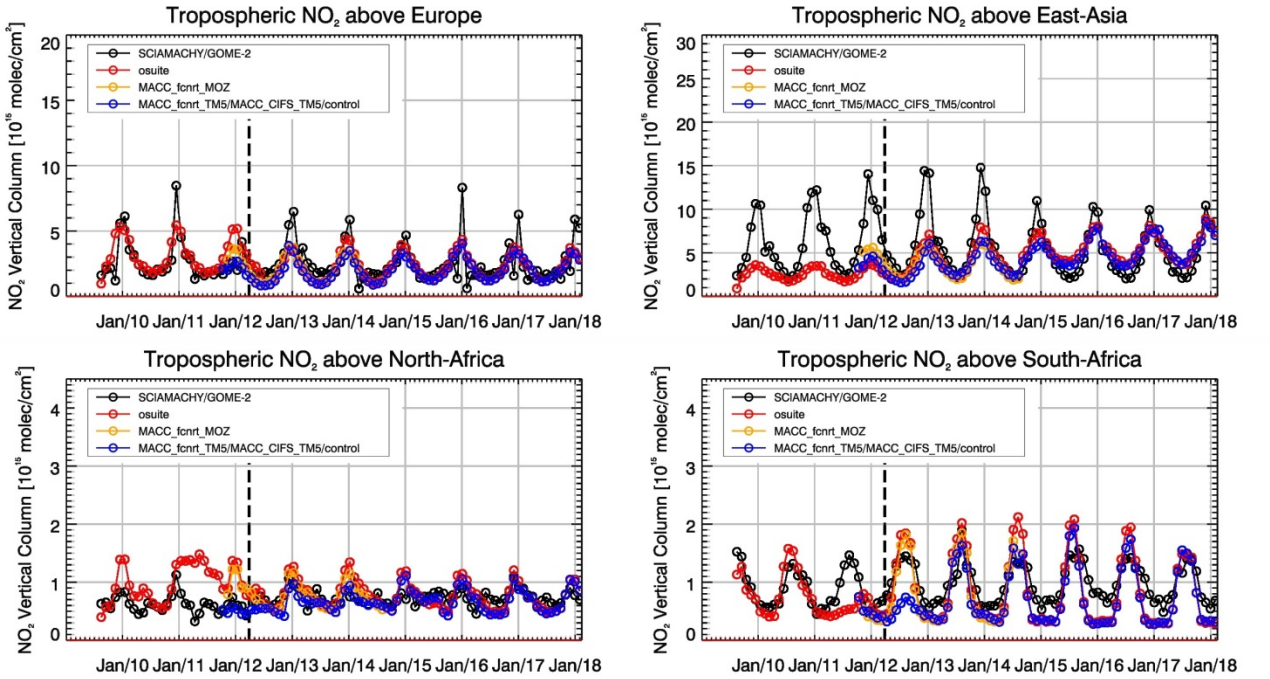


Figure 5.1.2: Time series of average tropospheric $NO_2$ columns [$10^{15}$ molec $cm^{-2}$] from SCIAMACHY (up to March 2012) and GOME-2 (from April 2012 onwards) compared to model results for different regions (see Annex 2 for definition of regions). Upper panels represent regions dominated by anthropogenic emissions, lower panels represent those dominated by biomass burning. The blue line shows MACC_fcnrt_TM5 from November 2011 to November 2012, MACC_CIFS_TM5 results from December 2012 to August 2014 and control results from September 2014 onwards (the model run without data assimilation is termed control since Sep 2014). Vertical dashed black lines mark the change from SCIAMACHY to GOME-2 based comparisons in April 2012.

Over regions where biomass burning is the major contributor to $NO_x$ emissions, seasonality and amplitude of model columns are determined by fire emissions. The seasonality for the two regions in Africa is simulated reasonably well for 2010 and after October 2011. In the time period in between, a bug in reading fire emissions lead to simulation errors for all MOZART runs. Over North-Africa, the o-suite shows improved results since an update in July 2012 and the change to IFS-CB05 in September 2014. However, tropospheric $NO_2$ columns around December are still overestimated by the models. Summertime $NO_2$ columns over North-Africa are underestimated compared to the satellite data from 2015 onwards. The models (especially the o-suite) strongly overestimate the seasonal cycle for South-Africa for 2014 -2016 with an overestimation of the seasonal maximum which usually occurs around August of each year (e.g. by a factor of 1.4 larger compared to GOME-2 retrievals in August 2016). However, summertime values are in better agreement with the upgrade of the o-suite in 2017. For 2014 model runs without data assimilation agree much better with satellite observations, in contrast to more recent CB05-based o-suite runs since 2015. For November 2015 and November 2016, satellite retrieved values over South-Africa do not decrease below 1x$10^{15}$ molec/$cm^2$, a feature which did not show up in the time series before. However, this changed again in November 2017.Details on the $NO_2$ evaluation can be found at: http://www.doas-bremen.de/macc/macc_veri_iup_home.html.

## 5.2 Evaluation against ground-based DOAS observations

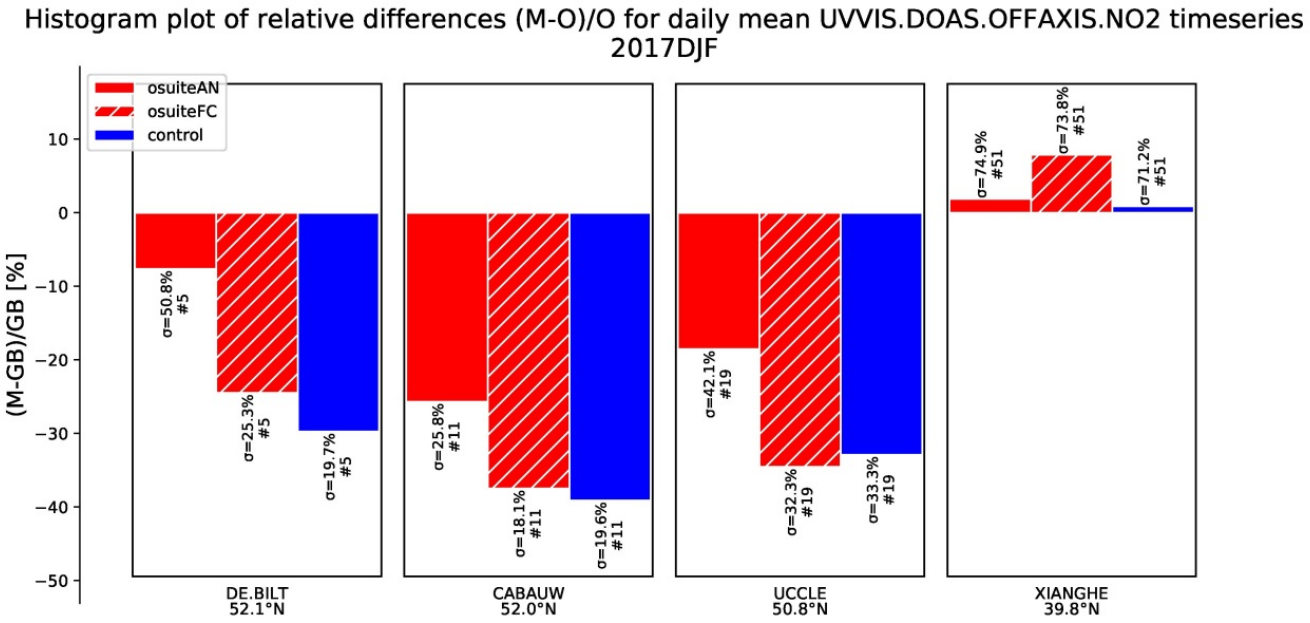


Figure 5.2.1: Table diagram showing the seasonal bias (December 2017 – February 2018) for four stations, sorted by latitude. The stations in Cabauw and De Bilt contributed with only a few measurements in February 2018.

In this section, we compare the $NO_2$ profiles of the CAMS models with UVVIS DOAS measurements at Xianghe (39.8°N, 117°E, station near Beijing, altitude 92m). Uccle (50°N, 4°E) and Cabauw and De Bilt.[1] This ground-based, remote-sensing instrument is sensitive to the $NO_2$ abundance in the lower troposphere, up to 1km altitude with an estimated uncertainty of 8%. Tropospheric $NO_2$ profiles and columns are validated (up to 3.5km). A description of the instruments and applied methodologies is the same all DOAS OFFAXIS measurements, see http://nors.aeronomie.be. It is important to mention here that the model partial column values between the surface and 3.5 km are calculated for the smoothed model profiles (see Fig. 5.2.1). This guarantees that the model levels where the measurement is not sensitive do not contribute to the observed bias. We should mention that the measurement data is still catalogued as rapid delivery and not in the consolidated NDACC database. During December 2017 - February 2018 the o-suite slightly overestimates at the high polluted Xianghe and falls within the measurement's uncertainty. At Uccle, all models underestimate with values up to 20%. The contributions from De Bilt and Cabauw confirm this underestimation even though the number of measurements is limited to February.

[1] No contribution from Reunion and OHP due to instrument failure.

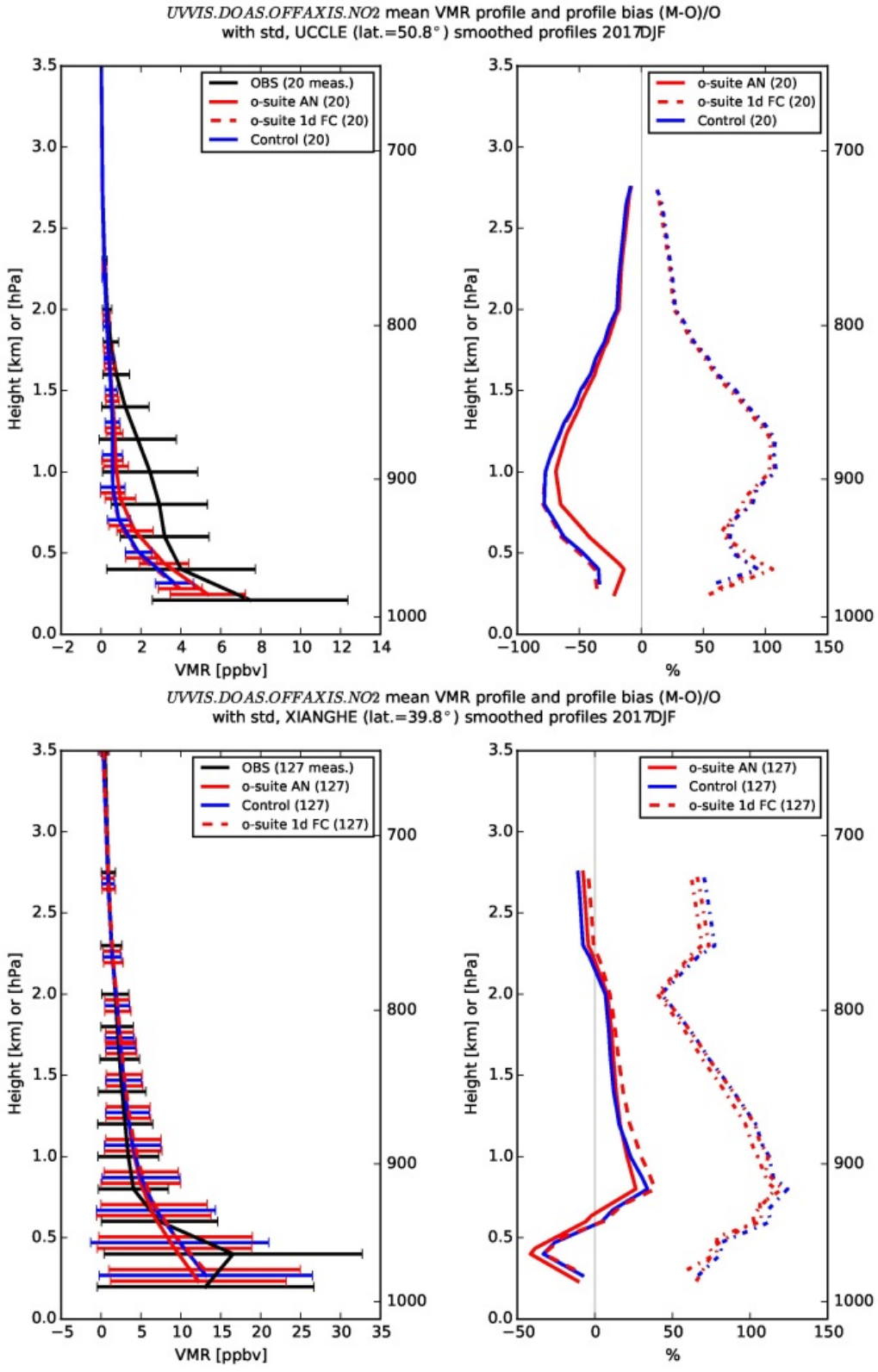


Figure 5.2.2: Seasonal mean tropospheric $NO_2$ profiles by o-suite (red) and Control (blue) compared to NDACC UVVIS DOAS data at Uccle (Brussels 50.8°N, 4°E, left top) and Xianghe (39.8°N, 117°E, right) for December 2017 – February 2018.

# 6. Formaldehyde

## 6.1 Validation against satellite data

In this section, simulations of tropospheric formaldehyde are compared to SCIAMACHY/Envisat HCHO satellite retrievals (IUP-UB v1.0) [Wittrock et al., 2006] for model data before April 2012 and to GOME-2/MetOp-A HCHO data (IUP-UB v1.0) [Vrekoussis et al., 2010] afterwards. As the retrieval is performed in the UV part of the spectrum where less light is available and the HCHO absorption signal is smaller than that of $NO_2$, the uncertainty of monthly mean HCHO columns is relatively large (20% – 40%) and both noise and systematic offsets have an influence on the results. However, absolute values and seasonality are retrieved more accurately over HCHO hotspots.

In Figure 6.1.1, monthly mean satellite HCHO columns are compared to model results for December 2017. The magnitude of oceanic and continental background values and the overall spatial distribution are well represented by the o-suite and control. The models overestimate values over Northern Australia and Central Africa which could be fire or biogenic emissions.

Time series in Fig. 6.1.2 highlight three cases:

- East-Asia and the Eastern US, where HCHO is dominated by biogenic emissions. Model results and measurements generally agree rather well. However, all model runs underestimate the yearly cycle over East-Asia since 2012. In contrast to MOZART runs, MACC_CIFS_TM5 overestimates satellite values for the Eastern US since the middle of 2013. However, the newer IFS-CB05 runs perform well for Eastern US since 2015. For recent years and both regions, there is virtually no difference between the most recent o-suite run with IFS-CB05 chemistry and the corresponding control run without data assimilation. The variability or “ups and downs” in HCHO columns observed by GOME-2 since December 2014 is due to the lack of data (caused by instrument degradation) for these regions during Northern Hemisphere winter months (see Fig. 6.1.1 for the spatial coverage of HCHO data in December 2017). This also explains the negative values in the GOME-2 time series for Eastern US which occur in the time series since December 2015 and is a likely reason for the relatively large underestimation of values during DJF 2016/2017 by the models compared to the retrievals. Summertime maxima are still underestimated by the now higher resolution runs over East-Asia for 2016 and 2017.
- North-Africa, where biomass burning as well as biogenic sources largely contribute to HCHO and its precursors. Satellite observations over North-Africa are generally overestimated by IFS-CB05 chemistry model runs and also the latest higher resolution model versions since July 2016.
- Indonesia, where HCHO is also dominated by biogenic sources and biomass burning. Old MOZART based model versions generally overestimate satellite values here (by a factor of 3 – 4 in the second half of 2010) and fail to reproduce the observed seasonality. This may be due to the use of fire emissions including El Nino years which experience much larger fire activities. MOZART simulations and observations agree much better since late 2012. IFS-CB05 runs agree very well with satellite retrieved ones for December 2014 to August 2015. For September and October 2015, satellite retrieved HCHO columns show a pronounced maximum. 2015 was a strong El Nino year, which caused droughts and higher fire activity in Indonesia. As for previous

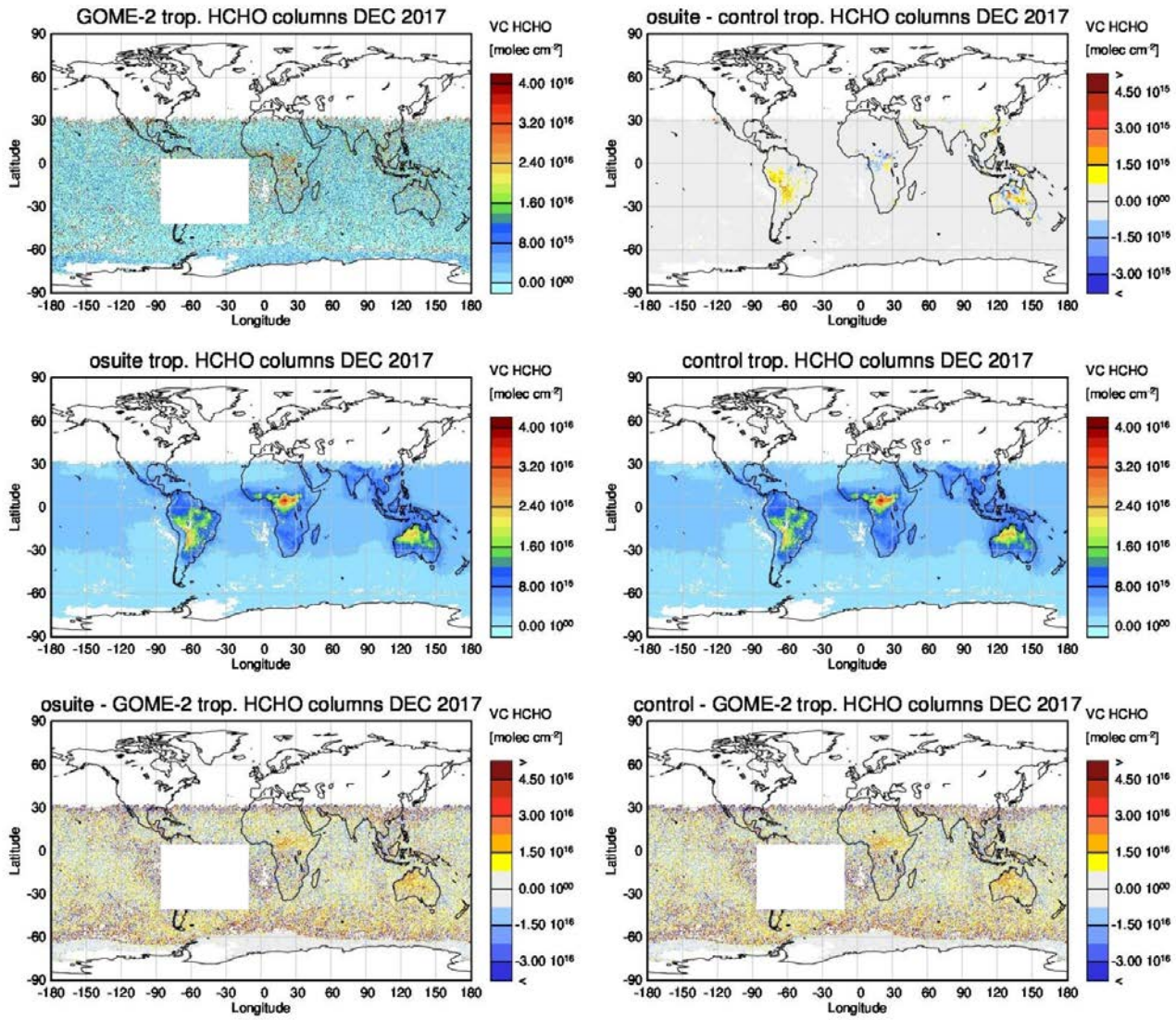


Figure 6.1.1: Global map comparisons of satellite retrieved and model simulated tropospheric HCHO columns [molec $cm^{-2}$] for December 2018. The top row shows monthly mean tropospheric HCHO columns retrieved by GOME-2, the second row shows the same but for model simulated averages. The third row shows differences of monthly means between models and GOME-2. GOME-2 data were gridded to model resolution (i.e. 0.4° deg x 0.4° deg). Model data were treated with the same reference sector subtraction approach as the satellite data. Satellite retrieved values in the region of the South Atlantic anomaly are not valid and therefore masked out (white boxes in all images except those which show model results only).

El Nino years, fire emissions used by IFS-CB05 seem to be largely overestimated, resulting in model simulated HCHO columns which are almost twice as large as those retrieved by GOME-2. Further investigations (see previous reports) show that this is not caused by cloud flagging applied to the satellite and model data. The recent higher resolution runs overestimate values over Indonesia as well. There is little variation from one month to another in both, satellite observations and model simulations since middle of 2016, apart from a decrease in retrieved HCHO columns for Dec 17/ Jan 18 which is not reproduced by the simulations. Models in general overestimate satellite observed HCHO columns since that time.

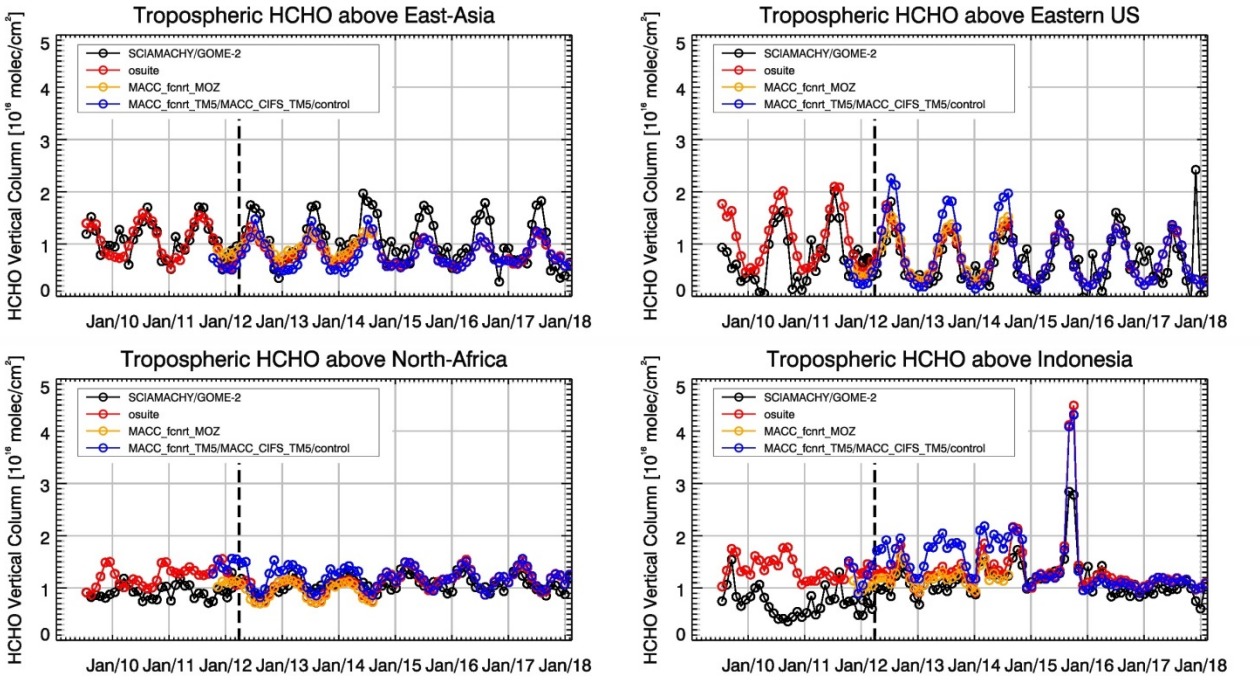


Figure 6.1.2: Time series of average tropospheric HCHO columns [$10^{16}$ molec $cm^{-2}$] from SCIAMACHY (up to March 2012) and GOME-2 (from April 2012 onwards) compared to model results for different regions. The blue line shows MACC_fcnrt_TM5 from November 2011 to November 2012, MACC_CIFS_TM5 results from December 2012 to August 2014 and control results from September 2014 onwards (the model run without data assimilation is termed control since Sep 2014). The regions differ from those used for $NO_2$ to better focus on HCHO hotspots: East-Asia (25-40°N, 110-125°E), Eastern US (30-40°N, 75-90°W), Northern Africa (0-15°N, 15°W-25°E) and Indonesia (5°S-5°N, 100-120°E). Negative satellite retrieved values over Eastern US are due to a lack of data (caused by instrument degradation) during Northern Hemisphere winter months for this region. Vertical dashed black lines mark the change from SCIAMACHY to GOME-2 based comparisons in April 2012.

Details on the HCHO evaluation can be found at:
http://www.doas-bremen.de/macc/macc_veri_iup_home.html.

## 6.2 Validation against UVVIS DOAS observations from the NDACC network

In this section, we compare the HCHO profiles of the CAMS models with UVVIS DOAS measurements at Reunion Le Port (20.1°S, 55.5°E, rural station, altitude 90m) and Xianghe (39.8°N, 117°E, station near Beijing, altitude 92m). Due to instrument failure, the Uccle (50.8°N, 4.36°E, urban) and Haute Provence (43.9°N, 5.71°E, rural) measurements are not displayed. These ground-based, remote-sensing instruments are sensitive to the HCHO abundance in the lower troposphere, up to 1km altitude. Tropospheric HCHO profiles and columns are validated (up to 3.5km). A description of the instruments and applied methodologies is the same as for the MWR $O_3$ and FTIR $O_3$ and CO validations see http://nors.aeronomie.be. It is important to mention here that the model partial column values between the surface and 3.5 km are calculated for the smoothed model profiles. This guarantees that the model levels where the measurement is not sensitive do not contribute to the observed bias. In this specific situation the smoothing of the model profiles implies a strong increase of the model column data by the MAXDOAS apriori (and only the relative difference plots should be considered).

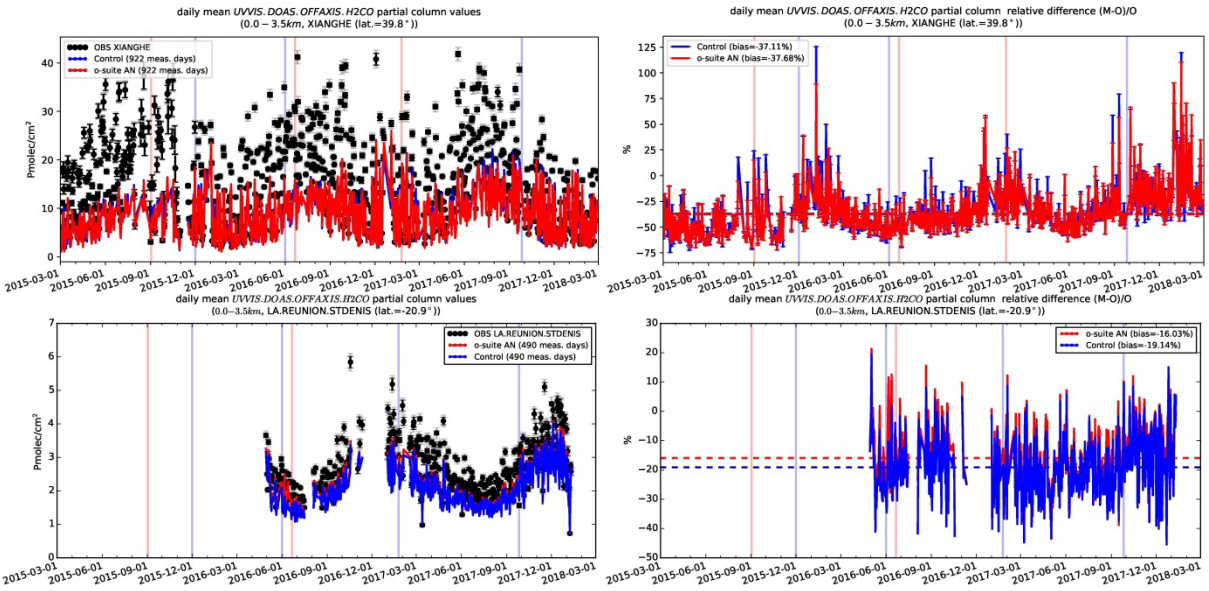


Figure 6.2.1: Daily mean relative differences of tropospheric HCHO columns (till 3.5km) by the o-suite (red) and the control run (blue) compared to NDACC UVVIS DOAS data at at Xianghe (39.8°N, 117°E, station near Beijing, altitude 92m) and Reunion Le Port (20.9°S, 55.5°E, island, altitude 90m, bottom) for the period March 2015 –February 2018. The number of measurements and median of differences is indicated in the legend (the overall measurement uncertainty is 10%). Vertical lines indicate the model upgrades.

We should mention that the measurement data is still catalogued as rapid delivery and not in the consolidated NDACC database. The measurements have been quality filtered on cloud conditions: only measurements under “clear sky” and “thin clouds” are used (see Gielen et al., 2014).

From Figure 6.2.1 we see little difference between the o-suite and the control run. Both models underestimate the observations below 1km. Although the background column values are well captured by the models, the high emission events are not.

# 7. Aerosol

## 7.1 Global comparisons with Aeronet and EIONET-Airbase

The comparison of the CAMS simulation of time series of aerosol optical depth can be compared for all Aeronet stations via: http://aerocom.met.no/cams-aerocom-evaluation/

More detailed evaluation including scores, maps, scatterplots, bias maps and histograms illustrating the performance of the aerosol simulation in the IFS system are made available through the AeroCom web interface . The model run can be compared here to eg the CAMS interim and other models, such as the AeroCom Median model.

Correlation, based on daily aerosol optical depth and NRT Aeronet observations, has no clear trend since 2011. The o-suite forecast at +3 days shows slightly lower correlation, as expected. See figure S3. An o-suite MNMB bias of plus 11-24 percent is found in DJF 2018.

Part of the month-to-month variation in correlation is due to the varying quality and coverage of the Aeronet network. This has been improved by the version 3 from Aeronet. We use therefore version 3 level 1.5 for all global comparison to Aeronet.

The regional performance of the o-suite model exhibits some seasonal variation in AOD depending on region (Fig. 7.1.1 a). For instance, the model performance in the North American winter season with respect to correlation seemed to be worst in 2011-2013 but seems to be more balanced now. Noteworthy is the persistent AOD overestimation over North America (Fig. 7.1.1 b), but also the change from underestimation to overestimation in East Asia since February 2017. The latitudinal display of model and Aeronet AOD in the period investigated here (Fig. 7.1.2) shows the positive bias against Aeronet NRT in the Southern Hemisphere.

The simulated aerosol size distribution may be validated to first order using the wavelength dependent variation in AOD, computed as Ångström exponent, with higher Ångström exponents indicative of smaller particles. Figure 7.1.3-a shows the temporal evolution of simulated and observed mean Ångström exponent, while the correlation is found in figure 7.1.3-b. We find in DJF 2017-2018 a positive bias of +10% (against -5% before October 2013). Temporal and spatial variability is rather high and correlation is lower than for AOD (Figure 7.1.3-b). Figure 7.1.4 shows that the Oct 2013 model changes are responsible for this shift in Ångström exponent. Less sea salt and more sulphate or organic matter shift the size distribution to smaller sizes. AOD due to sea salt decreased

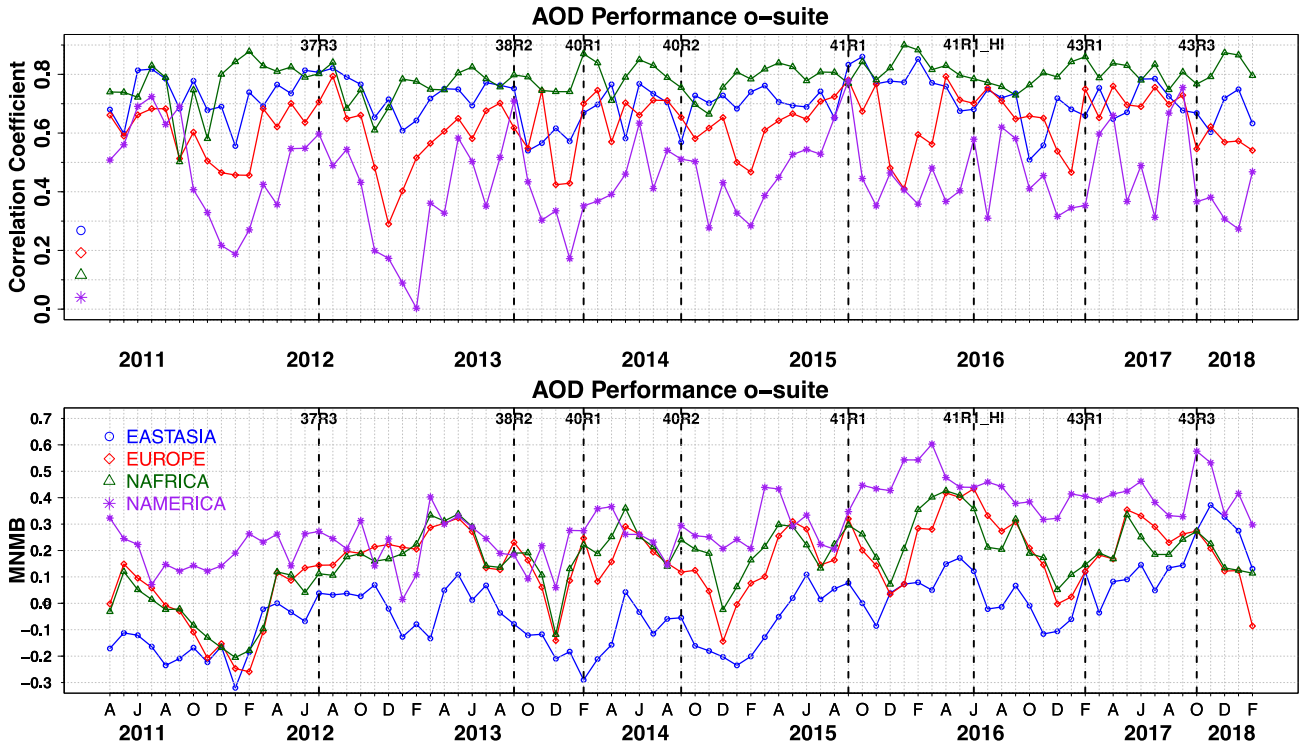


Figure 7.1.1. (a) top) Correlation coefficient and (b) bottom) modified normalized mean bias (MNMB) in AOD, since 2011, based on daily AOD comparison (Aeronet V3 level 1.5 data) in four world regions [ Eastasia(blue); Europe(red); NAfrica(green); NAmercia(purple) ] for the o-suite.

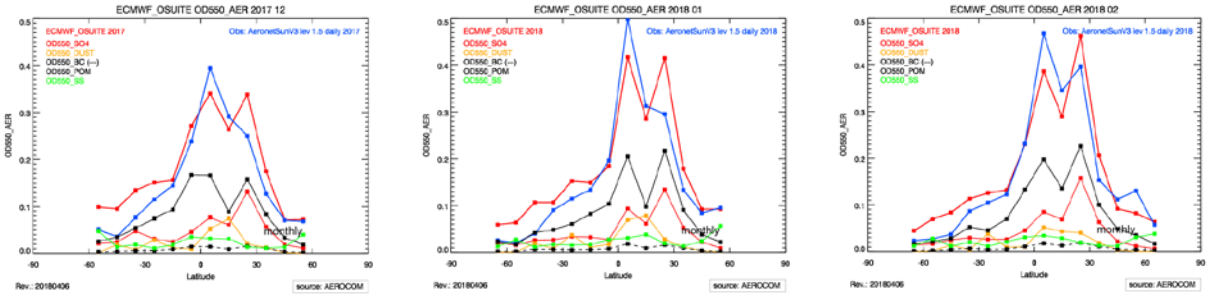


Figure 7.1.2. Aerosol optical depth of o-suite (red) compared to latitudinally aggregated Aeronet V3 level 1.5 data (blue) for the three months covered by this report.

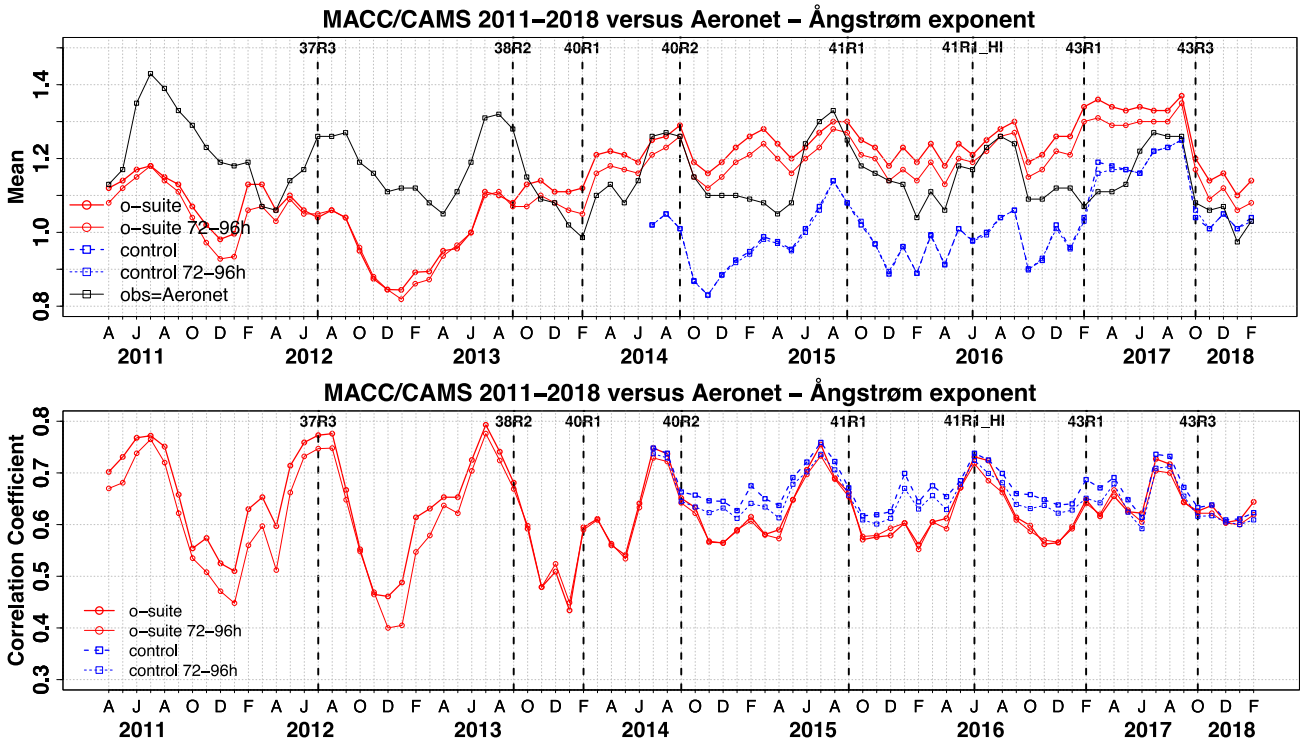


Figure 7.1.3. (top) Evolution of mean Ångström exponent in o-suite and control at Aeronet sites (Aeronet V3 level 1.5 data), based on matching monthly mean values. o-suite (thick red curve); o-suite at last forecast day (light red curve); control (blue dashed curve); control at last forecast day (light blue dashed curve). (bottom) Correlation using daily matching Ångström exponent.

by 50%, that to due organics decreased by 25%, while that of sulphate increased by 40%. The changes in the model since end of January 2017 indicate an increase of organics by 30% and decrease of sulphate of 40%. The latest model upgrade with a bugfix for sea salt and improved parameterisations for SO4 lead to sea salt increased with 45% while sulphate further decreased a bit. Organics seem to return to earlier level (since the change in February 2017) after a short period of increase in August and September.

The o-suite uses data assimilation to obtain a first guess aerosol field. In the forecast period, however, a-priori model parameterisations and emissions (except fire emissions, which are kept in the forecast equal to the latest GFAS emission values) determine more and more the shape and amplitude of the aerosol fields. The performance of the day three forecasted AOD fields as compared to the first guess is shown in Figure S3 in the summary of this report. Table 7.1.1 shows an average global decrease in total aerosol optical depth by 17% during the first four forecast days, dominated by sulphate and organics. Against Aeronet the o-suite forecast for day three has less bias in AOD. The control run with no assimilation shows significant less AOD (-33% compared to o-suite, see figure S3). All this supports the conclusion that either a-priori IFS aerosol and aerosol precursor sources are too small or sinks are too effective in the IFS model.

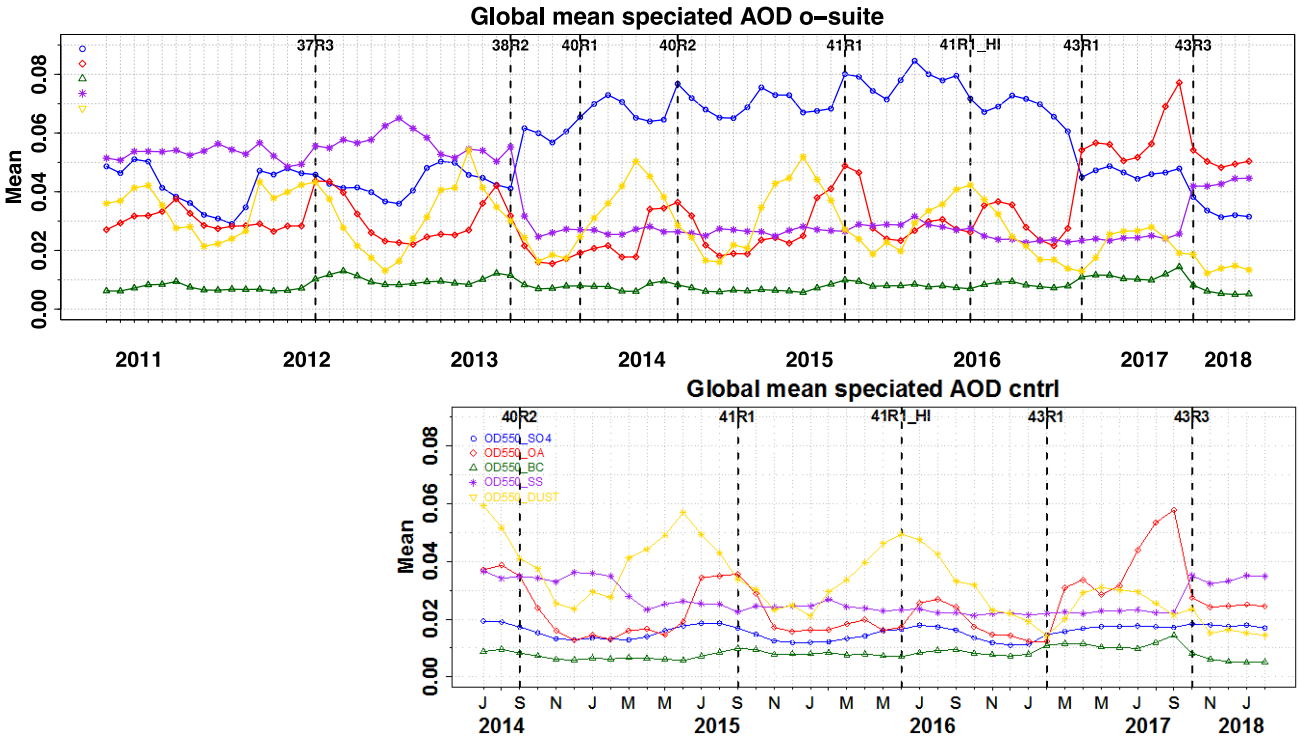


Figure 7.1.4. Evolution of the aerosol components of total AOD@550nm [OD550_SO4 = sulphate(blue); OD550_OA = organics(red); OD550_BC = black carbon(green); OD550_SS = sea salt(purple); OD550_DUST = dust(yellow) ] in o-suite and control simulation.

Table 7.1.1. Mean global total and speciated AOD in the o-suite for the last two periods covered by the VAL report and change after 3 forecast days.

| | o-suite | | o-suite | |
|---|---|---|---|---|
| | Mean SON 2017 0-24h | Change wrt to first day on day 4 | Mean DJF 2017/18 0-24h | Change wrt to first day on day 4 |
| AOD@550 | 0.166 | -17% | 0.145 | -19% |
| BC-OD@550 | 0.009 | -25% | 0.005 | -25% |
| Dust-OD@550 | 0.017 | 0% | 0.014 | 5% |
| OA-OD@550 | 0.061 | -21% | 0.049 | -25% |
| SO4-OD@550 | 0.040 | -25% | 0.031 | -25% |
| SS-OD@550 | 0.036 | -13% | 0.044 | -15% |

Surface concentration of particulate matter below 10 µm (PM10) from the o-suite experiment have been validated against data from 160 background IMPROVE and EMEP stations. A climatological average has been constructed from data in the period 2000-2009 as available in the EBAS database hold at NILU. The data availability is not the same at all stations, and sometimes covers only a few years. All time series used are documented via the CAMS-AeroCom web interface. In earlier evaluations the bias maps showed that both in North America and Europe a high bias appears at a few stations located in regions close to the coastlines. This is an indication that simulated PM10

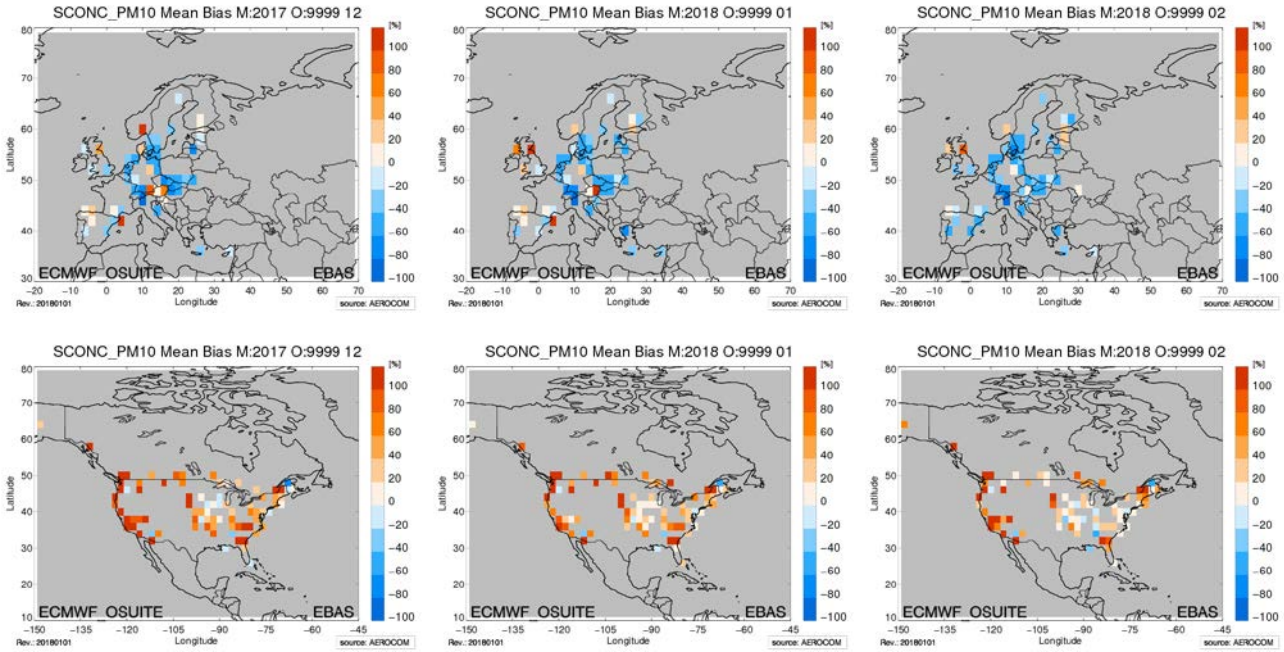


Figure 7.1.5. Bias [%] map of monthly mean PM10 concentrations at EMEP (Europe) and IMPROVE sites (North America); simulated o-suite versus EMEP/IMPOVE derived climatological average (2000-2009).

concentrations are high due to sea salt aerosols. This has changed with the implementation of recent model versions. Regional models using the sea salt concentrations as boundary condition should look into the PM10 definition as used in IFS.

A negative MNMB bias of -30% both in Europe and a +40% overestimate in North America appears (figure 7.1.5). Figure 7.1.6 is showing the evolution of mean observed and simulated PM10. The biggest change appeared in July 2017, the bias of both o-suite and control now becoming positive overall due to the weight and larger number of stations in North America. Shown is also the statistics of being within factor 2, a more robust metrics for a comparison to climatological data. This statistics has clearly increased over time, indicating best PM10 performance in summer months for the o-suite. O-suite is also better most of the times than the control simulation.

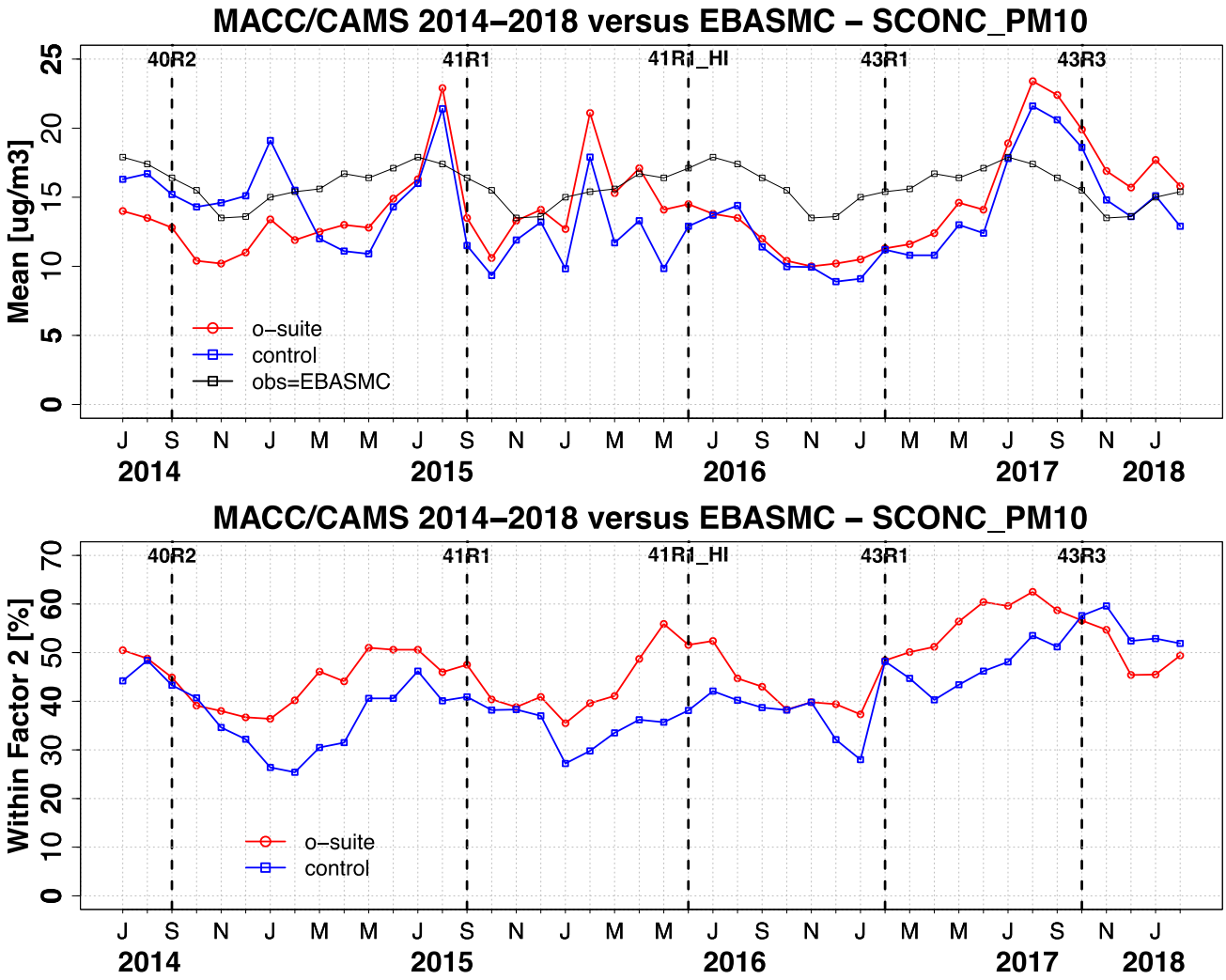


Figure 7.1.6. Temporal evolution of monthly mean average PM 10 concentrations at EMEP (Europe) and IMPROVE sites (North America) and data fraction within a factor 2 of observed; ca 160 sites, observed data averaged from data available in EBAS from 2000-2009.

## 7.2 Dust forecast model intercomparison: Validation of DOD against AERONET, and comparisons with Multi-model Median from SDS-WAS

72-hour forecasts (on 3-hourly basis) dust aerosol optical depth (DOD) from CAMS o-suite and control experiments have been validated for the period 1 December 2017 – 28 February 2018 against AERONET direct-sun cloud-screened observations, MODIS Collection 6 Level 3 (1º x 1º) and compare with the SDS-WAS Multi-model Median DOD. The SDS-WAS Multi-model Median DOD is obtained from twelve dust prediction models participating in the Sand and Dust Storm Warning Advisory and Assessment System (SDS-WAS) Regional Center for Northern Africa, Middle East and Europe (http://sds-was.aemet.es/).

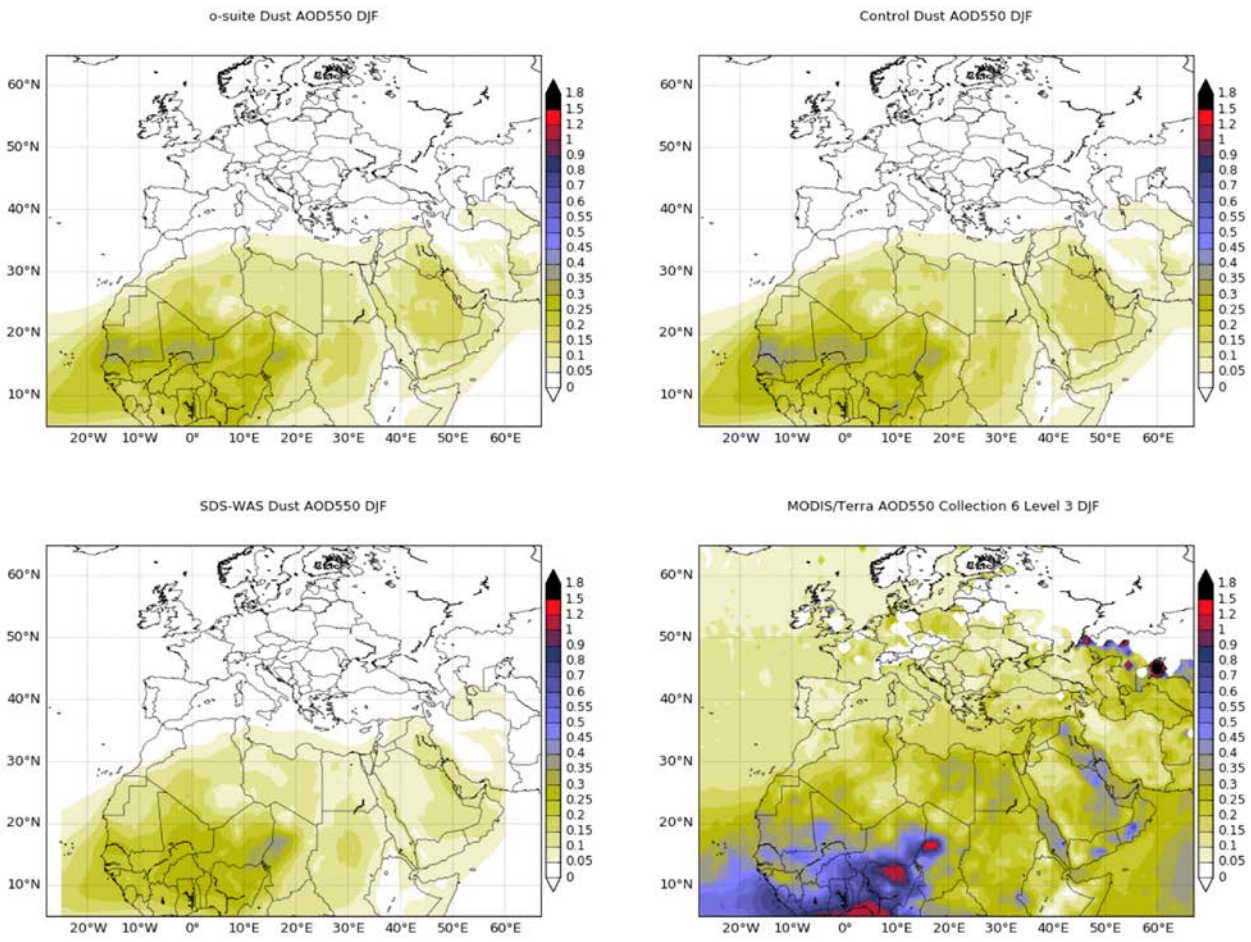


Figure 7.2.1: Averaged DOD 24h forecast from o-suite (top left) and control (top right), DOD of the multi-model SDS-WAS Median product (bottom left) as well as AOD from MODIS Collection 6 Level 3 combined Dark target and Deep Blue product (bottom right) for the study period.

For winter, dust activity is low, and the presence of biomass burning from Savanah fires are detected by satellites (see MODIS in Figure 7.2.1), and major dust activity is concentrated over the Bodélé Basin. CAMS model can simulate the main areas of dust activity in comparison with MODIS, although o-suite shows lower DOD values particularly, over the Bodélé (see Figure 7.2.1) in which the SDS-WAS Multi-model product presents a higher signal. In the Middle East, both CAMS experiments show maximum DOD concentrations over the whole Arabian Peninsula meanwhile MODIS and the SDS-WAS Multi-Model are localising the maximum DOD values in a smaller region of eastern Arabian Peninsula.

For December to February, o-suite is the model can reproduce the daily variability of AERONET observations with a correlation coefficient of 0.79 in average for all the AERONET sites in comparison with control with a correlation coefficient of 0.74. These results are closer to those obtained by the SDS-WAS Multi-model of 0.81. In terms of MB, both CAMS experiments (o-suite and control) as well as the SDS-WAS Multi-model underestimate the AERONET observations resulting in an MB of -0.08 for all these experiments.

Tropical North Atlantic (see Dakar in Figure 7.2.2 and Table 7.2.1) region presents the best results of the AERONET comparison. Both experiments can reproduce the daily variability with correlation coefficients of 0.92 (0.82) respectively for o-suite (control). Over the Sahara (see Tamanrasset in Figure 7.2.2 and Table 7.2.1), o-suite shows better results than control with an increase of the correlation coefficient from 0.64 (control) to 0.70 (o-suite) keeping the MB at 0 for both experiments. The SDS-WAS Median Multi-model presents better results than o-suite with a correlation coefficient of 0.84 for Sahara although it underestimates the observations with an MB of -0.03. Otherwise, in the Eastern Sahara (see Zinder Airport in Figure 7.2.2 and Table 7.2.1), control presents better skill scores than o-suite with a correlation coefficient of 0.80 for control (closer to the SDS-WAS Median Multi-model) in comparison with 0.72 of o-suite. In the Sahel, o-suite presents strong underestimations (MB of -0.30, slightly higher than control with MB of -0.29) despite that the model can reproduce the observed daily variability (with a correlation value of 0.58 for o-suite and 0.47 for control).

In the North-Western Maghreb, o-suite can reproduce the daily variability of the AERONET observations than control (with correlation coefficients of 0.81 for o-suite, 0.82 for control and 0.77 for the SDS-WAS Median Multi-model) although it shows higher underestimations (with MB of -0.01 for o-suite and control).

In the Middle East (see Table 7.2.1 and in Kuwait University AERONET site in Figure 7.2.3), o-suite and control shows similar performance scores than o-suite with a correlation coefficient of 0.77 for o-suite and 0.76 for control and MB of -0.06 for both experiments. These results are slightly better than the SDS-WAS Multi-model (with a correlation coefficient of 0.79 and MB of -0.07).

Over long-range transport regions, the performance of o-suite is particularly limited over sub-Tropical North Atlantic region with correlation values of 0.30 (see Table 7.2.1 as well as Santa Cruz de Tenerife AERONET sites in Figure 7.2.2) achieving worth results than control (with a correlation coefficient of 0.35). This is a consequence of the low AOD concentration observed during this period in these AERONET sites. Both CAMS models present low correlation coefficients (between 0.49 and 0.55) in Western Iberian Peninsula and Western Mediterranean in comparison with better correlation coefficients in Iberian Peninsula and Central-Eastern Mediterranean (between 0.73 and 0.89) as it is shown in Table 7.2.1. The worth scores in Western Iberian Peninsula and Western Mediterranean are directly linked to an exceptional period of frequent precipitations and snow during this period.

Otherwise, the comparison of 48h and 72h forecasts for both CAMS experiments shows that the prediction is stable during the 3-days forecasts with correlation coefficients of 0.79 (0.72), 0.75 (0.73) and 0.73 (0.72) respectively to 24, 48 and 72h forecasts for all the sites for o-suite (control). In the Sahara region, the correlation coefficient (r) is better at 48h and 72h than forecast (see Table 7.2.2).

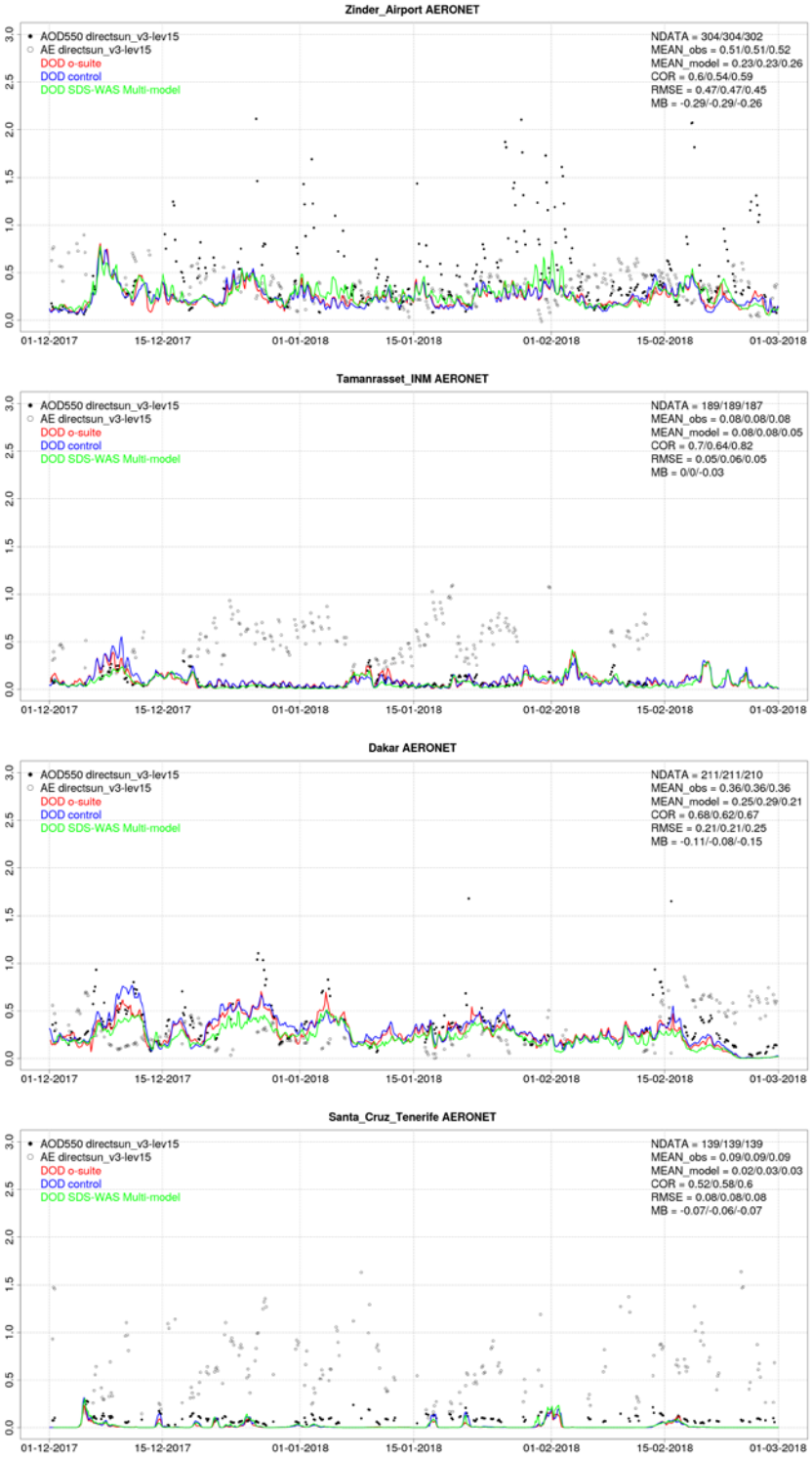


Figure 7.2.2: AOD from AERONET (black dots), DOD o-suite (red line), DOD control (blue line) and DOD Multimodel SDS-WAS Median (green line) for the study period over Zinder Airport (Eastern Sahara), Tamanrasset (Sahara), Dakar (Sahel) and Santa Cruz de Tenerife (sub-Tropical North Atlantic). Skill scores per each individual site and model (o—suite/control/SDS-WAS Multi-model) are shown in the upper right corner (NDATA: available 3-hourly values used for the calculations, MEAN observations, MEAN_model, COR, RMSE, MB).

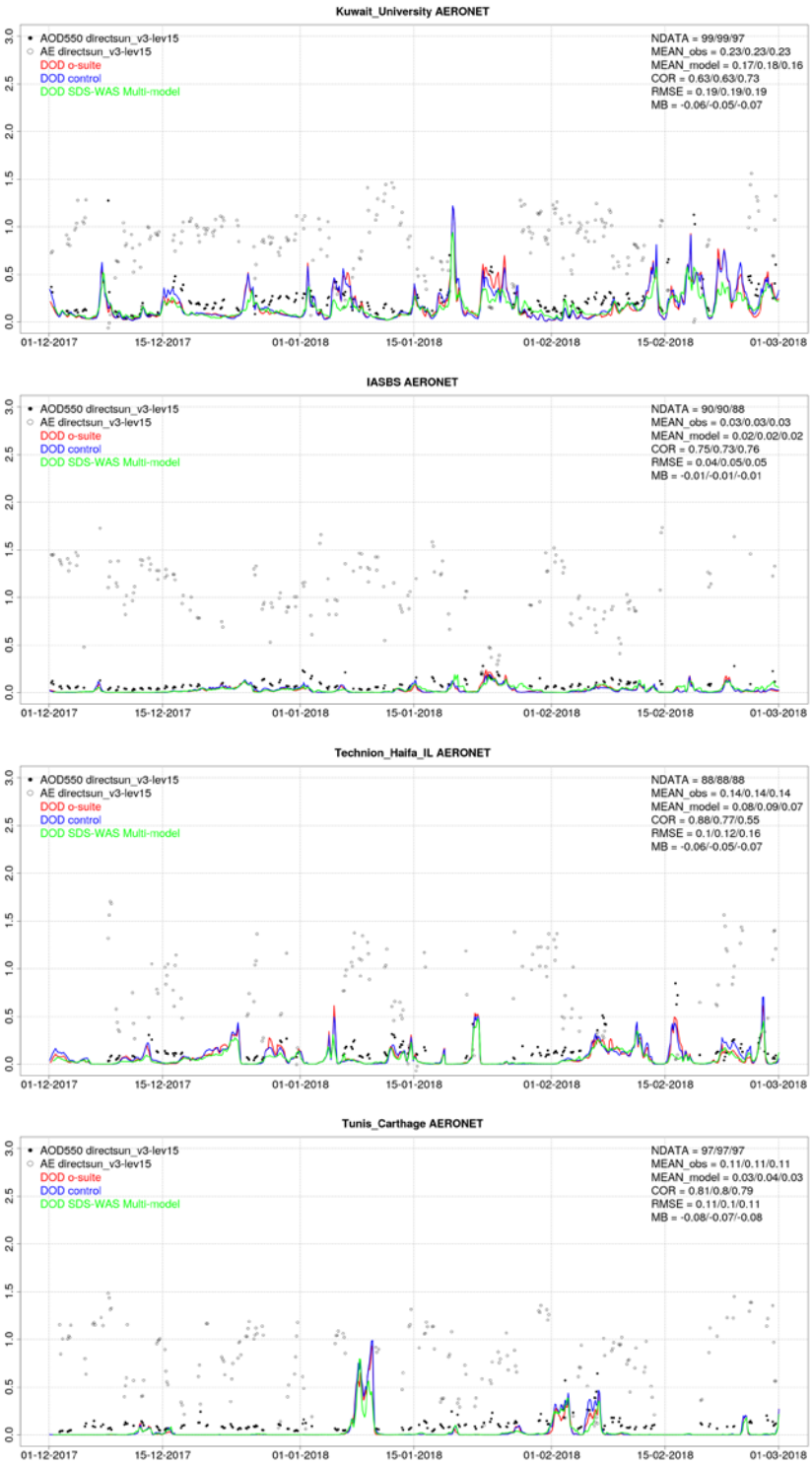


Figure 7.2.3: AOD from AERONET (black dots), DOD o-suite (red line), DOD control (blue line) and DOD Multimodel SDS-WAS Median (green line) for the study period over Kuwait University (Middle East), KAUST IABS (Middle East, Iran), Technion Haifa IL (Eastern Mediterranean) and Tunis Carthage (Central Mediterranean). Skill scores per each individual site and model (o—suite/control/ SDS-WAS Multi-model) are shown in the upper right corner (NDATA: available 3-hourly values used for the calculations, MEAN observations, MEAN_model, COR, RMSE, MB).

Table 7.2.1: Skill scores (MB, FGE, RMSE and r) of 24h forecasts for CAMS o-suite, CAMS control and SDS-WAS Multi-model Median for the study period, and the number of data (NDATA) used. Dust AOD (DOD) from AERONET is the reference.

| | | control | | | | o-suite DOD | | | | SDS-WAS Median DOD | | | |
|---|---|---|---|---|---|---|---|---|---|---|---|---|---|
| | NDATA | MB | FGE | RMSE | r | MB | FGE | RMSE | r | MB | FGE | RMSE | r |
| Sahara | 189 | 0.00 | 0.01 | 0.06 | 0.64 | 0.00 | 0.00 | 0.05 | 0.70 | -0.03 | -0.43 | 0.05 | 0.82 |
| Sahel | 1022 | -0.29 | -0.56 | 0.47 | 0.42 | -0.30 | -0.58 | 0.46 | 0.58 | -0.29 | -0.56 | 0.46 | 0.60 |
| Tropical North Atlantic | 74 | -0.10 | -0.88 | 0.16 | 0.89 | -0.10 | -0.90 | 0.15 | 0.92 | -0.16 | -1.12 | 0.22 | 0.92 |
| Subtropical North Atlantic | 190 | -0.04 | -0.41 | 0.07 | 0.35 | -0.05 | -0.45 | 0.08 | 0.30 | -0.04 | -0.42 | 0.08 | 0.36 |
| North Western Maghreb | 167 | -0.01 | 0.91 | 0.07 | 0.82 | -0.01 | 0.89 | 0.05 | 0.81 | -0.02 | 0.91 | 0.05 | 0.77 |
| Western Iberian Peninsula | 309 | -0.04 | -0.01 | 0.07 | 0.55 | -0.04 | -0.05 | 0.07 | 0.54 | -0.04 | -0.02 | 0.06 | 0.59 |
| Iberian Peninsula | 471 | -0.01 | 1.20 | 0.03 | 0.89 | -0.01 | 1.20 | 0.03 | 0.88 | -0.01 | 1.20 | 0.04 | 0.85 |
| Western Mediterranean | 1233 | -0.01 | 1.01 | 0.05 | 0.52 | -0.02 | 0.99 | 0.06 | 0.49 | -0.01 | 1.00 | 0.05 | 0.54 |
| Central Mediterranean | 793 | -0.03 | 0.61 | 0.10 | 0.81 | -0.03 | 0.58 | 0.10 | 0.83 | -0.04 | 0.59 | 0.11 | 0.82 |
| Eastern Mediterranean | 760 | -0.02 | 1.08 | 0.09 | 0.73 | -0.02 | 1.05 | 0.09 | 0.74 | -0.02 | 1.05 | 0.09 | 0.75 |
| Eastern Sahara | 121 | 0.03 | 0.62 | 0.07 | 0.80 | 0.01 | 0.54 | 0.07 | 0.72 | 0.00 | 0.47 | 0.06 | 0.77 |
| Middle East | 529 | -0.06 | 0.29 | 0.13 | 0.76 | -0.06 | 0.29 | 0.13 | 0.77 | -0.07 | 0.28 | 0.14 | 0.79 |

Table 7.2.2: Skill scores (MB, FGE, RMSE and r) of 48h and 72h forecasts for CAMS o-suite and CAMS control for the study period, and the number of data (NDATA) used. Dust AOD (DOD) from AERONET is the reference.

| | | 48h control | | | | 48h o-suite | | | | | 72h control | | | | 72h o-suite | | | |
|---|---|---|---|---|---|---|---|---|---|---|---|---|---|---|---|---|---|---|
| | NDATA | MB | FGE | RMSE | r | MB | FGE | RMSE | r | NDATA | MB | FGE | RMSE | r | MB | FGE | RMSE | r |
| Sahara | 185 | 0.00 | -0.01 | 0.05 | 0.70 | 0.00 | -0.04 | 0.05 | 0.73 | 181 | 0.00 | -0.03 | 0.05 | 0.73 | 0.00 | -0.05 | 0.05 | 0.76 |
| Sahel | 1014 | -0.29 | -0.57 | 0.47 | 0.43 | -0.30 | -0.60 | 0.48 | 0.51 | 1002 | -0.29 | -0.56 | 0.47 | 0.42 | -0.31 | -0.60 | 0.48 | 0.44 |
| Tropical North Atlantic | 74 | -0.10 | -0.88 | 0.15 | 0.90 | -0.10 | -0.89 | 0.16 | 0.89 | 71 | -0.09 | -0.84 | 0.16 | 0.88 | -0.09 | -0.84 | 0.16 | 0.88 |
| Subtropical North Atlantic | 187 | -0.04 | -0.40 | 0.08 | 0.35 | -0.04 | -0.43 | 0.08 | 0.33 | 187 | -0.04 | -0.37 | 0.08 | 0.36 | -0.04 | -0.39 | 0.08 | 0.34 |
| North Western Maghreb | 166 | 0.00 | 0.92 | 0.08 | 0.80 | -0.01 | 0.93 | 0.07 | 0.79 | 158 | -0.01 | 0.87 | 0.06 | 0.77 | -0.01 | 0.92 | 0.06 | 0.78 |
| Western Iberian Peninsula | 303 | -0.03 | 0.03 | 0.08 | 0.59 | -0.03 | 0.00 | 0.07 | 0.58 | 302 | -0.03 | 0.00 | 0.10 | 0.54 | -0.03 | -0.01 | 0.09 | 0.54 |
| Iberian Peninsula | 467 | -0.01 | 1.20 | 0.03 | 0.88 | -0.01 | 1.20 | 0.03 | 0.89 | 462 | -0.01 | 1.20 | 0.04 | 0.76 | -0.01 | 1.19 | 0.04 | 0.83 |
| Western Mediterranean | 1225 | -0.01 | 1.01 | 0.05 | 0.54 | -0.01 | 1.00 | 0.06 | 0.51 | 1217 | -0.01 | 1.01 | 0.06 | 0.47 | -0.01 | 1.00 | 0.06 | 0.47 |
| Central Mediterranean | 793 | -0.03 | 0.60 | 0.10 | 0.80 | -0.03 | 0.59 | 0.10 | 0.82 | 787 | -0.03 | 0.59 | 0.10 | 0.80 | -0.03 | 0.59 | 0.10 | 0.82 |
| Eastern Mediterranean | 744 | -0.02 | 1.07 | 0.10 | 0.69 | -0.02 | 1.05 | 0.10 | 0.69 | 738 | -0.02 | 1.07 | 0.10 | 0.69 | -0.02 | 1.05 | 0.10 | 0.70 |
| Eastern Sahara | 119 | 0.03 | 0.63 | 0.08 | 0.79 | 0.02 | 0.55 | 0.08 | 0.76 | 119 | 0.03 | 0.59 | 0.11 | 0.70 | 0.03 | 0.55 | 0.11 | 0.68 |
| Middle East | 524 | -0.06 | 0.29 | 0.14 | 0.73 | -0.07 | 0.28 | 0.14 | 0.75 | 519 | -0.07 | 0.28 | 0.14 | 0.74 | -0.07 | 0.26 | 0.14 | 0.75 |

## 7.3 Backscatter profiles

Technical specifications of data sources, evaluated parameters and methods are described in the observation characteristation report (Douros et al., 2017). In this section, the temporal and vertical variation of the backscatter coefficient (bsc) profiles are evaluated, statistically as bias, correlation, and standard deviation of o-suite '0001' and control run gsyg' vs ceilometers, and summarized in Taylor plots. Second topic is the reproduction of the planetary boundary layer (PBL), and thirdly, the representation of individual aerosol types is considered. Covariance plots of daily 2-D time-height sections serve for case studies and for development of a fractional skill score. The vertically integrated bsc is not in focus, because it reveals similar but less accurate information like AOD. As various hitherto case studies confirmed the reliability of the methodology our focus turns more towards evaluation metrics and interpretations aerosols representation in the model versions.

*Period Overview*

The model aerosol optical depth (AOD) and ceilometer overviews are used to select periods with significant aerosol plumes over Germany. Figure 7.3.1 shows the maximum AOD over Germany, separately for contributions of mineral dust (SD), sea salt (SS), carbonaceous matter (CM), black (BC) and organic carbon (OC), as well as sulfate (SU). Events in the DJF 2017/18 period have been discussed in previous reports, but are omitted in this report in favor of other topics:

- SD event on 08/09 Jan 2018
- elevated SS events due to stormy winter 2017/18 season

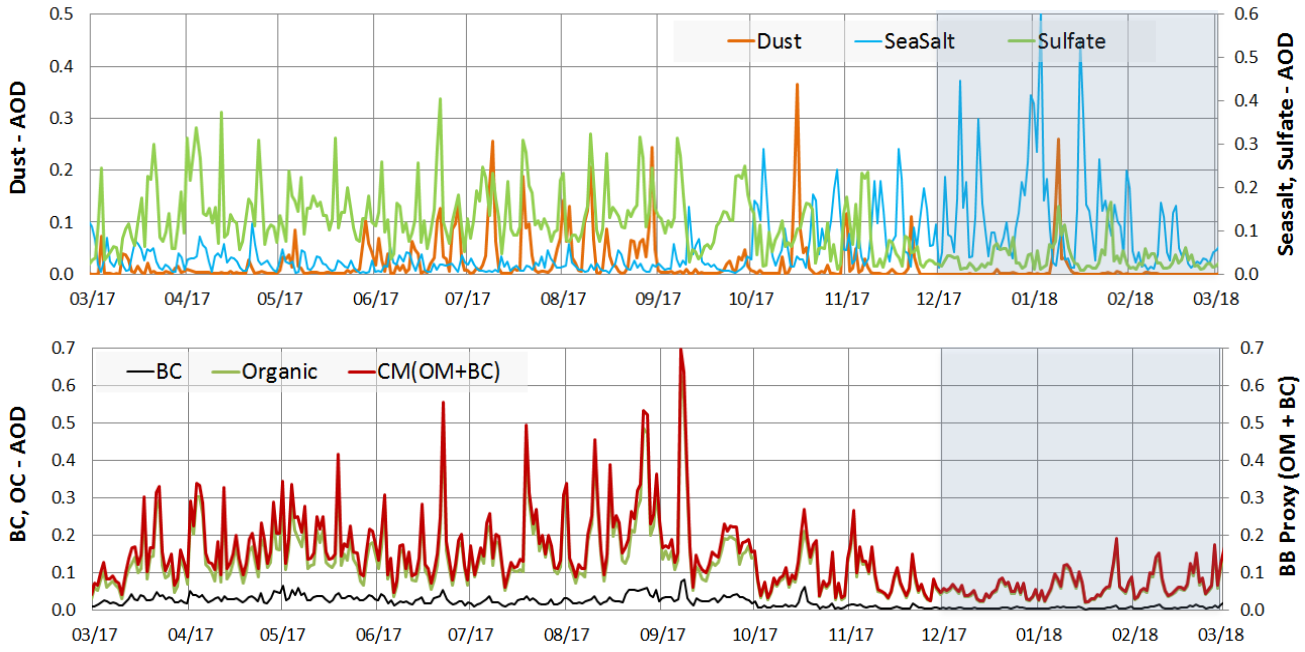


Figure 7.3.1: Maximum daily AOD over Germany for aerosols included in the IFS model from 03/2017 - 02/2018: sea salt (blue), dust (orange), sulfate (light green), black carbon (BC, black), organic matter (green), proxy for 'biomass burning' (as OC+BC - red). Note the different y-axes for the aerosol species.

Table 7.3.1: Correlation r, relative bias ($bsc_{model}/bsc_{ceilo}$) RB and modified normalized mean bias MNMB of osuite and control run vs ceilometer observations for 2017.

| | $r_{L40}$ | $r_{L45}$ | $r_{L50}$ | $RB_{L40}$ | $RB_{L45}$ | $RB_{L50}$ | $MNMB_{40}$ | $MNMB_{45}$ | $MNMB_{50}$ |
|---|---|---|---|---|---|---|---|---|---|
| **osuite** | 0.42 | 0.59 | 0.30 | 1.0 | 1.3 | 0.7 | 73 | 57 | -38 |
| **control** | 0.38 | 0.51 | 0.27 | 0.4 | 0.9 | 0.5 | -10 | -5 | -73 |

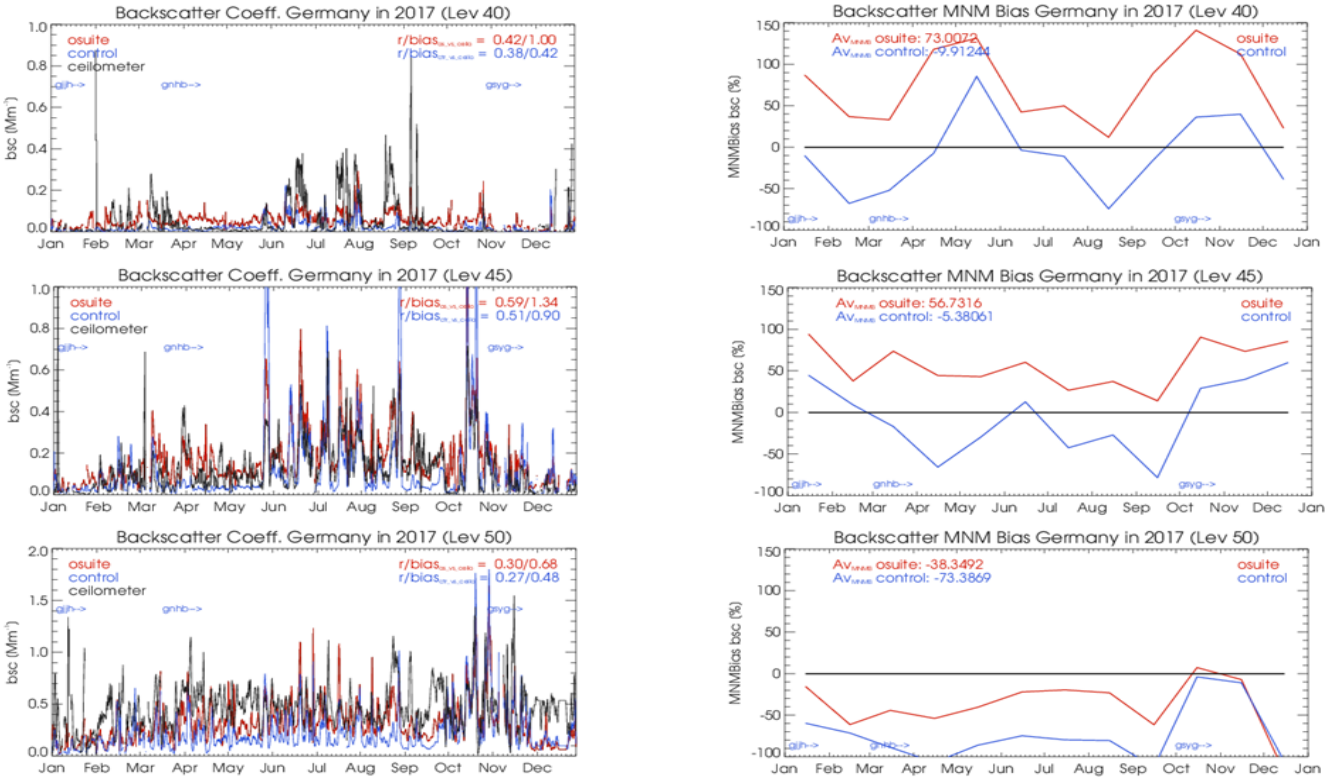


Figure 7.3.2: Variation of bsc at L40 (~4.3 km a.g.), L45 (~2.3 km a.g.), L50 (~1.0 km a.g.) during 2017. Each is averaged over 21 German ceilometer stations. The numbers are given in table 7.3.1.

*Temporal variation at selected model levels:*

Fig. 7.3.2 shows the temporal variation of bsc at different model levels (L40, L45, L50), averaged over 21 German ceilometer sites. The corresponding mean heights above ground are 4.3 km (L40), 2.3 km (L45), 1 km (L50). Pearson's r, relative bias (RB) as well as modified normalized mean biases (MNMB) at these model levels over the 2017 period are given in Table 7.3.1. Both runs exhibit a high bias in the FT and a low bias in the PBL. Owing to this opposite behavior, the best agreement is found near the top of the PBL, and so, owing to the seasonal variation of the PBL height, all metrics have a seasonal trend. Similar information, in a transposed way, is contained in the average vertical backscatter profiles in Figure 7.3.3. They also show that the assimilation (AOD) does not consistently improve the shape of the vertical profile.

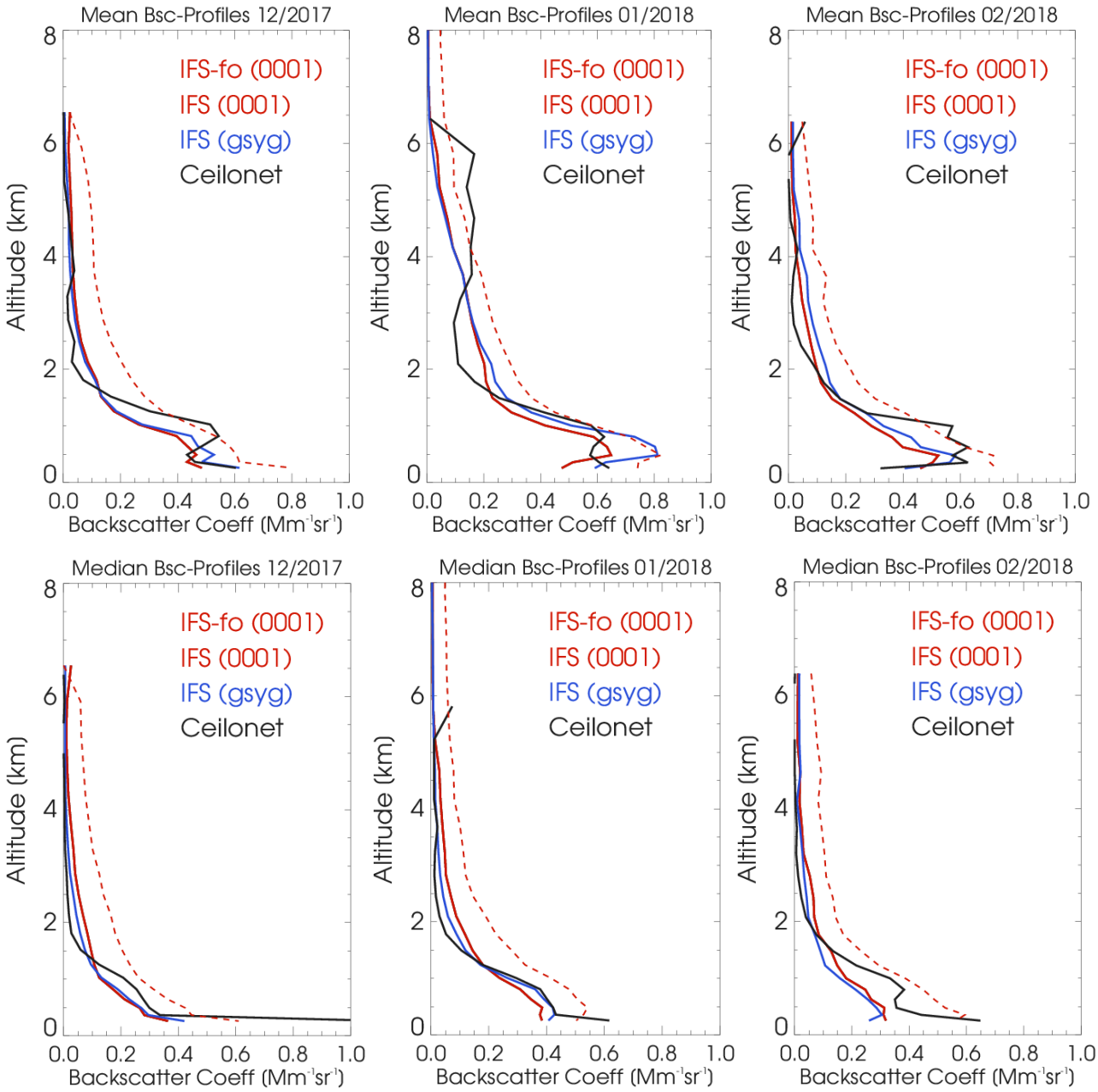


Figure 7.3.3: Monthly mean (upper panel) and median (lower panel) profiles of backscatter coefficients from osuite, control run gsyg, and ceilometers combined from 21 German stations in Dec 2017, Jan and Feb 2018. The profiles are partly contaminated by few remaining cloud artefacts.

*Mean profiles:*

Model bsc in the PBL are on average lower than observed (cf. Tab. 7.3.1), however more so in summer than in winter and very variable. While enhanced emissions of organic matter (OM) have been introduced in Jan 2017, nitrate and ammonia are still missing in the current model version, which contribute roughly 10-30% of aerosol mass (as $NO_3NH_4$ or $(NH_4)_2SO_4$) in the rural central European PBL. (According to pers. communication - S. Remy/G. Mann - nitrates and ammonium are ready in the current model and should get activated soon, maybe with the next update). Secondly, our forward operator (including mass→volume conversion) presently uses particle densities of the

pure materials, not taking into account that dry atmospheric particles are often porous (sponge-like, even fractal) with entrapped air owing to coagulation and variable internal mixing, and thus exhibit reduced bulk density. A high-biased particle density results in low-biased equivalent volume, and a corresponding underestimation of all optical properties, because these depend strongly on the particle size. Density reductions for accumulation mode particles, composed of hydrophilic and hydrophobic materials may be as high as a factor 1.5 (~1.3 for surface). Thirdly, the capping transport barrier at the PBL top is less effective in the model, diluting high PBL concentrations with clean FT air. Geometrically, however, the PBL height on average seems reasonable (cf. next section).

Monthly mean bsc profiles in the model roughly follow observations, except that the PBL top is too smooth (Fig 7.3.3) and the PBL too clean. The monthly mean bsc profiles suggest that the aerosol mass, added to the whole column by the assimilation (run 0001), results in overall higher aerosol load than in the control run (gsyg), but the assimilation fails to introduce a realistic step at the top of the PBL to lower values in the free troposphere (FT) as in the ceilometer profiles. Rather, the FT background is too high due to adding an assimilated portion there. This aerosol mass is missing in the PBL, yielding a too low amplitude (coded in the standard deviation) of the model compared to observations (reference) in the Taylor plots, too. The SD event around 8/9 Jan 2018 causes a low bias of the mean bsc profile while the median profiles (background) fit quite well. Highly polluted air from eastern Europe, continuously transported to Germany as of mid-Feb 18 is not captured by the model profiles.

*Planetary boundary layer height (BLH)*

Though definition, determination and evaluation of the BLH is challenging (and there is much discussion on how to do) we add a comparison (not evaluation!) of daily maximum Aerosol-BL and model-BL heights at the German ceilometer stations as proxies for the representation of THE planetary BLH, archived in MARS as parameter '159.128'. As explained in Douros et al. (2017), its information is coded in the measured aerosol gradient respective the modelled Richardson number (Ri > 0.25), which do not necessarily refer to the same atmospheric feature. Fig. 7.3.4 illustrates the steps to infer and compare BLH, including the large variability and the quality-control/interpretation issue. For the example day, 17 Jun 2017, the composite plot indicates little disturbance by clouds for the PBL diurnal cycle, the contour/bullet plot confirms the sanity of the approach and the time-series shows both, the reasonable median BLH (about few 100 m low bias) but also the tremendous variability, most of which should be removable by rigorous quality filtering, i.e. elimination of inapplicable days with multiple layers, clouds, fog, precipitation, missing aerosol gradients, e.g by injection of Saharan dust from the FT etc.

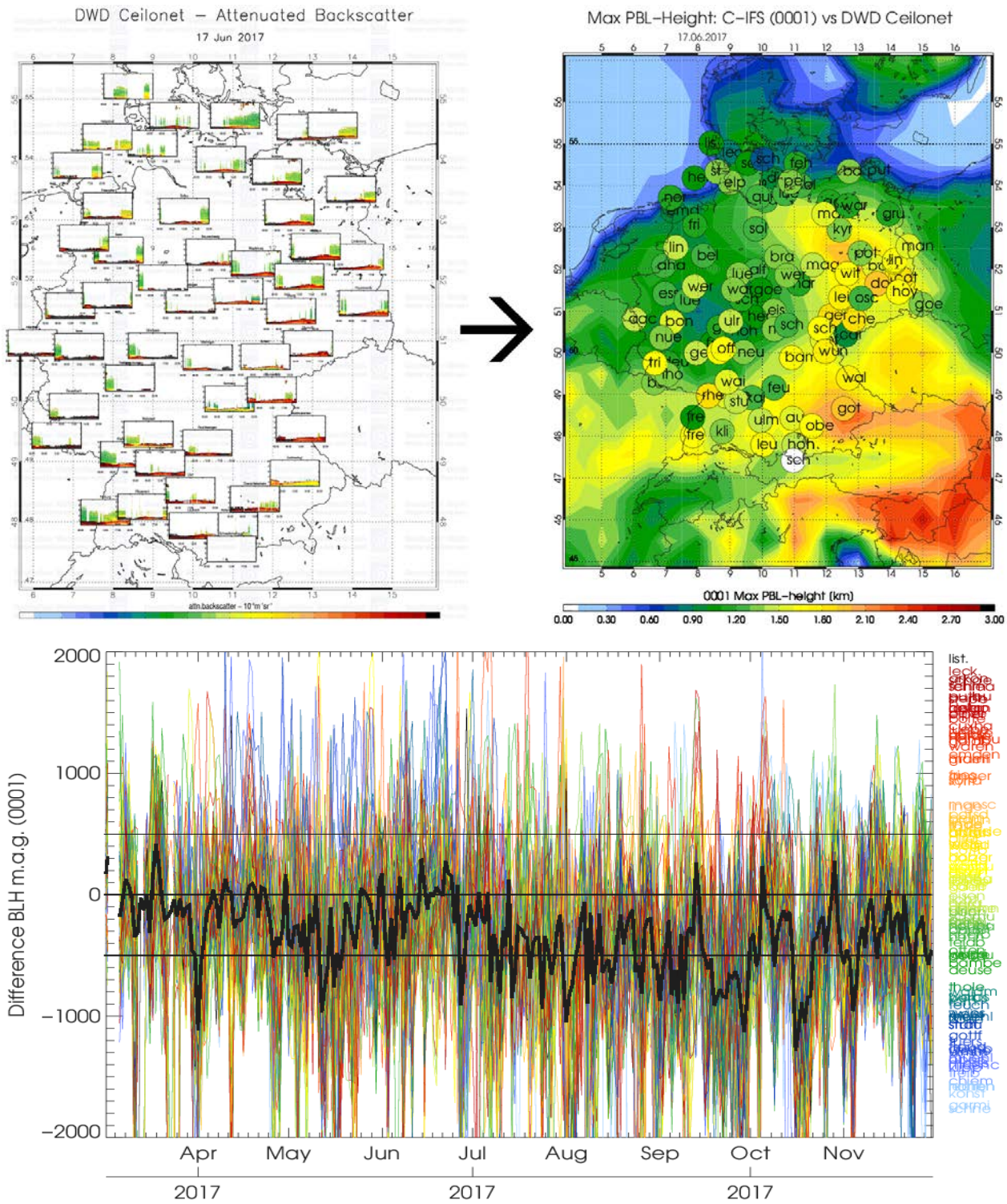


Fig. 7.3.4: Upper panel: Composite of ceilometer 2D time-height sections of attenuated backscatter over Germany and inferred daily maximum planetary boundary layer heights (color bullets) overlayed to model contour map of parameter z. Bottom: bias of Aerosol-BLH vs model-BLH for year 2017, inferred from >100 German ceilometer stations.

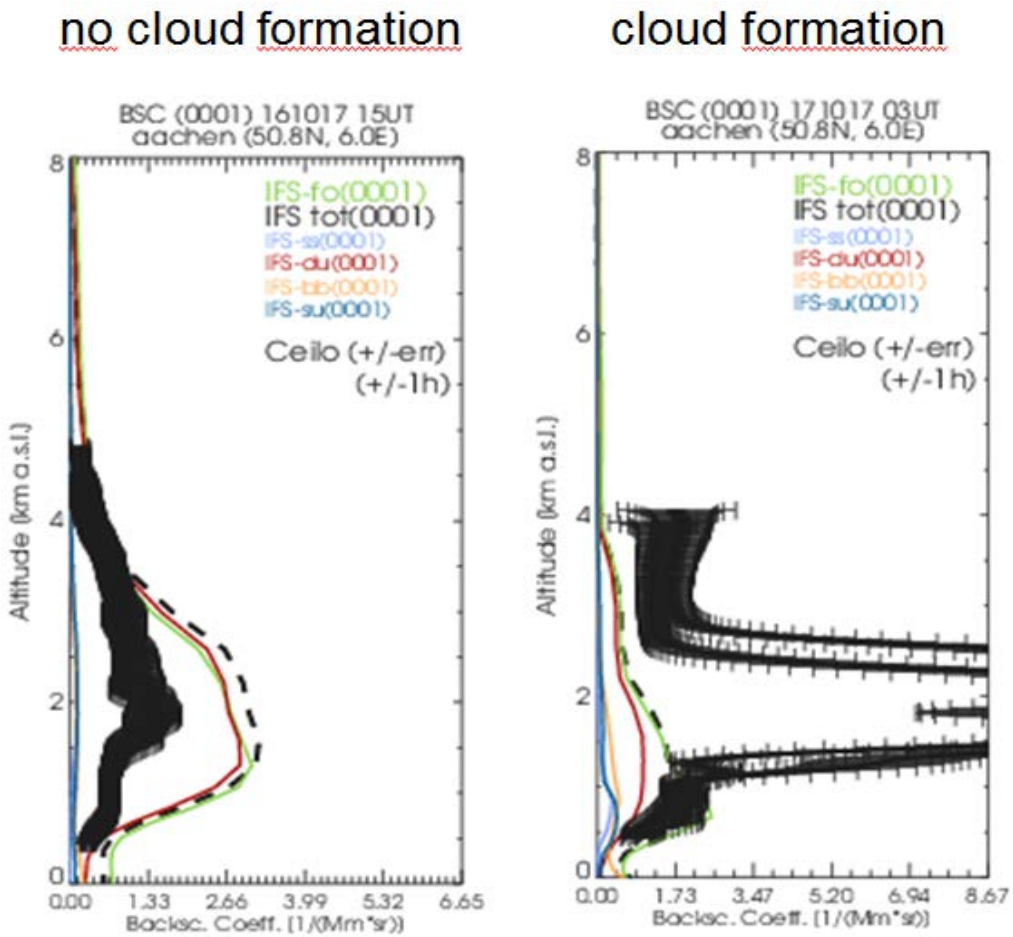


Figure 7.3.5: Profiles of backscatter coefficients from the ceilometer at Aachen on 16 and 17 Oct 2017, from the model and observations. The black dashed line is calculated with the DWD forward operator (FO), the green line using the ECMWF FO, namely, retrieving attenuated backscatter from ground from the MARS archive). Clouds formed in the SD air mass on 17 Oct, but not yet on 16 Oct 2018.

*Saharan Dust reproduction 16/17 Oct 2017 – dependency on observed reference*

Saharan dust events are generally reproduced and positioned fairly accurate in space and time, but the peak particle backscatter is often overestimated (cf. former reports and the typical example in Fig. 7.3.5). The case from 16/17 Oct 2017 was already discussed in the last NRT report, but shall be elaborated again to illustrate different information content of model evaluation w.r.t. backscatter-coefficients or mass concentrations. Though on both days, similar bsc are simulated by the model (largely dust), the observed bsc were less than half of those modelled, while on 17 Oct cloud formation dramatically increased the optical signal though most likely (as indicated shortly before and afterwards) the change of the dust load in terms of mass concentration was small.

Together with the considerable uncertainties imposed by hygroscopic growth BELOW saturation, this imposes a noticeable caveat on the interpretation of evaluation results where significant conversions are involved.

It is further shown, that for this dust example, the results achieved with the forward operator at ECMWF and with the one programmed by DWD, agree quite well. However, this is not always the case when other aerosol types dominate and particularly in presence of high relative humidity.

*Summary*

Backscatter coefficients are low-biased in the planetary boundary layer (PBL). Possible reasons are missing of ammonia and nitrate in the model (foreseen to be activated soon), assumption of too high particle densities (for pure compact materials) in the mass to backscatter conversion, and the lack of vertical transport barrier at the top of the PBL, causing dilution with free troposphere air. Free troposphere (FT) background backscatter coefficients are biased high, probably due to wrong re-distribution between PBL and FT. This is not fixed by the assimilation, which instead adds aerosol to the whole profile. The bsc bias on a specific level thus depends on its relative position w.r.t. to the BLH.

The SD plume (probably mixed with BB) spatial dispersion on 16 Oct 2017 closely matches the 3-D distribution observed by the German ceilometers. Though the total aerosol load likely does not change between both days, the model is high-biased by about a factor of 2 on 16 Oct, and seemly strongly low-biased on 17 Oct. This inconsistency is due to cloud formation on 17 Oct, which severely affects the optical properties and causes very high bsc signals. Heterogeneous condensation is not captured by the model.

The model BLH agrees reasonably (within few 100 m) with observations under favourable measurement conditions. Very often, however, meteorological conditions prevent formation, unambiguousness or detectability of the BLH or make the latter a challenge.

## 7.4 Aerosol validation over the Mediterranean

Three-hourly aerosol optical depth (AOD) and surface concentration (PM10 and PM2.5) from o-suite experiment and control experiment have been validated for the period 1 December 2017 – 28 February 2018 against AERONET direct-sun cloud-screened observations.

*Aerosol optical depth*

CAMS o-suite can reproduce the daily variability of AERONET observations. In Western, Central and Eastern Mediterranean, the correlation coefficient increase from 0.50, 0.66 and 0.63 to 0.59, 0.67 and 0.65, respectively for control and o-suite during winter (see the correlation coefficient by sites in Figure 7.4.1). Underestimations observed in the Mediterranean Basin in control are corrected in o-suite introducing overestimations in the whole Mediterranean Basin except in Italian sites. This results in an increase of MB from -0.02, -0.03 and 0 for control to 0.01, 0.01 and 0.01 for o-suite. The highest peaks on CAMS AOD simulations are linked to desert dust sources (see Palma de Mallorca, ETNA, Thessaloniki and IMS-METU-Erdemli AERONET sites in Figure 7.4.2). Dust activity was exceptional high over the Mediterranean during this winter. Different consecutive dust events were affecting the Mediterranean during end-January and early-February (see ETNA and Thessaloniki in Figure 7.4.2).

*Surface aerosol concentrations*

For winter, PM10 and PM2.5 results of CAMS o-suite and control show similar skill scores in comparison with EIONET observations (see Figure 7.4.3 and Figure 7.4.4) indicating the limited impact of the data assimilation at surface levels. From December to February, the modelled PM10/PM2.5 values are low (< 25 μg/m$^3$) except in the Mediterranean islands of Balears, Corsica and Cyprus (see Hospital Joan March and Venaco in Figure 7.4.4). At Hospital Joan March (in Western Mediterranean), these high PM10 and PM2.5 values (> 50 μg/m$^3$) are also observed in the EIONET observations although CAMS tends to overestimate the magnitude of these peaks that coincident with African dust intrusions. On the contrary, in Venaco, a PM10/PM2.5 maximum (> 200 μg/m$^3$) is predicted by both CAMS experiments on 5$^{th}$ January that it is not observed in the EIONET site (see Figure 7.4.4). This maximum aerosol peak has a primary contributor to maritime aerosols.

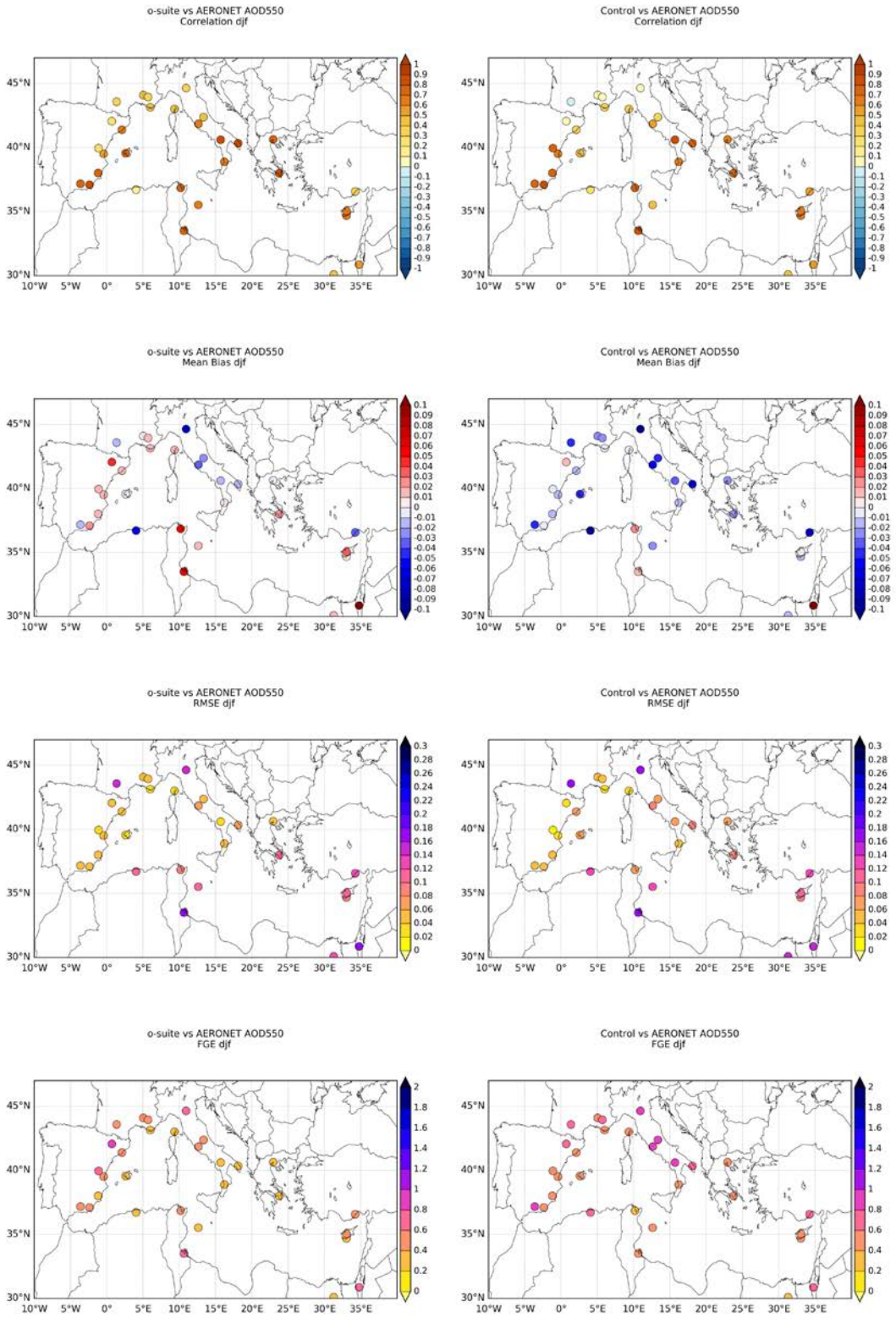


Figure 7.4.1: Skill scores (correlation coefficient, MB, RMSE and FGE) for 24-hour forecasts of CAMS o-suite and control for the study period. AOD from AERONET is the reference.

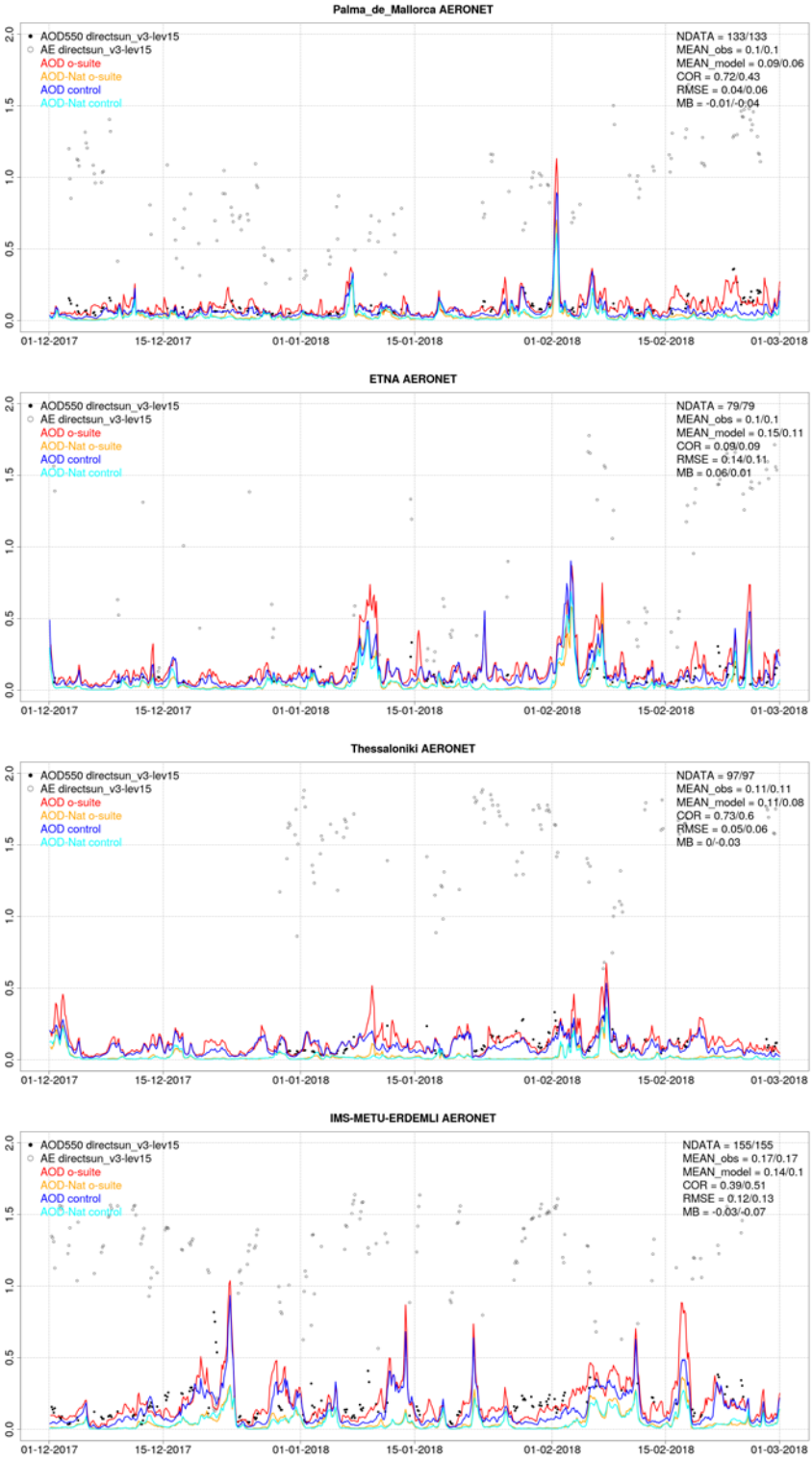


Figure 7.4.2: AOD from AERONET (black dot), AOD o-suite (red line), AOD control (blue line), AOD-Nat o-suite (orange line), AOD-Nat control (cyan line), for the study period over Palma de Mallorca (Spain), ETNA (Italy), Thessaloniki (Greece) and IMS-METU-Erdemli (Israel). AOD-Nat corresponds to the natural aerosol optical depth that includes dust and sea-salt. Skill scores per each individual site and model (o—suite/control) are shown in the upper right corner (NDATA: available 3-hourly values used for the calculations, MEAN observations, MEAN_model, COR, RMSE, MB).

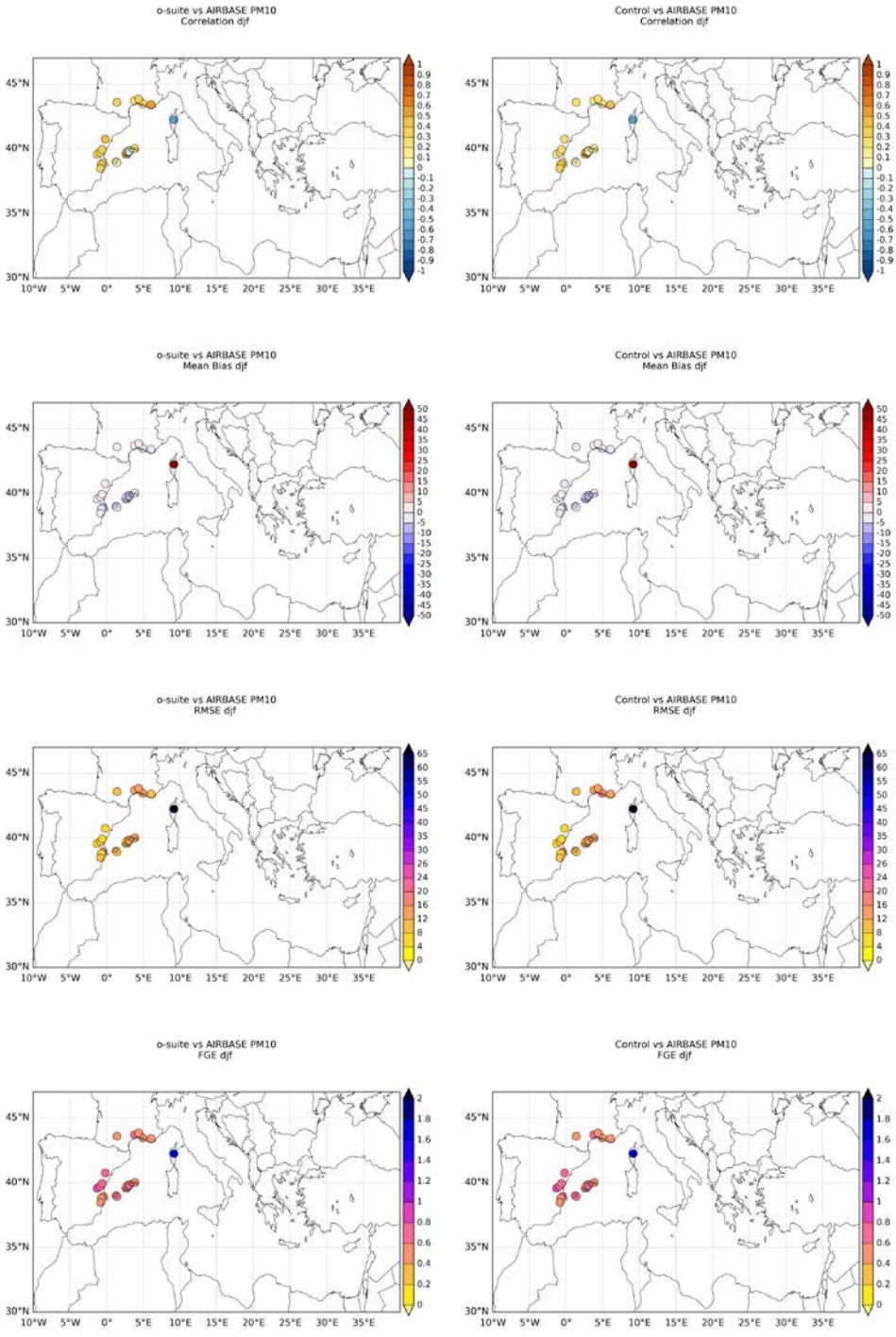


Figure 7.4.3: Skill scores (correlation coefficient, MB, RMSE and FGE) for 24-hour forecasts of CAMS o-suite and control for the study period. PM10 from Airbase are the reference. Only background suburban and rural available stations are displayed.

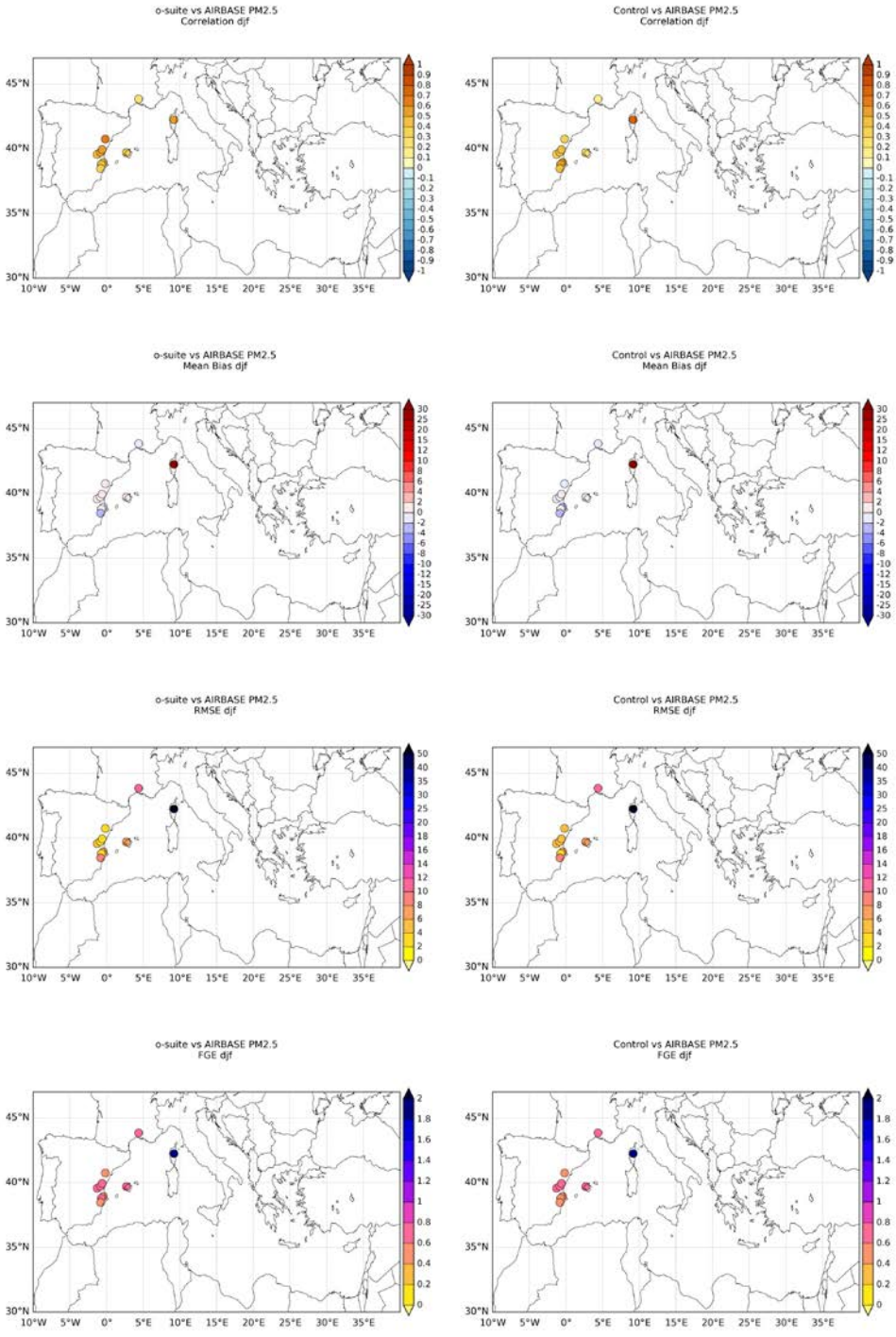


Figure 7.4.4: Skill scores (correlation coefficient, MB, RMSE and FGE) for 24-hour forecasts of CAMS o-suite and control for the study period. PM2.5 from Airbase are the reference. Only background suburban and rural available stations are displayed.

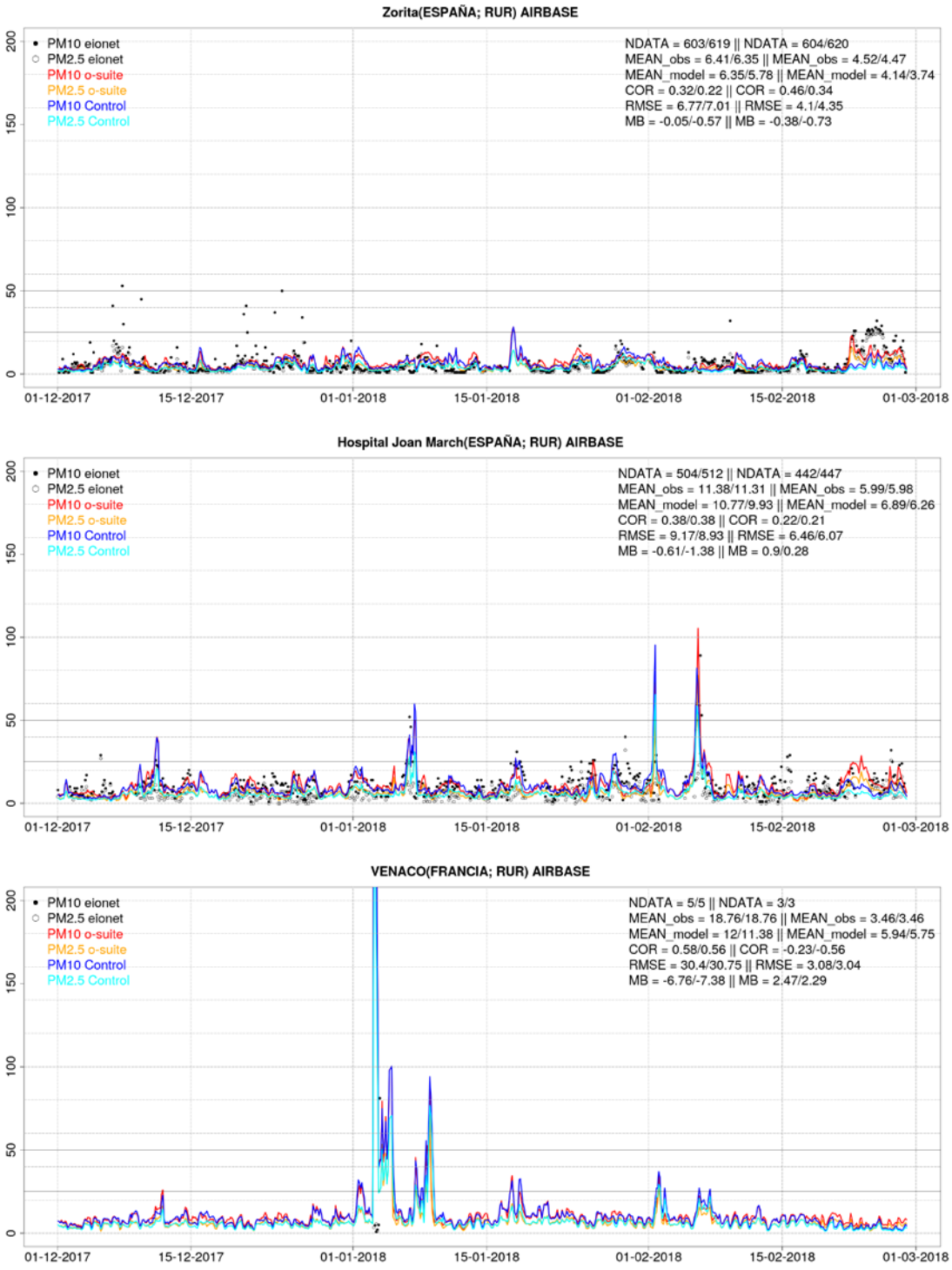


Figure 7.4.5: PM10 and PM2.5 Airbase observations (black and grey dots, respectively), PM10 and PM2.5 o-suite (red and orange lines, respectively) and PM10 and PM2.5 control (blue and cyan lines, respectively) for the study period over Alcudia (Balearic Islands, Spain) and Venaco (Corse, France). Skill scores per each individual site, model (o—suite/control) and PM10/PM2.5 are shown in the upper right corner (NDATA: available 3-hourly values used for the calculations, MEAN observations, MEAN_model, COR, RMSE, MB).

# 8. Stratosphere

## 8.1 Validation against ozone sondes

In this section, we present the results of the stratospheric ozone evaluation against ozone soundings from the NDACC, WOUDC, NILU and SHADOZ databases. The sondes have a precision of 3-5% (~10% in the troposphere for Brewer Mast) and an uncertainty of 5-10%. For further details see Cammas et al. (2009), Deshler et al. (2008) and Smit et al (2007). Model profiles of the o-suite are compared to balloon sondes measurement data of 44 stations for the period January 2013 to November 2017 (please note that towards the end of the validation period fewer soundings are available). As C-IFS-CB05 stratospheric composition products beyond $O_3$ in the o-suite is not useful we provide only a very limited evaluation of the control experiment. A description of the applied methodologies and a map with the sounding stations can be found in Eskes et al. (2016). Both runs, the o-suite and the control run, show MNMBs mostly within the range ±12%, for all regions and months (some exceptions with MNMBs of up to ±18% for single months in the high latitude regions). Figure 8.1.1. shows the results for the period February 2017 to February 2018.

Fig. 8.1.2 compares the averaged profiles in each region during January 2018. The vertical distribution of stratospheric ozone is quite well represented for all regions by the o-suite, with little overestimation in all latitude bands (MNMBs between -3 to 12% for DJF).

Except for the tropical region, the control run shows a strong overestimation of stratospheric ozone in the upper stratosphere, and an underestimation between 40hPa (Arctic 100 hPa) and 300 hPa.

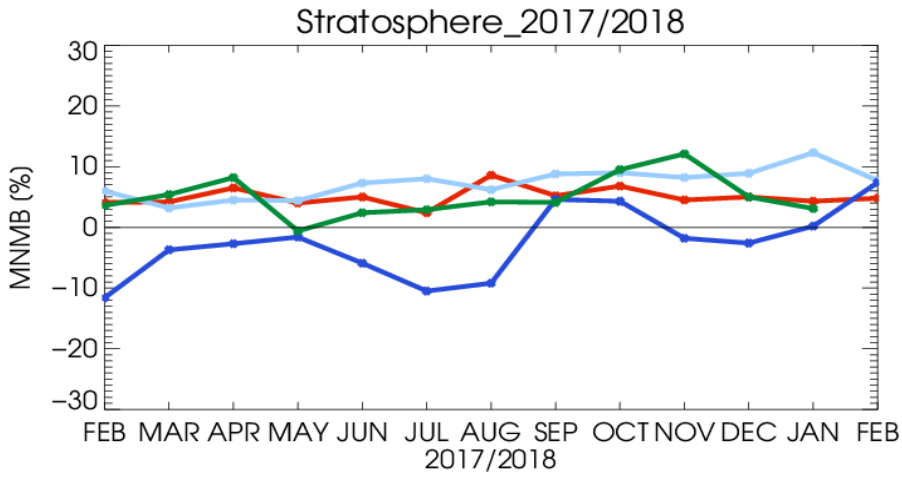


Figure 8.1.1: MNMBs (%) of ozone in the stratosphere from the o-suite against aggregated sonde data in the Arctic (light blue), Antarctic (dark blue) northern midlatitudes (red) and tropics (green).

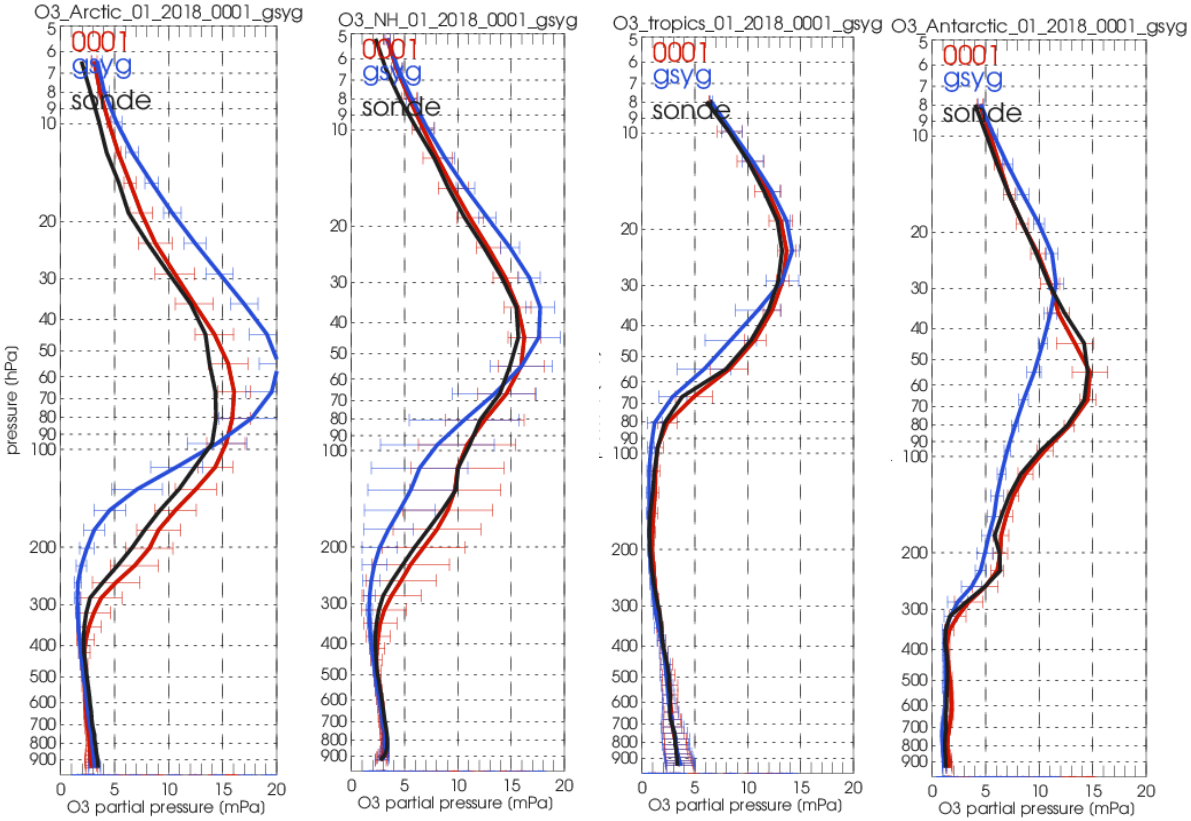


Figure 8.1.2: Comparison between mean $O_3$ profiles (units: mPa) of o-suite (red), and control (blue) in comparison with observed $O_3$ sonde profiles (black) for January 2018 for the various latitude bands: Arctic, NH-mid latitudes, Tropics and Antarctic.

## 8.2 Validation against observations from the NDACC network (MWR, LIDAR)

***UVVIS stratospheric columns***

Since the start of the CAMS27 project, the number of UVVIS Zenith ozone measurements have increased on NDACC. Currently fifteen sites provided data in the recent quarter allowing for a representative picture on the latitude dependence of the model data.

The systematic uncertainty of the UVVIS measurements is typically 5%, hence the relative biases for all sites for the o-suite (AN and 1d FC) are within the uncertainty ranges. The control run shows a sign change of the bias between the northern and southern hemisphere, see Figure 8.2.1.

The correlations between the sites and the model are presented in the Taylor diagrams in Fig 8.2.2. Again the Eureka station (nr 2) can be ignored from the plots because of the low measurements. Comparing the Taylor diagrams of the control and o-suite AN model shows the posivitive effect of assimilation. From the Taylor diagram for the o-suite (left), the Tropical stations (Izana, Reunion and Baura) are the stations whose correlation with the o-suite AN model is lowest (≤.9, left diagram) and where the std of the difference between model and measurement is highest (>0.6*std(model)). This is probably due to a numerical artefact because the ozone concentration is much less variable at the tropics which has an impact on the numerical interpretation of the computation of the correlation and the difference relative to the std of the model time series.

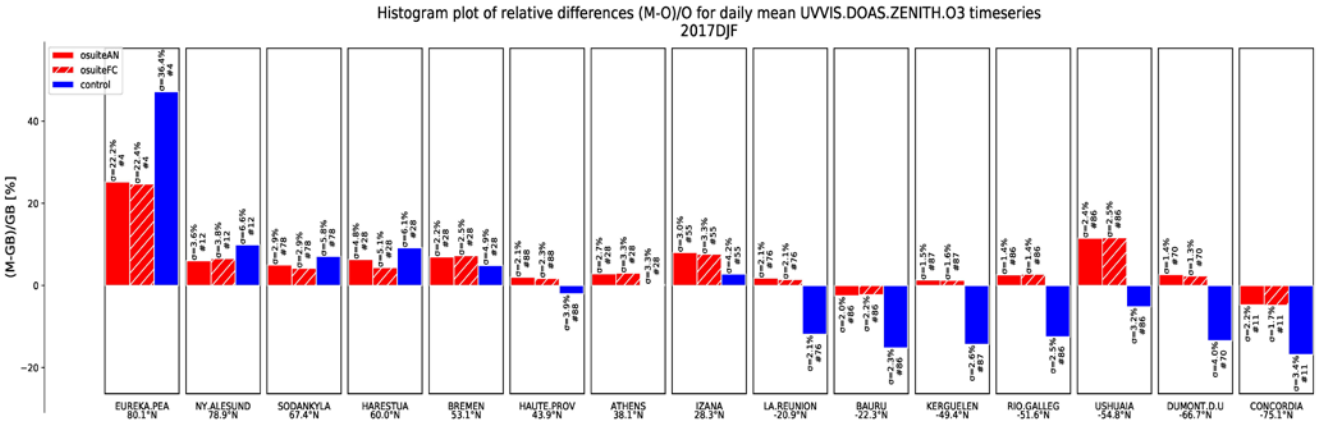


Figure 8.2.1: Relative biases during quarter DJF 2017 - 2018 for 15 UVVIS stations measuring stratospheric ozone columns with ZENITH measurement geometry (stations sorted with decreasing latitude). The relative bias of the control run is reversed when transitioning from the Northern to the Southern Hemisphere. The number of measurements at Eureka is limited, and the bias should be discarded.

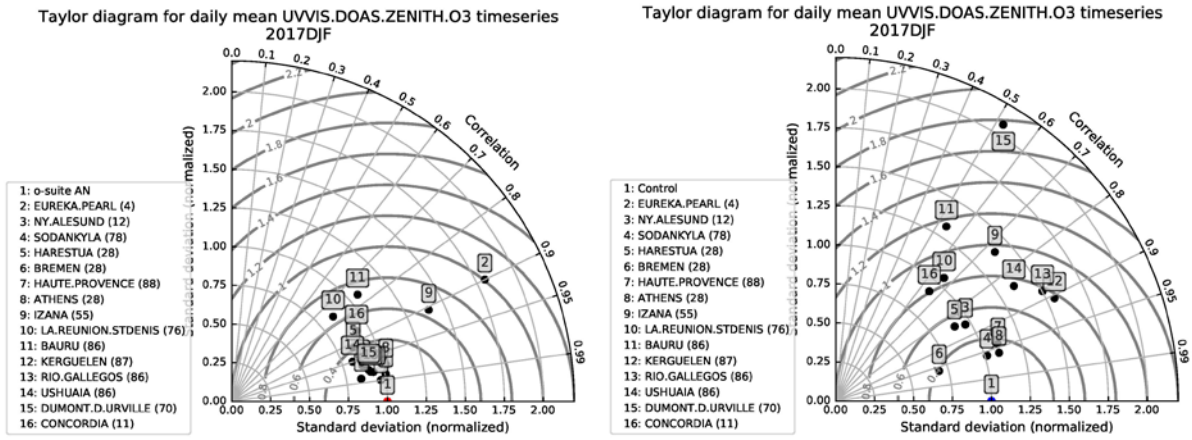


Figure 8.2.2: Taylor diagrams relating the standard deviations for the model and GB time series and their correlation. All time series are normalized such that the std of the model is 1. The increased correlation of all sites between control and o-suite shows the positive effect of assimilation.

### *Profile comparison using LIDAR and MWR*

In this section we present a comparison between the CAMS o-suite and control run models against MWR and LIDAR observations from the NDACC network. A detailed description of the instruments and applied methodologies for all NDACC instruments can be found in the Annex 2 and at http://nors.aeronomie.be. MWR (microwave) at Ny Alesund (79°N, 12°E, Arctic station) and Bern (47°N, 7°E, northern midlatitude station). LIDAR at Observatoire Haute Provence (OHP), France (43°N, 5.7°E, altitude 650m) and Hohenpeissenberg, Germany (47°N, 11°E, altitude 1km).

From table 8.2.1, the upper stratospheric partial column bias at Bern during Sept . 2015 –Dec. 2017 is nearly vanishing (uncertainty on the partial column is 6%). At Ny Alesund, o-suite overestimates the stratospheric ozone concentration with more than 10% during SON/DJF/MAM and the bias vanishes during summer JJA.

Table 8.2.1: Seasonal relative mean bias (MB, %), standard deviation (STD, %) of the partial (upper stratospheric 25km – 65km) ozone column for the considered period and number of observations used (NOBS), compared to NDACC microwave observations at Ny Alesund and Bern (mean bias and stddev in %).

| | | MAM | | | JJA | | | SON | | | DJF | | |
|---|---|---|---|---|---|---|---|---|---|---|---|---|---|
| | | MB | stddev | nobs | MB | stddev | nobs | MB | stddev | nobs | MB | stddev | nobs |
| o-suite | Ny.Ale | 11.73 | 7.93 | 191 | 0.17 | 5.61 | 218 | 10.28 | 9.32 | 195 | 18.29 | 5.80 | 71 |
| | Bern | -3.30 | 2.24 | 635 | -6.10 | 6.59 | 496 | -4.76 | 2.80 | 638 | -3.41 | 3.96 | 598 |

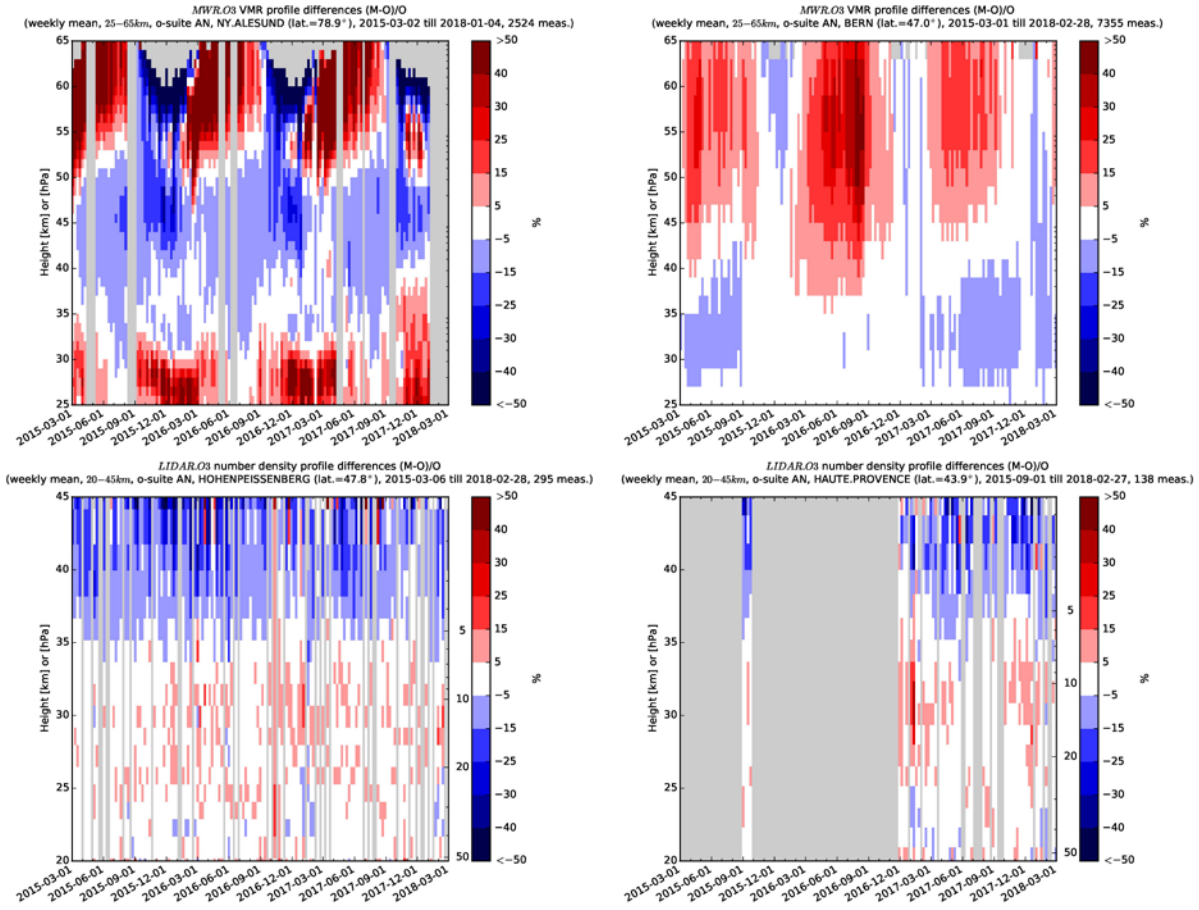


Figure 8.2.3: Comparison of the weekly mean profile bias between the $O_3$ mixing ratios of o-suite and the NDACC station at Ny Alesund, Bern, Hohenpeissenberg and OHP. For the LIDAR stations, the measurement uncertainty above 35km is comparable to the observed profile bias.

In MAM-JJA 2015-2017, both MWR stations observe a significant (i.e. comparable to the measurement uncertainty) overestimation of the upper stratospheric/mesospheric ozone content, and the converse is seen during autumn and winter SON-DJF, underestimating up to -30% (Ny Alesund), see also Figure 8.2.3. At BERN the difference between o-suite and MWR at 25-35km is negligible since Sept 2015 (compared to the MWR profile uncertainty).

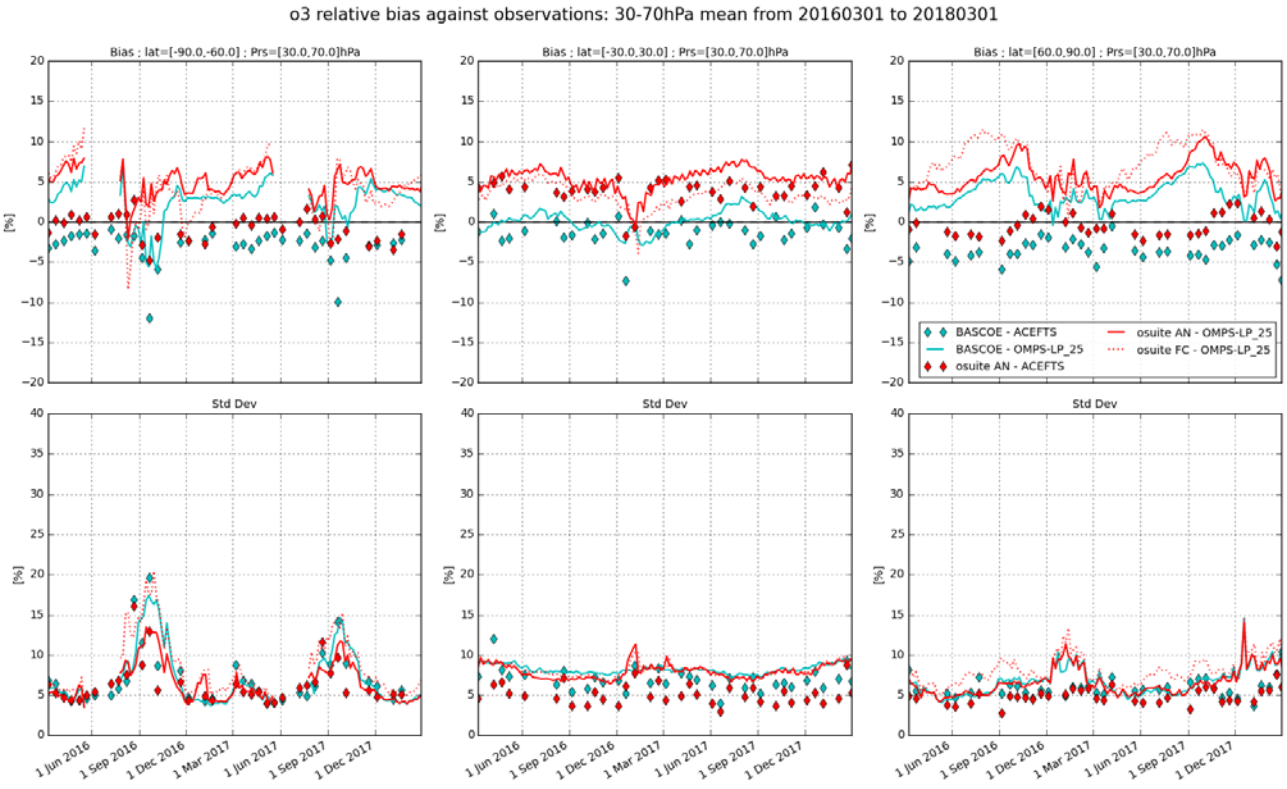


Figure 8.3.1: Time series comparing models to observations for the period 2016-03-01 to 2018-03-01 in the middle stratosphere (30-70hPa averages): o-suite analyses vs OMPS-LP (red, solid), o-suite forecasts 4$^{th}$ day vs OMPS-LP (red, dotted), o-suite analyses vs ACE-FTS (red markers), BASCOE vs OMPS-LP (cyan, solid) and BASCOE vs ACE-FTS(cyan markers). Top row, normalized mean bias (model-obs)/obs (%); bottom row, standard deviation of relative differences (%).

At OHP and Hohenpeissenberg (LIDAR), the o-suite slightly overestimates the observed ozone (<10%) between 25km and 35km. The uncertainty on the LIDAR concentration increases with altitude and above 35km the observed differences are comparable to the measurement uncertainty (>10%, see http://nors.aeronomie.be/projectdir/PDF/NORS_D4.2_DUG.pdf)

## 8.3 Comparison with dedicated systems and with observations by limb-scanning satellites

This section compares the output of the o-suite for the last period with observations by limb-scanning satellite instruments, using the methodology described by Lefever et al. (2015). We also include the comparisons for the o-suite 4$^{th}$ day forecasts (96h to 120h) of stratospheric ozone. These forecasts are represented by dotted lines in the figures.

All datasets are averaged over all longitudes and over the three most interesting latitude bands for stratospheric ozone: Antarctic (90°S-60°S), Tropics (30°S-30°N) and Arctic (60°N-90°N). In order to provide global coverage, the two mid-latitude bands (60°S-90°S and 60°N-90°N) are also included in some comparisons with satellite observations.

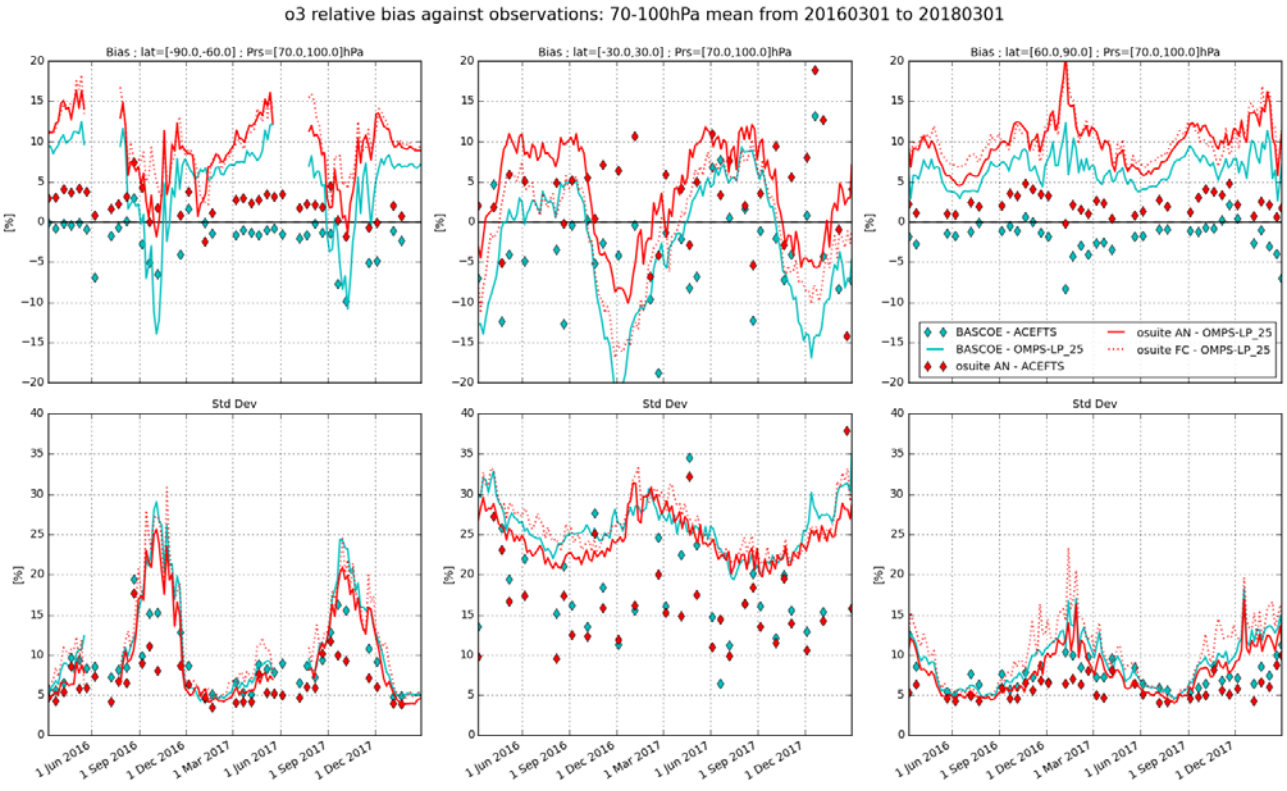


Figure 8.3.2: Time series comparing models to observations for the period 2016-03-01 to 2018-03-01 in the lower stratosphere (70-100hPa averages): o-suite analyses vs OMPS-LP (red, solid), o-suite forecasts 4$^{th}$ day vs OMPS-LP (red, dotted), o-suite analyses vs ACE-FTS (red markers), BASCOE vs OMPS-LP (cyan,solid) and BASCOE vs ACE-FTS(cyan markers). Top row, normalized mean bias (model-obs)/obs (%);bottom row, standard deviation of relative differences (%).

In this section, we use on one hand the version 2.5 of OMPS-LP (i.e. the Limb Profiler) and the version 3.6 of ACE-FTS. For reference, we include also the BASCOE analyses which are very constrained by the AURA MLS offline profiles.

Figure 8.3.1 and Figure 8.3.2 present, in the upper row, the timeseries over the last 24 months of the bias of the o-suite against the two satellite measurements for respectively two regions of the lower stratosphere and UTLS (30-70hPa and 70-100hPa); the bottom row of the figures shows the standard deviation of the differences and can be used to evaluate the random error in the analyses.

Compared to OMPS-LP in the 30hPa to 70hPa region, there is a systematic overestimation by the o-suite: up to 8% in the South polar region and in the tropics and up to 12% in the North polar region. Compared to OMPS-LP in the 70hPa to 100hPa region, the North polar bias increases up to 20% at various periods, while the variability of the bias is much stronger in the South polar region; the tropics exhibits a strong seasonal variation for the bias, with a high variability indicated by the standard deviation.

The agreement with ACE-FTS is much better: the bias is generally within ±5%, except in the tropics for 70hPa to 100hPa region, where the standard deviations indicate less reliable results.

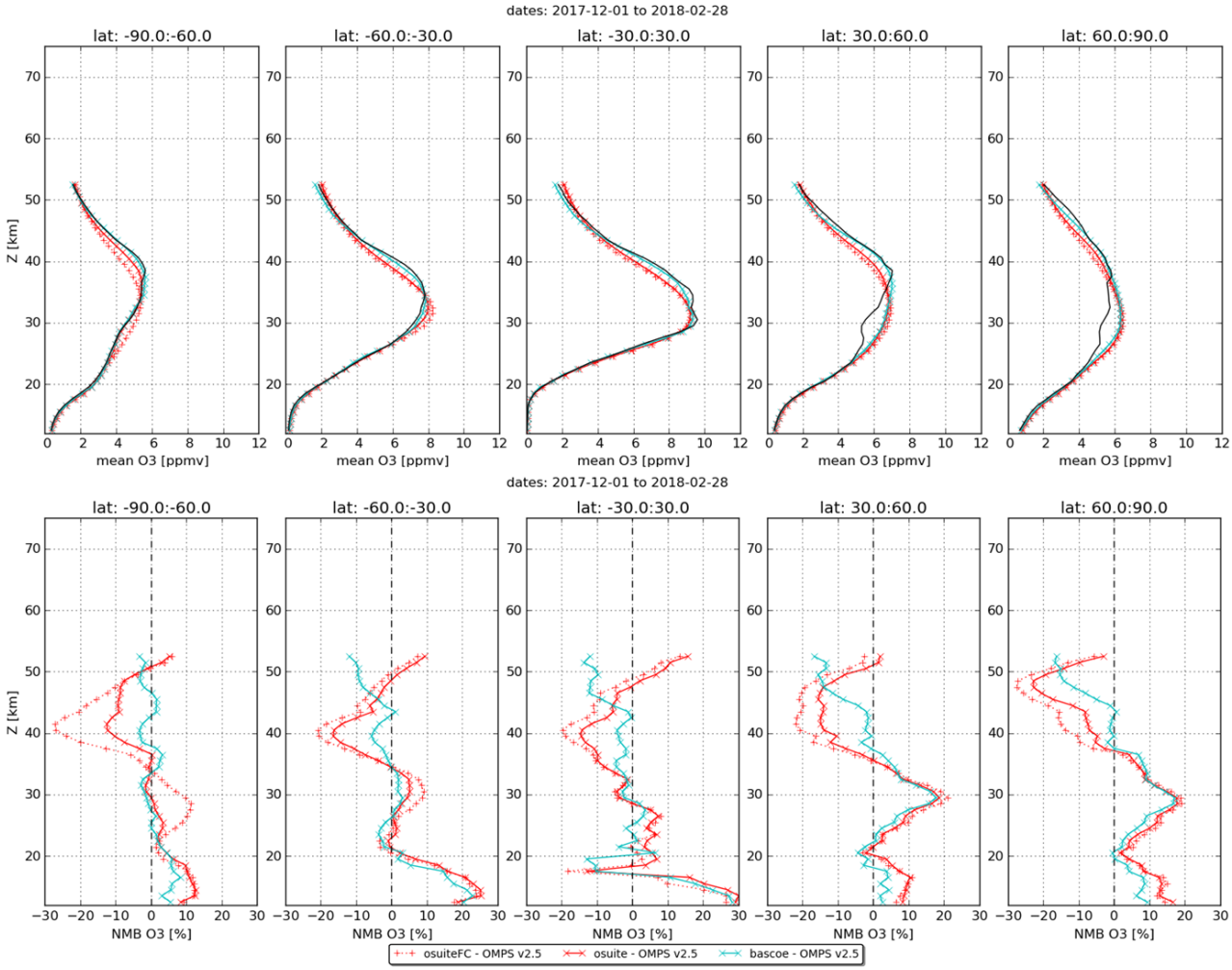


Figure 8.3.3: Mean value expressed in partial pressure (top) and normalized mean bias (bottom) of the ozone profile between o-suite analyses (red, solid), o-suite forecasts 4th day (red, dotted) and BASCOE (cyan line) with OMPS-LP v2 observations for the period September 2017 to November 2017.

The bias of BASCOE against the satellite observations for the considered regions is systematically lower, but follows a similar evolution as the o-suite.

Figure 8.3.3 and Figure 8.3.4 display vertical profiles of the relative biases between the o-suite or BASCOE and the satellite measurements. The difference is averaged over the most recent 3-month period considered in this validation report, i.e. December 2017 to March 2018.

The OMPS-LP profiles present a notch which is absent in the ACEFTS or MLS profiles (at around 30km for the north midlatitude and north polar region). Outside these anomalous zones, the relative bias between o-suite and OMPS-LP is <±10% between 18km and 35km (18km and 45km for BASCOE).

The negative bias above 40km is confirmed by the ACEFTS profiles, otherwise there is a good agreement in the middle and lower stratosphere.

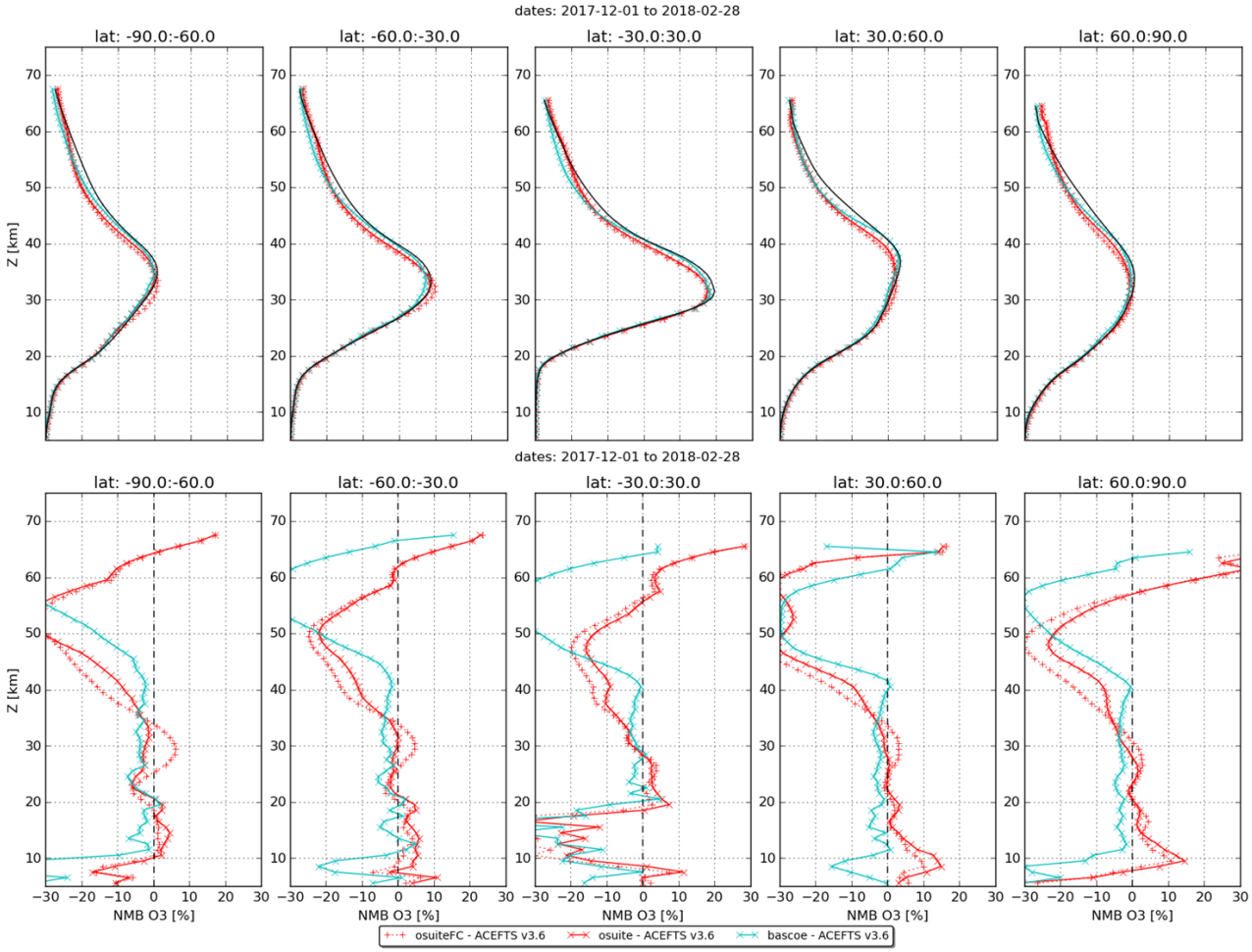


Figure 8.3.4: Mean value expressed in partial pressure (top) and normalized mean bias (bottom) of the ozone profile between o-suite analyses (red, solid), o-suite forecasts 4th day (red, dotted) and BASCOE (cyan line) with ACE-FTS observations for the period September 2017 to November 2017.

It must be noted that the different instruments have a variety of spatial and temporal coverage: for a 3 month period and over the latitude bands considered, OMPS and Aura MLS (not shown) provide daily data with more than 40000 valid profiles, while ACE-FTS provides around 750 profiles in the polar region and 150 profiles in the tropics.

## 8.4 Stratospheric $NO_2$

In this section, nitrogen dioxide from SCIAMACHY/Envisat satellite retrievals (IUP-UB v0.7) and GOME-2/MetOp-A satellite retrievals (IUP-UB v1.0) are used to validate modelled stratospheric $NO_2$ columns. Monthly mean stratospheric $NO_2$ columns from SCIAMACHY and GOME-2 have relatively small errors on the order of 20% in the tropics and in mid-latitudes in summer and even lower errors at mid-latitudes in winter. As the time resolution of the saved model files is rather coarse and $NO_x$ photochemistry in the stratosphere has a large impact on the $NO_2$ columns at low sun, some uncertainty is introduced by the time interpolation at high latitudes in winter.

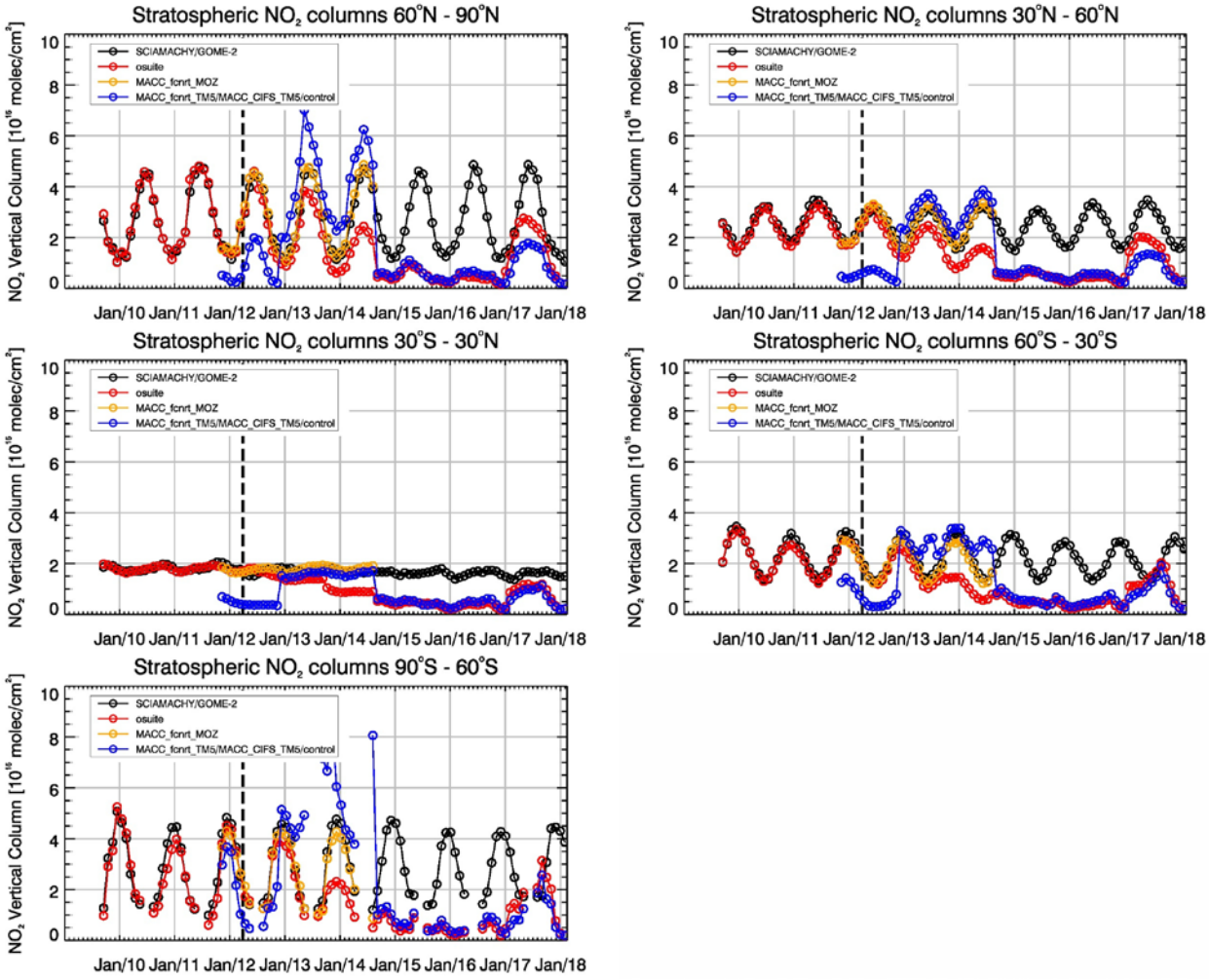


Figure 8.4.1: Time series of average stratospheric NO2 columns [1015 molec cm-2] from SCIAMACHY (up to March 2012) and GOME-2 (from April 2012) compared to model results for different latitude bands. See text for details. The blue line shows MACC_fcnrt_TM5 from November 2011 to November 2012, MACC_CIFS_TM5 results from December 2012 until August 2014 and control results from September 2014 onwards (the model run without data assimilation is termed control since Sep 2014). The vertical dashed black lines mark the change from SCIAMACHY to GOME-2 based comparisons in April 2012.

In this section, nitrogen dioxide from SCIAMACHY/Envisat satellite retrievals (IUP-UB v0.7) and GOME-2/MetOp-A satellite retrievals (IUP-UB v1.0) are used to validate modelled stratospheric $NO_2$ columns. Monthly mean stratospheric $NO_2$ columns from SCIAMACHY and GOME-2 have relatively small errors on the order of 20% in the tropics and in mid-latitudes in summer and even lower errors at mid-latitudes in winter. As the time resolution of the saved model files is rather coarse and $NO_x$ photochemistry in the stratosphere has a large impact on the $NO_2$ columns at low sun, some uncertainty is introduced by the time interpolation at high latitudes in winter.

As shown in Figure 8.4.1, amplitude and seasonality of satellite stratospheric $NO_2$ columns are poorly modelled with CB05-based chemistry runs including the more recent versions of the o-suite. The significant differences between observations and CB05 chemistry runs, i.e. a strong underestimation of satellite retrievals by models, can be explained by the missing stratospheric chemistry for these model versions. The only constraint on stratospheric $NO_x$ is implicitly made by

fixing the $HNO_3/O_3$ ratio at the 10 hPa level. This assumption, in combination with the changing model settings for stratospheric $O_3$ for control compared to MACC_CIFS_TM5, may explain some of the jumps we see in stratospheric $NO_2$. In any of these runs the stratospheric $NO_2$ is poorly constrained. It clearly indicates that stratospheric $NO_2$ in the latest versions of the o-suite is not a useful product and should be disregarded. However, model simulated values increased with the last upgrade of the osuite in February 2017, so that simulations are now closer to the satellite observations, especially for northern hemisphere latitude bands where seasonality seems to be reproduced (in contrast to the Southern Hemisphere where seasonality is not reproduced) by the new o-suite apart from the pronounced underestimation. O-suite values are larger than the control since February 2017 at all latitude bands.

Comparison of the o-suite from July 2012 until August 2014 with the other model runs and satellite observations shows that the previous version of the o-suite stratospheric $NO_2$ columns have a systematic low bias relative to those from MACC_fcnrt_MOZ and satellite observations for all latitude bands. For example, o-suite values are a factor of 2 smaller than satellite values between 60°S to 90°S for October 2013. Best performance was achieved with the MOZART chemistry experiments without data assimilation (MACC_fcnrt_MOZ, running until September 2014), especially northwards of 30°S. Details on the $NO_2$ evaluation can be found at: http://www.doas-bremen.de/macc/macc_veri_iup_home.html.

# 9. Validation results for greenhouse gases

This section describes the NRT validation of the pre-operational, high resolution forecast of $CO_2$ and $CH_4$ from 1st February 2017 to 1st March 2018 based on observations from 15 surface stations. Over this period the high resolution forecast corresponds to the experiments *ghqy*, see also Sec. 2.1.3. The same experiment is used for the validation of $CO_2$ and $CH_4$ simulations using ICOS surface data and TCCON total column data.

## 9.1 $CH_4$ and $CO_2$ validation against ICOS observations

Figures 9.1.1 and 9.1.2 show the $CO_2$ and $CH_4$ comparisons at four stations in South hemisphere (Amsterdam I.), North hemisphere (Mace Head, Trainou tall tower) and in the tropics (Lamto). The best agreement is obtained at the two north hemisphere sites for both $CO_2$ and $CH_4$. This is due particularly to the good representation of the wintertime pollution events observed regularly at MHD and TRN. The timing of those synoptic events are very well simulated even if their amplitudes are generally underestimated by 1 to 4% for $CO_2$. At the remote station of AMS, in South hemisphere, the model overestimates the amplitude of the seasonal $CO_2$ variation by ±1 ppm (±0.025%). At the same station, the CH4 concentrations are in pretty good agreement with the model until February 2017, when the model starts to diverge from the observations up to -2% (-40 ppb). At the tropical station of Lamto, the model show a poor correlation coefficient for CO2 ($r^2$=0.3). For $CH_4$ we observe a better correlation ($r^2$=0.5) but the model systematically underestimates the observed variabilities at synoptic and seasonal scales with a bias between -2% and -6%.

The figure 9.1.3 presents the annual metrics for all surface stations based on comparisons of the daily means mole fractions, with a distinction between measurements/simulation obtained for daytime (12-16hr local time) and nighttime (00-04hr local time). There is a significant improvement of the performance of the model when looking exclusively at daytime time series, especially for $CO_2$. The poorest correlation coefficients (lower than 0.6) for CO2 and CH4 are generally observed at tropical stations (CHC, GUY, LTO, RUN, STD) during nighttime. This feature can be explained by the more challenging landscape surroundings the monitoring sites. Tropical stations like LTO and GUY are located in places characterized by very strong biospheric sources. RUN and STD sites, both located on La Réunion Island are mountain/coastal sites with very strong emissions heterogeneity. In addition the infrastructure of the tropical sites is not as developed as in Europe where tall towers have been erected as part of ICOS in order to minimize the influence of local emissions. For the three tall towers (OHP, OPE, TRN) we see an improvement of the $CO_2$ correlation coefficient, and a decrease of the bias especially during nighttime, when going from the lowest to the highest sampling lines. For $CH_4$ there is much less differences between the different sampling levels of the towers. The two mountain station located in France (PDM, PUY) display even higher correlation coefficients. They sample free tropospheric air masses most of the time, which is an easier case for the atmospheric model.

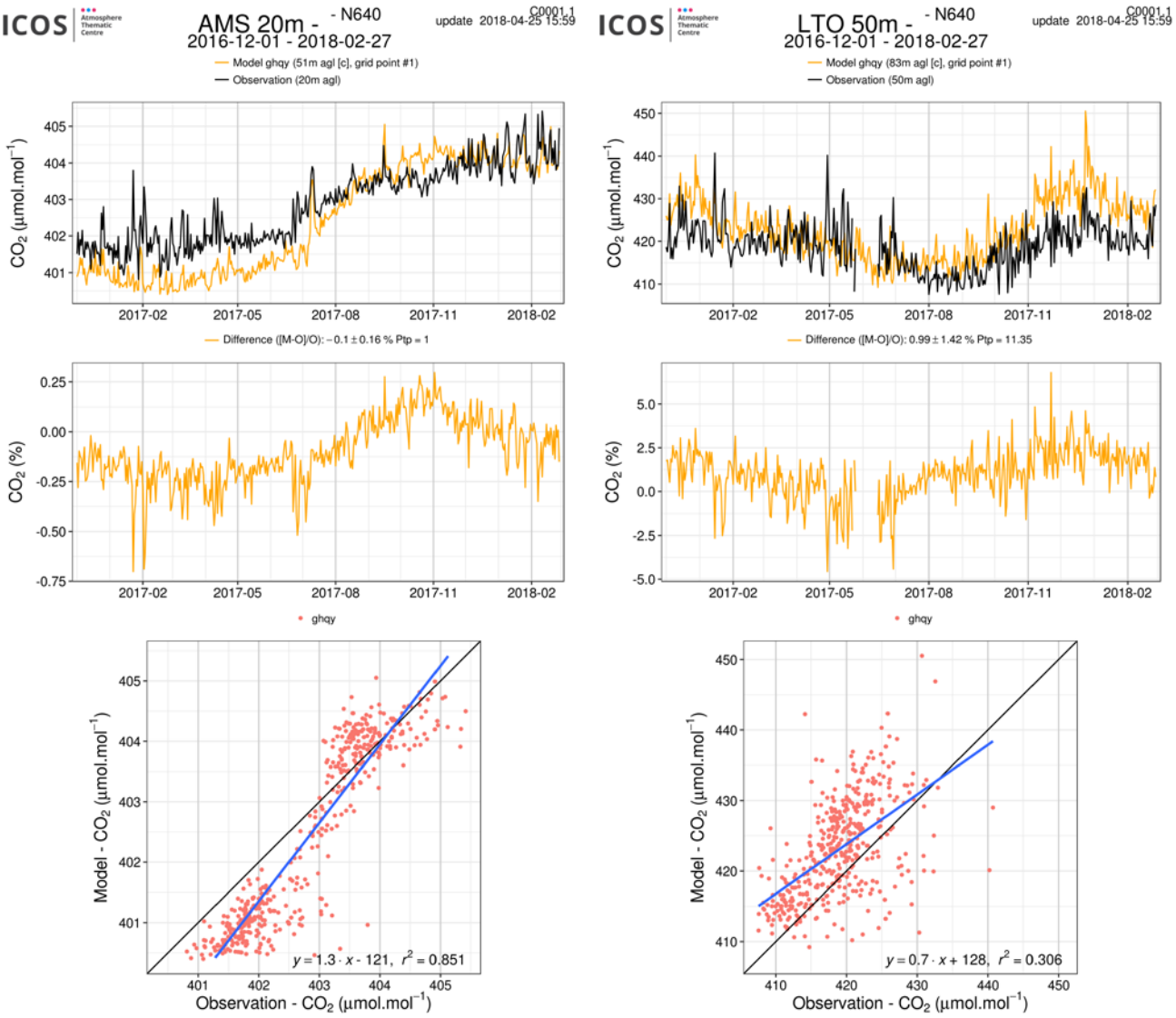
ICOS
AMS 20m - N640
2016-12-01 - 2018-02-27
update 2018-04-25 15:59
C0001.1
Model ghqy (51m agl [c], grid point #1)
Observation (20m agl)
CO2 (µmol.mol−1)
Difference ([M-O]/O): −0.1 ± 0.16 % Ptp = 1
CO2 (%)
ghqy
Model - CO2 (µmol.mol−1)
Observation - CO2 (µmol.mol−1)
y = 1.3 · x - 121, r2 = 0.851
ICOS
LTO 50m - N640
2016-12-01 - 2018-02-27
update 2018-04-25 15:59
C0001.1
Model ghqy (83m agl [c], grid point #1)
Observation (50m agl)
CO2 (µmol.mol−1)
Difference ([M-O]/O): 0.99 ± 1.42 % Ptp = 11.35
CO2 (%)
ghqy
Model - CO2 (µmol.mol−1)
Observation - CO2 (µmol.mol−1)
y = 0.7 · x + 128, r2 = 0.306

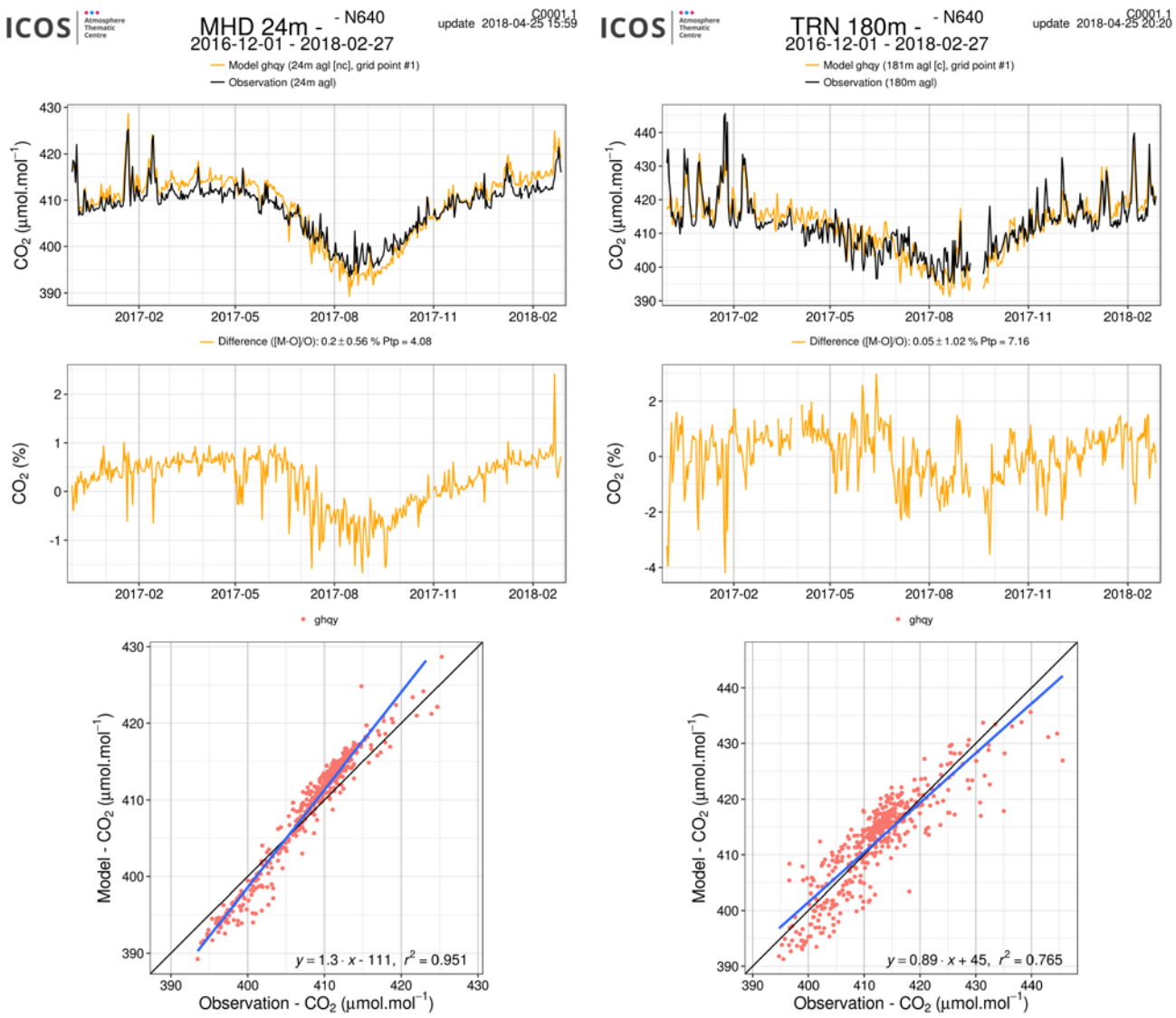


Figure 9.1.1: Above: Comparison of $CO_2$ daily means observed (black) and simulated (orange) at four stations (Amsterdam I., Mace Head, Lamto and Trainou tall tower). Middle: differences of the observations minus the simulations. Below: Linear fit between observations and simulations.

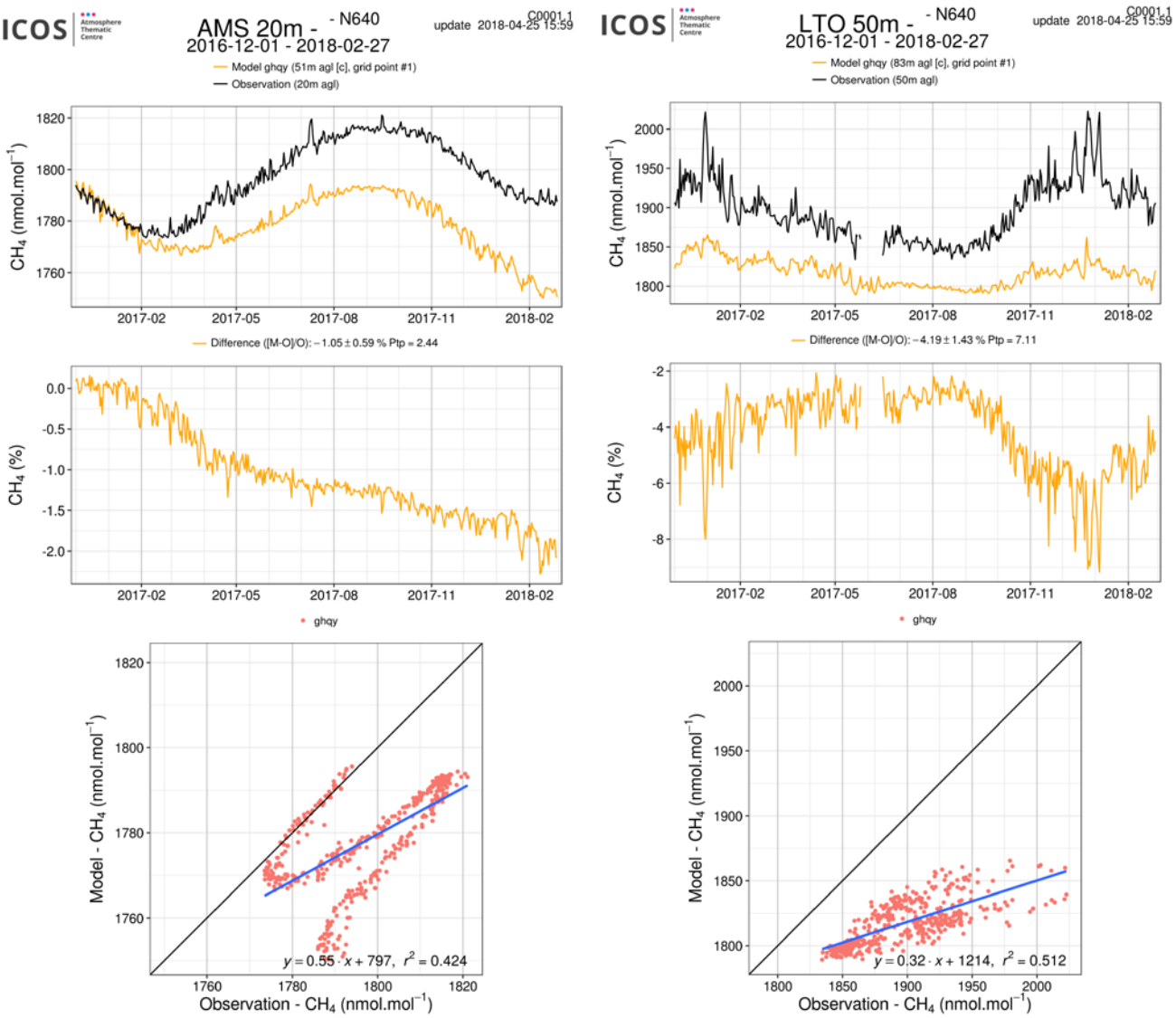
ICOS
AMS 20m - N640
2016-12-01 - 2018-02-27
update 2018-04-25 15:59
C0001.1
Model ghqy (51m agl [c], grid point #1)
Observation (20m agl)
CH4 (nmol.mol−1)
Difference ([M-O]/O): −1.05 ± 0.59 % Ptp = 2.44
CH4 (%)
ghqy
Model - CH4 (nmol.mol−1)
Observation - CH4 (nmol.mol−1)
y = 0.55 · x + 797, r2 = 0.424
ICOS
LTO 50m - N640
2016-12-01 - 2018-02-27
update 2018-04-25 15:59
C0001.1
Model ghqy (83m agl [c], grid point #1)
Observation (50m agl)
CH4 (nmol.mol−1)
Difference ([M-O]/O): −4.19 ± 1.43 % Ptp = 7.11
CH4 (%)
ghqy
Model - CH4 (nmol.mol−1)
Observation - CH4 (nmol.mol−1)
y = 0.32 · x + 1214, r2 = 0.512

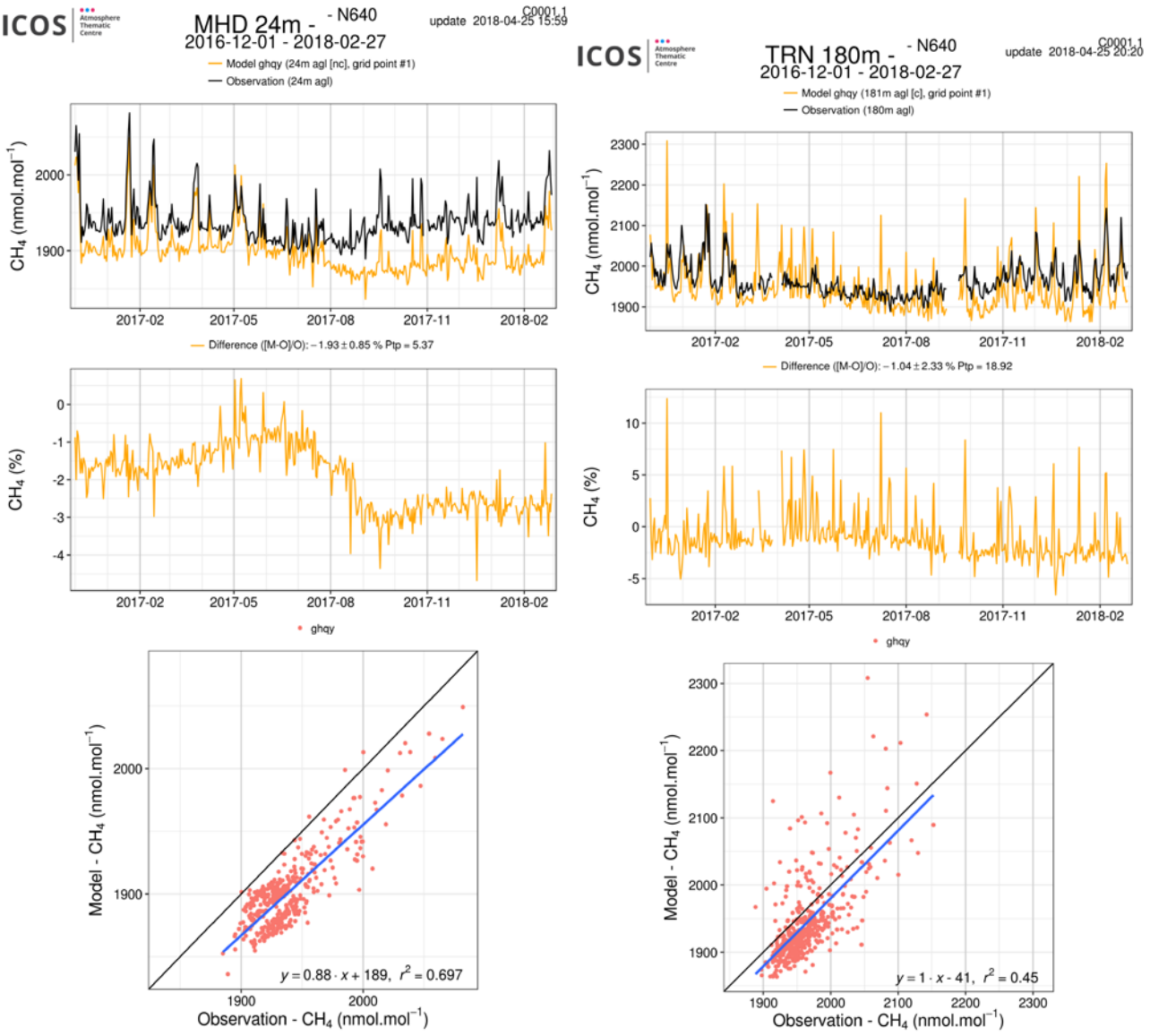


Figure 9.1.2: Same as figure 9.1.1, but for $CH_4$ .

In the last figure 9.1.4 we have merged all European stations in one category (Northern hemisphere), whereas other sites are split in two categories, namely southern hemisphere and tropics. From this synthesis we can conclude that the seasonal cycle of the $CO_2$ is overestimated over Europe. Positive biases up to 4 ppm in winter/spring are followed by negative biases up to -4 ppm in late summer and autumn. For $CH_4$ we observe an increase of bias and RMSE in each part of the world. Over the year the bias has doubled to reach about -50 ppb in early 2018.

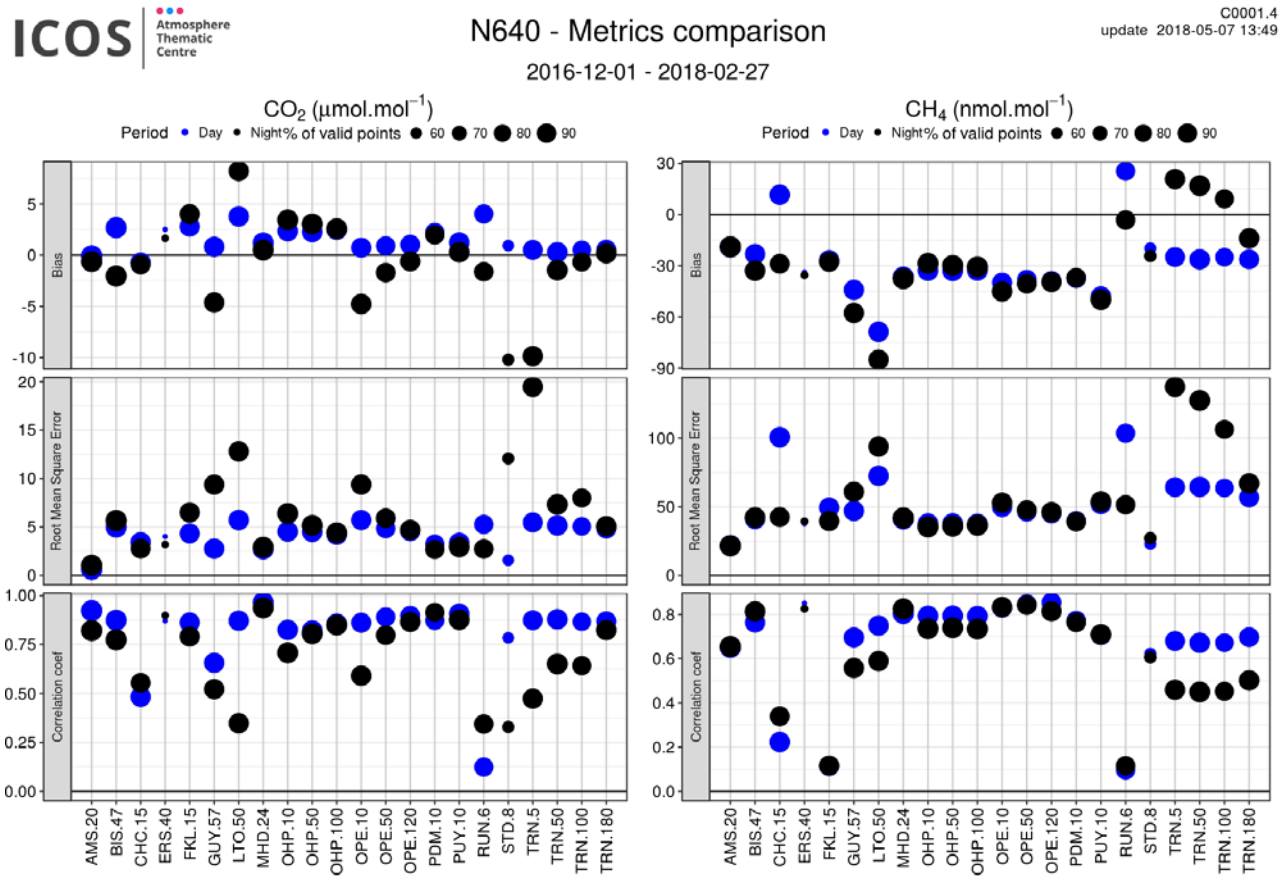


Figure 9.1.3: Annual metrics (bias, RMSE and coefficient correlation) calculated from the model-data comparison for daily means of CO2 (left) and CH4 (right) at the 15 sites (with multiple sampling heights at the last three sites). The size of each point relates to the percentage of available data. This figure uses GHQY experiment from 1st November 2016 to 1st December 2017. Daytime data (12-16 hr local time) are shown in blue, and nighttime data (00-04 hr local time) in black.

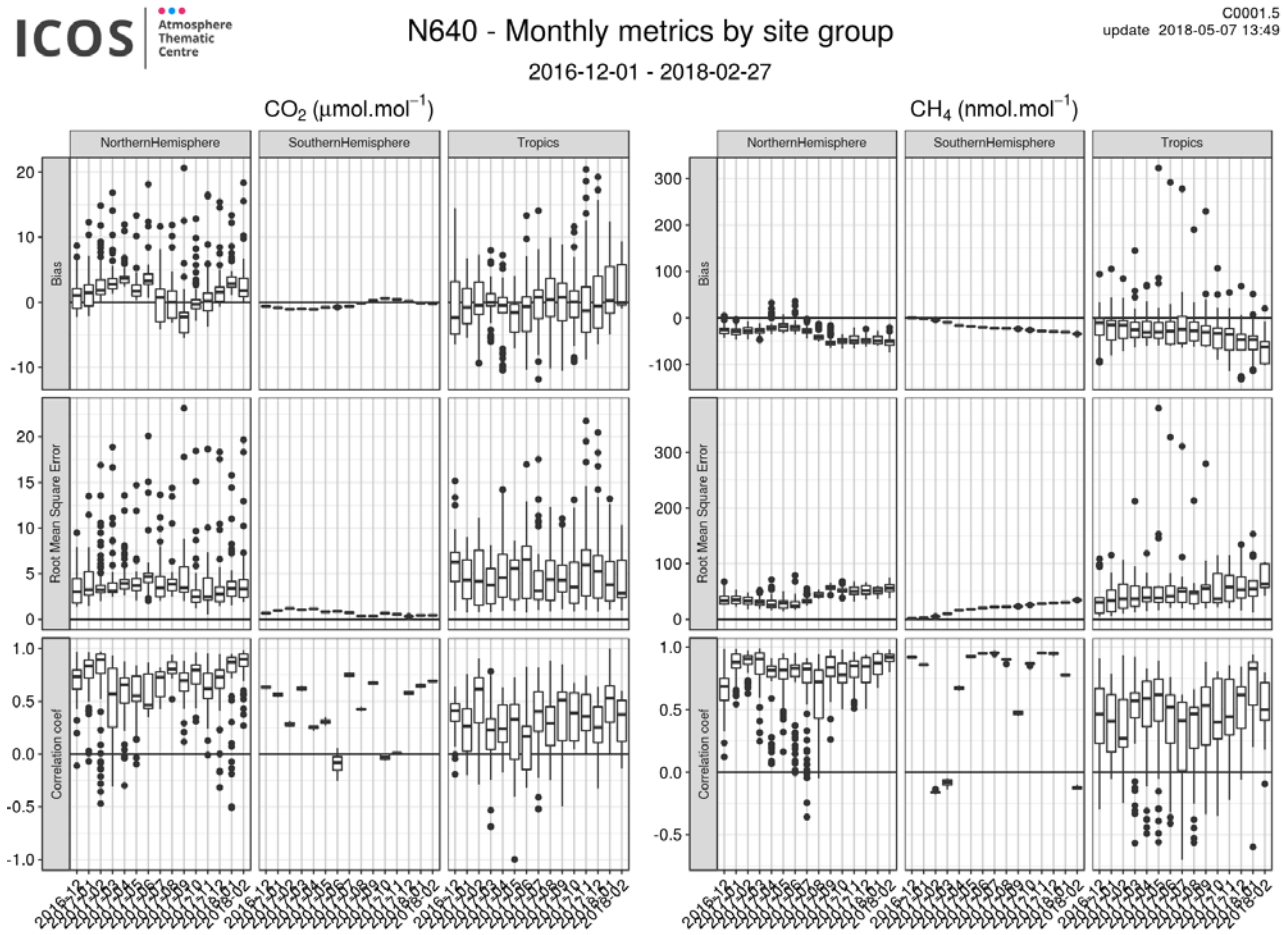


Figure 9.1.4: Annual metrics (bias, RMSE and coefficient correlation) calculated from the model-data comparison for daily means of $CO_2$ (left) and $CH_4$ (right) for three groups of stations: North hemisphere (Western Europe), Tropics and South hemisphere. This figure uses GHQY experiment from 1st November 2016 to 1st December 2017.

## 9.2 $CH_4$ and $CO_2$ validation against TTCON observations

For the validation column averaged mole fractions of $CO_2$ and $CH_4$ (denoted as XCO2 and XCH4) from the Total Carbon Column Observing Network (TCCON) are used. Column averaged mole fractions provide different information than the in situ measurements and are therefore complementary to the in situ data. For example if models suffer from problems in vertical transport, the combination of TCCON and surface in situ measurements will provide a means to detect this.

For the model validation the official TCCON data cannot be used due to its availability of typically one year after the measurement. Some TCCON sites are providing rapid delivery data (RD-TCCON data), which is available at least one month after the measurement. TCCON sites that deliver RD-TCCON data currently include Trainou (France), Bialystok (Poland) and Reunion (France). Over the course of the project more TCCON sites might contribute. This largely depends on funding for the fast data product.

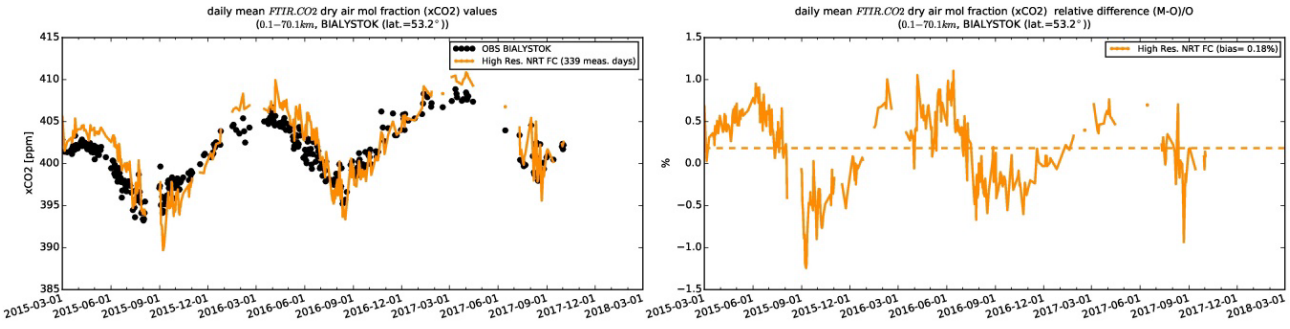


Figure 9.2.1: Time series of column averaged mole fractions (left) and relative difference (right) of carbon dioxide ($CO_2$) at the TCCON site Bialystok compared to high resolution NRT FC data (yellow)

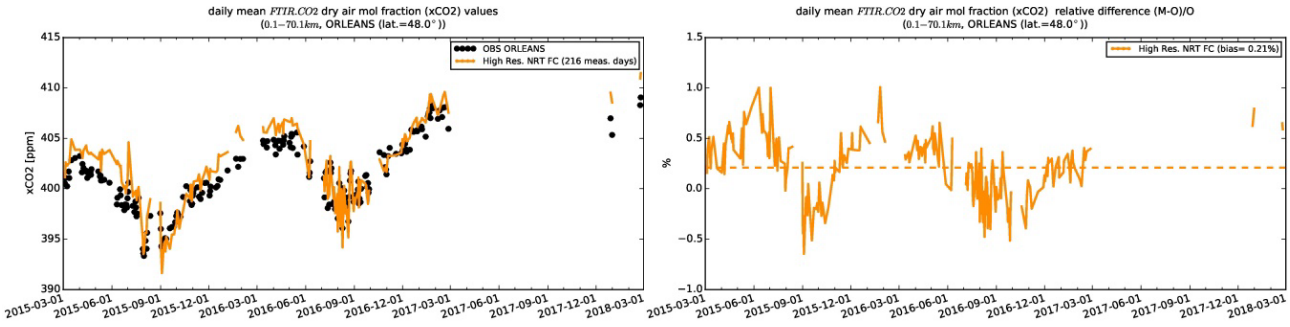


Figure 9.2.2: Time series of column averaged mole fractions (left) and relative difference (right) of carbon dioxide ($CO_2$) at the TCCON site Orleans compared to high resolution NRT FC data (yellow).

During the reporting period for this report several problems occurred at the TCCON sites Bialystok and Orleans resulting in gaps in the time series. These problems include a broken computer, problems with the spectrometer as well as the solar tracker. For some periods of the reporting period data might become available. However, a closer check of the data is required and therefore it is not included in this report.

The validation routines used for TCCON data are the same as used for the NDACC network and are documented in Langerock et al. (2015). The routines have been adapted to use the TCCON data format. Only measurements within 2.5h around local noon have been used for the comparison. The reason is that at high solar zenith angles the comparison worsens due to the averaging kernels. This issue is being investigated.

### 9.2.1 Evaluation against TCCON $CO_2$

The data presented in the Figures 9.2.1-9.2.3 show a comparison for the time period March 2015 – March 2018. At Bialystok (Fig. 9.2.1) and Orleans (Fig. 9.2.2) the difference between the model and the measurement shows a very similar seasonal pattern. Instrumental problems at both sites produce large gaps in the data and therefore do not allow new insights in the model comparison for last reporting period.

For Reunion Figure 9.2.3 nicely shows how the model comparison changed over time from slight underestimation until August 2015 to an overestimation in 2016 and 2017. One should note that the differences are well below 1%.

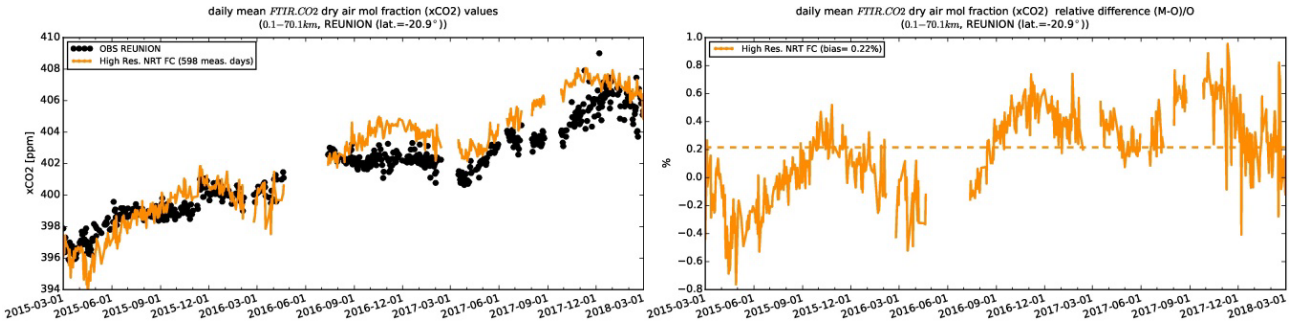


Figure 9.2.3: Time series of column averaged mole fractions (left) and relative difference (right) of carbon dioxide ($CO_2$) at the TCCON site Reunion compared to high resolution NRT FC data (yellow)

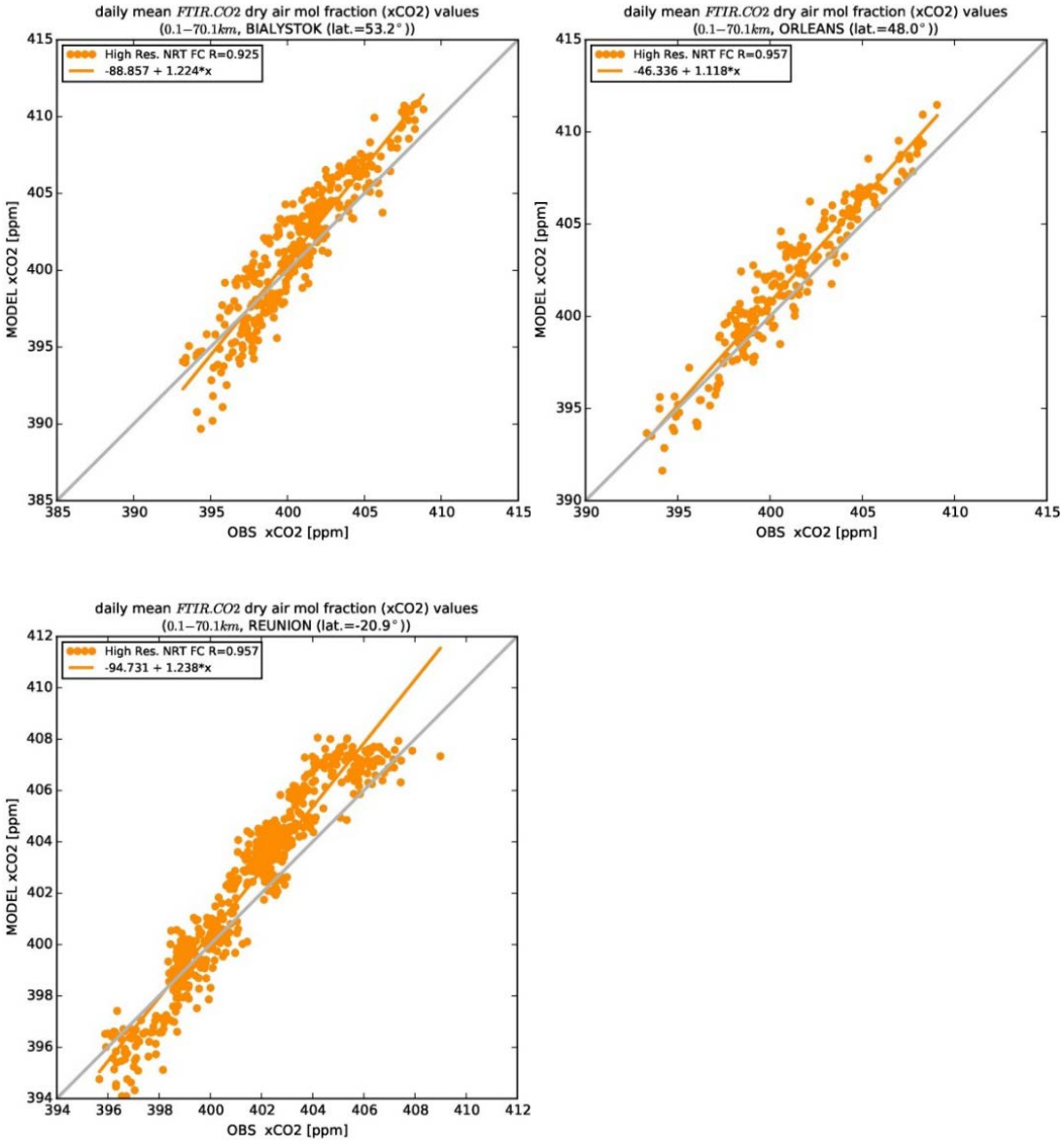


Figure 9.2.4: Scatter plots for the measured $CO_2$ column averaged mole fractions and the high resolution NRT FC data for the TCCON sites Bialystok (top left), Orleans (top right) and Reunion (bottom left).

### 9.2.2 Evaluation against TCCON $CH_4$

At Bialystok and Orleans the model comparison has not improved significantly over time. The high resolution model underestimates the XCH4 by about 1-1.5%. The control run and the o-suite both underestimate the XCH4 by 3-4% at Bialystok and Orleans. (Note: The last reporting period is excluded due to a lack of data arising from instrumental problems). At Reunion (Fig. 9.2.7) a step change in the high resolution model in March 2016 is the most striking feature. Directly after this step change the model agreed with the measurements. From March 2016 until February 2017 the model agreed with the measurements within 0.5%. From March 2017 until September 2017 the model showed variations, which are not seen in the measurements. From Sep 2017 onwards the variations in the comparison are not present anymore but the agreement is worse than 1%.

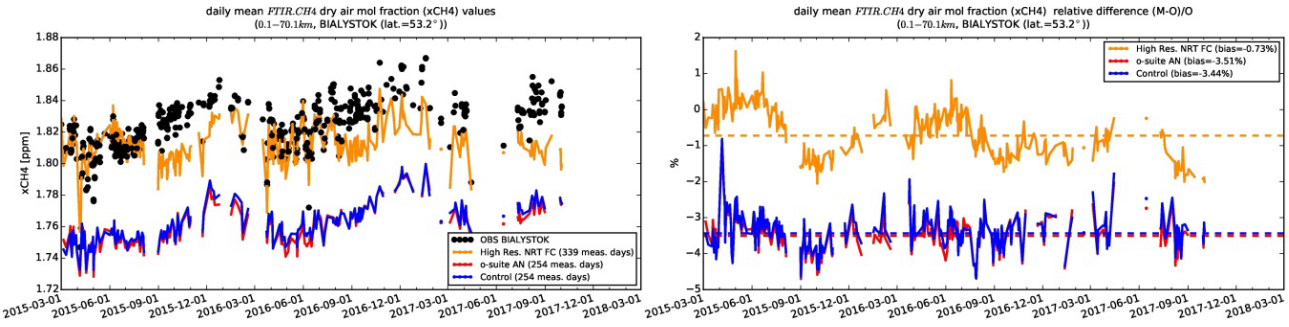


Figure 9.2.5: Time series of column averaged mole fractions (left) and relative difference (right) of methane ($CH_4$) at the TCCON site Bialystok compared to high resolution NRT FC data (yellow)

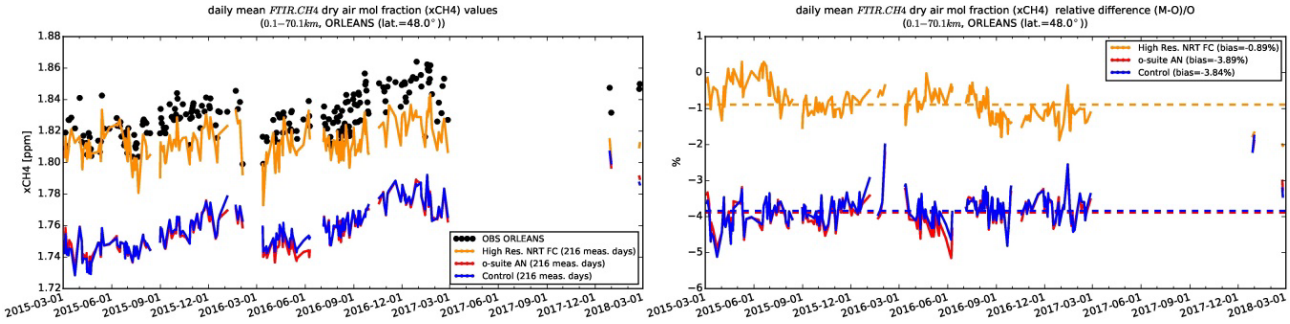


Figure 9.2.6: Time series of column averaged mole fractions (left) and relative difference (right) of methane ($CH_4$) at the TCCON site Orleans compared to high resolution NRT FC data (yellow).

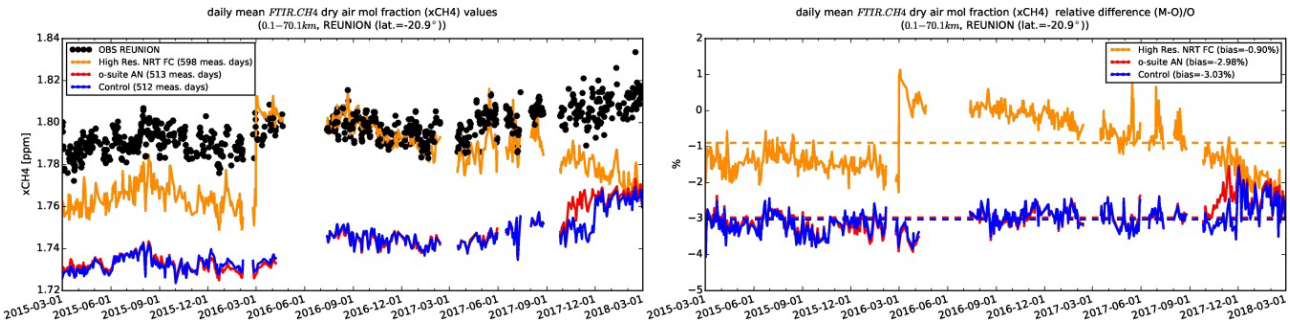


Figure 9.2.7: Time series of column averaged mole fractions (left) and relative difference (right) of methane ($CH_4$) at the TCCON site Reunion compared to high resolution NRT FC data (yellow).

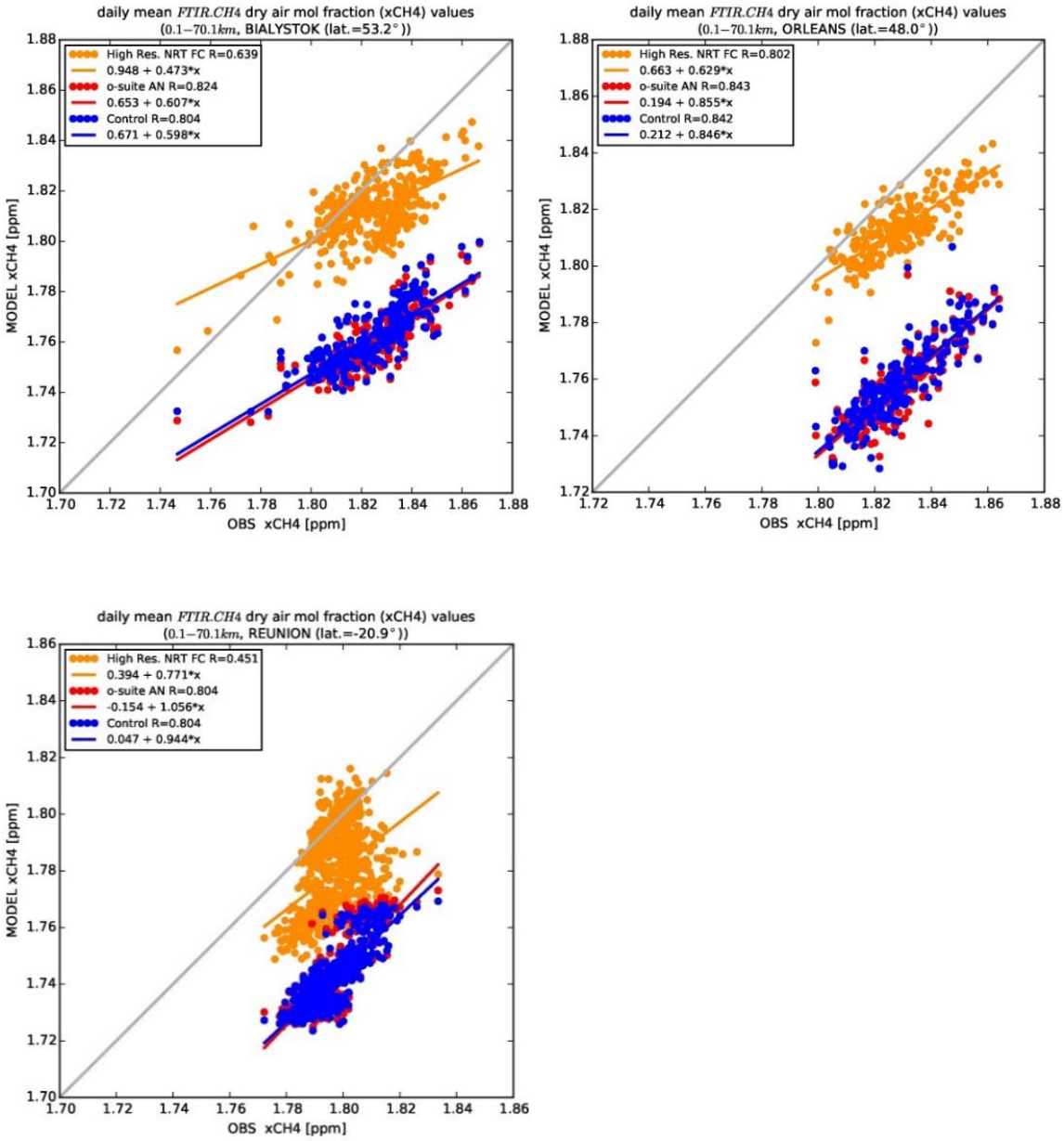


Figure 9.2.8: Scatter plots for the measured $CH_4$ column averaged mole fractions and the high resolution NRT FC data for the TCCON sites Bialystok (top left), Orleans (top right) and Reunion (bottom left).

# 10. Events

## 10.1 Dust over the Mediterranean: 31 January 2018 – 10 February 2018

During End-January and early-February, there was an intense dust activity over the Mediterranean. On 30th January an intense dust outbreak with origin in Algeria affected Southern Iberian Peninsula and Western Mediterranean (see Granada in Figure 10.1.1 and Figure 10.1.2). On 2nd February, a new dust event with origin in Algeria-Tunisia border was affecting Central-Eastern Mediterranean (see Rome Tor Vergata and Athens-NOA in Figure 10.1.1 and Figure 10.1.2) achieving high aerosol concentrations (up to 1.3 in Greece see Athens-NOA on 4th February in Figure 10.1.1). After this later event, the Eastern Mediterranean again affected by two more consecutive dust event with origin in Libya (see Athens-NOA in Figure 10.1.1 and Figure 10.1.3). This exceptional "dusty" period over the Mediterranean was associated with a strong and permanent pressure high system in the North Atlantic (not shown here) that was inducing African flow towards the Mediterranean.

CAMS AOD o-suite can timely reproduce the spatial distribution of the different dust plumes over the Mediterranean in comparison with AERONET (see Figure 10.1.1) and MODIS/Aqua (see Figure 10.1.2, Figure 10.1.3). However, a high AOD/DOD ratio is observed over the dust affected areas inducing DOD underestimations, particularly, this ratio is very high during 2-4 February event over Central Mediterranean (see Figure 10.1.3). Non-natural aerosols (mainly organic matter and sulphates) are contributing the main aerosol contributing to the total AOD during the days of the dust event.

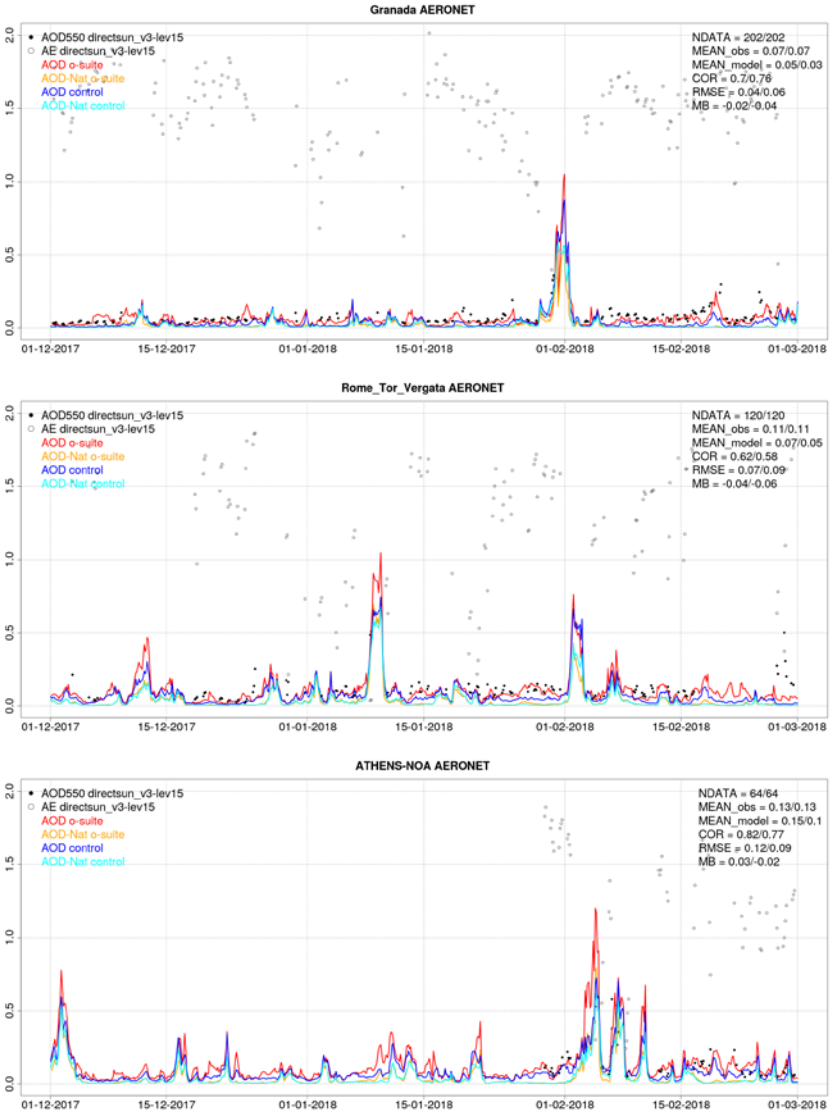


Figure 10.1.1: AOD from AERONET (black dot), AOD o-suite (red line), AOD control (blue line), AOD-Nat o-suite (orange line), AOD-Nat control (cyan line), for the study period over Granada (Spain), Rome Tor Vergata (Italy) and Athens-NOA (Greece). AOD-Nat corresponds to the natural aerosol optical depth that includes dust and sea-salt. Skill scores per each individual site and model (o—suite/control) are shown in the upper right corner (NDATA: available 3-hourly values used for the calculations, MEAN observations, MEAN_model, COR, RMSE, MB).

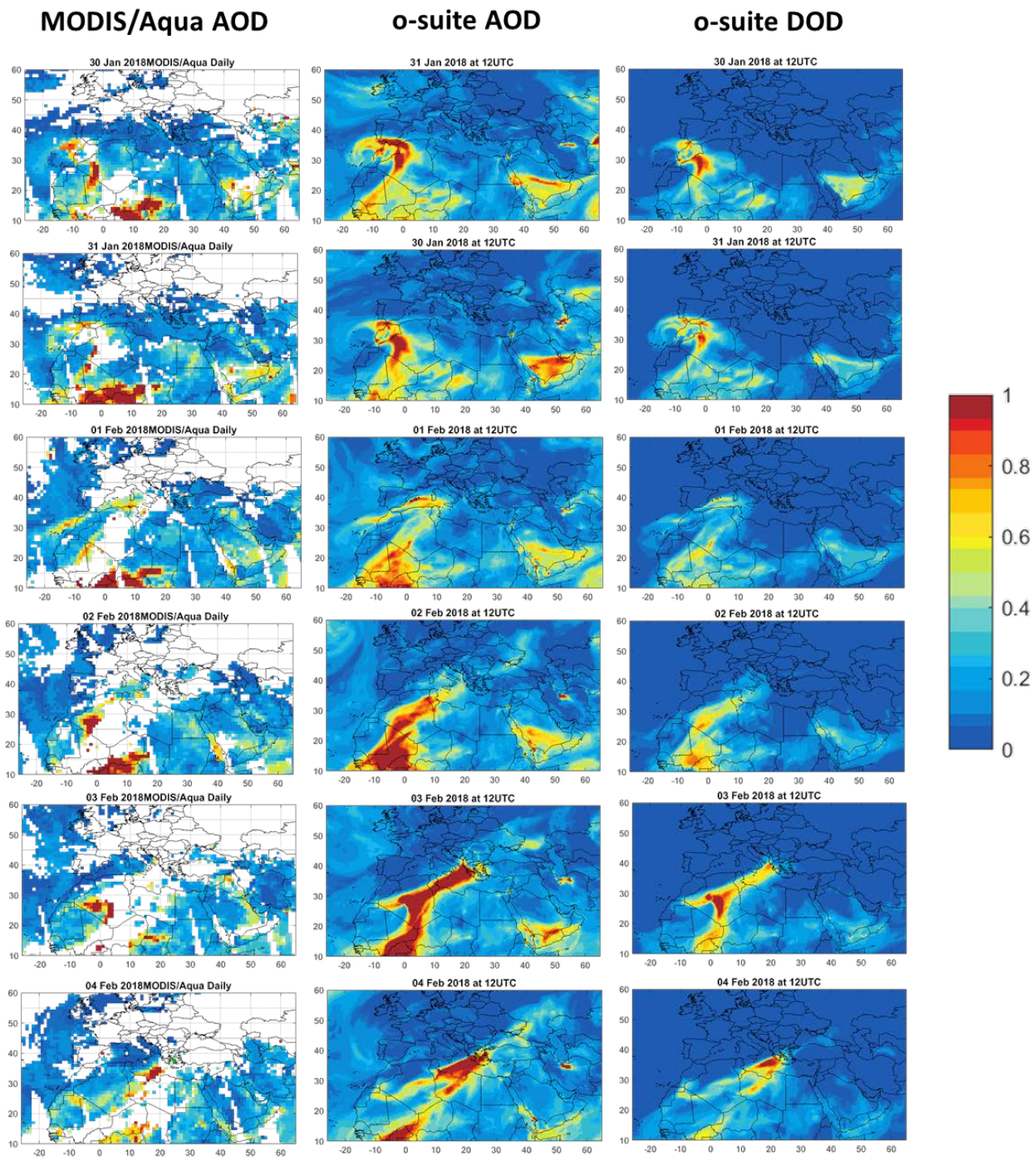


Figure 10.1.2. AOD and DOD at 12UTC from o-suite (central and right column) and AOD from MODIS-Aqua combined Dark Target and Deep Blue aerosol products (left column), from January 30 to February 4, 2018. MODIS-Aqua overpasses are around 12UTC over the study period.

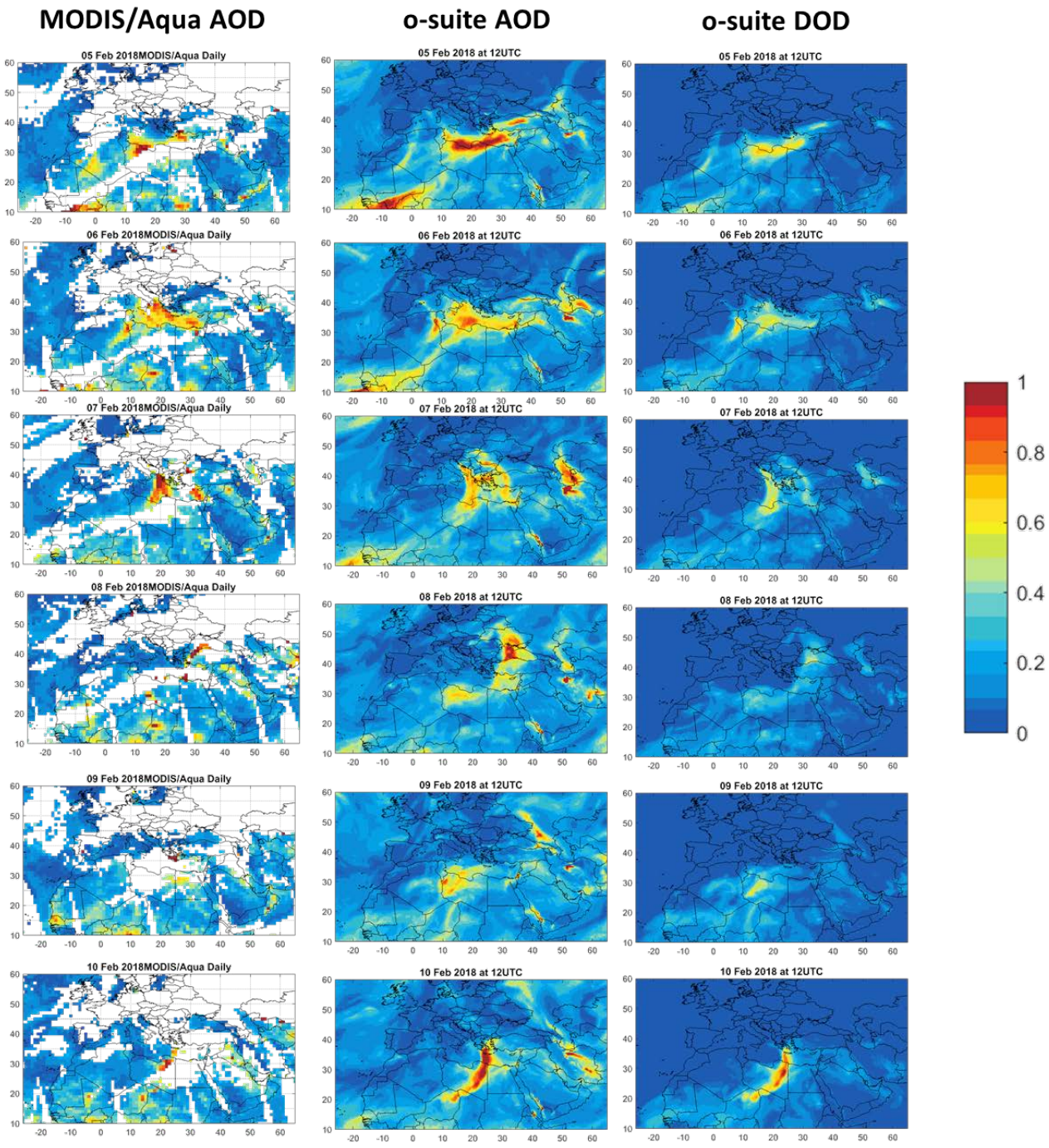


Figure 10.1.3. AOD and DOD at 12UTC from o-suite (central and right column) and AOD from MODIS-Aqua combined Dark Target and Deep Blue aerosol products (left column), for February 5-10, 2018. MODIS-Aqua overpasses are around 12UTC over the study period.

## 10.2 Fires in Portugal and Spain, 14-17 October 2017

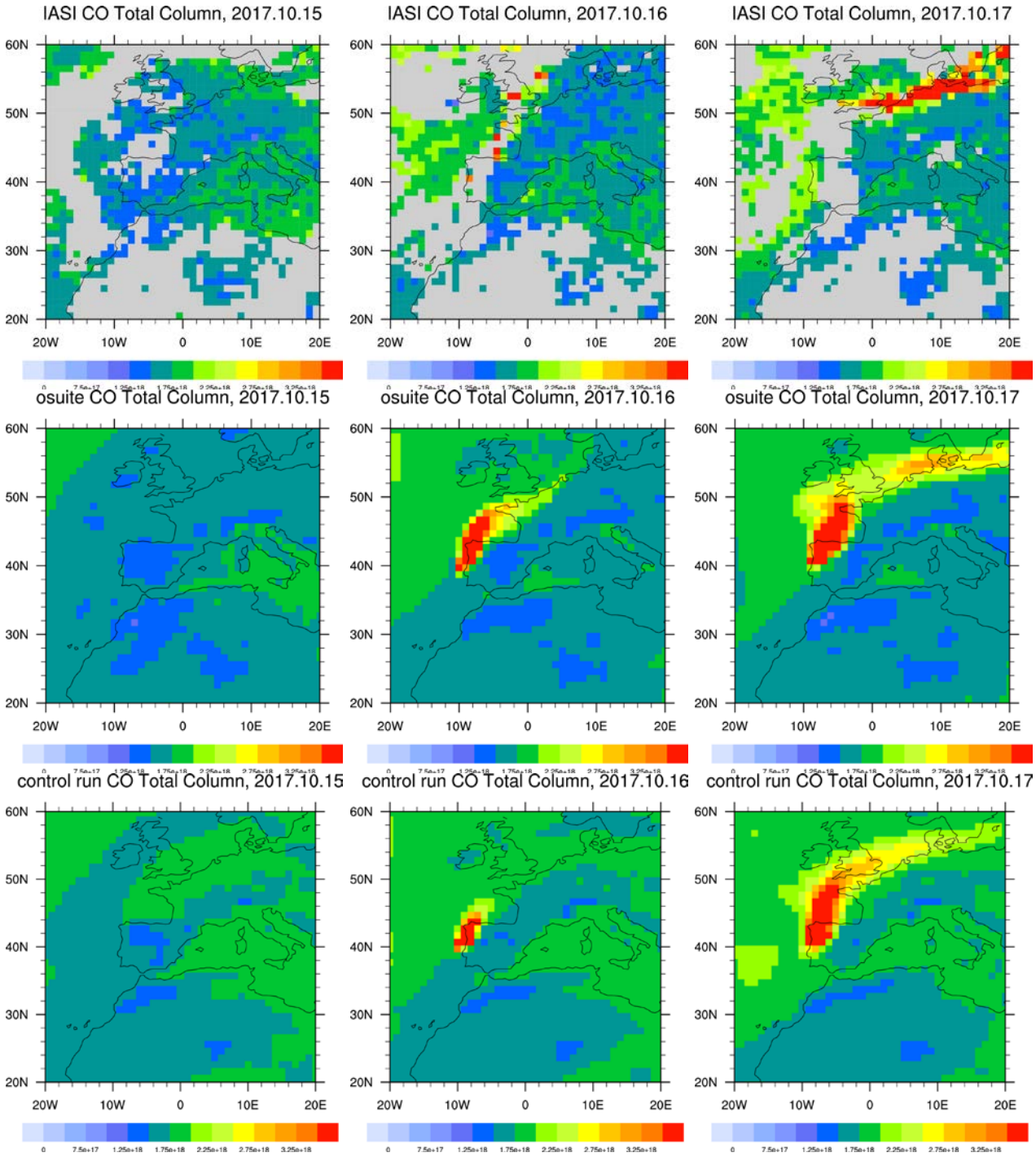


Figure 10.2.1. Comparison of IASI observations (top row) with CAMS-global o-suite (middle row) and control run (lowest row) for 15, 16 and 17 October 2017.

On the weekend of 14/15 October more than 140 wildfires broke out in central and northern Portugal and Galicia in Spain. The fires caused widespread devastation and more than 30 people were reported to have died.
(https://www.eumetsat.int/website/home/Images/ImageLibrary/DAT_3688467.html)

IASI data (Fig. 10.2.1) show rapidly increasing CO over the region starting from October 16th and north/northeastward transport across the ocean, but with many missing data points, especially over the location of the fire and the location of the plume. Both model simulations reproduce well the transport of CO as seen by IASI. The o-suite shows higher CO than the control run in the region of the fire. On the 17th October, the model simulations underestimate the CO plume over northern Europe, the location is correct, but the CO columns are higher in the IASI observations.

## 10.3 Dust over the North Atlantic: 13-16 October 2017

In mid-October 2017, a number of planes were forced to make emergency landings at Heathrow Airport as Storm Ophelia pulled a high concentration of aerosols into the London sky on 16th October. Five planes have reportedly made full emergency landings at the airport amid claims of the smell of smoke filling the cockpit. The rare spectacle was caused by Storm Ophelia pushing warm air (and dusty) from Africa northwards (see Figure 10.3.1). As the air moved north towards Ireland and the UK, it gathered smoke and tiny debris from recent wildfires in Spain and Portugal.

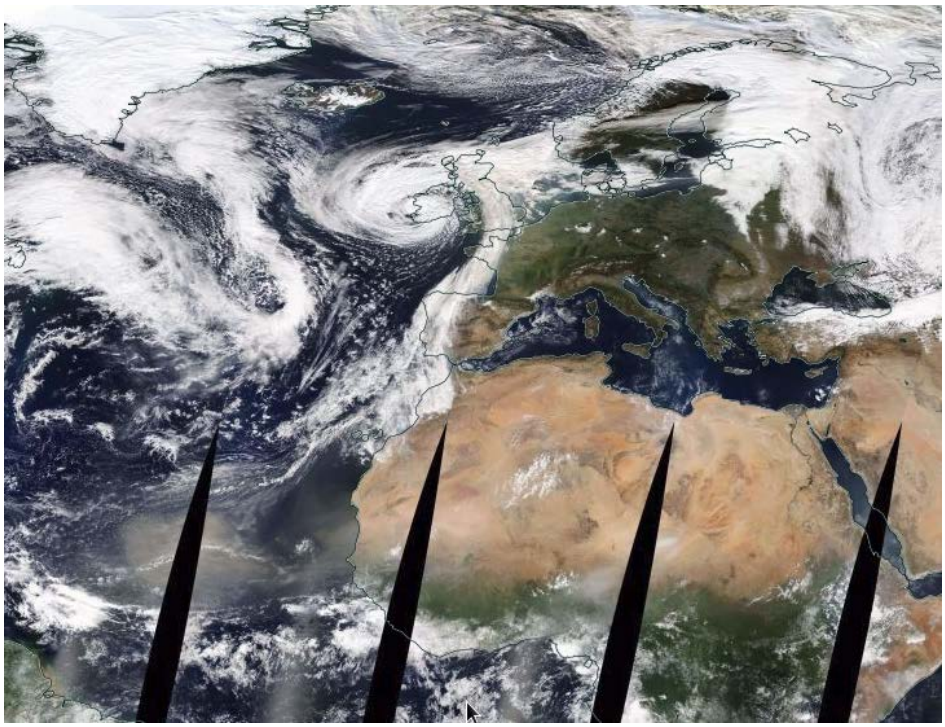

Figure 10.3.1. Daily composite image of MODIS-Aqua for 16th October. Satellite imagery shows high concentrations of airborne Saharan dust over the North Atlantic and a deep low centered over UK.

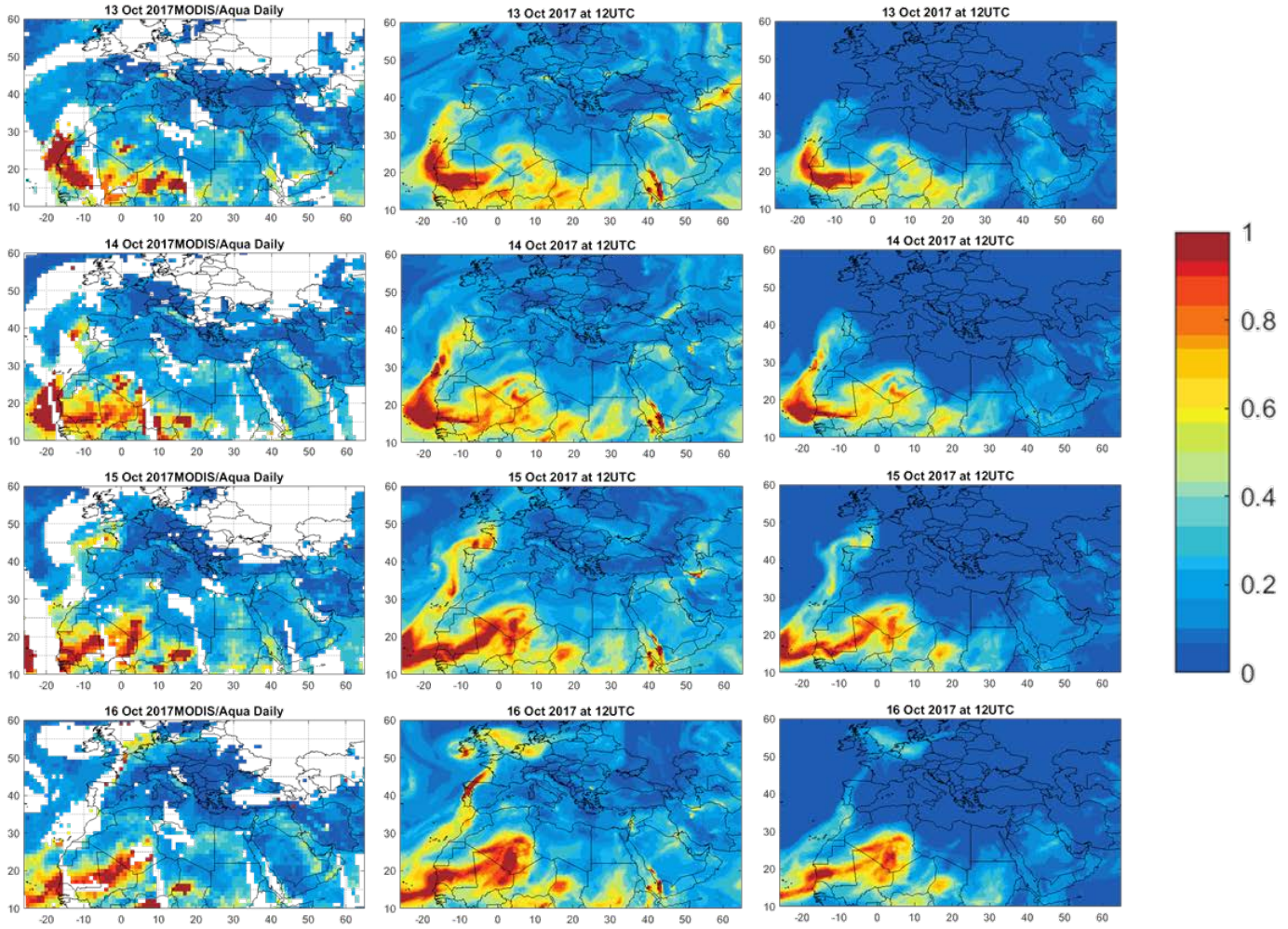


Figure 10.3.2. AOD and DOD at 12UTC from o-suite (central and right column) and AOD from MODIS-Aqua combined Dark Target and Deep Blue aerosol products (left column), for October 12-16, 2017. MODIS-Aqua overpasses are around 12UTC over the study period.

CAMS o-suite can timely reproduce the spatial distribution of the different dust plumes over the North Atlantic on 12-16 October and affected Northwestern Spain on 15 October and the United Kingdom on 16 October as observed by MODIS (Figure 10.3.2). The whole episode is well simulated by CAMS o-suite in the North Atlantic and Europe. We can see how CAMS o-suite tracks fairly well the changes in both shape and size of the dust layer throughout the dusty period and how the AOD levels are enhanced on 15 October in Northwestern Spain coinciding with the location of the fires. The magnitude of the event is overestimated by the model as shown the comparison with AERONET observations. Particularly in Coruna (Spain, see Figure 10.3.3), the control experiment predicts an unrealistic AOD peak above 3 that o-suite reduces to up 1.5.

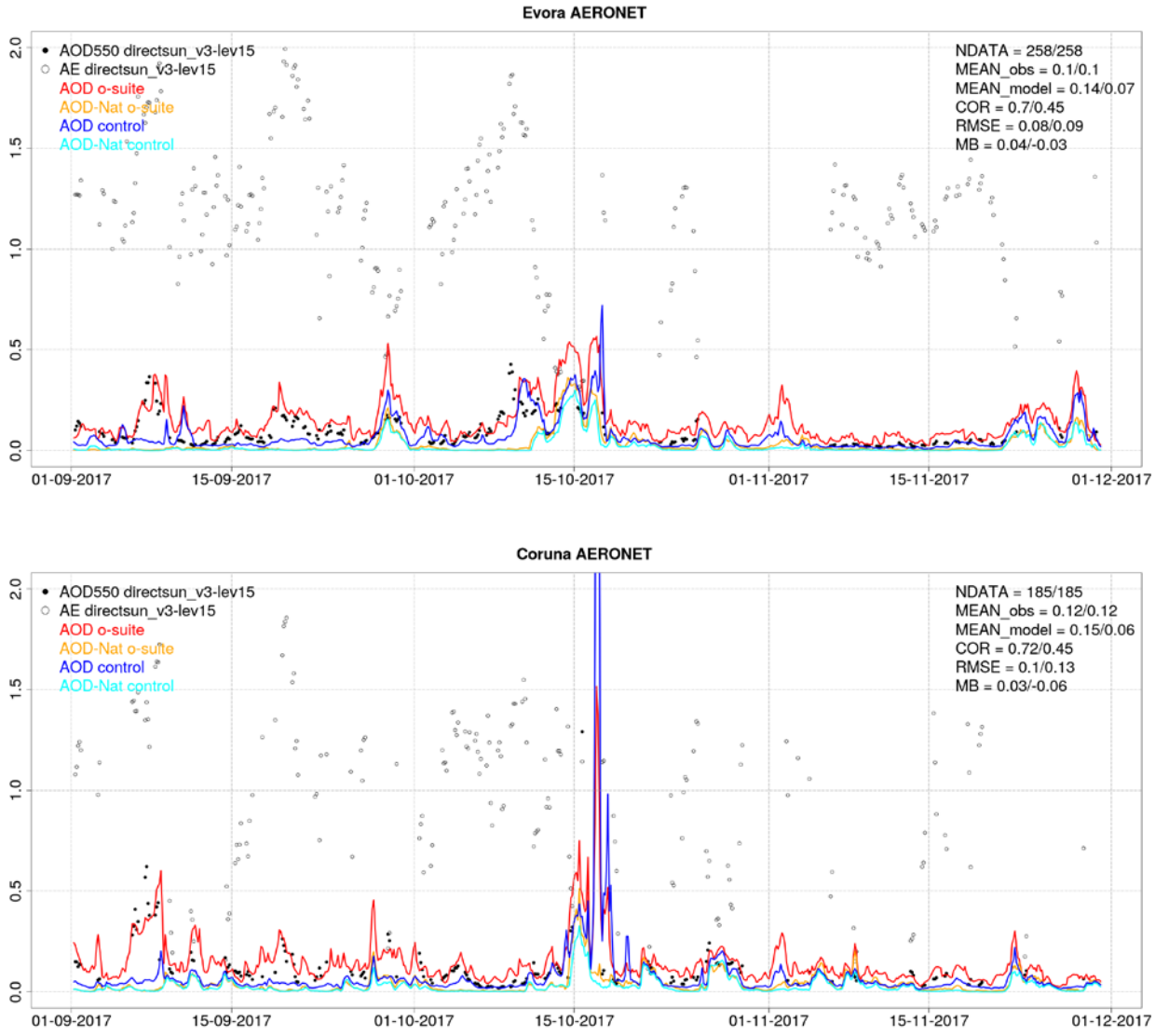


Figure 10.3.3: AOD from AERONET (black dot), AOD o-suite (red line), AOD control (blue line), AOD-Nat o-suite (orange line), AOD-Nat control (cyan line), for the study period over Evora (Portugal) and Coruna (Spain). AOD-Nat corresponds to the natural aerosol optical depth that includes dust and sea-salt. Skill scores per each individual site and model (o—suite/control) are shown in the upper right corner (NDATA: available 3-hourly values used for the calculations, MEAN observations, MEAN_model, COR, RMSE, MB).

# 11. References

*Agusti-Panareda, A., Monitoring upgrades of analysis/forecast system, MACC-III Deliverable D44.04, June 2015.*

*Bergamaschi, P., Frankenberg, C., Meirink, J. F., Krol, M., Villani, M. G., Houweling, S., Dentener, F., Dlugokencky, E. J., Miller, J. B., Gatti, L. V., Engel, A., and Levin, I.: Inverse modeling of global and regional CH4 emissions using SCIAMACHY satellite retrievals, J. Geophys. Res., 114, D22301, doi:10.1029/2009JD012287, 2009.*

*Benedetti, A., J.-J. Morcrette, O. Boucher, A. Dethof, R. J. Engelen, M. Fisher, H. Flentjes, N. Huneeus, L. Jones, J. W. Kaiser, S. Kinne, A. Mangold, M. Razinger, A. J. Simmons, M. Suttie, and the GEMS-AER team: Aerosol analysis and forecast in the ECMWF Integrated Forecast System. Part II : Data assimilation, J. Geophys. Res., 114, D13205, doi:10.1029/2008JD011115, 2009.*

*Boussetta, S., Balsamo, G., Beljaars, A., Agusti-Panareda, A., Calvet, J.-C., Jacobs, C., van den Hurk, B., Viterbo, P., Lafont, S., Dutra, E., Jarlan, L., Balzarolo, M., Papale, D., and van der Werf, G.: Natural carbon dioxide exchanges in the ECMWF Integrated Forecasting System: implementation and offline validation, J. Geophys. Res.-Atmos., 118, 1–24, doi: 10.1002/jgrd.50488, 2013.*

*Braathen, WMO Arctic Ozone Bulletin No 1/2016, DOI:10.13140/RG.2.1.4929.6403, 2016.*

*Cammas, J.P., Brioude J., Chaboureau J.-P., Duron J., Mari C., Mascart P., Nédélec P., Smit H., Pätz H.-W., Volz-Thomas A., Stohl A., and Fromm M., Injection in the lower stratosphere of biomass fire emissions followed by long-range transport: a MOZAIC case study. Atmos. Chem. Phys., 9, 5829-5846, 2009*

*Cariolle, D. and Teyssèdre, H.: A revised linear ozone photochemistry parameterization for use in transport and general circulation models: multi-annual simulations, Atmos. Chem. Phys., 7, 2183-2196, doi:10.5194/acp-7-2183-2007, 2007.*

*Dee, D. P. and S. Uppala, Variational bias correction of satellite radiance data in the ERA-Interim reanalysis. Quart. J. Roy. Meteor. Soc.,135, 1830-1841, 2009.*

*Deeter, M. N., Emmons, L. K., Edwards, D. P., Gille, J. C., and Drummond, J. R.: Vertical resolution and information content of CO profiles retrieved by MOPITT, Geophys. Res. Lett., 31, L15112, doi:10.1029/2004GL020235, 2004.*

*Deeter, M. N., et al. (2010), The MOPITT version 4 CO product: Algorithm enhancements, validation, and long-term stability, J. Geophys. Res., 115, D07306, doi:10.1029/2009JD013005.*

*Dentener, F., et al., 2006: Emissions of primary aerosol and precursor gases in the years 2000 and 1750 prescribed data-sets for AeroCom, Atmos. Chem. Phys., 6, 4321 – 4344.*

*Deshler, T., J.L. Mercer, H.G.J. Smit, R. Stubi, G. Levrat, B.J. Johnson, S.J. Oltmans, R. Kivi, A.M. Thompson, J. Witte, J. Davies, F.J. Schmidlin, G. Brothers, T. Sasaki (2008) Atmospheric comparison of electrochemical cell ozonesondes from different maufacturers, and with different cathode solution strengths: The Balloon Experiment on Standards for Ozonsondes. J. Geophys. Res.113, D04307, doi:10.1029/2007JD008975*

*Douros, J., S. Basart, A. Benedictow, A.-M. Blechschmidt, S. Chabrillat, Y. Christophe, H. Clark, E. Cuevas, H.J. Eskes, H. Flentje, K. M. Hansen, J. Kapsomenakis, B. Langerock, K. Petersen, M. Ramonet, A. Richter, M. Schulz, A. Wagner, T. Warneke, C. Zerefos, Observations characterisation and validation methods document, Copernicus Atmosphere Monitoring Service (CAMS) report, CAMS84_2015SC2_D.84.8.1.1-2017_observations_v2.pdf, October 2017. Available from: http://atmosphere.copernicus.eu/user-support/validation/verification-global-services.*

*Dupuy, E., et al.: Validation of ozone measurements from the Atmospheric Chemistry Experiment (ACE), Atmos. Chem. Phys., 9, 287-343, doi:10.5194/acp-9-287-2009, 2009.*

*Elbern, H., Schwinger, J., Botchorishvili, R.: Chemical state estimation for the middle atmosphere by four-dimensional variational data assimilation: System configuration. Journal of Geophysical Research (Atmospheres) 115, 6302, 2010.*

*Emmons, L. K., D. P. Edwards, M. N. Deeter, J. C. Gille, T. Campos, P. Nédélec, P. Novelli, and G. Sachse, Measurements of Pollution In The Troposphere (MOPITT) validation through 2006 Atmos. Chem. Phys., 9, 1795-1803, 2009*

*Errera, Q., Daerden, F., Chabrillat, S., Lambert, J. C., Lahoz, W. A., Viscardy, S., Bonjean, S., and Fonteyn, D., 4D-Var Assimilation of MIPAS chemical observations: ozone and nitrogen dioxide analyses, Atmos. Chem. Phys., 8, 6169-6187, 2008.*

*Errera, Q. and Ménard, R.: Technical Note: Spectral representation of spatial correlations in variational assimilation with grid point models and application to the belgian assimilation system for chemical observations (BASCOE), Atmos. Chem. Phys. Discuss., 12, 16763-16809, doi:10.5194/acpd-12-16763-2012, 2012.*

*Eskes, H., Wagner, A., Schulz, M., Christophe, Y., Ramonet, M., Basart, S., Benedictow, A., Blechschmidt, A.-M., Chabrillat, S., Clark, H., Cuevas, E., Flentje, H., Hansen, K. M., Im, U., Kapsomenakis, J., Langerock, B., Petersen, K., Richter, A., Sudarchikova, N., Thouret, V., Warneke, T., and Zerefos, C.: Validation report of the CAMS near-real time global atmospheric composition service December 2016 - February 2017, CAMS84_2015SC2_D84.1.1.7_2017DJF_v1.1, June 2017. Available from: http://atmosphere.copernicus.eu/user-support/validation/verification-global-services*

*Eskes, H., Huijnen, V., Arola, A., Benedictow, A., Blechschmidt, A.-M., Botek, E., Boucher, O., Bouarar, I., Chabrillat, S., Cuevas, E., Engelen, R., Flentje, H., Gaudel, A., Griesfeller, J., Jones, L., Kapsomenakis, J., Katragkou, E., Kinne, S., Langerock, B., Razinger, M., Richter, A., Schultz, M., Schulz, M., Sudarchikova, N., Thouret, V., Vrekoussis, M., Wagner, A., and Zerefos, C.: Validation of reactive gases and aerosols in the MACC global analysis and forecast system, Geosci. Model Dev., 8, 3523-3543, doi:10.5194/gmd-8-3523-2015, 2015.*

*Flemming, J., Huijnen, V., Arteta, J., Bechtold, P., Beljaars, A., Blechschmidt, A.-M., Diamantakis, M., Engelen, R. J., Gaudel, A., Inness, A., Jones, L., Josse, B., Katragkou, E., Marecal, V., Peuch, V.-H., Richter, A., Schultz, M. G., Stein, O., and Tsikerdekis, A.: Tropospheric chemistry in the Integrated Forecasting System of ECMWF, Geosci. Model Dev., 8, 975-1003, doi:10.5194/gmd-8-975-2015, 2015.*

*Flemming, J., Benedetti, A., Inness, A., Engelen, R. J., Jones, L., Huijnen, V., Remy, S., Parrington, M., Suttie, M., Bozzo, A., Peuch, V.-H., Akritidis, D., and Katragkou, E.: The CAMS interim Reanalysis of Carbon Monoxide, Ozone and Aerosol for 2003–2015, Atmos. Chem. Phys., 17, 1945-1983, doi:10.5194/acp-17-1945-2017, 2017.*

*Franco, B., et al., Retrievals of formaldehyde from ground-based FTIR and MAX-DOAS observations at the Jungfraujoch station and comparisons with GEOS-Chem and IMAGES model simulations, Atmos. Meas. Tech., 8, 1733-1756, 2015*

*Gielen, C., Van Roozendael, M., Hendrick, F., Pinardi, G., Vlemmix, T., De Bock, V., De Backer, H., Fayt, C., Hermans, C., Gillotay, D., and Wang, P.: A simple and versatile cloud-screening method for MAX-DOAS retrievals, Atmos. Meas. Tech., 7, 3509-3527, doi:10.5194/amt-7-3509-2014, 2014.*

*Granier, C. et al.: Evolution of anthropogenic and biomass burning emissions of air pollutants at global and regional scales during the 1980–2010 period. Climatic Change (109), 2011*

*Holben, B. N., Eck, T. F., Slutsker, I., Tanré, D., Buis, J. P., Setzer, A., Vermote, E., Reagan, J. A., Kaufman, Y. J., Nakajima, T., Lavenu, F., Jankowiak, I., and Smirnov A.: AERONET – a federated instrument network and data archive for aerosol characterization, Remote Sens. Environ., 66, 1–16, 5529, 5533, 5537, 5544, 1998.*

*Hommel, R., Eichmann, K.-U., Aschmann, J., Bramstedt, K., Weber, M., von Savigny, C., Richter, A., Rozanov, A., Wittrock, F., Khosrawi, F., Bauer, R., and Burrows, J. P.: Chemical ozone loss and ozone mini-hole event during the Arctic winter 2010/2011 as observed by SCIAMACHY and GOME-2, Atmos. Chem. Phys., 14, 3247-3276, doi:10.5194/acp-14-3247-2014, 2014.*

*Huijnen, V., et al.: The global chemistry transport model TM5: description and evaluation of the tropospheric chemistry version 3.0, Geosci. Model Dev., 3, 445-473, doi:10.5194/gmd-3-445-2010, 2010.*

*Inness, A., Blechschmidt, A.-M., Bouarar, I., Chabrillat, S., Crepulja, M., Engelen, R. J., Eskes, H., Flemming, J., Gaudel, A., Hendrick, F., Huijnen, V., Jones, L., Kapsomenakis, J., Katragkou, E., Keppens, A., Langerock, B., de Mazière, M., Melas, D., Parrington, M., Peuch, V. H., Razinger, M., Richter, A., Schultz, M. G., Suttie, M., Thouret, V., Vrekoussis, M., Wagner, A., and Zerefos, C.: Data assimilation of satellite-retrieved ozone, carbon monoxide and nitrogen dioxide with ECMWF's Composition-IFS, Atmos. Chem. Phys., 15, 5275-5303, doi:10.5194/acp-15-5275-2015, 2015.*

*Janssens-Maenhout, G., Dentener, F., Aardenne, J. V., Monni, S., Pagliari, V., Orlandini, L., Klimont, Z., Kurokawa, J., Akimoto, H., Ohara, T., Wankmueller, R., Battye, B., Grano, D., Zuber, A., and Keating, T.: EDGAR-HTAP: a Harmonized Gridded Air Pollution Emission Dataset Based on National Inventories, JRC68434, EUR report No EUR 25 299–2012, ISBN 978-92-79- 23122-0, ISSN 1831-9424, European Commission Publications Office, Ispra (Italy), 2012.*

*Jaross, G., Bhartia, P.K., Chen, G., Kowitt, M., Haken, M., Chen, Z., Xu, Ph., Warner, J., Kelly, T. : OMPS Limb Profiler instrument performance assessment, J. Geophys. Res. Atmos 119, 2169-8996, 2014.*

*Kaiser, J. W., Heil, A., Andreae, M. O., Benedetti, A., Chubarova, N., Jones, L., Morcrette, J.-J., Razinger, M., Schultz, M. G., Suttie, M., and van der Werf, G. R.: Biomass burning emissions estimated with a global fire assimilation system based on observed fire radiative power, Biogeosciences, 9, 527-554, doi:10.5194/bg-9-527-2012, 2012.*

*Kramarova, N. A., Nash, E. R., Newman, P. A., Bhartia, P. K., McPeters, R. D., Rault, D. F., Seftor, C. J., Xu, P. Q., and Labow, G. J.: Measuring the Antarctic ozone hole with the new Ozone Mapping and Profiler Suite (OMPS), Atmos. Chem. Phys., 14, 2353-2361, doi:10.5194/acp-14-2353-2014, 2014.*

*Lahoz, W. A., Errera, Q., Viscardy, S., and Manney G. L., The 2009 stratospheric major warming described from synergistic use of BASCOE water vapour analyses and MLS observations, Atmos. Chem. Phys. 11, 4689-4703, 2011*

*Lambert, A, et al., Aura Microwave Limb Sounder Version 3.4 Level-2 near real-time data user guide, http://disc.sci.gsfc.nasa.gov/Aura/data-holdings/MLS/documents/NRT-user-guide-v34.pdf*

*Langerock, B., De Mazière, M., Hendrick, F., Vigouroux, C., Desmet, F., Dils, B., and Niemeijer, S.: Description of algorithms for co-locating and comparing gridded model data with remote-sensing observations, Geosci. Model Dev., 8, 911-921, doi:10.5194/gmd-8-911-2015, 2015.*

*Lefever, K., van der A, R., Baier, F., Christophe, Y., Errera, Q., Eskes, H., Flemming, J., Inness, A., Jones, L., Lambert, J.-C., Langerock, B., Schultz, M. G., Stein, O., Wagner, A., and Chabrillat, S.: Copernicus stratospheric ozone service, 2009–2012: validation, system intercomparison and roles of input data sets, Atmos. Chem. Phys., 15, 2269-2293, doi:10.5194/acp-15-2269-2015, 2015.*

*Liu, Z., et al., Exploring the missing source of glyoxal (CHOCHO) over China, Geophys. Res. Lett., 39, L10812, doi: 10.1029/2012GL051645, 2012*

*Massart, S., Flemming, J., Cariolle, D., Jones, L., High resolution CO tracer forecasts, MACC-III Deliverable D22.04, May 2015, available from http://www.gmes-atmosphere.eu/documents/macciii/deliverables/grg*

*Morcrette, J.-J., O. Boucher, L. Jones, D. Salmond, P. Bechtold, A. Beljaars, A. Benedetti, A. Bonet, J. W. Kaiser, M. Razinger, M. Schulz, S. Serrar, A. J. Simmons, M. Sofiev, M. Suttie, A. M. Tompkins, and A. Untch: Aerosol analysis and forecast in the ECMWF Integrated Forecast System. Part I: Forward modelling, J. Geophys. Res., 114, D06206, doi:10.1029/2008JD011235, 2009.*

*Richter, A., Burrows, J. P., Nüß, H., Granier, C, Niemeier, U.: Increase in tropospheric nitrogen dioxide over China observed from space, Nature, 437, 129-132, doi: 10.1038/nature04092, 2005*

*Richter, A., Begoin, M., Hilboll, A., and Burrows, J. P.: An improved NO2 retrieval for the GOME-2 satellite instrument, Atmos. Meas. Tech. , **4**, 1147-1159, doi:10.5194/amt-4-1147-2011, 2011*

*Sindelarova, K., Granier, C., Bouarar, I., Guenther, A., Tilmes, S., Stavrakou, T., Müller, J.-F., Kuhn, U., Stefani, P., and Knorr, W.: Global data set of biogenic VOC emissions calculated by the MEGAN model over the last 30 years, Atmos. Chem. Phys., 14, 9317-9341, doi:10.5194/acp-14-9317-2014, 2014.*

*Smit, H.G.J., W. Straeter, B.J. Johnson, S.J. Oltmans, J. Davies, D.W. Tarasick, B. Hoegger, R. Stubi, F.J. Schmidlin, T. Northam, A.M. Thompson, J.C. Witte, I. Boyd: Assessment of the performance of ECC-ozonesondes under quasi-flight conditions in the environmental simulation chamber: Insights from the Juelich Ozone Sonde Intercomparison Experiment (JOSIE), J. Geophys. Res. 112, D19306, doi:10.1029/2006JD007308, 2007.*

*Solomon, S., Haskins, J., Ivy, D. J. and Min, F.: Fundamental differences between Arctic and Antarctic ozone depletion, PNAS 2014 111 (17) 6220-6225, doi:10.1073/pnas.1319307111, 2014.*

*Stavrakou,T., First space-based derivation of the global atmospheric methanol fluxes, Atm. Chem. Phys., 11, 4873-4898, 2013.*

*Strahan, S.E., A.R. Douglass, and P.A. Newman, The contributions of chemistry and transport to low arctic ozone in March 2011 derived from Aura MLS observations, J. Geophys. Res. Atmos., 118, 1563–1576, doi:10.1002/jgrd.50181, 2013.*

*Taha, G.; Jaross, G. R.; Bhartia, P. K.: Validation of OMPS LP Ozone Profiles Version 2.0 with MLS, Ozone Sondes and Lidar Measurements, American Geophysical Union, Fall Meeting 2014, abstract #A33J-3322, 2014.*

*Taylor, K.E.: Summarizing multiple aspects of model performance in a single diagram. J.Geophys. Res., 106, 7183-7192, 2001.*

*van der A, R. J. , M. A. F. Allaart, and H. J. Eskes, Multi sensor reanalysis of total ozone, Atmos. Chem. Phys., 10, 11277–11294, doi:10.5194/acp-10-11277-2010, www.atmos- chem-phys.net/10/11277/2010/, 2010*

*van der A, R., M. Allaart, H. Eskes, K. Lefever, Validation report of the MACC 30-year multi-sensor reanalysis of ozone columns Period 1979-2008, MACC-II report, Jan 2013, MACCII_VAL_DEL_D_83.3_OzoneMSRv1_20130130.docx/pdf.*

*van der A, R. J., Allaart, M. A. F., and Eskes, H. J.: Extended and refined multi sensor reanalysis of total ozone for the period 1970–2012, Atmos. Meas. Tech., 8, 3021-3035, doi:10.5194/amt-8-3021-2015, 2015.*

*Vrekoussis, M., Wittrock, F., Richter, A., and Burrows, J. P.: GOME-2 observations of oxygenated VOCs: what can we learn from the ratio glyoxal to formaldehyde on a global scale?, Atmos. Chem. Phys., **10**, 10145-10160, doi:10.5194/acp-10-10145-2010, 2010*

*Wittrock, F., A. Richter, H. Oetjen, J. P. Burrows, M. Kanakidou, S. Myriokefalitakis, R. Volkamer, S. Beirle, U. Platt, and T. Wagner, Simultaneous global observations of glyoxal and formaldehyde from space, Geophys. Res. Lett., 33, L16804, doi:10.1029/2006GL026310, 2006*

*WMO (2010), Guidelines for the Measurement of Atmospheric Carbon Monoxide, GAW Report No. 192, World Meteorological Organization, Geneva, Switzerland, 2010.*

*WMO (2013), Guidelines for the Continuous Measurements of Ozone in the Troposphere, GAW Report No. 209, World Meteorological Organization, Geneva, Switzerland, 2013.*

# Annex 1: Acknowledgements

Listed below are the authors contributing to the sections in this report. The authors contributing to the model description are also provided, as well as acknowledgements to the validation datasets.

***Tropospheric reactive gases reactive gases***

Annette Wagner, MPG (editor, O3 sondes, GAW data)
Hannah Clark, Valerie Thouret, CNRS-LA (IAGOS)
Harald Flentje, DWD (O3 sondes, GAW data)
Anne Blechschmidt and Andreas Richter, IUB Bremen (GOME-2 NO2, HCHO)
John Kapsomenakis, Christos Zerefos, AA (ESRL)
N. Sudarchikova, satellite IR observations (MPG)
Kaj Hansen, Ulas Im, AU (Arctic theme)
Bavo Langerock, BIRA (NDACC)

***Tropospheric aerosol***

Michael Schulz, MetNo (editor, Aerocom, Aeronet)
Anna Benedictow, Jan Griesfeller, MetNo (Aerocom, Aeronet)
Sara Basart, MTeresa Pay, Oriol Jorba, BSC-CNS (Aeronet, MODIS, AirBase, SDS-WAS NAMEE RC)
Emilio Cuevas, AEMET (Aeronet, MODIS, AirBase, SDS-WAS NAMEE RC)
Harald Flentje, DWD (Backscatter profiles)

***Stratospheric reactive gases***

Yves Christophe, BIRA (editor, model-satellite intercomparisons)
Simon Chabrillat, BIRA (model intercomparisons)
Annette Wagner, MPI-M ($O_3$ sondes)
Bavo Langerock, BIRA (NDACC FTIR, MWR, UVVIS DOAS, LIDAR)
Anne Blechschmidt and Andreas Richter, IUB-UB Bremen (SCIAMACHY/GOME-2 $NO_2$)

***Greenhouse gases***

Michel Ramonet, IPSL (ICOS)
Olivier Jossoud and Leonard Rivier, LSCE (ICOS)
Thorsten Warneke, UBC (TCCON)
Bavo Langerock, BIRA (TCCON)

***Reactive gases and aerosol modeling***

Johannes Flemming (ECMWF), Antje Inness (ECMWF), Angela Benedetti (ECMWF), Sebastien Massart (ECMWF), Anna Agusti-Panareda (ECMWF), Johannes Kaiser (KCL/MPIC/ECMWF), Samuel Remy (LMD), Olivier Boucher (LMD), Vincent Huijnen (KNMI), Richard Engelen (ECMWF)

***Acknowledgements for the validation datasets used***

We wish to acknowledge the provision of NRT GAW observational data by: Institute of Atmospheric Sciences and Climate (ISAC) of the Italian National Research Council (CNR), South African Weather Service, National Centre for Atmospheric Science (NCAS, Cape Verde), National Air Pollution Monitoring Network (NABEL) (Federal Office for the Environment FOEN and Swiss Federal Laboratories for Materials Testing and Research EMPA), Atmospheric Environment Division Global Environment and Marine Department Japan Meteorological Agency, Chinese Academy of Meteorological Sciences (CAMS), Alfred Wegener Institut, Umweltbundesamt (Austria), National Meteorological Service (Argentina), Umweltbundesamt (UBA, Germany)

We are grateful to the numerous operators of the Aeronet network and to the central data processing facility at NASA Goddard Space Flight Center for providing the NRT sun photometer data, especially Ilya Slutker and Brent Holben for sending the data.

The authors thank to all researchers, data providers and collaborators of the World Meteorological Organization's Sand and Dust Storm Warning Advisory and Assessment System (WMO SDS-WAS) for Northern Africa, Middle East and Europe (NAMEE) Regional Node. Also special thank to Canary Government as well as AERONET, MODIS, U.K. Met Office MSG, MSG Eumetsat and EOSDIS World Viewer principal investigators and scientists for establishing and maintaining data used in the activities of the WMO SDS-WAS NAMEE Regional Center (http://sds-was.aemet.es/).

We wish to acknowledge the provision of ozone sonde data by the World Ozone and Ultraviolet Radiation Data Centre established at EC in Toronto (http://woudc.org), by the Data Host Facility of the Network for the Detection of Atmospheric Composition Change established at NOAA (http://ndacc.org), by the Norwegian Institute for Air Research and by the National Aeronautics and Space Administration (NASA).

We wish to thank the NDACC investigators for the provision of observations at Ny Alesund, Bern, Jungfraujoch, Izaña, Xianghe, Harestua, Reunion Maido, Uccle, Hohenpeissen, Mauna Loa, Lauder and Haute Provence.

The authors acknowledge the NOAA Earth System Research Laboratory (ESRL) Global Monitoring Division (GMD) for the provision of ground based ozone concentrations.

The MOPITT CO data were obtained from the NASA Langley Research Center ASDC. We acknowledge the LATMOS IASI group for providing IASI CO data.

SCIAMACHY lv1 radiances were provided to IUP-UB by ESA through DLR/DFD.

GOME-2 lv1 radiances were provided to IUP-UB by EUMETSAT.

The authors acknowledge Environment and Climate Change Canada for the provision of Alert ozone data and Sara Crepinsek – NOAA for the provision of Tiksi ozone data. Surface ozone data from the Zeppelin Mountain, Svalbard are from www.luftkvalitet.info. Surface ozone data from the Villum Research Station, Station Nord (VRS) were financially supported by "The Danish Environmental Protection Agency" with means from the MIKA/DANCEA funds for Environmental Support to the Arctic Region. The Villum Foundation is acknowledged for the large grant making it possible to build VRS in North Greenland.

We acknowledge the National Aeronautics and Space Administration (NASA), USA for providing the OMPS limb sounder data (http://npp.gsfc.nasa.gov/omps.html) and the Aura-MLS offline data (http://mls.jpl.nasa.gov/index-eos-mls.php).

We thank the Canadian Space Agency and ACE science team for providing level 2 data retrieved from ACE-FTS on the Canadian satellite SCISAT-1.

The TCCON site at Orleans is operated by the University of Bremen and the RAMCES team at LSCE (Gif-sur-Yvette, France). The TCCON site at Bialystok is operated by the University of Bremen. Funding for the two sites was provided by the EU-project ICOS-INWIRE and the University of Bremen. The TCCON site at Réunion is operated by BIRA-IASB, in cooperation with UReunion and is funded by BELSPO in the framework of the Belgian ICOS program.

We acknowledge the provision of $CO_2$/$CH_4$ data from SNO-RAMCES/ICOS network coordinated by LSCE/OVSQ (CEA-CNRS-UVSQ, Université Paris-Saclay), as well as Laboratorio de Física de la Atmósfera (UMSA, Bolivia), Environmental Chemical Processes Laboratory (ECPL/UoC, Greece), Station Géophysique de LAMTO, Ivory Coast), C-CAPS/NUIG/EPA (Ireland), BIRA-IASB (Belgium) and the following research institutes in France: LaMP/OPGC, P2OA/LA/OMP, OPE/ANDRA, OHP/PYTHEAS, OPAR/LACY/OSUR, UMR EcoFoG, IPEV, IRD.

The European Environment Information and Observation Network (Eionet) Air Quality portal provides details relevant for the reporting of air quality information from EU Member States and other EEA member and co-operating countries. This information is submitted according to Directives 2004/107/EC and 2008/50/EC of the European Parliament and of the Council.

Copernicus Atmosphere Monitoring Service

ECMWF - Shinfield Park, Reading RG2 9AX, UK

Contact: info@copernicus-atmosphere.eu